Some properties of spout-fluid beds

SOME PROPERTIES OF SPOUT-FLUID BEDS

C. HEIL

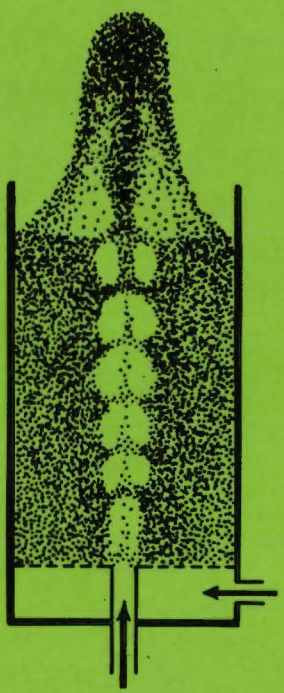

SOME PROPERTIES OF SPOUT-FLUID BEDS

SOME PROPERTIES OF SPOUT-FLUID BEDS

PROEFSCHRIFT

TER VERKRIJGING VAN DE GRAAD VAN DOCTOR IN DE TECHNISCHE WETENSCHAPPEN AAN DE TECHNISCHE HOGESCHOOL EINDHOVEN, OP GEZAG VAN DE RECTOR MAGNIFICUS, PROF. DR. S. T. M. ACKERMANS, VOOR EEN COMMISSIE AANGEWEZEN DOOR HET COLLEGE VAN DEKANEN IN HET OPENBAAR TE VERDEDIGEN OP VRIJDAG 18 MEI 1984 TE 16.00 UUR

DOOR

CORNELUS HEIL

GEBOREN TE RAVENSTEIN

Dit proefschrift is goedgekeurd door
de promotoren:

prof.ir.M.Tels
prof.dr.K.Rietema

Aan mijn ouders,
aan Willeke

Dankwoord

Het in dit proefschrift beschreven onderzoek is verricht in de vakgroep Fysische Technologie van de Technische Hogeschool Eindhoven.
Aan de leden hiervan die op enigerlei wijze bijdragen hebben geleverd aan de inhoud van dit proefschrift ben ik dank verschuldigd.

Het grootste deel van de werkzaamheden aan de opstellingen is voor rekening gekomen van Henk de Goeij. De inventiviteit en het vakmanschap waarmee technische problemen zijn opgelost zijn door mij als zodanig zeer gewaardeerd. De overige leden van de technische staf wil ik bedanken voor de assistentie bij de technische werkzaamheden.

Een zeer belangrijke bijdrage aan het werk is geleverd door de studenten die op gedeelten van dit onderzoek zijn afgestudeerd. In verband hiermee gaat mijn erkentelijkheid uit naar het werk van Hans Mennen, Jean Claessen en Sjef Voncken.

Vanaf deze plaats wil ik tevens wijlen prof.ir.A.L.Stuijts herdenken met wie ik vele discussies heb gevoerd over het prepareren van poreuze tracerdeeltjes van magnetisch materiaal. Hij wakkerde het enthousiasme in mij aan om een onderzoek met gebruikmaking van een grote inductieve spoel te starten.

In het bijzonder ben ik zeer erkentelijk voor de grote zorg waarmee Anniek van Bemmelen het proefschrift getypt heeft.

Tenslotte wil ik iedereen bedanken die op enigerlei wijze mij een morele steun is geweest en mij allerlei kleine werkzaamheden uit handen heeft genomen.

Acknowledgement

Part of this thesis was presented at the "Second International Symposium on Spouted Beds", held at Vancouver (B.C.), Canada on October 3-6, 1982.

The author wishes to express his gratitude to the Dutch Ministry of Education and Sciences (Ministerie van Onderwijs en Wetenschappen) who absorbed the cost of his trip to Vancouver.

The author wishes to thank the National Research Council of Canada and the University of British Columbia for providing grants in support of his stay in Vancouver.

The author also thanks Dr.Epstein and his coworkers for the hospitality they showed him during his visit to their laboratory.

Curriculum vitae

The author was born on January 9, 1955, in Ravenstein, The Netherlands. Following his secondary education at the "Jorislyceum" in Eindhoven, he began his studies at the Department of Physical Engineering of the Eindhoven University of Technology in 1972.
Graduate work, performed under the guidance of prof.dr.ir.G.Vossers in 1978, comprised the theoretical and experimental investigation into the optimisation procedure and the performance characteristics of horizontal axis wind turbines.
In 1979 he joined the Department of Chemical Engineering of the Eindhoven University of Technology where he worked for 4 years under the guidance of prof.ir.M.Tels.
The work that has been performed in that period comprised the investigation into the properties of spout-fluid beds.
In 1983 he joined the Department of Mechanical Engineering of the Delft University of Technology where he now works under the guidance of prof.ir.J.J.C. van Lier.

CONTENTS

SUMMARY

A spout-fluid bed is a type of fluid bed in which an orifice has been installed, at the center of the flat distributor plate. Spout gas is introduced into the bed through the nozzle. Fluidisation gas can be introduced into the bed through the remainder of the distributor plate.
This type of reactor has a broad potential applicability to processes in which solid/gas dispersions are treated that either show a wide spread in the distribution of the particle sizes or contain material which cannot be fluidised as such.
The investigation described in this thesis had two aims:

1. Measuring and modelling the pressure and flow distributions of the gas in the spout-fluid bed.
2. Measuring and modelling the mixing of the solids in the spout-fluid bed.

Several flow regimes can be generated in the bed by varying the spout and fluidisation gas flow rates:

1. the packed bed flow regime
2. the fluctuating spouted bed flow regime
3. the stable spouted bed flow regime.

The possibility of obtaining the several flow regimes, that is the possibility of contacting gas and solids in different ways by simply changing the rates of spout and fluidisation gas, is held to be a mature advantage of the spout-fluid bed.

Models were developed that describe the pressure and flow distributions in spout-fluid beds in the packed bed and stable spouted bed flow regimes fairly well.
Both pressure distribution models predict the bed pressures from the spout- and fluidisation gas flow rates and besides from variables that represent the geometrical properties of the bed and of the bed material only. This way of modelling differs from that used by many authors who have included in their analysis the maximum spoutable bed height which cannot be easily measured.
First a simple model was developed for a bed in the stable spouted bed

flow regime. In this model it is assumed that pressure and friction forces only determine the gas flow in the spout channel. Simple expressions for the pressure and flow distribution were obtained from this model.
Next, an extended model was developed that in addition includes the effects of inertial forces and interaction forces between the gas and the bed particles in the spout channel.
Calculated results of the simple model do not agree with pressures that were measured near the spout channel. The reason is that the influences of the inertial and interaction forces that occur in the gas flow through the spout channel are ignored.
Pressures that were calculated by means of the extended model agree better with the measured pressures than those that were calculated from the simple model.

The mixing behaviour of spout-fluid beds in the fluctuating spouted bed regime was investigated by measuring the circulation times of single tracer particles in these beds.
Mixing results from the variance in the circulation times of the bed particles. For this reason a mathematical description was derived of the variance in the circulation times and of the mixing rate in an apparatus in which a circulation flow occurs.
In the model that is described the variance in the circulation times is established by exchange of bed material between the separate particle trajectories.
In the model this exchange takes place as the bed particles that are entrained upward through the spout channel are deposited in random positions on the top surface of the annulus, subsequently move back towards various points on the spout channel wall along trajectories of different length, whence the particles again pass into the spout channel. The particles are dispersed through following these trajectories of different lengths. The dispersion is expressed in terms of a dispersion coefficient.
The mixing in the spout-fluid beds was investigated by means of a tracer particle with high magnetic permeability. Circulation times of this particle were measured by noting the periods of time that elapsed between each two successive passages of the tracer particle between

the two poles of an inductive coil. The coil was placed around the bed at the position of the top of the annulus.
Circulation time distributions are shown for several values of the spout and fluidisation gas velocities and for two bed heights.
The mixing model appears to describe the mixing behaviour of spout-fluid beds reasonably well. The dispersion coefficient and the downward particle velocity appear to depend on the bed height and on the spout and fluidisation gas velocities.

SAMENVATTING

Een spout-fluid bed is een soort fluid bed waarin een uitstroompijpje is geplaatst dat uitmondt in het midden van de verdeelplaat. Door dit pijpje wordt spoutgas aan het bed toegevoerd. Fluidisatiegas wordt via het overgebleven deel van de verdeelplaat aan het bed toegevoerd.
Dit type reactor heeft toepassingsmogelijkheden die een breed terrein beslaan op het gebied van processen aangaande mengsels van gas en vaste stof, waarbij de deeltjes van de vaste stof een grote spreiding vertonen in de deeltjesgrootte-verdeling of materiaal bevatten dat zelf niet als zodanig gefluidiseerd kan worden.
Het onderzoek dat beschreven is in dit proefschrift had twee doelen:
1. Het meten en het modelleren van de druk- en snelheidsverdeling van het gas in het spout-fluid bed.
2. Het meten en het modelleren van de menging van de vaste stof in het spout-fluid bed.

Verscheidene stromingsregimes kunnen in het bed verkregen worden door de spout- en fluidisatiegasdebieten te variëren:
1. het gepakte bed stromingsregime
2. het fluctuerend spouted bed stromingsregime
3. het stabiel spouted bed stromingsregime.
De mogelijkheid om de verschillende stromingsregimes te verkrijgen, dat is de mogelijkheid om gas en vaste stof op verschillende manieren met elkaar in contact te brengen door eenvoudigweg de spout- en fluidisatiegasdebieten te veranderen, wordt als een groot voordeel beschouwd van het spout-fluid bed.

Modellen werden ontwikkeld die de druk- en snelheidsverdeling van gas in spout-fluid bedden in het gepakte bed en het stabiel spouted bed stromingsregime redelijk goed beschrijven.
Beide modellen geven de drukken in het bed uit de spout- en fluidisatiegasdebieten en uit variabelen die de geometrische eigenschappen van het bed en van het bedmateriaal representeren. Deze wijze van modelleren verschilt van wat gebruikelijk is bij vele auteurs die in hun analyses de maximale hoogte van een te spouten bed gebruiken, welke niet gemakkelijk gemeten kan worden.

Voor een bed in het stabiel spouted bed regime werd eerst een eenvoudig model ontwikkeld. In dit model wordt aangenomen dat alleen de druk- en weerstandskrachten de gasstroming in het spoutkanaal bepalen. Eenvoudige uitdrukkingen voor de druk- en snelheidsverdeling van het gas werden hieruit verkregen.
Een uitgebreid model werd daarna ontwikkeld dat bovendien de effecten van traagheids- en interactiekrachten tussen gas en beddeeltjes in het spoutkanaal in rekening bracht.
Berekende resultaten van het eenvoudige model komen niet overeen met de drukken die in de buurt van het spoutkanaal werden gemeten. De oorzaak hiervan is het feit dat de invloeden van de traagheid- en interactiekrachten, die de gasstroming in het spoutkanaal mede bepalen, verwaarloosd werden. Drukken die werden berekend met het uitgebreide model komen beter met de gemeten drukken overeen dan de drukken die werden berekend met het eenvoudige model.

Het menggedrag van spout-fluid bedden in het fluctuerend spouted bed regime werd onderzocht door de circulatietijden van een enkel tracerdeeltje in deze bedden te meten.
Menging is het gevolg van spreiding in de circulatietijden van het bedmateriaal. Daarvoor werd een wiskundige formulering afgeleid van de spreiding in de circulatietijden en van de snelheid waarmee de menging verloopt in een apparaat waarin een circulatiestroming plaatsvindt.
In het beschreven model komt de spreiding in de circulatietijden van het bedmateriaal tot stand door uitwisseling van het bedmateriaal tussen de afzonderlijke stroombanen. Deze uitwisseling heeft plaats als de beddeeltjes, die naar boven meegevoerd worden in het spoutkanaal, willekeurig verspreid worden over de top van de annulus en vervolgens terugstromen naar de verschillende punten van de wand van het spoutkanaal langs stroombanen van verschillende lengte, waar de deeltjes het spoutkanaal weer ingaan. De deeltjes ondergaan dispersie bij het volgen van deze stroombanen van verschillende lengte. De dispersie wordt uitgedrukt in termen van een dispersiecoefficient.
De menging in de spout-fluid bedden werd onderzocht door middel van een tracerdeeltje met een hoge magnetische permeabiliteit. Circulatietijden van dit tracerdeeltje werden gemeten door de tijd vast te stellen die verstreek tussen elke twee achtereenvolgende passages van het tracer-

deeltje tussen de twee polen van een spoel. De spoel was rond het bed geplaatst op de hoogte van de top van de annulus.
Circulatietijden worden getoond voor enkele waarden van de spout- en fluidisatiegassnelheden en voor twee bedhoogten.
Het mengmodel blijkt het menggedrag van fluctuerende spout-fluid bedden redelijk goed te beschrijven. De dispersiecoefficient en de neerwaartse deeltjessnelheid blijken van de bedhoogte en van de spout- en fluidisatiegassnelheden af te hangen.

1. INTRODUCTION

A spout-fluid bed is a type of fluidised bed in which an orifice through which spout gas is introduced has been placed at the center of the flat gas distributor plate at the bottom of the bed.
Fluidisation gas is introduced through the gas distributor plate (figure 1.1). The fluidisation gas causes an increasingly loosely packed bed structure with increasing gas velocity.
Spout gas is introduced in order to induce an overall circulation of the bed material.

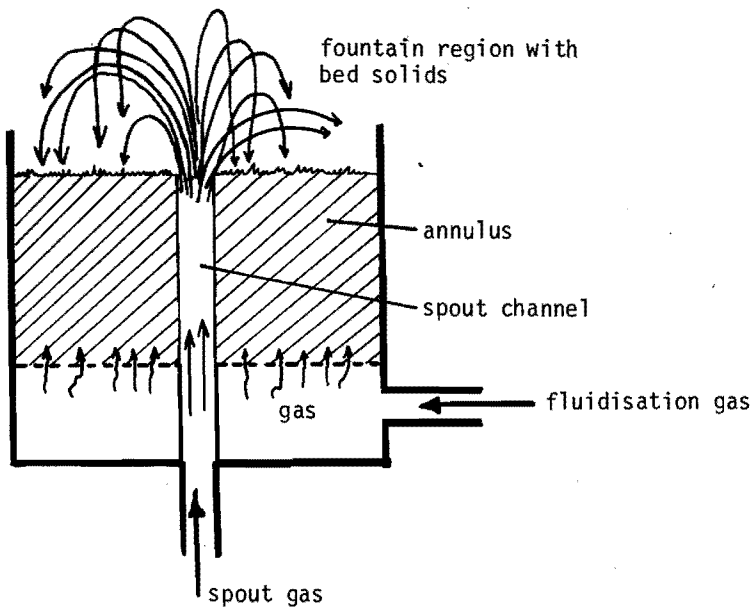

Figure 1.1. Schematic view of a spout-fluid bed.

The present investigation of spout-fluid bed reactors was prompted by an interest in the possible technical applicability of spout-fluid beds to operations for use in chemical engineering and physical technology [1]. The apparatus can be regarded as a combination of a spouted bed and a fluidised bed. It was therefore supposed at the outset of this investigation that the spout-fluid bed might combine some of the valuable properties of fluidised and spouted beds.

Fluidised beds are highly suitable for handling finely dispersed solid materials or for contacting a gas with such materials (figure 1.2). Baeyens and Geldart [5] have characterised powders according to their fluidisation, bubbling, slugging and spouting behaviour. The powders were classified as A, B, C and D powders according to their sizes and densities. Figure 1.3 shows a table that summarizes some fluidisation characteristics of the 4 powder groups. Figure 1.4 gives a powder classification diagram for fluidisation in air at ambient conditions.

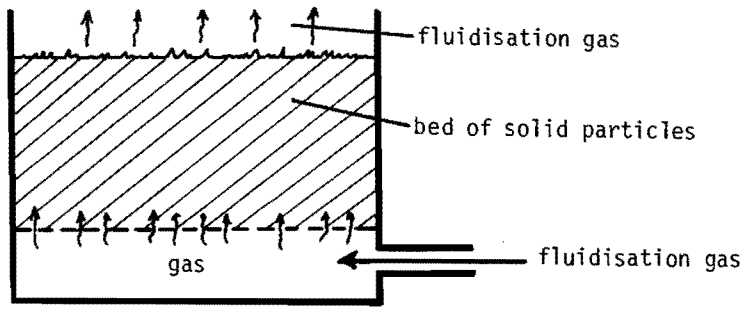

Figure 1.2. Schematic view of a fluid bed.

Group	C	A	B	D
Approx size/density ranges μm/g cm^{-3}	< 30/any	30/5 to 200/0.8	50/4 to 1000/1	> 400/4 to > 1200/1
Bed expansion	very small	large	small	very small
Bed collapse rate	very slow	slow	fast	fast
Bubble shape	channels	⊖	⊖	○
Solids mixing rate	very low	very high	high	moderate
Gas back mixing	none	very high	moderate	low
Mode of slugging	channels	axi-symmetric slugs break down at high gas flows	axi-symmetric → a-symmetric at high gas flows	a-symmetric
Spouting	channels	only in very shallow beds	only in shallow beds	yes
Wall/bed heat transfer coefficient	very low	high	high to moderately high	low

Figure 1.3. Summary of some fluidisation characteristics of the four powder groups. (from [5])

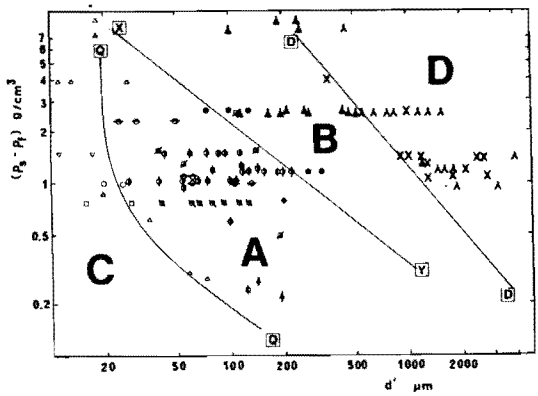

Figure 1.4. Powder classification diagram for fluidisation on air (ambient conditions). (from [5])

The behaviour of fine particles in a fluidised bed differs in some ways from the behaviour of coarse particles. When a fluidised bed of particles smaller than 100 micrometer (A and C powders) is operated at the minimum fluidisation condition the cohesion forces are of great importance when compared to the gravitational and fluid drag forces that are acting on the individual particles. For this reason a fluidised bed that contains finely dispersed material is stable when it is operated below the minimum bubbling velocity. The individual particles have little mobility due to the influence of cohesion forces. The fluidised bed is then operated in a homogeneous fluidisation regime. With increasing fluidisation gas velocity the fluid drag forces begin to dominate. Individual particles in the bed obtain the possibility of moving in the bed in a similar way as do molecules in a liquid as a result of Brownian movement. The bed becomes unstable and part of the fluidisation gas now flows through the bed as gas bubbles.

In a fluidised bed that contains coarse particles (B or D powders) the cohesion forces between the individual particles can be neglected with respect to the gravitational and fluid drag forces. A bed of coarse particles is therefore unstable at the minimum fluidisation condition. Spouted beds are highly suitable for handling coarse particles (figure 1.5) as opposed to fluidised beds. When spout gas is introduced into a

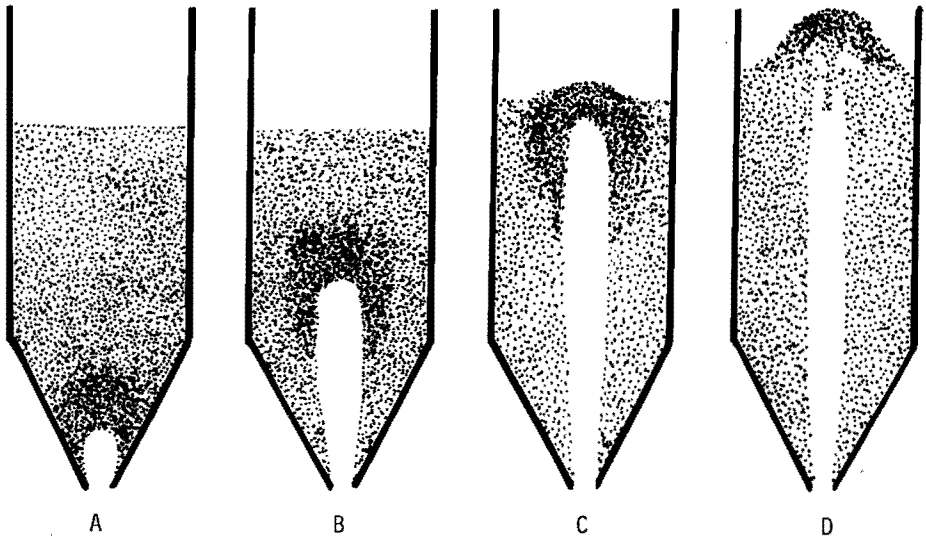

Figure 1.5. View of the several flow regimes in a spouted bed.

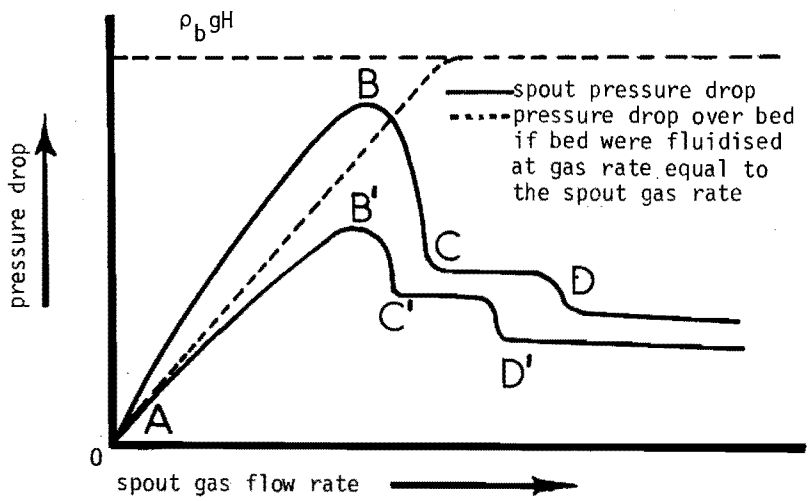

Figure 1.6. Example of a pressure drop over a spouted bed. Letters in the figure correspond to figure 1.5.

spouted bed several flow regimes can be obtained by adjusting the spout gas rate. When the gas rate is increased from zero an internal cavity is formed (figure 1.5A and B). A pressure drop exists between the orifice and the top of the bed that is high with respect to the fluidisation pressure drop when fluidisation gas only should be introduced at a rate equal to the spout gas rate (figure 1.6). The internal cavity becomes unstable at increasing spout gas rate.
A spout channel is then formed between the orifice and the top of the bed (figure 1.5C and D). The pressure drop over the bed becomes relatively low (figure 1.6).
At still higher spout gas rates an overall circulation of the solid bed material is maintained. The annulus solids are partly flowing into the spout channel at the bottom and are partly entrained from the spout channel wall along the whole length of the spout channel and blown up into the fountain. From this fountain region the solids are spread out over the upper surface of the annulus. The circulation flow pattern thus consists of an upwards flow of solids in the spout channel and a downward flow of solids in the annulus. The downward solids flow in the annulus can be regarded as having a certain degree of axial dispersion and moving countercurrently to the spout gas that has penetrated into the annulus.

Good mixing of the solids in a spouted bed reactor is established when a large variation exists in the circulation times of the solids together with a sufficient degree of transversal exchange between the individual particle trajectories. Transversal exchange is pronounced in the fountain region of the spouted bed.

An unfavourable situation occurs when bed materials are used that show a large variation in shape and size:
Under these circumstances segregation can be expected to take place in both fluidised and spouted beds. Segregation in a spouted bed is suppressed to a certain extent because of the dynamic circulation behaviour.
The advantages of the use of a fluidised bed and a spouted bed for handling fine and coarse particles respectively seem to suggest that a combination of both might be suitable for handling dispersions that

contain both fine and coarse solid bed material. It might also be possible to use the spout-fluid bed for handling mixed dispersions which contain material that cannot be fluidised as such.
Moreover the spout-fluid bed is also more flexible because the spout and fluidisation gas rate can of course be adjusted independently.
The different flow regimes that can be generated in a spout-fluid bed by varying the ratio of the rates of spout gas and fluidisation gas have already been discussed above. The possibility of obtaining several flow regimes, that is a possibility of contacting gas and solids in different ways by simply changing the rates of spout and fluidisation gas, is held to be a mature advantage of the spout-fluid bed.

Spout-fluid beds were first described by Chatterjee [2]. He pointed out that spout-fluid beds provide a possibility to overcome both some limitations that are inherent to fluidised beds and a number of limitations that are characteristic of spouted beds. Other useful properties of spout-fluid beds are, in the opinion of Chatterjee, the high rate of circulation and the thorough mixing of the solid particles, the accuracy with which both spouting and fluidisation phenomena can be controlled and the fact that the minimum flow rates that are required to maintain spouting and fluidisation conditions are lower than those needed in spouted and fluidised beds.
At the first International Symposium on Spouted Beds two papers on spout-fluid beds were presented by Nagarkatti and Chatterjee [3] and by Littman, Vukovic, Zdanski and Grbavcic [4].
Nagarkatti et al. studied bed properties at several values of the flow rate, particle diameter, orifice diameter and bed height. Littman et al. measured the minimum value of the total rate of spout and fluidisation gas as a function of bed height and orifice diameter for a bed that was spout-fluidised with water.
A large number of publications deal with the fluid dynamic behaviour of spouted and fluidised beds. Publications on circulation systems behaviour in general and on the mixing and circulation properties of spouted beds in particular are also available.
Some of these articles will be discussed in the appropriate chapters of this thesis.

This work first presents the different flow regimes of a spout-fluid bed (chapter 2). A description is given of the apparatus that were used for the investigation into these flow regimes. The experimental results are presented by means of pressure drop characteristics and by means of a diagram that shows which flow regime occurs in a given spout-fluid bed as a function of the spout and fluidisation gas velocity. Some photographs that show some flow regimes in a flat model of a spout-fluid bed are also presented in chapter 2. A theoretical model from which the pressure distribution in spout-fluid beds can be calculated is presented in chapter 3. The model applies to beds in the packed bed regime (without spout channel) as well as in the stable spouted bed regime.
First a simple model is considered that assumes a linear relationship between pressure drop and gas velocity in the spout channel. Calculated results of this models are shown in plots of isobars and plots with lines of equal vertical velocity. An extension of the flow model that includes the effect of inertial forces in the gas flow and the effect of interaction with entrained bed particles in the spout channel is considered also. The equation of motion of the bed solids in the spout channel is applied to obtain a relation between the hold-up in the spout channel and the circulation rate of the spout-fluid bed.
Experiments on the determination of the pressure distribution in some spout-fluid beds are discussed in chapter 4. The measured data are compared to the model results and are discussed.
Experimental and theoretical results on the mixing and circulation behaviour of the spout-fluid bed are presented in the chapters 5 and 6. Chapter 5 describes the solids circulation flow and the dispersion in that flow in a spout-fluid bed that is being operated in the fluctuating spouting regime in terms of circulation time distribution functions. The experimental determination of the circulation time distribution under various conditions is described in chapter 6.

Literature

[1] Ginneken, C.P.M. van
Ph.D.Thesis, Eindhoven University of Technology, 1982

[2] Chatterjee, A.
Ind.Eng.Chem.Process.Des.Develop. 9, 340 (1970)

[3] Nagarkatti, A. and Chatterjee, A.
Can.J.Chem.Eng. 52, 185 (1974)

[4] Littman, H., Vukovic, D.V., Zdanski, F.K., Grbavcic, Z.B.
Can.J.Chem.Eng. 52, 174 (1974)

[5] Baeyens, J. and Geldart, D.
Proceedings of the International Symposium "Fluidisation and its Applications", Toulouse, October 1-5, 1973

2. FLOW REGIMES IN SPOUT-FLUID BEDS

2.1 Introduction

When both spout and fluidisation gas rates are varied various flow regimes occur each of which is marked by definite characteristics. The occurence of these flow regimes appears to depend not only on the fluidisation and spout gas rates, but also on the geometric proportions of the bed, on the properties of the bed solids and on the properties of the spout and fluidisation gases.
These flow regimes will be discussed in the following paragraphs on the basis of our experiments in which two different solids were used to make up the beds. These solids were two kinds of river-sand, here indicated by "P" and "Q" respectively, which differ only slightly in their particle size distributions (figure 2.1) and in their gas velocity to pressure drop relation (figure 2.2). It is seen from figure 2.2 that the solids P and Q have values of the minimum fluidisation velocity of about 20 cm/s and about 32 cm/s respectively.
Air is supplied as both spout and fluidisation gas. No state of homogeneous fluidisation for the bed solids P and Q used in the experiments exists. This is the case for all materials that consist of coarse particles. At the minimum fluidisation condition the interaction forces between the particles can be neglected with respect to the gravitational and fluid drag forces. An instability then exists in the bed and the fluidised bed shows rising gas bubbles. This is the so-called heterogeneous fluidisation state.

2.2 The flow regimes

The various flow regimes were investigated in two experimental spout-fluid beds:

I. A 15.2 cm diameter bed the main part of which was a Quick-fit Visible Flow gas column (figure 2.3).
   Fluidisation gas was introduced through a sintered copper distributor plate at the bottom. Spout gas was introduced through a nozzle at the center of the distributor plate. Different bed heights and nozzle diameters were applied in these experiments. Bed solid P only was used in this spout-fluid bed apparatus.

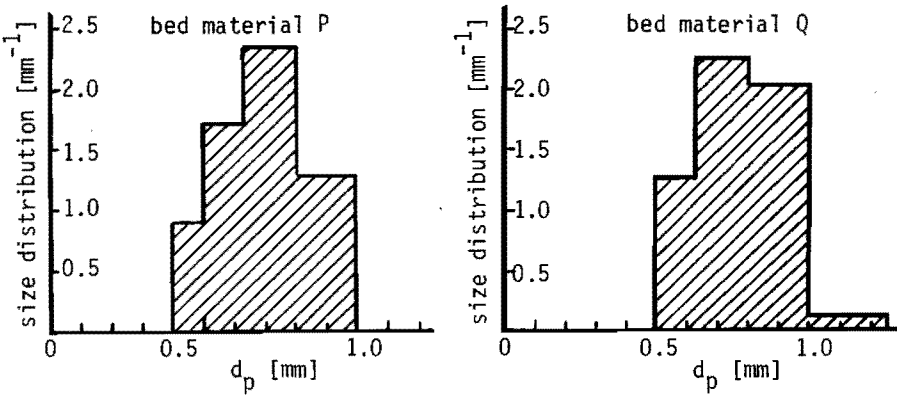

Figure 2.1. Particle size distribution of the used bed materials.

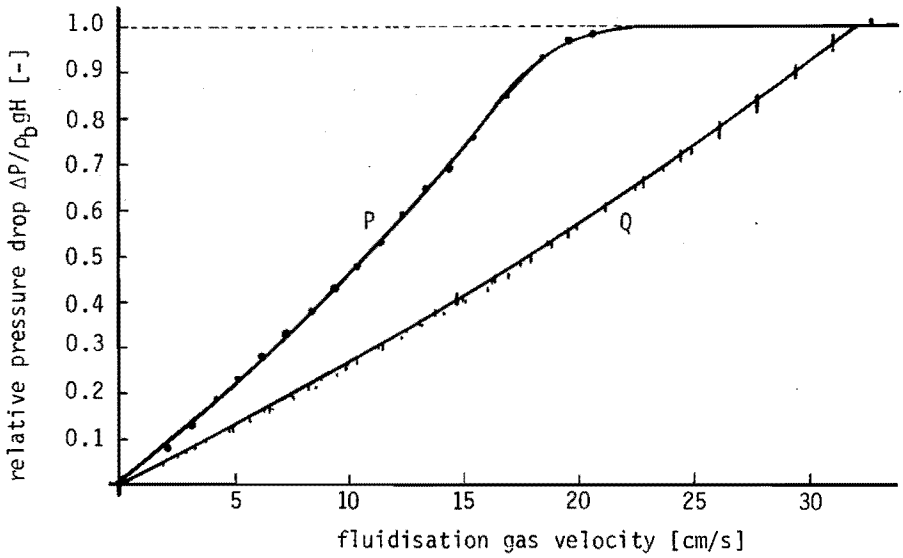

Figure 2.2. Fluidisation pressure drop characteristics of the used bed materials.

1. glass column (diameter = 15.2 cm)
2. disengagement zone
3. outlet of spout-fluidisation gas to dust bag
4. inlet of spout gas
5. inlet of fluidisation gas
6. sintered copper distributor plate
7. fluidisation gas buffer
8. pressure probe (moveable)
9. pressure tap
10. sand bed

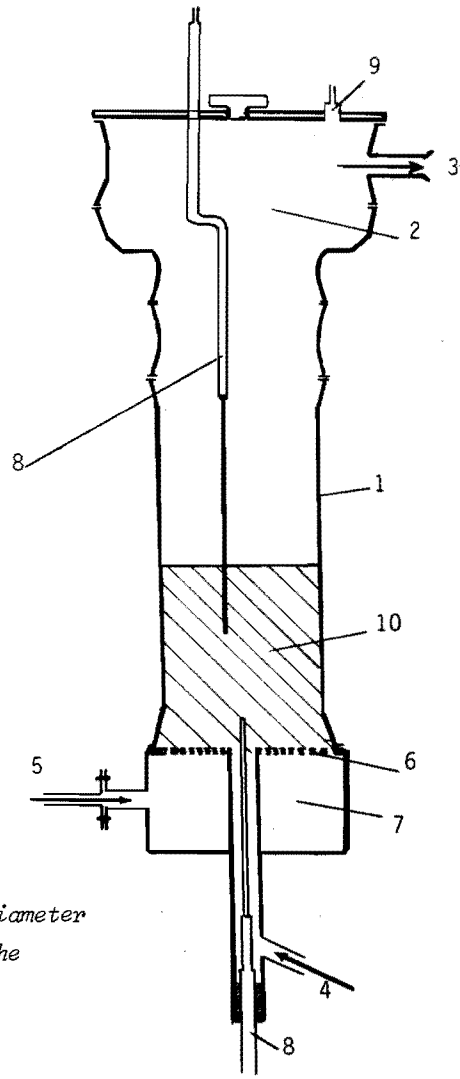

Figure 2.3. View of the 15.2 cm diameter spout-fluid bed and the pressure probes.

II. A 45 cm diameter spout-fluid bed which consisted of a stainless steel section and some Quick-fit Visible Flow glass sections (figure 2.4).

As in the case of apparatus I, different bed heights were applied in the experiments that were carried out in this apparatus. Bed solid Q only was used in this apparatus.

1. Stainless steel measurement section
2. glass column (diameter = 45 cm)
3. outlet of spout-fluidisation gas to dust bag
4. inlet of spout gas
5. inlet of fluidisation gas
6. fluidisation gas buffer
7. pressure taps

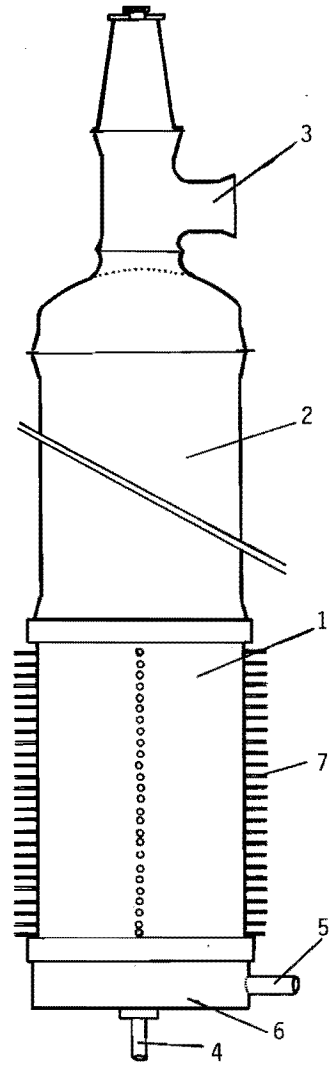

Figure 2.4. View of the 45 cm diameter spout-fluid bed and the pressure probes.

The occurence of the various flow regimes can be deduced from the way in which the pressure drop over the bed varies when varying spout gas rate at constant fluidisation gas velocity. This spout pressure drop was measured by means of a pressure probe that is inserted in the spout orifice of apparatus I and is placed near the spout orifice of apparatus II. Also a pressure probe is placed at the top of the bed. The pressure drop over the bed was recorded in this way while the spout gas flow rate was increased and decreased respectively at constant fluidisation gas velocity.

Several flow regimes were found to exist (figs. 2.5 and 2.6), viz. the packed bed regime (A), the bubbling (B), the fluctuating spouting (C) and the stable spouting (D) regimes.
Figure 2.5 shows examples of the plots of the time average of the pressure drop versus the spout gas flow rate and superficial spout gas velocity as measured in the 15.2 cm spout-fluid bed.

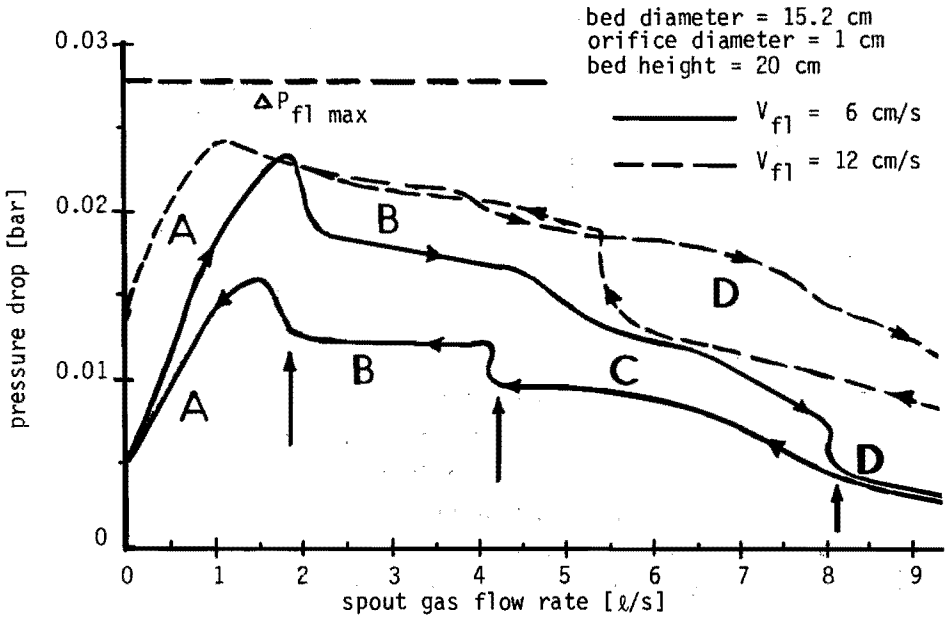

Figure 2.5. Example of a time average spout pressure drop measured during increase resp. decrease of spout gas flow rate. Transitions are marked with an arrow. Spout gas flow rate = 4 ℓ/s corresponds to superficial spout gas velocity = 22.0 cm/s.

The packed bed regime does not show a spout channel. At sufficiently high spout gas flow rates the spout gas forms an internal cavity that is quite stable and does not easily collapse (figure 2.6A). Spout gas percolates through the arch into the bed. This results in a pressure drop over the bed that is relatively high compared to the pressure drop that would exist over the bed when the bed was aerated with a gas rate equal to the sum of the rates of the spout and fluidisation gas that were introduced.

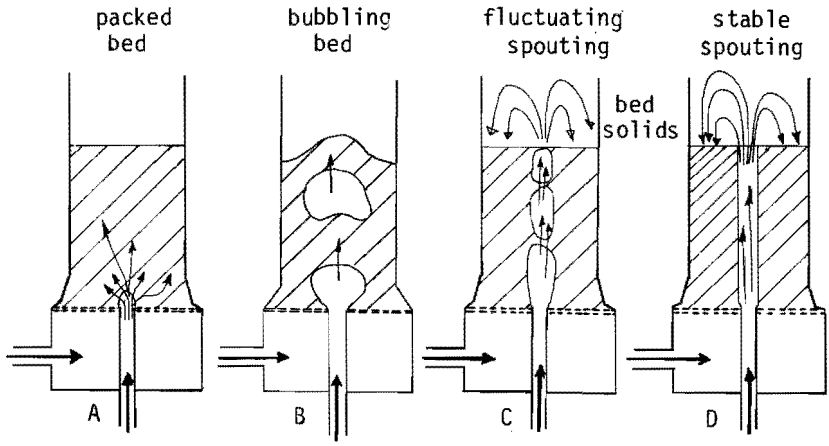

Figure 2.6. Schematic view of flow regimes in a spout-fluid bed.

The bubbling regime is characterised by individual, well defined bubbles that rise from the orifice to the top of the bed (figure 2.6B). In this flow regime the pressure drop shows irregular fluctuations with a frequency between 5 and 10 Hz. These fluctuations correspond to the formation of the bubbles at the orifice.

The fluctuating spouting regime is to be regarded as a regime that is intermediate between the bubbling and the stable spouting regimes. The pressure drop here shows periodic fluctuations of higher frequency (higher than 10 Hertz) than is the case in the bubbling regime. These fluctuations reflect a pulsating upwards flow of mixtures of the spout gas and the bed material. One might say that in this regime the bed is attempting to form a continuous spout channel between the orifice and the top of the bed. However, these attempts are not yet successful because parts of the channel wall keep collapsing and inject bed material into the spout channel (figure 2.6C). These frequent collapses of parts of the channel wall cause the periodic fluctuations in the pressure drop with time.

When the spout gas flow rate is increased further the channel wall becomes stable. The system then has entered the stable spouted bed regime (figure 2.6D). In this regime the pressure drop over the bed is lower than in any of the other regimes that have been discussed so far. The pressure drop shows no variation with time.

The pressure drop characteristic in figure 2.5 gives rise to the existence of some hysteresis in the transition between the stable spouted and fluctuating spouting bed regime (see D in figure 2.5). It can be seen that this hysteresis effect is larger when more fluidisation gas is introduced. This hysteresis is caused by the fact that there is a difference in the pressure over the bed that is needed to maintain a stable spout channel wall. This difference in pressures becomes larger when fluidisation gas is introduced also and is inherent to the stability or rigidity of the annulus region and to the amount of spout gas that crosses the spout-annulus interface. This hysteresis effect will be treated in section 4.4 also.

Some photographs of the flow regimes that have been mentioned above are shown in figure 2.8 [1]. These photographs were taken in a two-dimensional model of a spout-fluid bed which is shown in figure 2.7.

1. perspex plates
2. gas outlet to dust bag
3. inlet of spout gas
4. inlet of fluidisation gas
5. fluidisation gas buffer

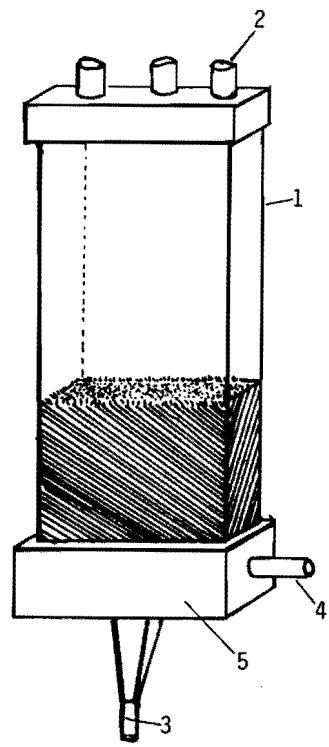

Figure 2.7. View of the two-dimensional (flat) model of the spout-fluid bed.

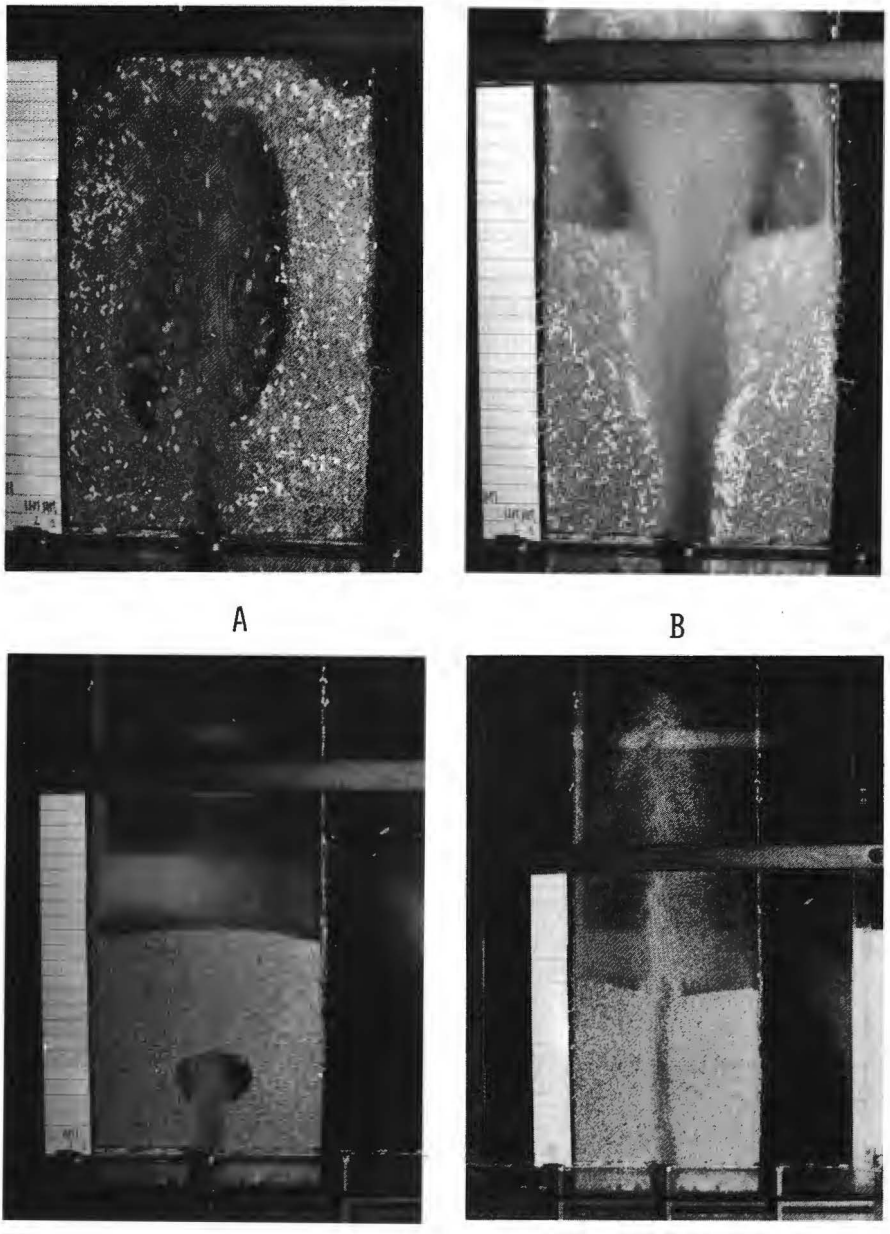

Figure 2.8. Photographs of the flow regimes in a two-dimensional model of the spout-fluid bed.

It can be seen from the pictures that the high speed photograph A in figure 2.8 shows the bubbling character of the fluctuating spouting regime in the form of a fast rising bubble.
The low speed photograph B shows the spouting character of this regime in the form of a spout channel with a collapsing spout wall and a pulsating upwards flow of solids.
The bubbling and spouting characters are two ways to express the same flow regime. This can be explained by considering the flow of the solid material around a fast rising bubble in the bed (figure 2.9). The spout channel is blown up above the rising bubble while the spout channel is collapsing beneath the bubble.

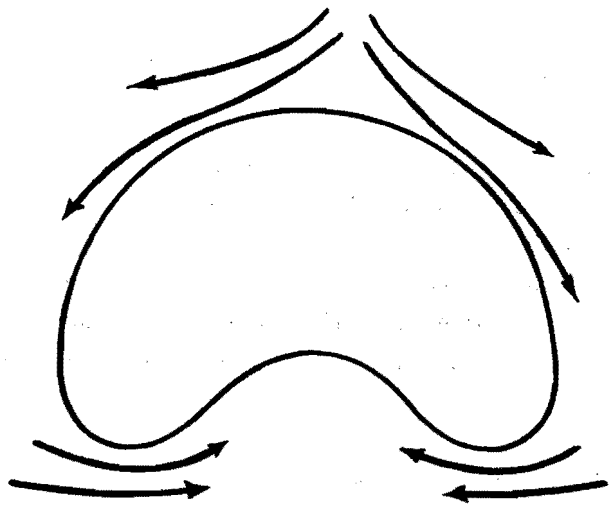

Figure 2.9. The flow of solids around a rising bubble.

Photograph C shows an internal cavity that is formed at a sufficiently high spout gas rate when the bed is being operated in the packed bed regime. Photograph D gives a view of the fountain and the spout channel when the bed is being operated in the stable spouted bed regime.

Capacity probes were used to measure the variations in bed porosity at some points in the spout-fluid bed. Figure 2.10 gives a sketch of the capacity probes and of the capacitance bridge that was used to measure

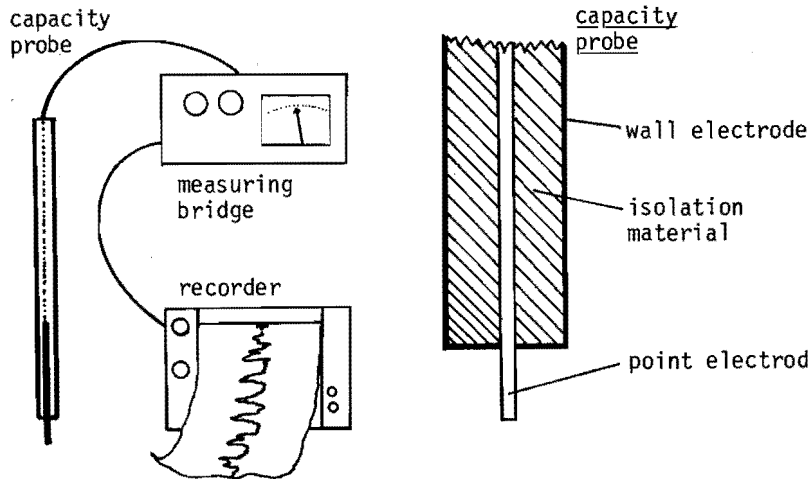

Figure 2.10. Sketch of the capacity probe and the measuring bridge.

its signal. When positioned near the spout orifice the probe can be used to determine the frequency with which bubbles are formed at the orifice in the bubbling regime.
When used in the fluctuating spouting regime the capacity probe indicates the frequency with which the wall of the spout channel is collapsing. An example of the measured signals of the capacity probe is shown in figure 2.11.

Pressure drop measurements were obtained in the 15.2 cm diameter bed with a 1 cm and a 2 cm diameter nozzle. The bed was filled with sand "P" (figs. 2.1A and 2.2A). Bed depths between 20 cm and 40 cm were applied. The bed depth was measured in the packed bed regime. The bed depths measured in the spouting regime were slightly larger than that in the packed bed regime because of the occurence of gas bubbles or a spout channel inside the bed.

Results of some pressure drop measurements carried out with a 1 cm diameter nozzle and while increasing and decreasing spout gas rate at different fluidisation gas rates are given in figure 2.12. The superficial spout gas velocity that corresponds to each value of the spout gas rate is shown in this figure. For reasons of comparison

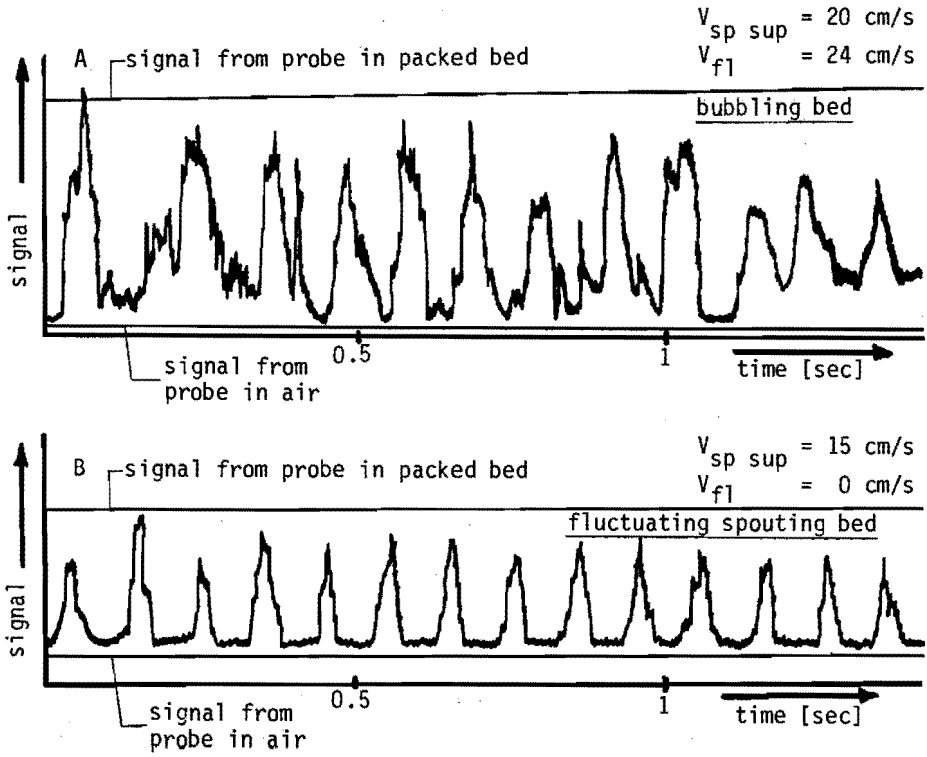

Figure 2.11. Example of a measured signal of the capacity probe. The probe is placed near the spout orifice.
A: in bubbling bed.
B: in fluctuating spouting bed.

figure 2.12 also shows the pressure drop over the bed that occurs at minimum fluidisation velocity ($\Delta P_{fl\ max}$).
The measurements described in figure 2.12 were started with the bed in the packed bed regime. The spout gas flow rate was first increased slowly until the stable spouted bed regime had been reached. The spout gas rate was then decreased slowly until the packed bed regime had become established again.
It is seen from this figure that the pressure drop over the bed increases with increasing fluidisation gas velocity in all flow regimes. It should also be noted from figure 2.12 that the spout gas rate at which the transition occurs from the packed bed regime to the bubbling

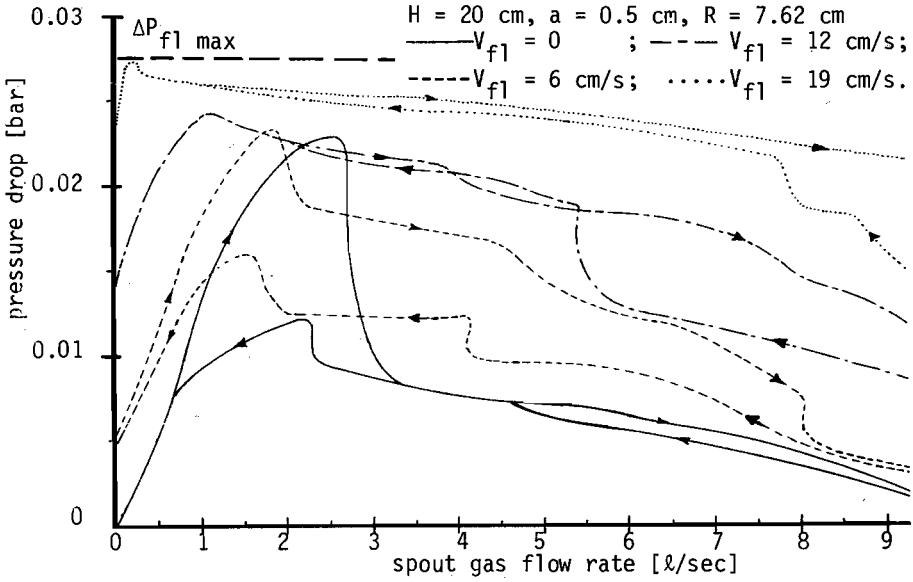

Figure 2.12. Pressure drop over the spout-fluid bed for various fluidisation gas velocities. The pressure drop ($\Delta P_{fl\ max}$) over the bed that occurs at minimum fluidisation velocity. Spout gas flow rate = 4 ℓ/s corresponds to superficial spout gas velocity = 22.0 cm/s.

or fluctuating spouting regimes decreases with increasing fluidisation gas rate.

In the transition from the bubbling or fluctuating spouting regime to stable spouted bed regime, on the other hand, the spout gas rate at which this transition occurs increases with increasing fluidisation gas rate.

Figure 2.13 gives some plots of the pressure drop over the bed versus spout gas flow rate and superficial spout gas velocity for zero fluidisation gas flow rate for various bed heights and a nozzle diameter of 1 cm (purely spouted bed).

Figure 2.13 like figure 2.12 also shows the pressure drop that would occur in the different beds at minimum fluidisation velocity ($\Delta P_{fl\ max}$). As already mentioned earlier figure 2.13 gives time average pressure drops over the bed. The occurence of the several flow regimes can be obtained from the time average pressure over the bed in dependence on

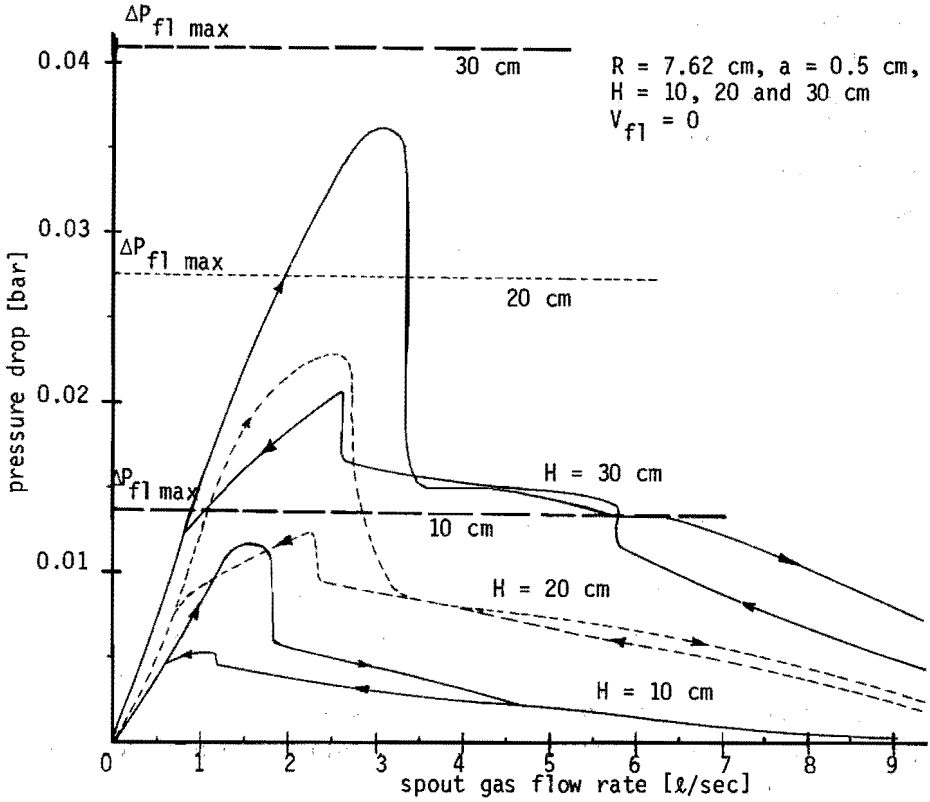

Figure 2.13. Pressure drop over the bed for various bed heights at zero fluidisation gas velocity. The pressure drop over the different bed ($\Delta P_{fl\ max}$) at minimum fluidisation velocity. Spout gas flow rate = 4 ℓ/s corresponds to superficial spout gas velocity = 22.0 cm/s.

the spout and fluidisation gas rates and from the dynamic part of the pressure signal. It was already indicated that no fluctuation exists in the pressure drop over the bed when the bed is in the packed bed and in the stable spouted bed regime. It can be found from figure 2.13 and from the dynamic part of the measured pressure that the transition from the packed bed regime to bubbling or fluctuating spouting regime are shifted to a higher value of the spout gas rate when the bed height increases.

There is a difference in the ways the pressure drop reacts to increasing spout gas rate on the one hand, and to decreasing spout gas rate on the other hand. This hysteresis has already been mentioned in many publications on spouted beds (see for example [2]).
The difference in the reaction of the bed is caused by the way the particles are packed in the bed (the microstructure of the bed) and on whether an internal cavity or spout exists in the bed (the macrostructure of the bed).
In the increasing spout gas rate branches of the curves in the figures 2.12 and 2.13 the pressure drop depends on the initial structure of the bed while in the decreasing spout gas branches of the pressure drop curves that start from the stable spouting regime the pressure drop is dependent on the structure of the stable spouted bed.
In the stable spouted bed the particles are thoroughly mixed so that no differences can exist in the way the bed is packed at the various points in the space between the spout channel and the bed wall.
It follows that when one wishes to measure well defined bed properties, such measurements are best carried out by first bringing the bed in the stable spouting regime and then reducing the spout gas rate. In this way a uniform microstructure of the bed is obtained with a measured local porosity of about 0.42.
It also follows that when one wishes to investigate the transition line between the stable spouting regime and the bubbling or fluctuating spouting regime, the measurements are best carried out at decreasing spout gas rate. The transition between the packed bed regime and the bubbling or fluctuating spouting regime, however, is best measured at increasing spout gas rate, after decreasing the spout gas rate from the stable spouted bed regime until near zero in order to obtain a bed without internal cavity and with a uniform structure of the bed material with known porosity of about 0.42.

Figure 2.14 presents a diagram that shows which flow regime exists in a spout-fluid bed with given bed diameter of 15.2 cm, spout orifice diameter of 1 cm and particles sizes between 0.4 and 0.8 mm as a function of the flow rates of both spout and fluidisation gas and of the bed height. The left hand curves represent the transition lines between the packed bed regime and the bubbling or fluctuating spouting regimes.

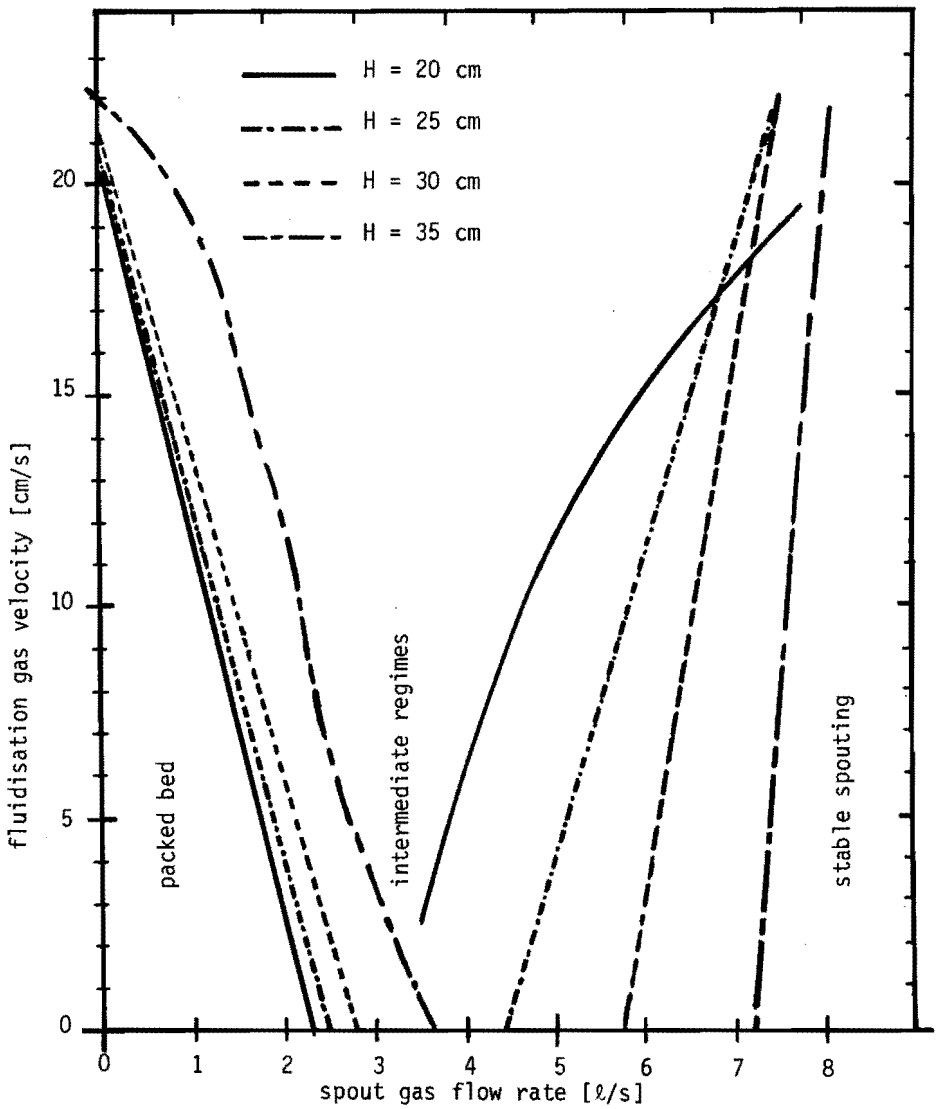

Figure 2.14. Measured limits of flow regimes for the 15.2 cm diameter spout-fluid bed for various bed heights (orifice diameter = 1 cm). Spout gas flow rate = 4 ℓ/s corresponds to superficial spout gas velocity = 22.0 cm/s.

The right hand curves represent the transition lines between the last called regimes and the stable spouted flow regime. It is seen that the left hand curves are straight for bed heights H = 10, 20, 25 and 30 cm and that all left hand curves intersect the vertical axis at the bubble point of the bed material, that is equal to the minimum fluidisation velocity of the bed material in this case. Figure 2.14 also shows some straight transition lines for the transition to the stable spouting regime for H = 25, 30 and 35 cm.

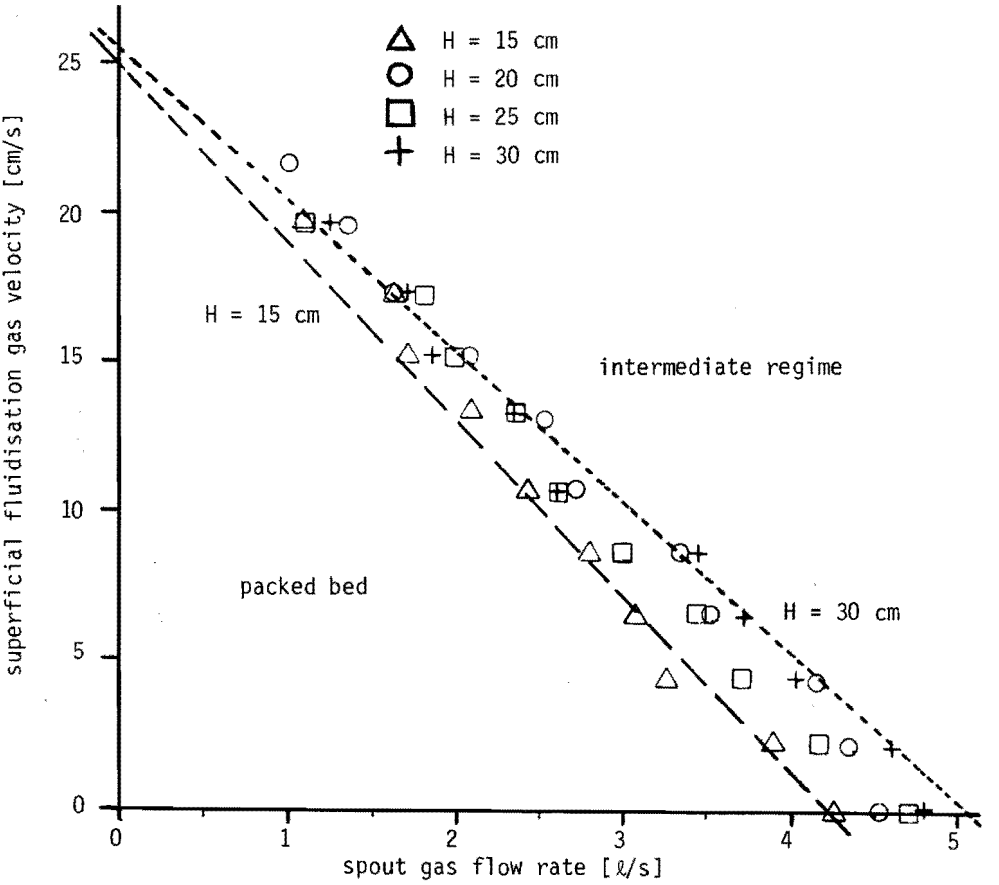

Figure 2.15. Measured limits of flow regimes for the 15.2 cm diameter spout-fluid bed for various bed heights (orifice diameter = 2 cm). Spout gas flow rate = 4 ℓ/s corresponds to superficial spout gas velocity = 22.0 cm/s.

Figure 2.15 presents a flow regime diagram for the case of a spout-fluid bed that is fitted with a 2 cm diameter spout orifice. No stable spouted bed regime exists in this bed. There is a critical orifice diameter to bed diameter ratio above with no stable spout channel can exist [2]. When a 2 cm diameter orifice is used the critical value of this ratio is exceeded.
Figure 2.15 therefore only shows transition lines between the packed bed regime and the fluctuating or bubbling flow regime. It is again seen that all transition lines are almost straight and intersect the vertical axis at the bubbling point of the bed material. The high value of the bubbling velocity (25 cm/s) is explained by the fact that some bed material Q has been mixed up in the bed material P.

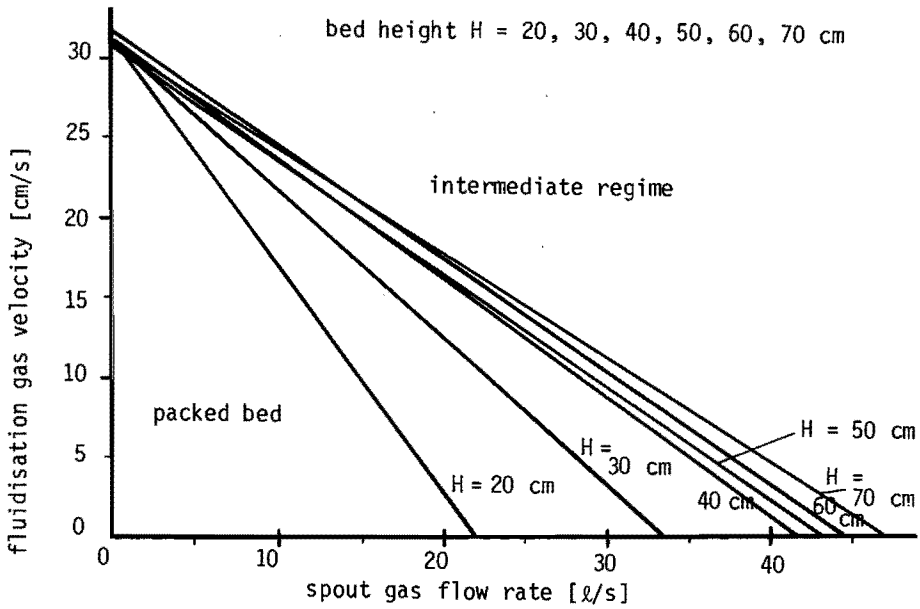

Figure 2.16. Measured limits of flow regimes for the 45 cm diameter spout-fluid bed for various bed heights (orifice diameter = 3 cm). Spout gas flow rate = 40 ℓ/s corresponds to superficial spout gas velocity = 25.2 cm/s.

Transition lines between the packed bed regime and the bubbling or fluctuating spouting regimes were determined in the 45 cm spout-fluid

bed that was fitted with a 3 cm diameter spout orifice. Transitions to the stable spouted bed regime were not measured because of the high rate of spout gas that had to be introduced into the bed and the bad controllability of the high spout and fluidisation gas rates. Figure 2.16 shows a diagram of the measured transition lines. These lines intersect the vertical axis at the bubbling velocity of material Q (32 cm/s), and are straight for all bed heights.

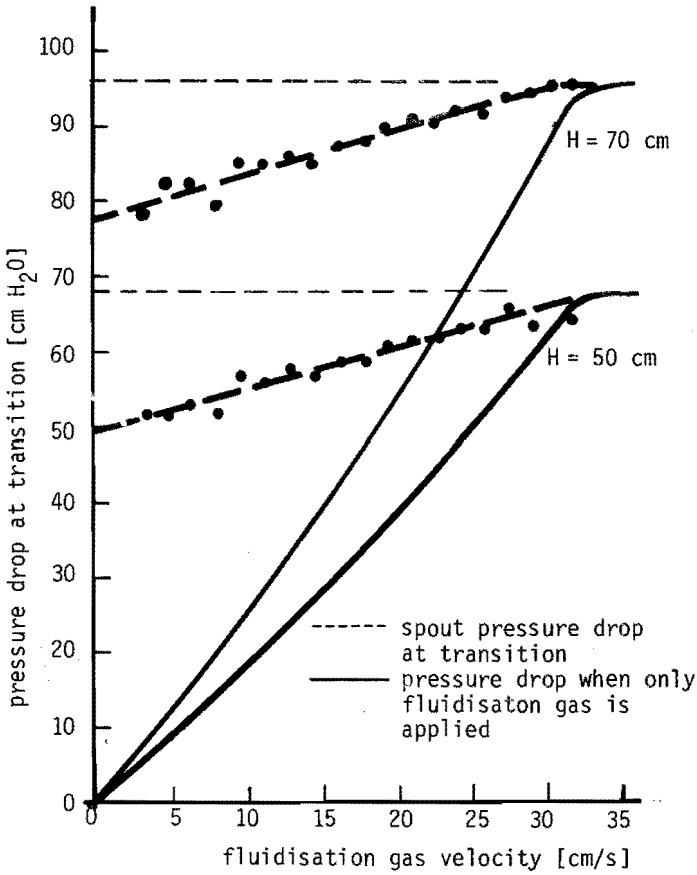

Figure 2.17. Measured spout pressure drop at the transition between packed bed and intermediate regimes for the 45 cm diameter bed at bed height H = 70 cm and H = 50 cm (orifice diameter = 3 cm).

Figure 2.17 presents the spout pressure drop at the transition between the packed bed regime and the bubbling regime as a function of the superficial fluidisation gas velocity. Figure 2.17 also shows the pressure drop that would result if fluidisation gas only were passed through the bed as a function of the superficial fluidisation gas velocity. It should be noted that the spout pressure drop becomes equal to the fluidisation pressure drop at the point where the superficial fluidisation gas velocity reaches the minimum fluidisation velocity. This fact is readily understood: It was mentioned above that no homogeneous fluidisation occurs in beds that consist of coarse sand that was used in the experiments. Thus bubbles must begin to occur in the bed at the minimum fluidisation velocity. The point in figure 2.17 that indicates the fluidisation pressure drop at minimum fluidisation velocity must therefore lie on the curve that shows the spout pressure drop at the transition between the packed bed regime and the bubbling regimes.

Literature

[1] van der Horst, H., M.Sc.Thesis, Eindhoven University of Technology, Laboratory for Physical Technology (sept. 1978).

[2] Mathur, K.B. and Epstein, N., "Spouted beds", Academic Press, New York (1974).

3. MODEL FOR THE PRESSURE DISTRIBUTION IN SPOUT-FLUID BED REACTORS

3.1 Introduction

3.1.1 Summary

This chapter presents a calculation model that predicts the pressure and flow distributions in spout-fluid beds for two flow regimes, the packed bed flow regime and the stable spouted bed flow regime. The model is applicable both to two-dimensional and cylindrical spout-fluid beds.
The calculated pressure distribution in the annulus of a spout-fluid bed that is being operated in the stable spouted bed regime depends to a large extent on the assumptions that have been made concerning the spout gas flow through the channel.
To derive a flow model of the spouted bed flow regime we first assume a flow in the spout channel that is determined by pressure and friction forces only. It is also assumed that a linear relationship exists between the friction force and the local gas velocity in the spout channel.
These assumptions result in a simple expression for the pressure and flow distribution in the spout-fluid bed.
Some examples of results that can be obtained from this model are given. Calculated pressures are presented by plots of isobars for beds of different height under several conditions in the two flow regimes. Calculated flow distributions are given by plots of curves which represent sets of points where the vertical components of the local gas velocity are the same.
An extension of this simplified flow model for the spouted bed regime is given at the end of this chapter.
It is now assumed that the gas flow in the spout channel is not only determined by pressure and friction forces but also by inertial forces and by forces that result from the interaction between the gas flow and bed particles. The bed particles are entrained from the spout channel wall and are then accelerated upwards.
The extended model describes the influences that all of the above types

of forces, i.e. inertial forces, pressure forces, wall friction forces and interaction forces between gas flow and entrained particles have on the flow. The extended model also assumes that a quadratic relationship exists between the wall friction and interaction forces and the local gas velocity in the spout channel. Results of this model are shown and are compared to the former model that somewhat unrealistically assumes a linear relationship between pressure drop and local gas velocity in the spout channel.

3.1.2 Literature survey

Several authors have previously investigated the pressure distribution in a spouted bed.
Most of the models these authors have published deal with the pressure and velocity profile as a function of the bed height while the radial dependence of the pressure and flow profiles in the annulus is neglected. The authors assume boundary conditions that they suppose exist at the top of the bed. These boundary conditions are applicable only when the bed height is equal to the maximum spoutable bed height, that is the maximum height of a bed in which a stable spout channel can be formed.
A spouted bed model that is based on more fundamental assumptions is discussed in more detail in this section. This model is believed to be more fundamental than the spouted bed models published sofar. It will be used as a starting point for the model that is developed in section 3.3 and 3.4. In addition some publications are discussed that deal with the changes that occur in the physical characteristics of a spout-fluid bed when the fluid flow, particle diameter and bed height are varied. Some physical characteristics of interest are the maximum flow rates for fluidisation, spouting and spout-fluidisation, and the bed pressure drop at minimum spout-fluidisation.
Literature is also available that reviews theories concerning pressure drop and flow in the annulus of a spouted bed (for example [2] and [6]).

Mamuro and Hattori [1] considered a segment of the annulus of a bed in the stable spouting regime and the forces that act on this segment. From mass and force balances over the spout-annulus interface they

derived a differential equation that defines the spout to annulus cross flow along the spout channel. They solved this differential equation using a boundary condition which postulates that at the top of the bed the flow velocity is equal to the minimum fluidisation velocity when the bed is equal to the maximum spoutable bed height.
For this special case the solution of the differential equation results in

$$V_z = V_{mf}(1 - (1 - z/H_m)^3)$$

where V_z = vertical flow velocity in the annulus at height z
V_{mf} = minimum fluidisation velocity
H_m = maximum spoutable bed height, and
z = vertical coordinate (height) in the bed.

For the cases where the bed height H is smaller than H_m, and thus $V_z < V_{mf}$ at the top of the bed where z=H, Mamuro and Hattori propose the equation

$$V_z = V_{z=H}(1 - (1 - z/H)^3)$$

where $V_{z=H}$ = vertical flow velocity at the top of the bed, and
H = bed height.

With this equation the vertical flow velocity and pressure drop over a spouted bed can be calculated, using Darcy's law, provided that $V_{z=H}$ is known.

Epstein et al. [2] have shown experimentally that at z=H when $H=H_m$ V_z is normally less than V_{mf}. To make the model of Mamuro and Hattori more acceptable they propose replacing the boundary condition at z=H and $H=H_m$ by

$$V_z = V_{z=H_m} \quad \text{and} \quad \frac{dV_z}{dz} = 0$$

The Mamuro-Hattori equation then changes to

$$V_z = V_{z=H_m}(1 - (1 - z/H_m)^3)$$

where $V_{z=H_m}$ = vertical flow velocity at the top of the bed z=H when $H=H_m$.

Grbavcič et al. [3] found that for a given solid material and spouting fluid in a column of fixed geometry, that is with constant H_m, the measured upward fluid flow velocity V_z and pressure gradient at any given height z in the annulus are independent of the bed height H. This observation which was first reported by Thorley et al. [4] yields an extension of the Mamuro-Hattori equation

$$\frac{V_z}{V_{z=H}} = \frac{1 - (1 - z/H_m)^3}{1 - (1 - H/H_m)^3}$$

The authors found that this equation better describes the experimental results than the original equation of Mamuro and Hattori.

In a study by Epstein and Levine [5] the particle Reynolds number at the top of the annulus was found to range from 38 to 285, that is almost two orders of magnitude in excess of Re for which Darcy's law is normally applicable. A rederivation of the Mamuro-Hattori model in which Darcy's law was not assumed to be valid was therefore in order. Epstein and Levine modified the theory of Mamuro and Hattori using the quadratic relationship

$$\frac{dP}{dz} = K_1 V_z + K_2 V_z^2$$

where the constants K_1 and K_2 were evaluated from experiments. This extension of the Mamuro-Hattori model to cover the flow with high particle Reynolds number outside the range where Darcy's law is applicable proved to give no better results than the original model.

Mathur and Epstein [6] have argued that the poor sensibility of the solution of the equation of Epstein and Levine to the characteristic parameter K_1/K_2V_{mf} causes the original solution of Mamuro-Hattori to be valid even for flow with high particle Reynolds number.

However, Mathur and Epstein based their argument on empirical grounds only [6].

Yokogawa et al. [7] used a flow model that includes the shear stress at the spout channel - annulus interface and at the bed wall respectively. Unlike the Mamuro and Hattori model, the Yokogawa model employs Darcy's law to calculate the horizontal pressure at the spout channel wall that counteracts the radial stresses of the solids in the bed. In addition he used the boundary condition $dV_z/dz = 0$ at $z=H$. The correctness of several elements of Yokogawa's model are open to doubt:

1. The boundary condition $dV_z/dz = 0$ at $z=H$ may not be applicable when $H < H_m$.
2. Darcy's law may not apply.

Lefroy and Davidson [8] have found empirically that at mimimum spouting velocity the pressure profile in the spout channel could be approximated by a quarter cosine function of the height z in the bed (figure 3.1).

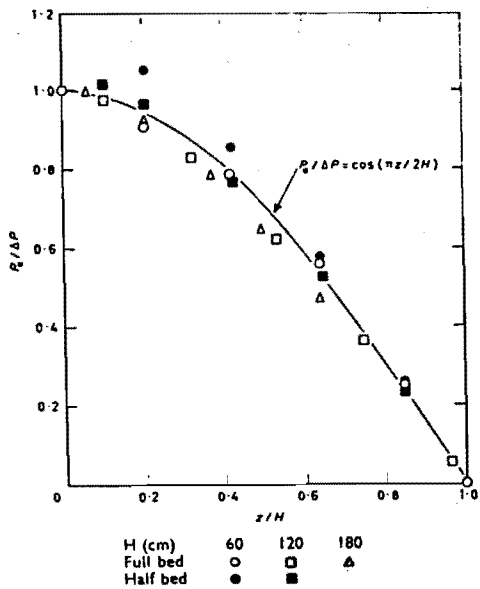

Figure 3.1. Pressure P_a at the spout wall as a function of height z. (Kale seeds. D_c = 30.5 cm, a = 1.27 cm). (from [8]).

$$P_{sp}(z) - P_H = \Delta P_s \cos(\pi z/2H)$$

where P_{sp} = pressure in the spout channel at height z
P_H = pressure above the bed, and
ΔP_s = pressure drop over the spouted bed.

Their theory starts from the assumption that Darcy's law is valid and from the conservation of the gas mass in the bed. They used the quarter cosine function as a boundary condition for the differential equation that describes a harmonic pressure distribution in the annulus of the bed. The pressure distribution in the annulus is thus found to be:

$$P(r,z) - P_H = \Delta P_s \cos mz \frac{I_0(mr)K_1(mR) + K_0(mr)I_1(mR)}{I_0(ma)K_1(mR) + K_0(ma)I_1(mR)}$$

where $m = \pi/2H$
a = spout channel radius, and
R = bed radius.

I_0, I_1, K_0 and K_1 are the usual symbols for Bessel functions of different kinds.
When $H/R > 4$ the pressure is assumed to be independent of the radial position r. It is then found that when $H=H_m$

$$P(z) - P_{H_m} = (\Delta P_s)_{H_m} \cdot \cos(\pi z/2H_m)$$

and

$$- \frac{dP}{dz} = (\Delta P_s)_{H_m} \cdot \frac{\pi}{2H_m} \sin(\pi z/2H_m)$$

When the pressure gradient at the top of the bed is assumed to correspond to that for minimum fluidisation at $z=H=H_m$ it follows that

$$(\Delta P_s)_{H_m} \cdot \frac{\pi}{2H_m} = - \left(\frac{dP}{dz}\right)_{mf} = (\Delta P_{fl})_{H_m}/H_m$$

so that $(\Delta P_s)_{H_m} = \frac{2}{\pi}(\Delta P_{fl})_{H_m}$

where $(\Delta P_s)H_m$ = pressure drop over a spouted bed at maximum spoutable bed height ($H=H_m$)

$(\Delta P_{fl})H_m$ = pressure drop over a fluidized bed with height $H=H_m$ at minimum fluidisation condition.

This equation does not cover the experimental data as well as do either the Mamuro model or its modification. Lefroy and Davidson have generalized this equation to all values of H lower than H_m by including a factor B in such a way that B=1 when $H=H_m$.

$$P(z) - P_H = B \cdot \frac{2}{\pi}(\Delta P_{fl})_H \cos(\pi z/2H)$$

where B = a multiplication factor, and

$(\Delta P_{fl})_H$ = pressure drop over fluidized bed with bed height H at minimum fluidisation condition.

Lefroy and Davidson also used fluid and particle momentum balances in the spout channel to describe the interaction forces between spout gas and entrained bed particles. They derived approximate values of H_m and of the spout channel radius using an analysis of the entrainment and of the equilibrium conditions at the spout channel - annulus interface.

At the First International Symposium on Spouted Beds two papers were presented [9,10] that discuss the pressure drop and flow characteristics of a spout-fluid bed at the minimum spout-fluidisation condition. Nagarkatti and Chatterjee [9] studied spout-fluid beds with conical and flat gas distributors. They investigated the physical characteristics of the bed at different values of the flow of fluid, particle diameter, orifice diameter and of the bed height. Nagarkatti and Chatterjee used the Mamuro-Hattori model which yields a simple equation for fluid flow in the annulus of a spouted bed as already mentioned:

$$V_z = V_{mf}(1 - (1 - z/H_m)^3) \qquad \text{for high beds and}$$

$$V_z = V_{z=H}(1 - (1 - z/H)^3) \qquad \text{for shallow beds.}$$

Fluidising the annulus would be possible by increasing the fluid flow

through the annulus. The minimum external flow for fluidisation, supplied through the gas distributor plate, of a spouted bed system where a flow of fluid through the annulus already takes place would therefore be given by the difference of V_{mf} and V_z:

$$V_{ext,f} = V_{mf} - V_z$$

where $V_{ext,f}$ = minimum external flow for fluidisation supplied through the sieve plate to the annulus

V_z = vertical flow velocity in the annulus of the spouted bed at height z.

The right hand side of the above equation may be written as a fraction of V_{mf}:

$$V_{ext,f}/V_{mf} = 1 - \phi(H,a,d_p)$$

where ϕ = a function of the bed height, spout orifice diameter and of the particle size.

Nagarkatti and Chatterjee have determined the exact minimum spout-fluid flow rate from a phase diagram they measured (figure 3.2). The minimum spout-fluid flow rate is obtained from the straight transition line between the unstable spouting regime (U.S. in figure 3.2) and the unstable spout-fluidisation regime (U.S.F.) by adding the spout and fluidising flows that correspond to any point of this line.
A correlation which these authors derived to calculate minimum spout-fluid flow rate from the equations of Mathur and Gishler and Mamuro and Hattori was found to give values that agree reasonably well with the experimentally found minimum spout-fluid flow rate.

Littman et al. [10] studied the properties of a liquid phase spout-fluid bed. They presented data on the minimum spouting velocity, the minimum spout-fluid flow rate and the spout pressure drop at minimum spouting.
The liquid phase spout-fluid bed shows some characteristics that are a blend of both spouting and fluidisation. Littman et al. also suggest

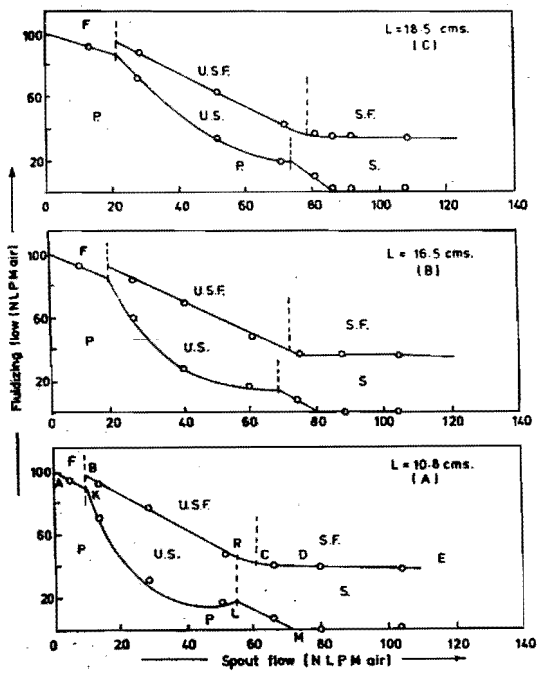

Figure 3.2. Phase diagram (d_p = 0.600 mm, a = 2.5 mm).
P = packed bed; U.S. = unstable spouted bed; F = fluidised bed; U.S.F. = unstable spout-fluidised bed; S = spouted bed; S.F. = spout-fluidised bed.
(from [9]).

that spout-fluid beds provide an important link between spouting and fluidisation and permit the design of beds that possess the characteristics of both in varying proportions.
The failure of the correlations developed by Mathur and Gishler [16] and by Malek and Lu [11] to predict the spouting data of Littman indicates that gas phase and liquid phase systems do not behave in the same manner.

3.1.3 Conclusions from literature

Many authors have discussed the ways in which the gas pressure and velocity vary in the annulus as functions of the bed height in the bed, but they neglect the radial variations in the gas pressure and

the gas flow distribution. The behaviour of the flowing solids in the spouted bed depends, however, to a large extent on the radial variations in the vertical component of the gas velocity. The stability of a spout-fluid bed in the stable spouted bed regime, on the other hand, depends on the behaviour of these flowing solids.
In literature boundary conditions are taken at the top of the bed. These boundary conditions are applicable only to beds that are operated at their maximum spoutable bed height. It is obvious, however, that the spouting behaviour of a bed is not determined by the fluid flow at the top of the bed only. It is to be noted also that a theoretical and experimental verification of the maximum spoutable bed height is not available in those cases where hysteresis occurs in the bed. Hysteresis is found to occur in beds that consist of relatively small particles. This is due to the high internal friction of such bed material.
$dV_z/dz = 0$ is most often used as boundary condition at the top of the bed. This condition follows directly from the law of conservation of fluid mass and from the assumption that the pressure above the bed is uniform. This boundary condition therefore applies to all spouted beds.

Lefroy and Davidson have developed a model from basic principles (harmonic pressure distribution). It is again noted that these authors first develop their model for beds that are operated at their maximum spoutable bed height and subsequently generalise the model to include beds that are less high.
However, the multiplication factor B in their generalised model cannot cover the fluid and solids behaviour in a bed that is less high than the maximum spoutable bed height because of the complex equilibrium at the wall of the spout channel.
It therefore seems useful to develop a pressure distribution model that takes into account the influence of the bed geometry and the influence of the spout channel and bed material properties.
The pressure distribution model then can be used as a means to analyse the relation between the pressure and fluid flow velocity inside the spout channel on the one hand and the relation between the pressure and flow distribution in the annulus on the other hand.

3.2 Basic assumptions

3.2.1 Momentum equations for the gas and solid phase

The Navier-Stokes' equations can be applied to describe both the flow of the gas and the movements of the solid phase in the bed [12,13]. The equation of motion of the gas phase in the annulus reads

$$\varepsilon\rho_g \frac{D\vec{V}}{Dt} = -\varepsilon\vec{\nabla}.\bar{\bar{\tau}}_c - \vec{\nabla}.\bar{\bar{R}}_c - \varepsilon\vec{\nabla}p + \varepsilon\rho_g\vec{g} + \vec{F}_s \qquad (3\text{-}1)$$

and the equation of motion of the solid phase in the annulus is

$$(1-\varepsilon)\rho_d \frac{D\vec{V}_d}{Dt} = -(1-\varepsilon)\vec{\nabla}.\bar{\bar{\tau}}_c - \vec{\nabla}.(1-\varepsilon)\bar{\bar{T}}_d - (1-\varepsilon)\vec{\nabla}p + (1-\varepsilon)\rho_d\vec{g} - \vec{F}_s \qquad (3\text{-}2)$$

The symbols that are used in these equations are defined in the list of symbols.
It follows from equation (3-1) that the flow of the gas phase is influenced by shear stresses, $\bar{\bar{\tau}}_c$, by the space averaged Reynolds stresses, $\bar{\bar{R}}_c$, by a pressure gradient, by gravitational forces and by a slip force $\vec{F}_s$, that acts between the solid phase and the gas phase. The velocity $\vec{V}_d$ of the solid phase in equation (3-2) is determined by shear stresses in the gas phase, by shear stresses due to interaction between the separate particles themselves which are represented by the stress tensor $\bar{\bar{T}}_d$, by a pressure gradient, gravitational forces and by the slip force $\vec{F}_s$. Equation (3-1) will be used in sections 3.2.2 and 3.2.4 to describe the gas flow in the annulus and in the spout channel respectively.

3.2.2 Gas flow in the annulus

The flows of gas and solids are assumed to be stationary while inertial forces, gravitational forces, forces due to the Reynolds' stresses and forces due to internal stresses are neglected in the equation of motion for the gas flow in the annulus.
Equation (3-1) can thus be reduced to

$$\varepsilon\vec{\nabla}p = \vec{F}_s \qquad (3\text{-}3)$$

It will be assumed in accordance with the propositions advanced by Lefroy and Davidson [8] that Darcy's law determines the slip force $\vec{F}_s$ between the gas phase and the solids

$$\vec{F}_s = - \frac{\eta}{K} (\vec{V} - \vec{V}_d) \tag{3-4}$$

Equation (3-4) applies when a laminar interstitial gas flow regime is assumed to exist between the solids of the annulus. Equation (3-4) is a good approximation for most bed materials which are not too coarse (A and B powders in figure 1.4) and for flow velocities below the minimum fluidisation velocity.
The law of conservation of mass applied to the flows of the gas and solid phase:

$$\frac{\partial \varepsilon \rho_g}{\partial t} + \text{div } \varepsilon \rho_g \vec{V} = 0 \tag{3-5}$$

$$\frac{\partial (1-\varepsilon)\rho_d}{\partial t} + \text{div } (1-\varepsilon)\rho_d \vec{V}_d = 0 \tag{3-6}$$

The porosity ε, the gas density ρ_g and the solid phase density ρ_d are assumed to be constant. Equations (3-5) and (3-6) then reduce to:

$$\text{div } \vec{V} = 0 \tag{3-7}$$

$$\text{div } \vec{V}_d = 0 \tag{3-8}$$

Combining the equations (3-3), (3-4), (3-7) and (3-8) and assuming a constant gas viscosity and dense phase*) permeability in the annulus of the bed yields a harmonic pressure distribution in the porous part of the bed:

$$\text{div grad } P = - \frac{\eta}{K} (\text{div } \vec{V} - \text{div } \vec{V}_d) = 0 \tag{3-9}$$

For cylindrical beds equation (3-9) is represented by:

$$\frac{1}{r} \frac{\partial}{\partial r} r \frac{\partial P}{\partial r} + \frac{\partial^2 P}{\partial z^2} = 0 \tag{3-10}$$

*) dense phase: mixture of gas and bed particles

where P is assumed to have an axial symmetric distribution.
For two-dimensional beds equation (3-9) can be written as:

$$\frac{\partial^2 P}{\partial x^2} + \frac{\partial^2 P}{\partial z^2} = 0 \qquad (3\text{-}11)$$

where P is assumed to be independent of the y-coordinate, that is in the direction of the depth of the bed.

3.2.3 The gas distributor plate

The pressure distribution in a spout-fluid bed depends to a great extent on the flow of fluidisation gas that is introduced through the gas distributor plate. In general the introduction of fluidisation gas results in a constant pressure gradient and a homogeneous velocity distribution in the bed. A pressure gradient in vertical direction exists in the vicinity of the gas distributor plate. This gradient depends on the local velocity of the gas that is penetrating through the gas distributor plate. Two cases can be distinguished:

a. The permeability of the distributor plate (K_z) is comparable to or much greater than the permeability of the dense phase (K_1).
b. The permeability of the plate is much smaller than that of the dense phase.

In the last case the local velocity of the gas that is penetrating the sieve plate only depends on the pressure P_{fl} beneath the plate and is independent of the radial coordinate r. In this case the boundary condition becomes

$$-\left(\frac{\partial P}{\partial z}\right)_{z=0} = \frac{\eta}{K_1} V_{fl} \qquad (3\text{-}12)$$

In case a. there is a complex boundary condition at the plate. The local gas velocity now depends also on the local pressure just above the distributor plate at z=0. The boundary condition then becomes

$$-\left(\frac{\partial P}{\partial z}\right)_{z=0} = \frac{\eta}{K_1} V_{fl}(r) = \frac{K_z}{K_1 \delta} (P_{fl} - P(r,o)) \qquad (3\text{-}13)$$

where $V_{fl}(r)$ is the local velocity of the fluidisation gas that is

penetrating the plate at z=0 and in this case depends on r.

K_1 and δ are the permeability and thickness of the distributor plate respectively, and

P_{fl} is the pressure beneath the plate.

A recursion relation exists in equation (3-13) because both $V_{fl}(r)$ and $P(r,o)$ follow from the pressure distribution just above the plate at z=0 and are dependent on the radial position.

3.2.4 Gas flow in the spout channel

The calculated pressure distribution in the annulus of a bed at stable spouting depends to a large extent on the boundary condition at the wall of the spout channel and thus on the assumptions that have been made concerning the flow of spout gas in the channel. The gas flow is defined by inertial forces, forces due to shear stresses, forces due to Reynolds' stresses, by pressure forces and by slip forces according to (3-1).

Assuming the gas flow to be stationary and neglecting gravitational forces equation (3-1) reduces to (appendix 3-V)

$$\varepsilon\rho_g \vec{V}.\vec{\nabla}\vec{V} = - \varepsilon\vec{\nabla}.\bar{\bar{\tau}}_c - \varepsilon\vec{\nabla}P + \vec{F}_s - \vec{\nabla}.\bar{\bar{R}}_c \qquad (3\text{-}14)$$

Mean values of the spout gas velocity and of the forces in the spout channel are obtained by integrating equation (3-14) over the transverse section of the spout channel.

$$\frac{1}{2}\rho_g \frac{d}{dz} V_{sp}^2 = - \frac{\lambda}{2a} \cdot \frac{1}{2}\rho V_{sp}^2 - \frac{dP_{sp}}{dz} - \frac{\beta}{\varepsilon}(V_{sp} - V_p)^2 \qquad (3\text{-}15)$$

It is seen that the internal stress contribution of (3-14) results after integration in a spout gas to channel wall interaction term that is related to V_{sp} by a quadratic relationship. The slip force contribution in equation (3-14) results in a gas to particle interaction force term that is proportional to the square of their slip velocities. From the continuity equation for the gas mass at the spout channel to annulus interface it follows that

$$\frac{dV_{sp}}{dz} = -\frac{2}{a} V_{ra} \qquad (3\text{-}16)$$

where V_{ra} is the radial component of the gas velocity at the spout channel wall.

The hold-up in the spout channel is assumed to be small (thus $\varepsilon \approx 1$) so that the effect of the presence of particles in the spout channel is expressed by the interaction drag term $\beta(V_{sp}-V_d)^2$ only. It is also assumed that the velocity V_d of the entrained particles in the spout channel is small with respect to the gas velocity V_{sp}. This assumption will be verified from results of measurements that are discussed later. A relationship proposed by Barnea and Mizrahi [15] is used to find the factor β in equation (3-15). This leads to

$$\beta = 0.75\ C_D(1-\varepsilon)\{1 + (1-\varepsilon)^{1/3}\}/d_p \qquad (3\text{-}17)$$

where C_D = drag coefficient of one particle
$1-\varepsilon$ = hold-up in the spout channel, and
d_p = particle diameter.

This relation for β is valid for turbulent flow of fluid through disperse media of high porosity.
For the value of C_D the drag coefficient of a sphere in a turbulent flow has been taken, thus $C_D = 0.42$.
Equation (3-17) is linearized in the interval $0<(1-\varepsilon)<0.01$.
It follows that the gas to particle interaction term $\beta(V_{sp}-V_d)^2$ can be approximated by the relation

$$\beta(V_{sp}-V_d)^2 = (0.384.(1-\varepsilon)/d_p).V_{sp}^2 \qquad (3\text{-}18)$$

Bed particles are entrained from the spout channel wall at an entrainment rate that depends on the shear stress that is caused by the gas flow in the spout channel, the normal pressure due to spout to annulus cross flow, and on the strength of the bed material (cohesion, angle of internal friction). The strength of the bed material in the annulus in turn depends on the fluid velocity in the annulus near the spout channel.

In general one can assume that bed particles are entrained from the spout channel wall over the whole length of the channel. The particle hold-up of the spout channel thus increases from zero at the bottom to a value $1-\varepsilon_s$ at the top of the bed. To include the effect of this increase of the number of particles it is assumed that the hold-up is a linear function of the height z:

$$1-\varepsilon = (1-\varepsilon_s)\,\frac{z}{H} \tag{3-19}$$

Here $1-\varepsilon_s$ is the hold-up at the top of the spout channel and is assumed to have a small value.
It will be shown in section 3.4.5 that this assumption is a fair approximation of the spout channel hold-up when the entrainment rate is assumed to be constant over the length of the spout channel.
The interaction forces between the gas flow and the particles in the spout channel are used to increase the kinetic and gravitational energy of the entrained particles. The interaction forces between the gas flow and the spout channel wall lead to the existence of a shear stress at the channel wall and cause particles to be entrained.

3.3 Packed bed gas flow in spout-fluid beds

3.3.1 Cylindrical beds

Differential equation (3-10) is applied to the calculation of the gas flow patterns in cylindrical beds, when it is assumed that Darcy's law is valid in the dense phase.
Assume that

$$P(r,z) = P_r(r) \cdot P_z(z) \tag{3-20}$$

Substitution of (3-20) into (3-10) yields

$$P_z \cdot \frac{1}{r}\frac{d}{dr}\, r\,\frac{dP}{dr} + P_r\,\frac{d^2P_z}{dz^2} = 0 \tag{3-21}$$

The solutions of (3-21) are

$$\begin{aligned} P_r &= \text{linear combination of } I_0(\alpha r) \text{ and } K_0(\alpha r) \\ P_z &= \text{linear combination of } \sin \alpha z \text{ and } \cos \alpha z \end{aligned} \tag{3-22}$$

or the equivalent solution

$$\begin{aligned} P_r &= \text{linear combination of } J_0(\alpha r) \text{ and } Y_0(\alpha r) \\ P_z &= \text{linear combination of } \sinh(\alpha z) \text{ and } \cosh(\alpha z) \end{aligned} \tag{3-23}$$

where α is a non-zero constant.
When $\alpha=0$ the solution of (3-21) is

$$\begin{aligned} P_r &= \text{linear function of } \ln r \\ P_z &= \text{linear function of } z \end{aligned} \tag{3-24}$$

$J_0(\alpha r)$ and $Y_0(\alpha r)$ are Bessel functions of zero order and of the first and second kind respectively while $I_0(\alpha r)$ and $K_0(\alpha r)$ are modified Bessel functions of the first and second kind respectively and of zero order (Abramowitz and Stegun [14]).
There are some specific solutions of equation (3-21) for the pressure distribution that obey the boundary conditions

$$\left(\frac{\partial P}{\partial r}\right)_{r=R} = 0 \tag{3-25}$$

and because P is the pressure relative to that above the bed

$$P(z=H) = 0 \tag{3-26}$$

The general solution of equation (3-21) can be written as

$$P(r,z) = \sum_n A_n P_{r,n}(r) \cdot P_{z,n}(z) \tag{3-27}$$

where $P_{r,n}(r)$ and $P_{z,n}(z)$ are the n^{th} solution of the differential equation (3-21) in the r and z respectively that obeys the boundary conditions (3-25) and (3-26) for $P_{r,n}(r)$ and $P_{z,n}(z)$:

$$\begin{aligned} \left(\frac{dP_{r,n}}{dr}\right)_{r=R} &= 0 \\ P_{z,n}(z=H) &= 0 \end{aligned} \tag{3-28}$$

The gas flow in a bed that is operated in the packed bed flow regime is now described in this section. Solution (3-23) will be used because of the boundary conditions at the bottom (z=0).
The following solutions are valid in the packed bed flow regime:

$$
\begin{aligned}
P_{r,n}(r) &= 1 && (n=0)\\
&= J_0(\alpha_n r) && (n=1,2,3\ldots)\\
P_{z,n}(z) &= H-z && (n=0)\\
&\quad \sinh \alpha_n(H-z) && (n=1,2,3\ldots)
\end{aligned}
\qquad (3\text{-}29)
$$

The general solution becomes (using (3-23) and (3-24))

$$
P(r,z) = A_0(H-z) + \sum_{n=1}^{\infty} A_n J_0(\alpha_n r)\sinh \alpha_n(H-z) \qquad (3\text{-}30)
$$

In this cylindrical case α_n must satisfy boundary condition (3-28), so that

$$
\frac{1}{\alpha_n}\left[\frac{d}{dr} J_0(\alpha_n r)\right]_{r=R} = -J_1(\alpha_n R) = 0 \qquad (3\text{-}31)
$$

The roots of $J_1(\alpha_n R) = 0$ are available from Abramowitz and Stegun [14] where numerical values of the roots are given. An approximation equation for calculation of the roots is also given.

$A_0, A_1, \ldots, A_n$, . are to be determined from the boundary condition at the height of the orifice and at the gas distributor plate (z=0):
Gas flows through the orifice (r<a) and through the sieve plate (a<r<R) at a velocity that is independent of r:

$$
\begin{aligned}
-\left(\frac{\partial P}{\partial z}\right)_{z=0} &= \frac{\eta}{K_1} V_{sp} = \frac{\eta}{K_1}\frac{Q_0}{\pi a^2} && \text{for } r<a\\
&= \frac{\eta}{K_1} V_{fl} = \frac{\eta}{K_1}\frac{Q_1}{\pi(R^2-a^2)} && \text{for } a<r<R\\
&= A_0 + \sum_{n=1}^{\infty} A_n\alpha_n \cosh \alpha_n H\, J_0(\alpha_n r)
\end{aligned}
\qquad (3\text{-}32)
$$

where V_{sp} = local spout gas velocity at the orifice (z=0)
V_{fl} = local fluidisation gas velocity at the sieve plate (z=0)
Q_0 = spout gas flow rate, and
Q_1 = fluidisation gas flow rate.

It is assumed that Darcy's law applies to the gas flow through the orifice even at the relative high velocities near the orifice.

Boundary condition (3-32) can be decomposed by means of Fourier series development in terms of $J_o(\alpha_n r)$, n=0,1,2,..,... (Appendix 3-II).
This leads to an expression for the pressure distribution that applies in the case where a cylindrical bed is operated in the packed bed flow regime:

$$P(r,z) = \frac{\eta}{K_1} \frac{Q_o + Q_1}{\pi R^2} (H-z) + \\ + \frac{\eta}{K_1} (V_{sp}-V_{fl}) \cdot \frac{2a}{R^2} \sum_{n=1}^{\infty} \frac{J_1(\alpha_n a)}{J_o^2(\alpha_n R)} \frac{J_o(\alpha_n r)\sinh \alpha_n(H-z)}{\alpha_n^2 \cosh \alpha_n H} \qquad (3\text{-}33)$$

where α_n is the n^{th} root of $J_1(\alpha_n R) = 0$ as was stated above.

3.3.2 Two-dimensional (flat) beds

Differential equation (3-11) is applied to the calculation of the gas flow patterns in two-dimensional beds when it is again assumed that Darcy's law applies in the dense phase.
Assume that

$$P(x,z) = P_x(x) \cdot P_z(z) \qquad (3\text{-}34)$$

Substitution of (3-34) into (3-11) yields

$$P_z \frac{d^2P_x}{dx^2} + P_x \frac{d^2P_z}{dz^2} = 0 \qquad (3\text{-}35)$$

The solutions of (3-35) are

$$\begin{aligned} P_x &= \text{linear combination of } \sinh \alpha x \text{ and } \cosh \alpha x \\ P_z &= \text{linear combination of } \sin \alpha z \text{ and } \cos \alpha z \end{aligned} \qquad (3\text{-}36)$$

or the equivalent solution

$$\begin{aligned} P_x &= \text{linear combination of } \sin \alpha x \text{ and } \cos \alpha x \\ P_z &= \text{linear combination of } \sinh \alpha z \text{ and } \cosh \alpha z \end{aligned} \qquad (3\text{-}37)$$

where α is a non-zero constant.
When α=0 the solution of (3-35) is

$$\begin{aligned} P_x &= \text{linear function of } x \\ P_z &= \text{linear function of } z \end{aligned} \qquad (3\text{-}38)$$

Solutions (3-37) and (3-38) are used to describe the gas flow in a two-dimensional spout-fluid bed that is operated in the packed bed flow regime.

A solution of (3-35) can be obtained in a manner similar to that which was used in the case of the cylindrical bed by applying Fourier series development of the boundary conditions at the orifice and at the sieve plate (z=0) to the general solution of P(x,z) (Appendix 3-I). It is again assumed that Darcy's law applies at the orifice and at the sieve plate while gas flows through the orifice ($|x|<a$) and through the sieve plate ($a<|x|<R$) at a velocity that is independent of x.

The result is

$$P(x,z) = \frac{\eta}{K_1}\frac{Q_o+Q_1}{2RD}(H-z) + \frac{\eta}{K_1}(V_{sp}-V_{fl}) \cdot \frac{2}{a}\sum_{n=1}^{\infty}\frac{\sin \alpha_n a}{\alpha_n^2 \cosh \alpha_n H}\cos \alpha_n \sinh \alpha_n(H-z) \qquad (3\text{-}39)$$

where in this case $\alpha_n = n\pi/R$, $n = 1,2,....$

3.3.3 Results obtained from the models for the packed bed flow regime

Calculations were carried out by means of the models that were described in the sections 3.3.1 and 3.3.2. Use was made of dimensionless forms of the equations (3-33) and (3-39). The dimensionless variables that were chosen are (appendix 3-III):

$H^* = H/R$	dimensionless bed height
$a^* = a/R$	dimensionless radius of orifice
$z^* = z/H$	dimensionless vertical position in bed
$r^* = r/R$	dimensionless radial position in cylindrical bed
$x^* = x/R$	dimensionless horizontal position in flat bed
$Q_o^* = Q_o/(Q_o+Q_1)$	dimensionless spout gas flow rate.

It should be noted that in the case of the two-dimensional beds the variables R and a denote one half of the bed and one half of the orifice width respectively.

The dimensionless pressure P^* is derived by dividing the actual pressure

drop, P, by the pressure drop that would exist over a bed of identical height, H, if this bed were aerated at a gas rate equal to the sum of the fluidisation and spout gas rates that is used in the experiment that is being considered under circumstances where Darcy's law applies. Thus

$$P^* = P/\left(\frac{\eta}{K_1}\frac{Q_o+Q_1}{\pi R^2}H\right) \qquad \text{for cylindrical beds} \qquad (3\text{-}40A)$$

and

$$P^* = P/\left(\frac{\eta}{K_1}\frac{Q_o+Q_1}{2RD}H\right) \qquad \text{for two-dimensional beds} \qquad (3\text{-}40B)$$

The dimensionless vertical gas velocity V_z^* is derived in the same manner:

$$V_z^* = V_z/\left(\frac{Q_o+Q_1}{\pi R^2}\right) \qquad \text{for cylindrical beds} \qquad (3\text{-}40C)$$

and

$$V_z^* = V_z/\left(\frac{Q_o+Q_1}{2RD}\right) \qquad \text{for two-dimensional beds} \qquad (3\text{-}40D)$$

The local linear gas velocity in the vertical direction in the bed can be found from the pressure distribution by

$$V_z = -\frac{K_1}{\eta}\frac{\partial P}{\partial z} \qquad (3\text{-}40E)$$

as it is assumed here that Darcy's law applies. From (3-40E), (3-33) and (3-39) it follows for V_z that:

$$V_z = \frac{Q_o+Q_1}{\pi R^2} + (V_{sp}-V_{fl})\frac{2a}{R^2}\sum_{n=1}^{\infty}\frac{J_1(\alpha_n a)}{J_o^2(\alpha_n R)}\frac{J_o(\alpha_n r)\cosh\alpha_n(H-z)}{\alpha_n\cosh\alpha_n H}$$

for cylindrical beds (3-41)

and

$$V_z = \frac{Q_o+Q_1}{2RD} + (V_{sp}-V_{fl})\frac{2}{a}\sum_{n=1}^{\infty}\sin\alpha_n a\,\frac{\cos\alpha_n x\cosh\alpha_n(H-z)}{\alpha_n\cosh\alpha_n H}$$

for two-dimensional beds (3-42)

Plots of isobars calculated from equations (3-33) and (3-39) are given in figures 3.3 and 3.4 for some beds where no fluidisation gas is introduced. In addition figures 3.5 and 3.6 show plots of the flow distribution in these beds. The curves in these figures represent the collection of points with equal vertical components of the local linear gas velocity. Figures 3.3 and 3.5 give results calculated for a cylindrical bed while figures 3.4 and 3.6 show similar results for a two-dimensional bed.

It is seen from the figures 3.3 and 3.4 that the pressure distribution tends to be flat at the top of the bed and to be spherical or cylindrical near the orifice. It can easily be seen that in the cylindrical bed the pressure P near the orifice is approximated by a spherical distributions, which is a harmonic distribution in a three-dimensional space. The pressure is then related to the distance s to the orifice by

$$P \sim 1/s^2$$

The pressure near the orifice of a two-dimensional bed, on the other hand, is approximated by a cylindrical distribution, which is a harmonic distribution in a two-dimensional space.

In this case the pressure P is related to the distance s to the orifice by

$$P \sim 1/s$$

It follows from above that the dimensionless pressure near the orifice of a cylindrical bed is considerably higher than the dimensionless pressure near the orifice in a comparable two-dimensional bed.

The flow distributions that are presented in figures 3.5 and 3.6 show that the region with the highest vertical velocity in the bed is located just around the spout orifice.

Figure 3.7 presents results of calculations that were carried out for cylindrical beds into which both fluidisation gas and spout gas are introduced. The figure shows a pattern of isobars that is more horizontal near the sieve plate than in the case when spout gas only is introduced.

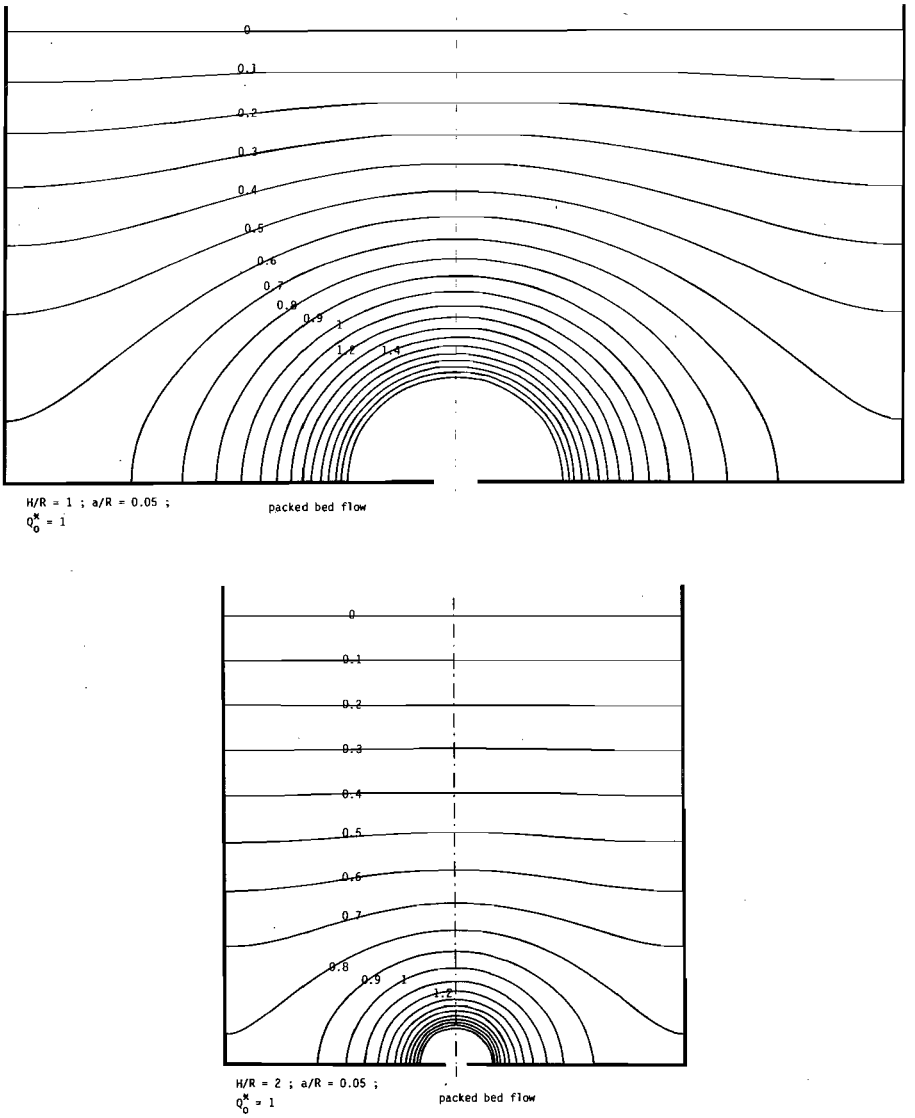

Figure 3.3. Calculated distribution of the dimensionless pressure P in some cylindrical beds. Introduction of spout gas only. P* calculated from eq. (3-33) and (3-40A) (packed bed flow regime assuming Darcy's law).*
$Q_o^* = 1$; a = 0.05; H* = 1 and 2 respectively.*

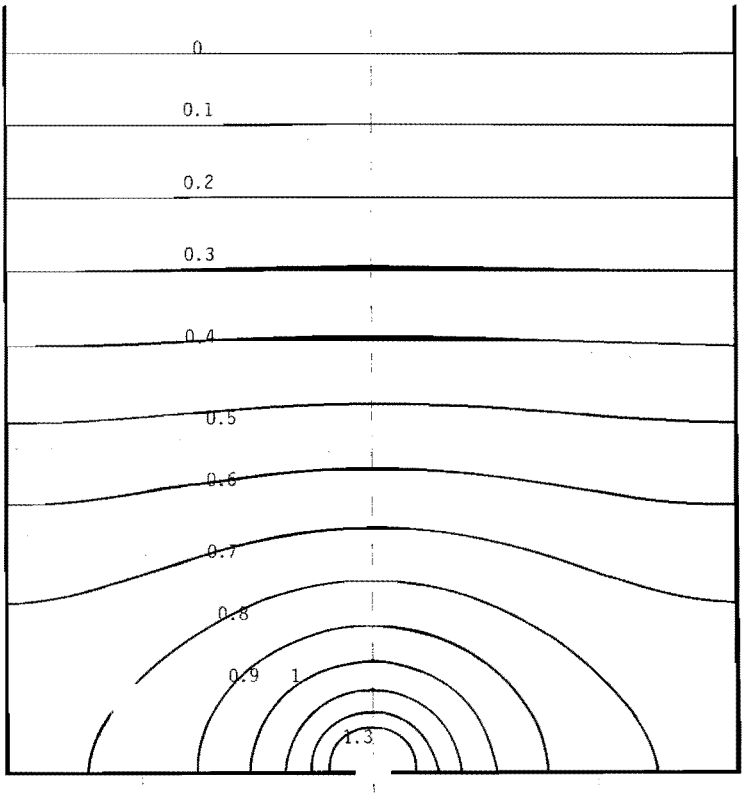

Figure 3.4. Calculated distribution of the dimensionless pressure P in a two-dimensional bed. Introduction of spout gas only. P* is calculated from eq. (3-39) and (3-40B) (packed bed flow regime assuming Darcy's law).*
$Q_o^* = 1$; $a^* = 0.05$; $H^* = 2$.

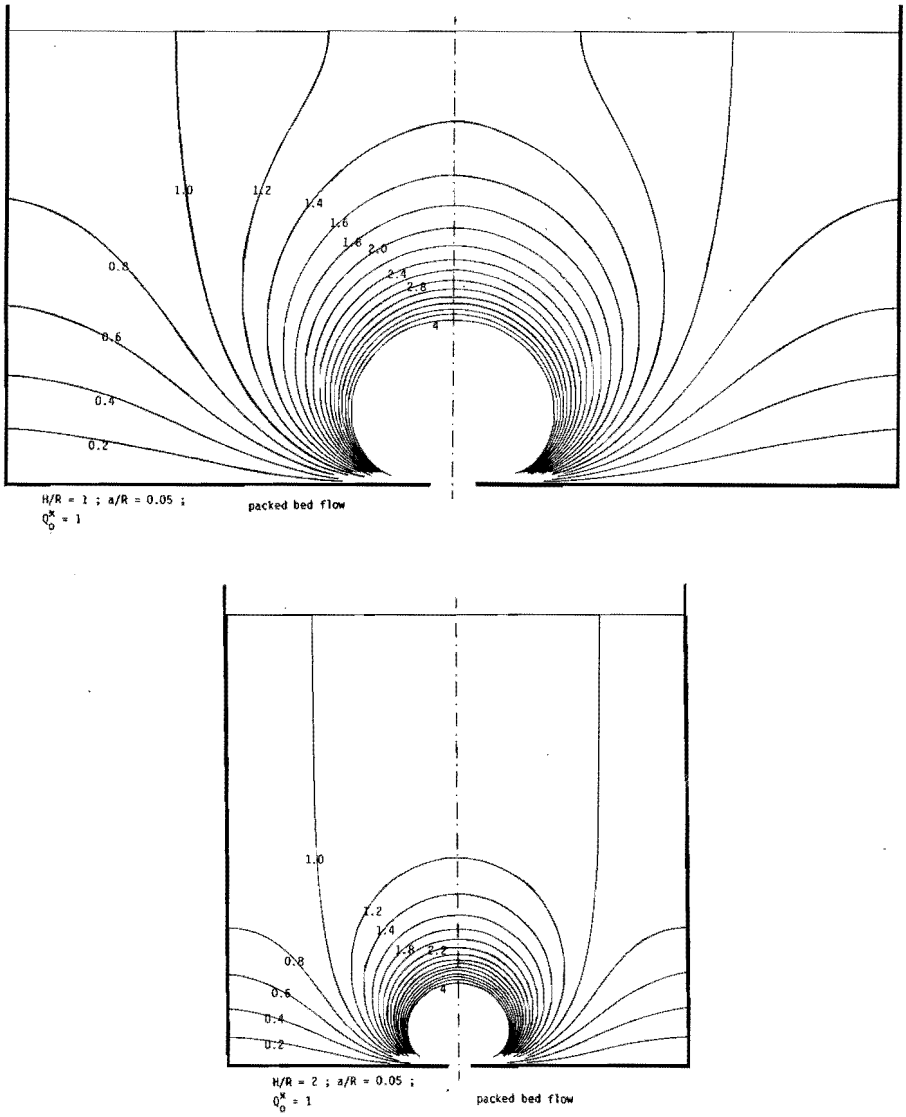

Figure 3.5. Calculated distribution of the dimensionless vertical velocity V_z^* *in some cylindrical beds. Introduction of spout gas only.* V_z^* *is calculated from eq. (3-41) and (3-40C). (Packed bed flow regime assuming Darcy's law).*
$Q_o^* = 1$; $a^* = 0.05$; $H^* = 1$ *and* 2 *respectively.*

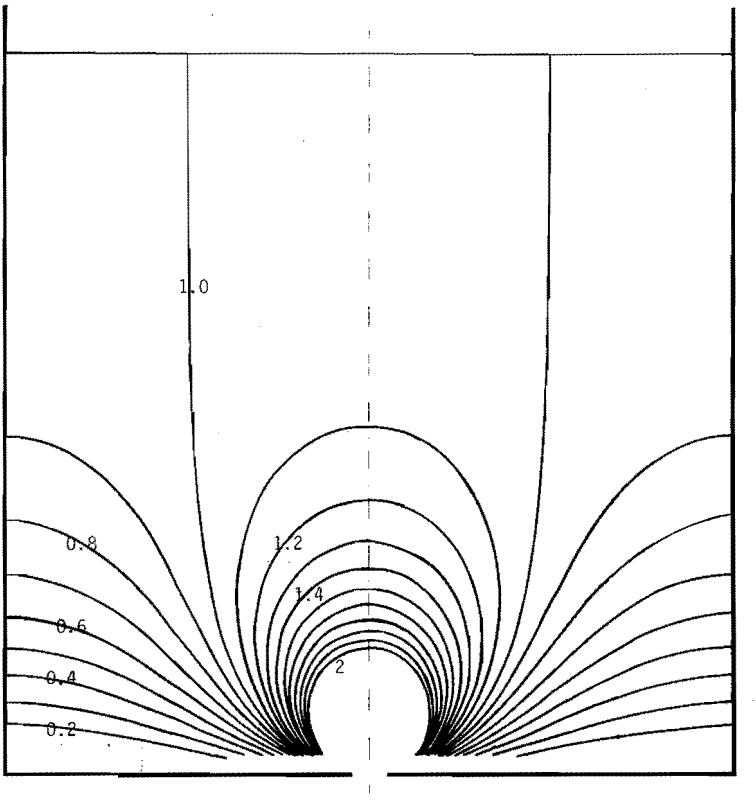

Figure 3.6. Calculated distribution of the dimensionless vertical velocity V_z^* *in a two-dimensional bed. Introduction of spout gas only.* V_z^* *is calculated from eq. (3-42) and (3-40D). (Packed bed flow regime assuming Darcy's law).*
$Q_o^* = 1$; $\alpha^* = 0.05$; $H^* = 2$.

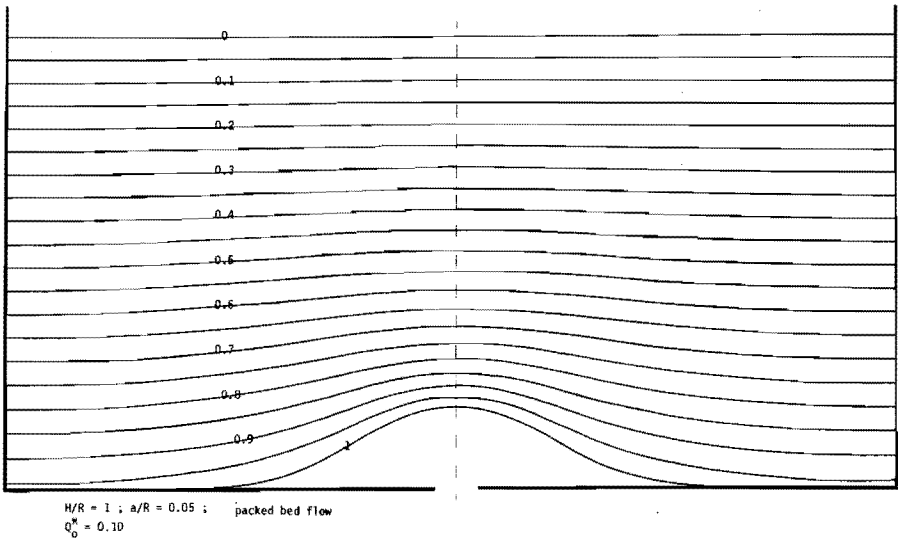

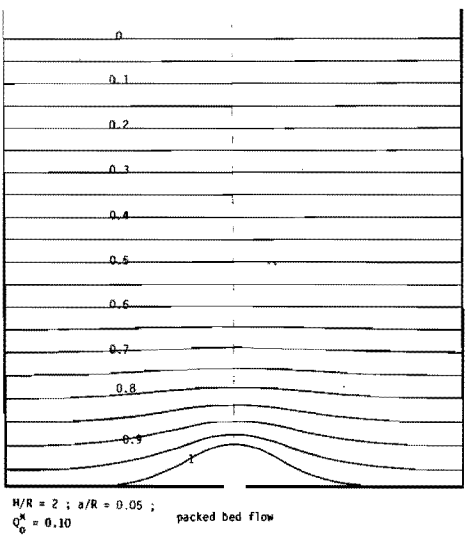

Figure 3.7. Calculated distribution of the dimensionless pressure P^* in some cylindrical beds, with introduction of fluidisation gas. (Packed bed flow regime assuming Darcy's law).
$Q_o^* = 0.10$; $a^* = 0.05$; $H^* = 1$ and 2 respectively.

3.4 Stable spouted bed flow in spout-fluid beds

3.4.1 Cylindrical beds

3.4.1.1 Gas flow in the annulus

The gas flow in a bed that is being operated in the stable spouted bed regime is determined in this section.
There are some specific solutions of equation (3-21) for the pressure distribution in this regime, that obey the boundary condition

$$\left(\frac{\partial P}{\partial r}\right)_{r=R} = 0$$

$$\left(\frac{\partial P}{\partial z}\right)_{z=0} = \frac{\eta}{K_1}\frac{Q_1}{\pi(R^2-a^2)} = \frac{\eta}{K_1} V_{fl} \qquad (3\text{-}43)$$

$$P(z=H) = 0$$

Using (3-22) and (3-24) the general solution of (3-21) can be written as equation (3-27) (section 3.3.1). The following solutions are now valid:

$$\begin{aligned} P_{r,n} &= 1 && \alpha = 0 \\ P_{r,n} &= K_o(\alpha_n r)I_1(\alpha_n R) + I_o(\alpha_n r)K_1(\alpha_n R) && \alpha = \alpha_n \neq 0 \\ P_{z,n} &= H-z && \alpha = 0 \\ P_{z,n} &= \cos \alpha_n z && \alpha = \alpha_n \neq 0 \end{aligned} \qquad (3\text{-}44)$$

α can take only discrete values according to boundary condition $P(z=H) = 0$ of (3-43). It follows from (3-44) that

$$\alpha_n = (n + \tfrac{1}{2})\pi/H$$

in the case of the stable spouted bed regime.

The solution for the pressure distribution in the annulus of the bed therefore is

$$P(r,z) = \sum_{n=0}^{\infty} A_n \cos \alpha_n z \; \frac{K_o(\alpha_n r)I_1(\alpha_n R) + I_o(\alpha_n r)K_1(\alpha_n R)}{K_o(\alpha_n a)I_1(\alpha_n R) + I_o(\alpha_n a)K_1(\alpha_n R)} +$$

$$+ \frac{\eta}{K_1} \cdot V_{fl}(H-z) \qquad (3\text{-}45)$$

It should again be noted that it is assumed that Darcy's law applies to the gas flow in the annulus while a uniform flow of fluidisation gas takes place through the sieve plate (z=0) and that this flow is independent of the radius r. It is also seen that the scaling term that is added as the nominator in equation (3-45) yields a simple expression for the pressure $P_{sp}(z)$ in the spout channel

$$P_{sp}(z) \equiv P(r=a,z) = \sum_{n=0}^{\infty} A_n \cos \alpha_n z + \frac{\eta}{K_1} V_{fl}(H-z) \qquad (3\text{-}46)$$

3.4.1.2 Gas flow in the spout channel

It follows from a mass balance over the gas contained in a volume-element that includes the interface between spout channel and annulus that

$$\frac{dV_{sp}}{dz} \cdot \pi a^2 = -2\pi a V_r(r=a,z) = 2\pi a \frac{K_1}{\eta} \left(\frac{\partial P}{\partial r}\right)_{r=a} \qquad (3\text{-}47)$$

From equations (3-45) and (3-47) it follows for the gas velocity V_{sp} in the spout channel that

$$\frac{dV_{sp}}{dz} = \frac{2}{a}\frac{K_1}{\eta}\left(\frac{\partial P}{\partial r}\right)_{r=a} = -\frac{2}{a}\frac{K_1}{\eta} \sum_{n=0}^{\infty} A_n B_n \alpha_n \cos \alpha_n z \qquad (3\text{-}48)$$

where $$B_n = \frac{K_1(\alpha_n a)I_1(\alpha_n R) - I_1(\alpha_n a)K_1(\alpha_n R)}{K_o(\alpha_n a)I_1(\alpha_n R) + I_o(\alpha_n a)K_1(\alpha_n R)}$$

Integrating equation (3-48) yields

$$V_{sp}(z) = V_{spo} - \frac{2}{a}\frac{K_1}{\eta} \sum_{n=0}^{\infty} A_n B_n \sin \alpha_n z \qquad (3\text{-}49)$$

where V_{spo} is the spout gas velocity at the orifice at z=0 given by $V_{spo} = Q_o/\pi a^2$.

This section now first presents a simple procedure for the gas flow computation in the spout channel. It is assumed in the simple model that the pressure gradient is linearly proportional to the local spout gas velocity so that

$$\frac{dP_{sp}}{dz} = -\frac{\eta}{K_o} V_{sp} \tag{3-50}$$

A spout channel permeability K_o is thus assigned to the spout channel in this simple approximation. It describes the effect of interactions between the spout channel gas and the spout channel wall and entrained bed particles in the spout channel.

The coefficients A_o, A_1,..., A_n,... can be determined by combining equation (3-46) for $P_{sp}(z)$, equation (3-49) for $V_{sp}(z)$ and equation (3-50) that provides a relationship between pressure and gas velocity in the spout channel.
Substituting (3-49) into (3-50) and integrating equation (3-50) yields an expression for $P_{sp}(z)$:

$$P_{sp}(z) = \frac{\eta}{K_o} V_{spo}(H-z) - \frac{2}{a}\frac{K_1}{K_o} \sum_{n=0}^{\infty} \frac{A_n B_n}{\alpha_n} \cos \alpha_n z \tag{3-51}$$

Equation (3-51) satisfies the boundary condition at z=H: $P_{sp}(z=H) = 0$. Equation (3-51) for $P_{sp}(z)$ must be identical to equation (3-46) that was derived earlier from expression (3-45) for the pressure distribution in the annulus. Therefore

$$\sum_{n=0}^{\infty} A_n \cos \alpha_n z + \frac{\eta}{K_1} V_{fl}(H-z) \equiv \frac{\eta}{K_o} V_{spo}(H-z) - \frac{2}{a}\frac{K_1}{K_o} \sum_{n=0}^{\infty} \frac{A_n B_n}{\alpha_n} \cos \alpha_n z \tag{3-52}$$

so that

$$\sum_{n=0}^{\infty} A_n \left(1 + \frac{2}{a}\frac{K_1}{K_o}\frac{B_n}{\alpha_n}\right).\cos \alpha_n z \equiv \left\{\frac{\eta}{K_o} V_{spo} - \frac{\eta}{K_1} V_{fl}\right\}.(H-z) \tag{3-53}$$

To determine A_n (n=0,1,2,...) the right hand side of equation (3-53) can be decomposed in terms of cos $\alpha_n z$ by Fourier series development (see Appendix 3-I). The result is

$$H-z \equiv \sum_{n=0}^{\infty} \frac{2H \cos \alpha_n z}{\alpha_n{}^2 H^2} \tag{3-54}$$

Thus

$$\sum_{n=0}^{\infty} A_n\left(1 + \frac{K_1}{K_o}\frac{2}{a}\frac{B_n}{\alpha_n}\right)\cos \alpha_n z \equiv \left(\frac{\eta}{K_o} V_{spo} - \frac{\eta}{K_1} V_{fl}\right) \sum_{n=0}^{\infty} \frac{2H}{\alpha_n{}^2 H^2} \cos \alpha_n z \tag{3-55}$$

It follows from equation (3-55) that for each coefficient of cos $\alpha_n z$:

$$A_n = \frac{2H\left(\frac{\eta}{K_o} V_{spo} - \frac{\eta}{K_1} V_{fl}\right)}{\alpha_n{}^2 H^2\left(1 + \frac{2}{a}\frac{K_1}{K_o}\frac{B_n}{\alpha_n a}\right)} \tag{3-56}$$

As was stated above the pressure distribution in a cylindrical spout-fluid bed in the stable spouted bed regime can be written in accordance with equation (3-45), with a simple calculation model using B_n which is defined by (3-48) and A_n that is defined by (3-56) while $\alpha_n = (n+\frac{1}{2})\pi/H$. $P_{sp}(z)$ is defined by equation (3-46).

3.4.2 Two-dimensional beds

The calculation of the pressure distribution in two-dimensional beds that are operated in the stable spouted bed regime is very similar to the calculation procedure that was described in section 3.4.1.
It is noted again that it is assumed in the calculations that Darcy's law applies to the gas flow in the annulus.

The solutions (3-36) and (3-38) that were derived in section 3.3.2 are applied in this section.
The general solution becomes

$$P(x,z) = \sum_{n=0}^{\infty} A_n \cos \alpha_n z \frac{\cosh \alpha_n (R-x)}{\cosh \alpha_n (R-a)} + \frac{\eta}{K_1} V_{fl}(H-z) \tag{3-57}$$

where $\alpha_n = (n+\frac{1}{2})\pi/H$

and $V_{fl} = Q_1/2(r-a)D$

A mass balance over the gas contained in a volume-element that includes the interphase between spout channel and annulus now yields

$$\frac{dV_{sp}}{dz} \cdot 2D \cdot a = -2DV_x(x=a,z) = 2D \frac{K_1}{\eta} \left(\frac{\partial P}{\partial x}\right)_{x=a} \qquad (3\text{-}58)$$

Application of the simple relationship (3-50) that assumes a linear proportionality between pressure gradient and local gas velocity in the spout channel leads to an expression for A_n (n=0,1,2,...) in a manner similar to the derivat that was given for the cylindrical bed in section 3.4.1.:

$$A_n = \frac{2H(\frac{\eta}{K_o} V_{spo} - \frac{\eta}{K_1} V_{fl})}{\alpha_n^2 H^2 (1 + \frac{1}{a} \frac{K_1}{K_o} \frac{B_n}{\alpha_n a})} \qquad (3\text{-}59)$$

where $V_{spo} = Q_o/2Da$.

The pressure distribution in a two-dimensional spout-fluid bed that is operated in the stable spouted bed regime can thus be written according to (3-57) with a simple calculation model using A_n that is defined by (3-59) while

$$B_n = \frac{\sinh \alpha_n(R-a)}{\cosh \alpha_n(R-a)} = \tanh \alpha_n(R-a) \qquad \text{and}$$

$$\alpha_n = (n+\tfrac{1}{2})\pi/H$$

The pressure in the spout channel is again equal to the pressure at the spout channel-annulus interface:

$$P_{sp}(z) = P(x=a,z) = \sum_{n=0}^{\infty} A_n \cos \alpha_n z + \frac{\eta}{K_1} V_{fl}(H-z)$$

3.4.3 Model results for the stable spouted bed flow regime

Plots of isobars calculated from equations (3-45) and (3-57) are given in figures 3.8 and 3.9 for some beds where no fluidisation gas was introduced. In addition figures 3.10 and 3.11 show plots of the flow distribution in these beds. Figures 3.8 and 3.10 give results calculated for a cylindrical bed while figures 3.9 and 3.11 show similar results for a two-dimensional bed. It is seen in these figures that the pressure distribution also tends to be flat at the top when the bed is operated in the stable spouted bed regime. The flow distributions that are presented in figures 3.10 and 3.11 show that the region with the highest vertical velocity is located just around the bottom section of the spout channel. Figure 3.12 presents results of calculations that were carried out for cylindrical beds in the stable spouted bed regime into which both fluidisation gas and spout gas are introduced. The figure shows a pattern of isobars that is more horizontal than in the case when spout gas is introduced only, as was the case for the packed bed regime.

3.4.4 Extended model for stable spouted bed flow

It was stated in section 3.2.4 that the calculated pressure distribution in a spout-fluid bed that is operated in the stable spouted bed regime depends to a large extent on the assumptions that have been made concerning the pressure distribution in the spout channel. It was pointed out that spout gas flow is determined by inertial forces, pressure forces, by interaction forces between the gas and entrained bed particles and by friction forces between the gas and the channel wall. Sections 3.4.1 and 3.4.2 present a simple model that assumes the existence of a linear relationship between pressure gradient and local gas velocity in the spout channel while inertial forces and interaction forces with bed particles are neglected. This model gives a fair description of the pressure distribution in the annulus, as will be shown in chapter 4, except for the region near the spout channel. This was to be expected because a high rate of spout gas crosses the spout channel-annulus interface causing a sharp decrease of the gas velocity in the spout channel. This is illustrated in figure 3.13 which shows the cal-

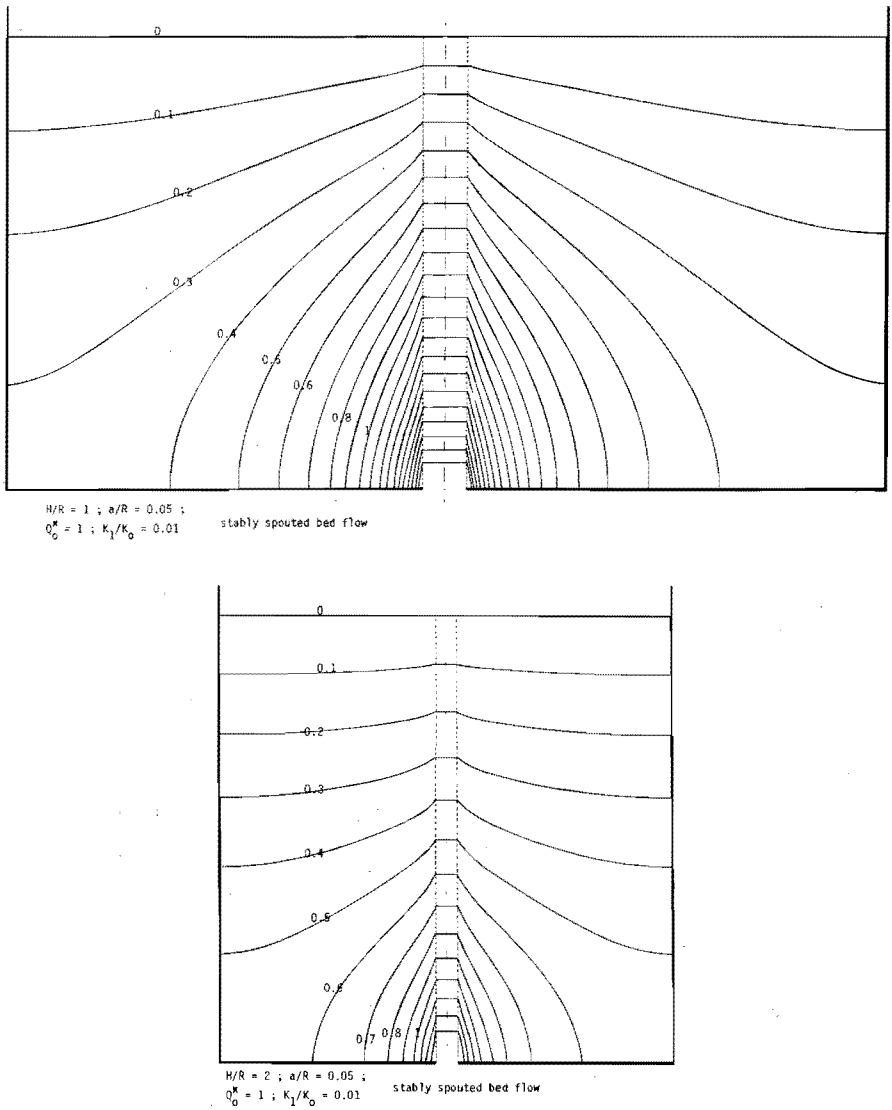

Figure 3.8. Calculated distribution of the dimensionless pressure P in some cylindrical beds with introduction of spout gas only. (Stable spouted bed regime assuming Darcy's law).*
$Q_o^* = 1$; $K_1/K_o = 0.01$; $a^* = 0.05$; $H^* = 1$ and 2 respectively.
P calculated from eq. (3.45), (3-56) and (3-40A).*

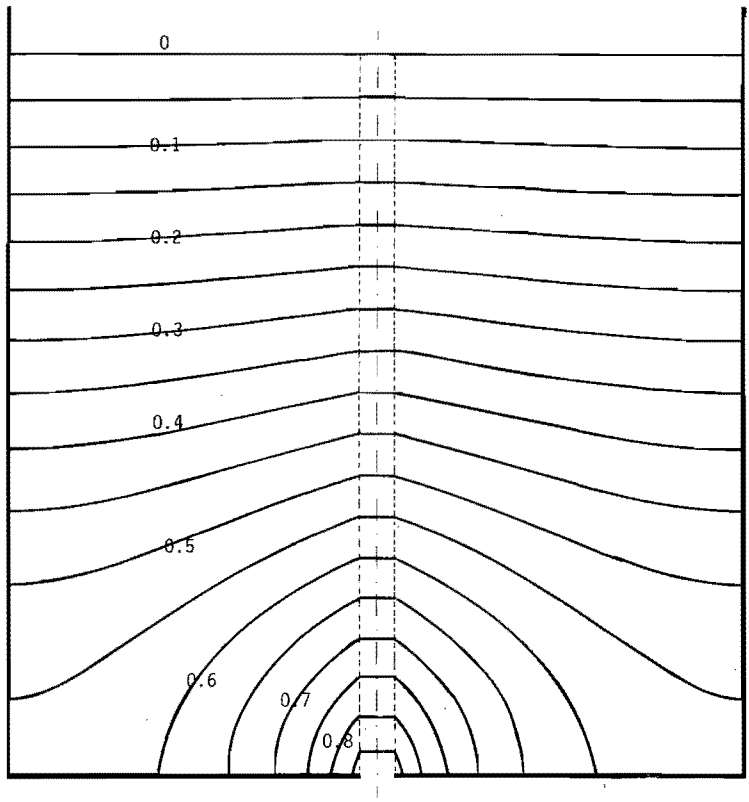

Figure 3.9. Calculated distribution of the dimensionless pressure. P in a two-dimensional bed with introduction of spout gas only. (Stable spouted bed regime assuming Darcy's law).*
$Q_o^* = 1$; $K_1/K_o = 0.01$; $a^* = 0.05$; $H^* = 2$.
P calculated from eq. (3-57), (3-59) and (3-40B).*

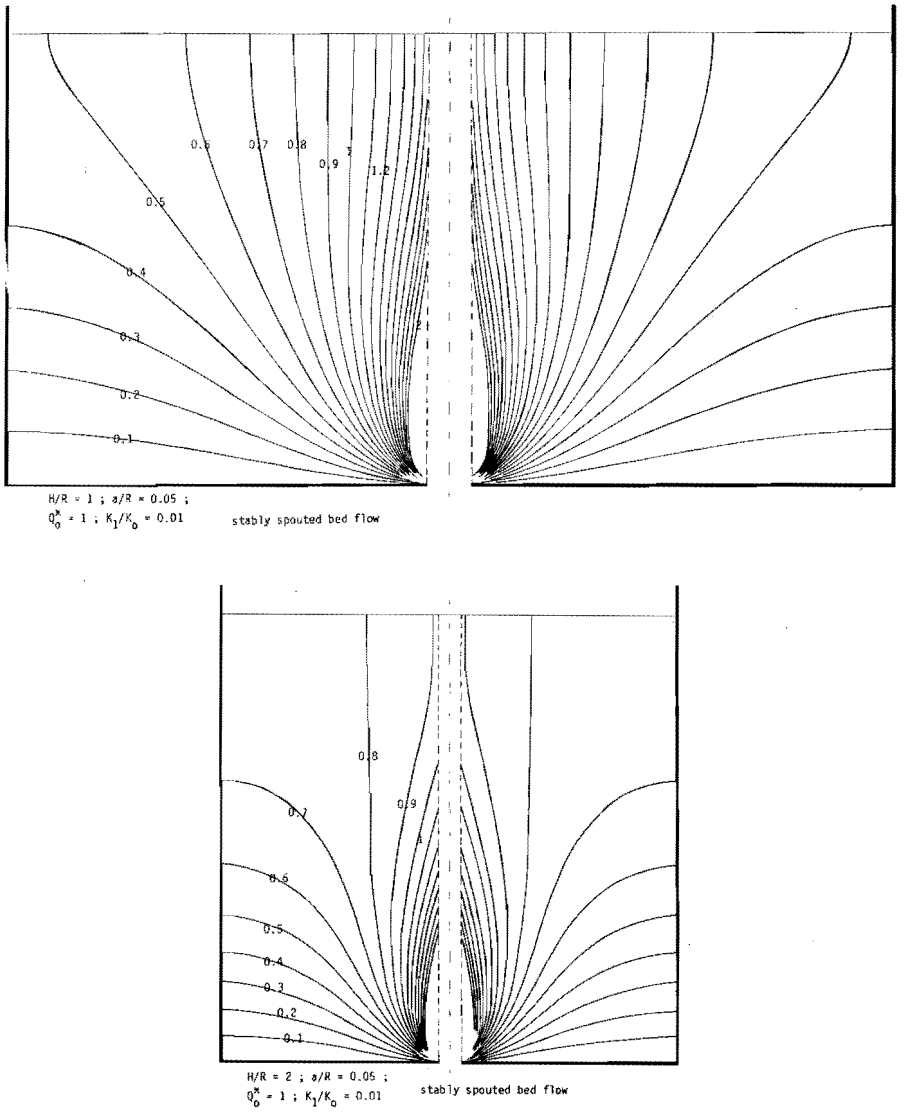

Figure 3.10. Calculated distribution of the dimensionless vertical velocity V_z^* in some cylindrical beds with introduction of spout gas only.

$Q_o^* = 1$; $K_1/K_o = 0.01$; $a^* = 0.05$; $H^* = 1$ and 2 respectively.

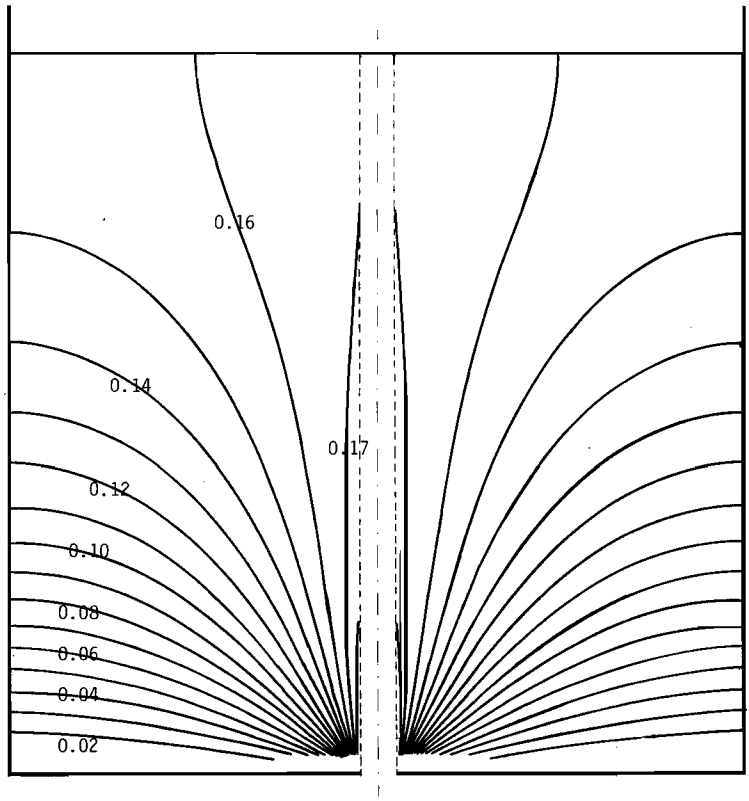

Figure 3.11. Calculated distribution of the dimensionless vertical velocity V_z^* *in a two-dimensional bed with introduction of spout gas only. (Stable spouted bed regime assuming Darcy's law).* $Q_o^* = 1$; $K_1/K_o = 0.01$; $a^* = 0.05$; $H^* = 2$.

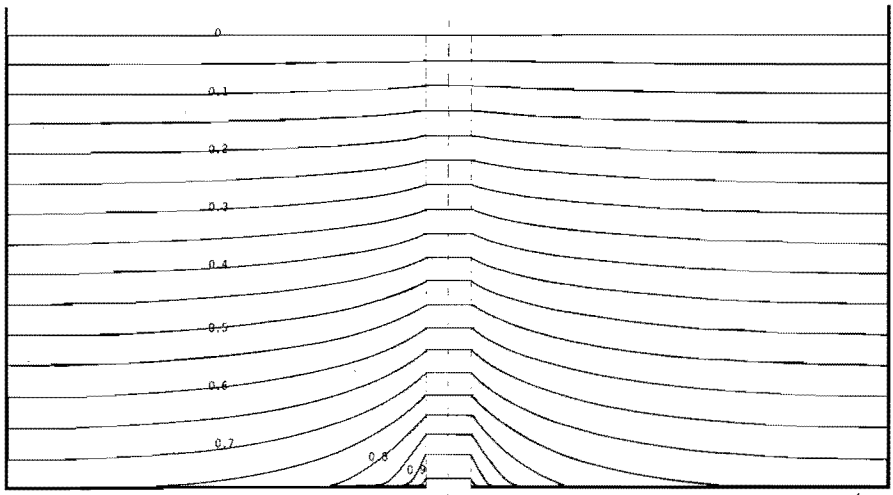

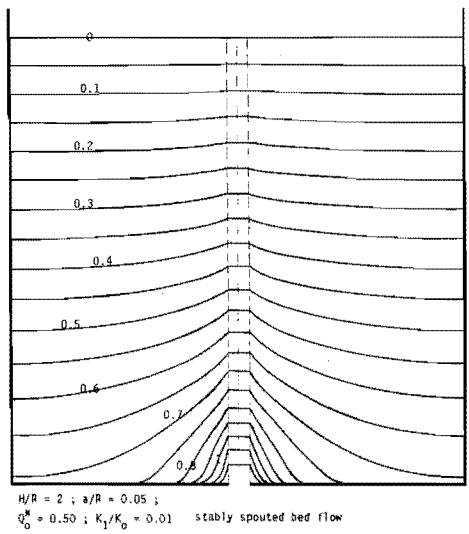

Figure 3.12. Calculated distribution of the dimensionless pressure P in some some cylindrical beds with introduction of fluidisation gas. (Stable spouted bed regime assuming Darcy's law).
$Q^* = 0.30$ and 0.50 respectively; $a^* = 0.05$; $K_1/K_o = 0.01$;
$H^* = 1$ and 2 respetively.

culated pressure distribution in a spout fluid bed with

bed height H = 20 cm

bed radius R = 7.6 cm

spout channel radius a = 0.5 cm

spout gas flow rate Q_o = 4 ℓ/s

No fluidisation gas was introduced.

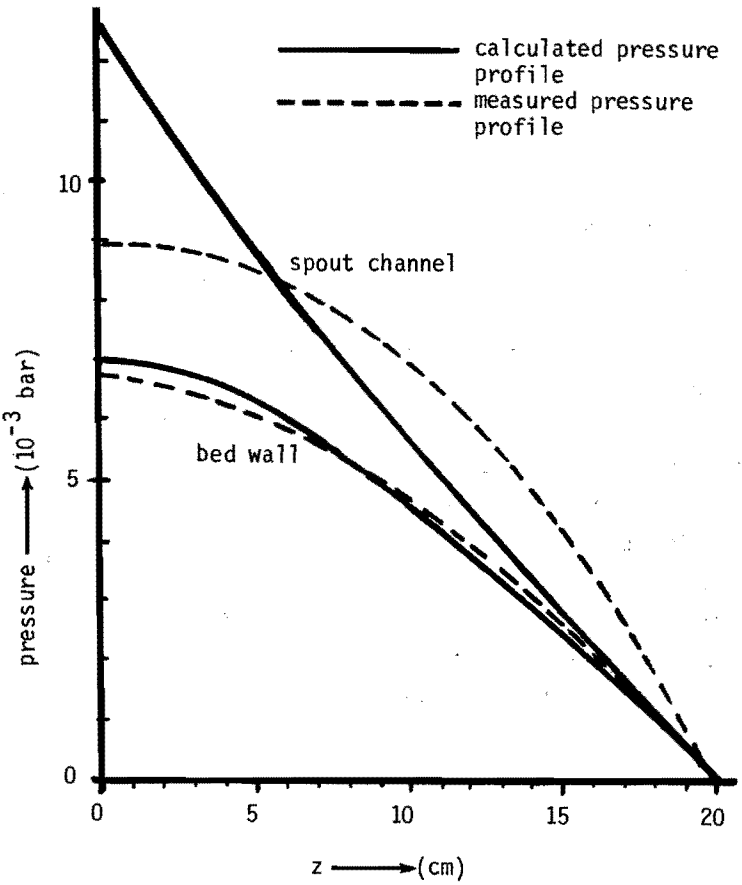

Figure 3.13. Example of a comparison between the calculated and measured pressure profile in the spout channel and at the bed wall in a bed at stable spouting while only spout gas is introduced. Calculated pressures were obtained with the simple pressure distribution model, using H = 20 cm; R = 7.6 cm; a = 0.5 cm; Q_o = 4 ℓ/s.

The minimum fluidisation velocity V_{mf} of the bed material was 22 cm/s. Figure 3.13 also shows an example of a measured pressure profile at the bed wall and in the spout channel (dotted lines).
It is seen that the measured pressure profile at the bed wall can be fitted fairly well by means of the simple flow model. The measured pressure profile in the spout channel shows, however, a negligible pressure gradient at the bottom of the bed. This pressure gradient increases in the direction towards the top of the bed. This can be understood from the momentum equation (3-14) or (3-15):

Inertial forces cause a positive pressure gradient due to deceleration of the gas flow.

Interaction forces cause a negative pressure gradient due to momentum transfer to the entrained bed particles and momentum transfer to the spout channel wall.

At the bottom section of the spout channel the inertial forces compensate the interaction forces between the gas flow and the entrained bed particles and the interaction forces between the gas flow and the spout channel wall. The inertial forces decrease with increasing height above the orifice because the rate of gas transfer to the annulus region and thus the deceleration of the gas in the spout channel decreases. The interaction forces rapidly increase because the number of entrained particles increases.
This causes an increase of the absolute value of the pressure gradient in the direction towards the top of the bed although the gas velocity in the spout channel slightly decreases in the same direction.
The interaction forces between the gas flow in the spout channel and the particles were neglected in the model on which the calculated curve in figure 3.13 is based, while the calculated curve did not account for the deceleration of the gas and the inertial forces caused by this deceleration either (compare figure 3.14). The interaction forces between the gas flow and the wall of the spout channel were assumed to be linearly proportional to the gas velocity.

To obtain insight into the magnitude of the inertial forces and of the interaction forces in the spout channel the above model now will be extended to provide an improved description of the gas flow in the spout channel.

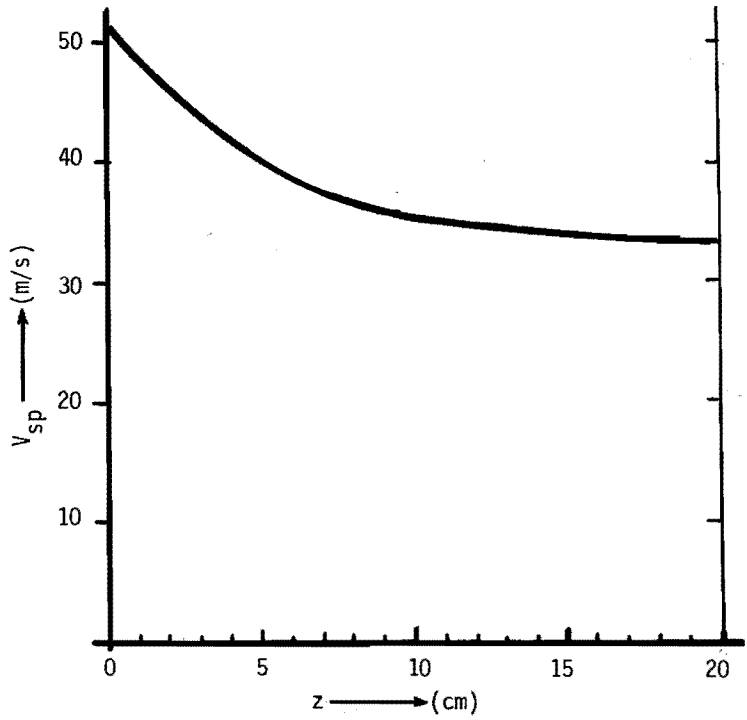

Figure 3.14. Calculated gas velocity in the spout channel using the simple pressure distribution model for the stable spouted bed regime, using H = 20 cm, R = 7.6 cm, a = 0.5 cm, Q_o = 4 ℓ/s. No fluidisation gas is introduced.

We start from equation (3-15) and assume that $\varepsilon \approx 1$. The momentum equation that is integrated over the cross section of the spout channel reads

$$\frac{1}{2}\rho_g \frac{d}{dz} V_{sp}^2 = -\frac{dP_{sp}}{dz} - \beta(V_{sp}-V_p)^2 - \frac{\lambda}{2a}\frac{1}{2}\rho_g V_{sp}^2 \qquad (3\text{-}60)$$

where λ is the friction factor for turbulent flow in rough pipes. This friction factor is discussed in more detail in Appendix 3-IV.
It is assumed that the hold-up of bed particles in the spout channel can be approximated by a linear relationship with respect to the height z:

$$1-\varepsilon = (1-\varepsilon_s)\cdot\frac{z}{H} \qquad (3\text{-}61)$$

This linear approximation results from the assumption of a constant particle entrainment rate at the spout channel wall. It will be shown later that the hold-up in the spout channel can indeed be approximated by this linear relationship ($1-\varepsilon$ is the hold-up at height z, $1-\varepsilon_s$ is the hold-up at the top of the spout channel).

Equation (3-60) can be rewritten using (3-18) and (3-61) and the assumption that $V_{sp} \gg V_d$ to obtain

$$\frac{1}{2}\rho_g \frac{d}{dz} V_{sp}^2 = -\frac{dP_{sp}}{dz} - \left(\frac{\lambda}{4a} + 0.384\,\frac{1-\varepsilon}{d_p}\right)\rho_g V_{sp}^2 \qquad (3\text{-}62)$$

The interaction term now has the form $(C + D\,\frac{z}{H})V_{sp}^2$ where $C = \lambda\rho_g/4a$ and $D = 0.384\,\rho_g(1-\varepsilon_s)/d_p$.

The pressure distribution in the annulus is given by equation (3-45) while the pressure $P_{sp}(z)$ and the gas velocity $V_{sp}(z)$ are described by equation (3-46) and (3-49) respectively. Thus

$$P(r,z) = \sum_{n=0}^{\infty} A_n \cos \alpha_n z \; \frac{K_o(\alpha_n r)I_1(\alpha_n R) + I_o(\alpha_n r)K_1(\alpha_n R)}{K_o(\alpha_n a)I_1(\alpha_n R) + I_o(\alpha_n a)K_1(\alpha_n R)} + \frac{\eta}{K} V_{fl}(H-z) \qquad (3\text{-}63)$$

with $\alpha_n = (n+\frac{1}{2})\pi/H$.
Equation (3-63) is thus valid in the annulus ($a \leq r \leq R$)

$$P_{sp}(z) = P(a,z) = \sum_{n=0}^{\infty} A_n \cos \alpha_n z + \frac{\eta}{K_1} V_{fl}(H-z) \qquad (3\text{-}64)$$

$$V_{sp}(z) = V_{spo} - \frac{2}{a}\frac{K_1}{\eta} \sum_{n=0}^{\infty} A_n B_n \sin \alpha_n z \qquad (3\text{-}65)$$

where V_{spo} = spout gas velocity at the orifice (z=0), and
V_{fl} = fluidisation gas velocity at the sieve plate (z=0).

From (3-65) it follows that

$$V_{sp}^2 = V_{spo}^2 + \frac{4}{a^2}\frac{K_1^2}{\eta^2} \sum_{k=0}^{\infty} \sum_{\ell=0}^{\infty} A_k A_\ell B_k B_\ell \sin \alpha_k z . \sin \alpha_\ell z$$

$$- \frac{4}{a}\frac{K_1}{\eta} V_{spo} \sum_{k=0}^{\infty} A_k B_k \sin \alpha_k z \qquad (3\text{-}66)$$

Integrating momentum equation (3-62) from height z to the top of the bed z=H yields

$$\frac{1}{2}\rho(V_{spH}^2 - V_{sp}^2) = P_{sp} - \int_z^H (C + D\frac{z}{H})V_{sp}^2\, dz \qquad (3\text{-}67)$$

where V_{spH} = gas velocity in the spout channel at z=H.

The left hand term of equation (3-67) is equal to

$$\frac{1}{2}\rho_g \frac{4}{a^2}\frac{K_1^2}{\eta^2}\sum_{k=0}^{\infty}\sum_{\ell=0}^{\infty} A_k A_\ell B_k B_\ell\{(-1)^{k+\ell} - \sin\alpha_k z \sin\alpha_\ell z\}$$

$$-\frac{1}{2}\cdot\frac{4}{a}\frac{K_1}{\eta}V_{spo}\sum_{k=0}^{\infty} A_k B_k\{(-1)^k - \sin\alpha_k z\}$$

where $\alpha_k = (k+\frac{1}{2})\pi/H$, and
B_k is defined by equation (3-48).

The first right hand term of equation (3-67) equals (compare eq.(3-64)):

$$\sum_{n=0}^{\infty} A_n \cos\alpha_n z + \frac{\eta}{K_1}V_{fl}(H-z)$$

The second right hand term of equation (3-67) becomes

$$-V_{spo}^2\{C(H-z) + \frac{1}{2}D\frac{H^2-z^2}{H}\} + \frac{4}{a^2}\frac{K_1^2}{2}\sum_{k}^{k\neq\ell}\sum_{\ell} A_k A_\ell B_k B_\ell C\{\frac{\sin(\alpha_k-\alpha_\ell)z}{2(\alpha_k-\alpha_\ell)} - \frac{\sin(\alpha_k+\alpha_\ell)z}{2(\alpha_k+\alpha_\ell)} -$$

$$-\frac{4}{a^2}\frac{K_1^2}{\eta^2}\sum_m A_m^2 B_m^2 C\{\frac{1}{2}(H-z) + \frac{1}{4\alpha_m}\sin 2\alpha_m z\} +$$

$$+\frac{4}{a^2}\frac{K_1^2}{\eta^2}\sum_{k}^{k\neq\ell}\sum_{\ell} A_k A_\ell B_k B_\ell \frac{D}{H}\{z\frac{\sin(\alpha_k-\alpha_\ell)z}{2(\alpha_k-\alpha_\ell)} - z\frac{\sin(\alpha_k+\alpha_\ell)z}{2(\alpha_k+\alpha_\ell)} +$$

$$+\frac{\cos(\alpha_k-\alpha_\ell)z - (-1)^{k-\ell}}{2(\alpha_k-\alpha_\ell)^2} - \frac{\cos(\alpha_k+\alpha_\ell)z - (-1)^{k+\ell+1}}{2(\alpha_k+\alpha_\ell)^2}\} -$$

$$-\frac{4}{a^2}\frac{K_1^2}{\eta^2}\sum_m A_m^2 B_m^2 \frac{D}{H}\{\frac{1}{4}(H^2-z^2) + \frac{z\sin 2\alpha_m z}{4\alpha_m} + \frac{\cos 2\alpha_m z}{8\alpha_m^2} + \frac{1}{8\alpha_m^2}\} -$$

$$- \frac{4}{a}\frac{K_1}{\eta} V_{spo} \sum_k A_k B_k \{-C \frac{\cos \alpha_k z}{\alpha_k} + \frac{D}{H} (\frac{\sin \alpha_k z - (-1)^k}{\alpha_k^2} - \frac{z \cos \alpha_k z}{\alpha_k})\}$$

on the condition that $\alpha_i = (i+\frac{1}{2})\pi/H$ according tot (3.65).

In order to determine A_n (n=0,1,2,...) by means of the momentum equation (3-64) the successive terms of (3-63) have to be developed in terms of the functions cos $\alpha_n z$ with $\alpha_n = (n+\frac{1}{2})\pi/H$ and n=0,1,2,... by Fourier series development (Appendix 3-I).

After Fourier series development and placing the coefficients of the terms of (3-67) back in (3-67) A_n (n=0,1,2,...) can be found from

$$\frac{1}{2}\rho_g \frac{4}{a^2}\frac{K_1^2}{\eta^2} \sum_k \sum_\ell A_k A_\ell B_k B_\ell \frac{(-1)^{k+\ell+n}}{H} \{\frac{\alpha_n}{(\alpha_k-\alpha_\ell)^2-\alpha_n^2} + \frac{\alpha_n}{(\alpha_k+\alpha_\ell)^2-\alpha_n^2} + \frac{2}{\alpha_n}\} -$$

$$- \frac{1}{2}\frac{4}{a}\rho_g \frac{K_1}{\eta} V_{spo} \sum_k A_k B_k \frac{2}{H} (\frac{\alpha_k}{\alpha_n} \cdot \frac{(-1)^{n-k}\ \alpha_k-\alpha_n}{\alpha_k^2-\alpha_n^2}) =$$

$$= A_n + \frac{\eta}{K_1} V_{fl} \frac{2}{H}\frac{1}{\alpha_n^2} - V_{spo}^2 \frac{2}{H}(\frac{C}{\alpha_n^2} + \frac{D}{H}(-1)^n \frac{1}{\alpha_n^3}) +$$

$$+ \frac{4}{a^2}\frac{K_1^2}{\eta^2} \sum_k \sum_\ell A_k A_\ell B_k B_\ell \frac{C}{H}\{\frac{1}{(\alpha_k-\alpha_\ell)^2-\alpha_n^2} - \frac{1}{(\alpha_k+\alpha_\ell)^2-\alpha_n^2}\} +$$

$$+ \frac{4}{a^2}\frac{K_1^2}{\eta^2} \sum_k \sum_\ell A_k A_\ell B_k B_\ell \frac{D}{H}\frac{2}{H}(-1)^{k+\ell+n}\{\frac{-\alpha_n}{((\alpha_k-\alpha_\ell)^2-\alpha_n^2)^2} - \frac{\alpha_n}{((\alpha_k+\alpha_\ell)^2-\alpha_n^2)^2} -$$

$$- \frac{1}{2\alpha_n}\frac{1}{(\alpha_k-\alpha_\ell)^2-\alpha_n^2} - \frac{1}{2\alpha_n}\frac{1}{(\alpha_k-\alpha_\ell)^2-\alpha_n^2}\} + \frac{4}{a}\frac{K_1}{\eta} V_{spo} A_n B_n C/\alpha_n +$$

$$+ \frac{4}{a}\frac{K_1}{\eta} V_{spo} \sum_k A_k B_k \frac{D}{H}\frac{2}{H}\frac{1}{\alpha_n}(-1)^{n-k} \frac{\alpha_k^2 - (-1)^{n-k}.2\alpha_k\alpha_n + \alpha_n^2}{(\alpha_k^2-\alpha_n^2)^2} \qquad (3\text{-}68)$$

Rearranging equation (3-68) results in a shorter expression:

$$A_n\left(1 + \frac{4}{a}\frac{K_1}{\eta} V_{spo} \frac{B_n C}{\alpha_n}\right) = \frac{2}{H}\frac{1}{\alpha_n^2}\left\{\left(C + \frac{D}{H}\frac{(-1)^n}{\alpha_n} V_{spo}^2 - \frac{\eta}{K_1} V_{fl}\right\} +\right.$$

$$+ \frac{4}{a^2}\frac{K_1^2}{\eta^2}\sum_k\sum_\ell A_k A_\ell B_k B_\ell \frac{1}{H} (-1)^{k+\ell+n} \cdot \left\{\frac{1}{2}\rho_g \left(\frac{\alpha_n}{(\alpha_k-\alpha_\ell)^2-\alpha_n^2} +\right.\right.$$

$$+ \frac{\alpha_n}{(\alpha_k+\alpha_\ell)^2-\alpha_n^2} + \frac{2}{\alpha_n}\Big) - C\left(\frac{1}{(\alpha_k-\alpha_\ell)^2-\alpha_n^2} - \frac{1}{(\alpha_k+\alpha_\ell)^2-\alpha_n^2}\right) +$$

$$\left. + \frac{2D}{H}(-1)^{k+\ell+n}\frac{1}{2\alpha_n}\left(\frac{(\alpha_k+\alpha_\ell)^2+\alpha_n^2}{((\alpha_k-\alpha_\ell)^2-\bar{\alpha}_n^2)^2} + \frac{(\alpha_k+\alpha_\ell)^2+\alpha_n^2}{((\alpha_k+\alpha_\ell)^2-\alpha_n^2)^2}\right)\right\} -$$

$$- \frac{4}{a}\frac{K_1}{\eta} V_{spo}\sum_k A_k B_k \frac{2}{H}\left\{\frac{1}{2}\rho_g \frac{\alpha_k}{\alpha_n}\frac{(-1)^{n-k}\,\alpha_k-\alpha_n}{\alpha_k^2-\alpha_n^2} +\right.$$

$$\left. + \frac{D}{H}\frac{1}{\alpha_n}(-1)^{n-k} \cdot \frac{\alpha_k^2 - (-1)^{n-k}\,2\alpha_k\alpha_n + \alpha_n^2}{(\alpha_k^2-\alpha_n^2)^2}\right\} \qquad (3\text{-}69)$$

where $C = \dfrac{\lambda\rho_g}{4a}$

and $D = \dfrac{0.384(1-\varepsilon)\rho_g}{d_p}$

A procedure to calculate A_n (n=0,1,2,...) from the recursion relation (3-69) can be deduced as follows:

The first approximation is

$$A_n^{(1)} = \frac{2}{H}\frac{1}{\alpha_n^2}\frac{(C + D.(-1)^n/\alpha_n H)V_{spo}^2 - \eta/K_1.V_{fl}}{1 + 4/a.V_{spo}.C.B_n/\alpha_n} \qquad (3\text{-}69A)$$

Each subsequent approximation for A_n (n=0,1,2,...) can be obtained from the previous one by means of the relationship

$$A_n(p) = A_n(1) + \frac{4}{a^2}\frac{K_1^2}{\eta^2}\sum_{k=0}^{\infty}\sum_{\ell=0}^{\infty} A_k(p-1)A_\ell(p-1)B_kB_\ell \frac{1}{H}\frac{\{\text{term 1}\}}{1+4/a.V_{spo}.C.B_n/\alpha_n}$$

$$- \frac{4}{a}\frac{K_1}{\eta} V_{spo} \sum_{k=0}^{\infty} A_k(p-1)B_k \cdot \frac{2}{H} \frac{\{\text{term 2}\}}{1 + 4/a.V_{spo}.C.B_n/\alpha_n} \qquad (3\text{-}69B)$$

where

$$\text{term 1} = \frac{1}{2}\rho_g (-1)^{k+\ell+n} \left(\frac{\alpha_n}{(\alpha_k-\alpha_\ell)^2-\alpha_n^2} + \frac{\alpha_n}{(\alpha_k+\alpha_\ell)^2-\alpha_n^2} + \frac{2}{\alpha_n}\right)$$

$$- C\left(\frac{1}{(\alpha_k-\alpha_\ell)^2-\alpha_n^2} - \frac{1}{(\alpha_k+\alpha_\ell)^2-\alpha_n^2}\right) \qquad (3\text{-}69C)$$

$$+ \frac{2D}{H}(-1)^{k+\ell+n}\frac{1}{2\alpha_n}\left(\frac{(\alpha_k-\alpha_\ell)^2+\alpha_n^2}{((\alpha_k-\alpha_\ell)^2-\alpha_n^2)^2} + \frac{(\alpha_k+\alpha_\ell)^2+\alpha_n^2}{((\alpha_k+\alpha_\ell)^2-\alpha_n^2)^2}\right)$$

$$\text{term 2} = \frac{1}{2}\rho_g \frac{\alpha_k}{\alpha_n}\frac{(-1)^{n-k}(\alpha_k-\alpha_n)}{\alpha_k^2-\alpha_n^2} + \frac{D}{H}\frac{(-1)^{n-k}}{\alpha_n}\frac{\alpha_k^2-(-1)^{n-k}2\alpha_k\alpha_n+\alpha_n^2}{(\alpha_k^2-\alpha_n^2)^2} \qquad (3\text{-}69D)$$

with $C = \lambda\rho_g/4a$

and $D = 0.384(1-\varepsilon_s)\rho_g/d_p$.

It is seen from the extended equation (3-69) and from the calculation procedure (3-69A,B,C,D) that the first approximation $A_n^{(1)}$, letting $1-\varepsilon_s=0$ i.e. no bed particles in the spout channel, is identical to the A_n that resulted from the simple calculation model that is derived in section 3.4.1. In the case of a turbulent spout channel flow the apparent permeability K_o of the spout channel is written as

$$K_o = \eta/\left(\frac{\lambda}{2a} \cdot \frac{1}{2}\rho_g V_{spo}\right) \qquad (3\text{-}70)$$

where this spout channel permeability is related to the spout gas velocity at the orifice in accordance with Appendix 3-IV.

Figure 3.15 shows the results of calculations obtained with the extended model that has been developed in the present section for a bed with $H = 20$ cm, $R = 7.6$ cm, $d_p = 0.56$ mm, $v_{mf} = 22$ cm/s, $Q_o = 4$ ℓ/s, $a = 0.5$ cm while no fluidisation gas is introduced.
The results that are presented in this figure can be compared to figure 3.13 which shows an example of measured pressure profiles at the bed wall and in the spout channel. It can be seen that the cal-

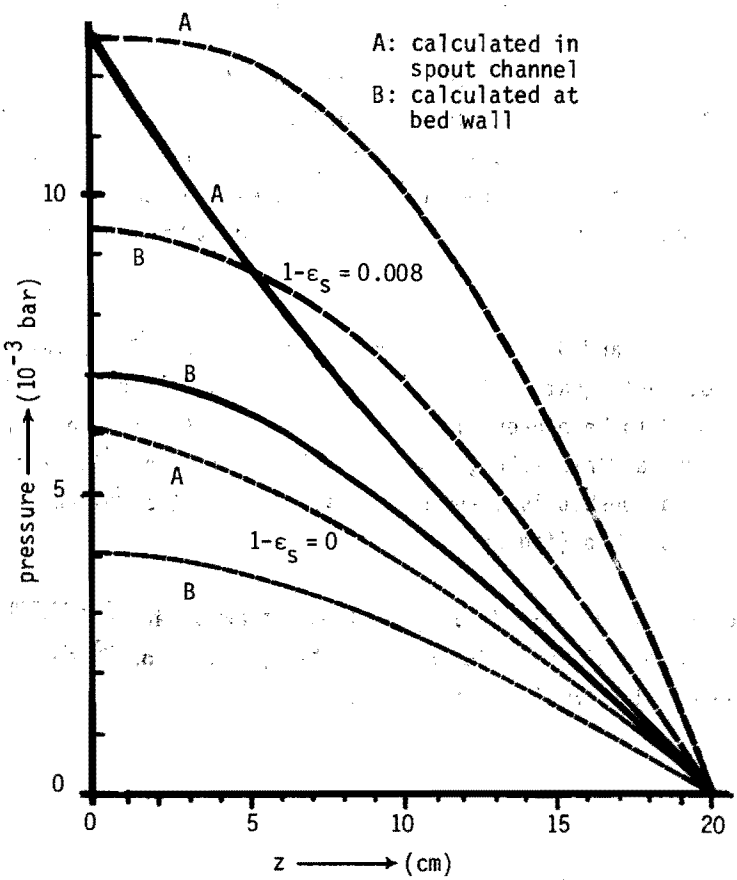

Figure 3.15. Calculated pressure profiles in the spout channel and at the bed wall in a bed in the stable spouted bed regime while only spout gas is introduced. Calculated pressures were obtained with the simple pressure distribution model (———) and with the extended model (------), using $H = 20$ cm, $R = 7,6$ cm, $a = 0,5$ cm, $Q_o = 4$ ℓ/s while $1-\varepsilon_s$ is set to 0.0 and 0.008 respectively.

culated results of the extended model show good agreement with the measured curves, provided that suitable values of the spout channel radius a and of the hold-up in the spout channel have been found to fit the extended model to the experimental pressure profile. The results presented in figure 3.15 are compared to similar results for the same bed under the same conditions that were obtained by means of the simple calculation model (section 3.4.3). It is seen that when the presence of entrained particles in the spout channel is ignored ($1-\varepsilon_s=0$) the pressures that are calculated from the extended model are much lower than those that are obtained from the simple model. Taking the effect of entrained bed particles into account leads to a higher pressure gradient in the spout channel. This causes the pressure in the bed to be higher than when the presence of entrained particles in the spout channel is neglected (see the dotted curves for the case $1-\varepsilon_s = 0.008$ in figure 3.15).

Figures 3.16A and B show the contribution of each of the terms of the Navier-Stokes' equation (3-15) both for the case where no particles are assumed to be present in the spout channel (no interaction forces between gas and particles, figure 3.16A) and for the case where a linear relationship is assumed to exist between the hold-up and the height in the bed (figure 3.16B).

The hold-up of entrained bed particles can be obtained from the equation of motion of the solid phase in the spout channel and will be discussed in the next section 3.4.5.

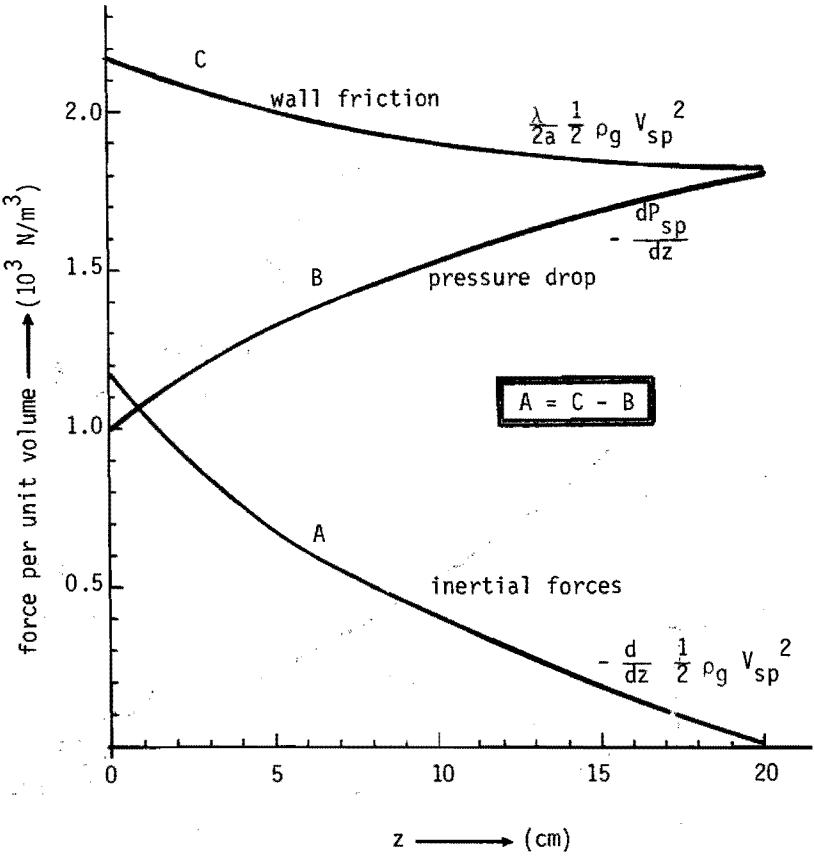

Figure 3.16A The contribution of each of the terms of the Navier-Stokes' equation (3-15) for the gas flow in the spout channel (no interaction forces between gas and entrained bed particles). H = 20 cm, a = 0.7 cm, R = 7.6 cm, Q_o = 5 ℓ/s, $1-\varepsilon_s$ = 0.0.

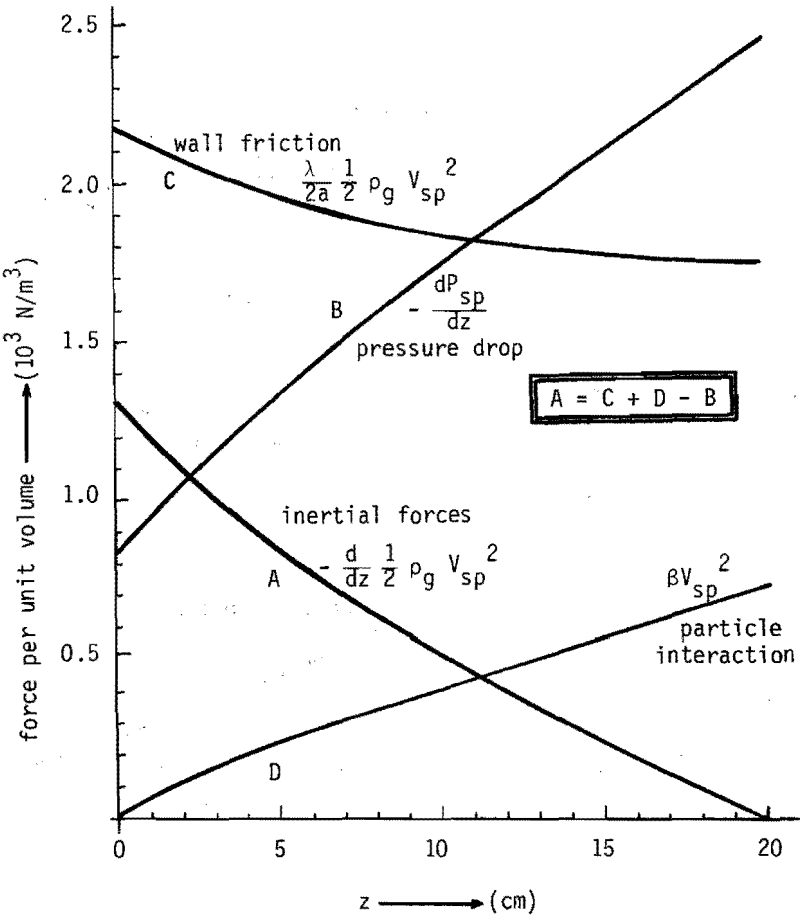

Figure 3.16B The contribution of each of the terms of the Navier-Stokes' equation (3-15) for the gas flow in the spout channel.
H = 20 cm, a = 0.7 cm, R = 7.6 cm, Q_o = 5 ℓ/s, $1-\varepsilon_s$ = 0.001.

3.4.5 The dispersed phase in the spout channel

Bed particles are entrained from the spout channel wall and are accelerated upwards in the spout channel (figure 3.17).
The equation of motion (momentum balance) can be applied to the flow of the solids in the spout channel (appendix 3-V).

$$\rho_d \frac{d}{dz}(1-\varepsilon) V_d^2 = -(1-\varepsilon)\frac{dP_{sp}}{dz} - \rho_d g(1-\varepsilon) + \frac{0.384(1-\varepsilon)\rho_g}{d_p} V_{sp}^2 \qquad (3\text{-}71)$$

The solids motion is thus defined by inertial forces, pressure forces, gravitational forces and by interaction forces with the gas flow.
The interaction force is again represented by a modified form of the relation proposed by Barnea and Mizrahi [15]. The particle velocity is

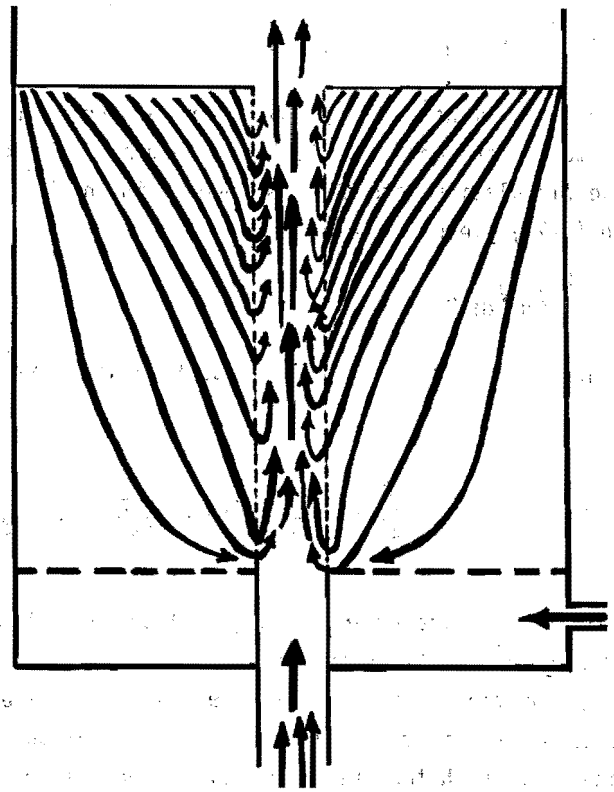

Figure 3.17. View of the flow of solids in the spout-fluid bed at stable spouting.

assumed to be negligible with respect to the gas velocity in the same manner as in equation (3-18).
It follows from equation (3-71) that

$$\rho_d \quad \frac{1}{1-\varepsilon}\frac{d}{dz}(1-\varepsilon)\,V_d^2 = -\frac{dP_{sp}}{dz} - \rho_d g + \frac{0.384}{d_p}\rho_g V_{sp}^2 \qquad (3\text{-}72)$$

A mass balance can be set up over a volume-element of the spout channel that includes the interface between spout channel and annulus. This mass balance provides a relation between the particle flow rate $(1-\varepsilon)V_d$ in the spout channel and the solids circulation rate W of the spout-fluid bed.
The mass balance can be written as

$$\rho_d \frac{d}{dz}(1-\varepsilon)V_d = \frac{2}{a}\rho_d V_{da} = \frac{2}{a}\cdot\rho_d\frac{W}{2\pi aH} \qquad (3\text{-}73)$$

where V_{da} (= entrainment velocity (m/s)) and a (spout channel radius) are assumed to be constant over the whole length of the spout channel and W is the circulation rate that is induced in the bed (m^3/s).
Integrating (3-73) yields

$$\rho_d (1-\varepsilon)V_d = \frac{2}{a}\rho_d V_{da} z \qquad (3\text{-}74)$$

Combining equation (3-72) and (3-74) leads to a differential equation in V_d:

$$\rho_d \quad \frac{V_d}{z}\frac{d}{dz}(zV_d) \quad = \rho_d\left(\frac{V_d^2}{z} + \frac{1}{2}\frac{d}{dz}V_d^2\right) = -\frac{dP_{sp}}{dz} - \rho_d g + \frac{0.384}{d_p}V_{sp}^2 \qquad (3\text{-}75)$$

where the right hand side of equation (3-75) can be calculated from the pressure profile in the spout channel.
Figure 3.18 shows the calculated particle velocity in the spout channel for two cases of the assumed maximum hold-up $1-\varepsilon_s$ at the top of the spout channel for which the pressure profile and gas velocity in the spout channel is calculated. A mean circulation time of 100 seconds has been taken in order to calculate the hold-up in the spout channel. This value is a reasonable value for a bed of a height of 20 cm that

is operated in the stable spouted bed regime. When the circulation flow includes the whole bed volume the circulation rate can be obtained from the mean circulation time t_m by the relationship

$$W = \pi(R^2-a^2).H/t_m \qquad (3\text{-}76)$$

The hold-up in the spout channel can be derived from the particle velocity V_d and the circulation rate W by means of equations (3-73) and (3-74):

$$1-\varepsilon = \frac{2}{a} V_{da} \cdot z/V_d \qquad (3\text{-}77)$$

where $V_{da} = W/2\pi aH$ and W according to equation (3-76).

Figure 3.18 shows the calculated results of the particle hold-up in the spout channel for two cases of the assumed maximum hold-up $1-\varepsilon_s$ at the top of the spout channel for which the pressure profile and gas velocity in the spout channel were computed ($1-\varepsilon_s=0$ and 0.008 respectively).
It is seen that the assumption which was made earlier in this chapter, according to which the hold-up increases linearly with increasing height z, agrees reasonably well with the calculated hold-up in the spout channel. It will be recalled that this calculation was carried out under the assumption that the entrainment velocity V_{da} is nearly constant over the spout channel.

It is noted that the hold-up increases linearly with constant entrainment velocity V_{da} over the length of the channel only when V_d is constant in the spout channel. Figure 3.18 shows that the dotted curves obey this condition at $z/H > 0.5$.
In cases where a high particle velocity occurs in the spout channel the slip velocity $V_{sp}-V_d$ rather than the gas velocity V_{sp} should be used to calculate the interaction forces between gas and particles. The use of the gas velocity V_{sp} rather than the slip velocity $V_{sp}-V_d$ in the calculations causes the calculated pressure drop to be too high and the calculated gas velocity to be too low in the upper part of the spout channel.

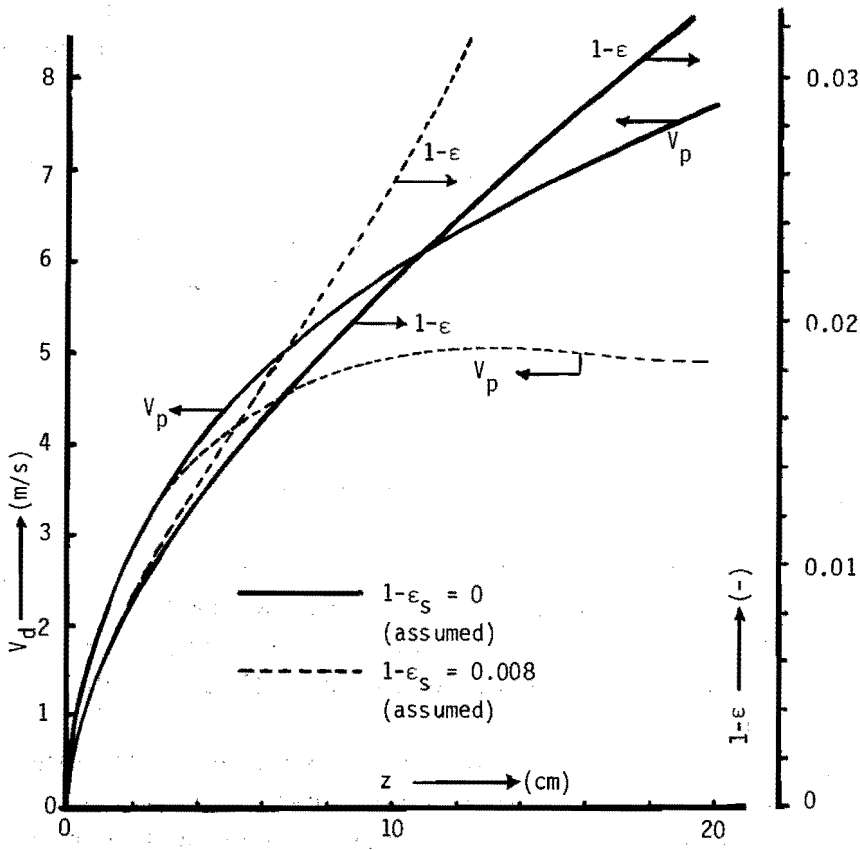

Figure 3.18. Calculated particle velocity V_d and the particle hold-up $1-\varepsilon$ in the spout channel. H = 20 cm, a = 0.5 cm, R = 7.6 cm, Q_o = 4 l/s. No fluidisation gas is introduced. The maximum hold-up $1-\varepsilon_s$ for the calculation of the pressure profile and gas velocity in the spout channel has been set to 0 and 0.008 while the assumed mean circulation time t_m of the bed particles was 100 sec.

Literature

1. Mamuro, T. and Hattori, H.
   J.Chem.Eng.Japan 1, 1 (1968)
   correction in J.Chem.Eng.Japan 3, 119 (1970).
2. Epstein, N., Lim, C.J. and Mathur, K.B.
   Can.J.Chem.Eng. 56, 436 (1978).
3. Grbavcič, Z.B., Vukovič, D.V., Zdanski, F.K. and Littman, H.
   Can.J.Chem.Eng. 54, 33 (1976).
4. Thorley, B., Saunby, J.B., Mathur, K.B. and Osberg, G.L.
   Can.J.Chem.Eng. 37, 184 (1959).
5. Epstein, N. and Levine, S.
   "Non Darcy Flow and Pressure Distribution in a Spouted Bed"
   Proc. 2nd. Eng.Foundation Conference on Fluidization,
   pp.98-103, Cambridge University (1978).
6. Mathur, K.B. and Epstein, N.
   "Spouted Beds"
   Academic Press, New York (1974).
7. Yokogawa, A., Ogino, E. and Yoshii, N.
   Trans.Jap.Soc.Mech.Engrs. 38, 148 (1972).
8. Lefroy, G.A. and Davidson, J.F.
   Trans.Instn.Chem.Engrs. 47, T120 (1969).
9. Nagarkatti, A. and Chatterjee, A.
   Can.J.Chem.Eng. 52, 185 (1974).
10. Littman, H., Vukovič, D.V., Zdanski, F.K. and Grbavcič, Z.B.
    Can.J.Chem.Eng. 52, 174 (1974).
11. Malek, M.A. and Lu, B.C.Y.
    Ind.Eng.Chem.Process Des.Develop. 4, 123 (1965).
12. Heil, C. and Tels. M.
    "Pressure Distribution in Spout-Fluid Bed Reactors"
    Proc. 2nd. International Symposium on Spouted Beds, Vancouver,
    Canada, Oct.3-6, 1982.
13. Rietema, K. and van den Akker, H.E.A.
    Int.J. of Multiphase Flow, in press.
14. Abramowitz, M. and Stegun, I.A.
    "Handbook of Mathematical Functions",
    Dover Publications, Inc., 7th printing, New York, page 355.

15. Barnea, E. and Mizrahi, J.
Chem.Eng.J. 5, 171 (1973).
16. Mathur, K.B. and Gishler, P.E.
AIChE Journal 1, 157 (1955).

APPENDIX 3.I

The functions $\cos n\pi x/R = \cos \alpha_n x$ in equation (3-39) are orthogonal functions on the interval $-R \leq x \leq R$. This means that

$$\int_{-R}^{R} \cos \frac{m\pi x}{R} \cos \frac{n\pi x}{R}\, dx = \begin{cases} 0 & \text{for } m \neq n = 0 \\ R & \text{for } m = n \neq 0 \\ 2R & \text{for } m = n = 0 \end{cases}$$

An even function f(x) can thus be expressed in terms of $\cos n\pi x/R$, n=0,1,2,...:

$$f(x) = \tfrac{1}{2}a_0 + \sum_{n=1}^{\infty} a_n \cos \frac{n\pi x}{R}$$

$$\text{with } a_n = \frac{1}{R} \int_{-R}^{R} f(x) \cos \frac{n\pi x}{R}\, dx = \frac{2}{R} \int_{0}^{R} f(x) \cos \frac{n\pi x}{R}\, dx$$

The functions $\cos \frac{(n+\frac{1}{2})\pi z}{H} = \cos \alpha_n z$ in the equations (3-45) and (3.57) are orthogonal functions on the interval $0 \leq z \leq H$ so that

$$\int_{0}^{H} \cos \alpha_m z \cos \alpha_n z\, dz = \begin{cases} 0 & \text{for } m \neq n \\ \tfrac{1}{2}H & \text{for } m = n \end{cases}$$

under the condition that $\alpha_n = (n+\frac{1}{2})\pi/H$.

A function f(z) with property f(z=H) = 0 can thus be expressed in terms of $\cos \alpha_n z = \cos \frac{(n+\frac{1}{2})\pi}{H} z$, n=0,1,2,3,... by

$$f(z) = \sum_{n=0}^{\infty} a_n \cos \alpha_n z$$

$$\text{with } a_n = \frac{2}{H} \int_{0}^{H} f(z) \cos \alpha_n z\, dz$$

APPENDIX 3.II

The functions $J_o(\alpha_n r)$ in the equations (3.30) and (3.32) are orthogonal functions on the surface of the circle with radius R, so that

$$\int_0^R J_o(\alpha_m r)\, J_o(\alpha_n r)\, r\, dr = 0 \qquad \text{for } m \neq n$$
$$= \tfrac{1}{2}R^2 . J_o^2(\alpha_n R) \qquad \text{for } m = n$$

where $\alpha_n R$ is a root of $J_1(\alpha_n R) = 0$.

A function f(r) can thus be expressed in terms of $J_o(\alpha_n r)$ n=0,1,2,3,... by:

$$f(r) = \sum_{n=0}^{\infty} a_n\, J_o(\alpha_n r)$$

$$\text{with } a_n = \frac{2}{R^2 J_o^2(\alpha_n R)} \int_0^R f(r)\, J_o(\alpha_n r)\, r\, dr$$

APPENDIX 3.III

The expressions for the pressure distributions have to be made in dimensionless form in order to obtain general results from the theoretical model.
Consider the expressions (3-33), (3-39), (3-45), (3-56), (3-57) and (3-59) and assume

$$H^* = H/R$$
$$a^* = a/R$$
$$z^* = z/R$$
$$x^* = x/R$$
$$r^* = r/R$$
$$Q_o^* = \frac{Q_o}{Q_o+Q_1}$$

The pressure P is related to the pressure drop over the bed that would result if the spout gas and fluidisation gas were introduced together into the bed homogeneously as fluidisation gas.

Therefore

$$P^* = \frac{P}{\frac{n}{K_1}\frac{Q_o+Q_1}{2RD} \cdot H} \qquad \text{in the two-dimensional bed}$$

or

$$P^* = \frac{P}{\frac{n}{K_1}\frac{Q_o+Q_1}{\pi . R^2} \cdot H} \qquad \text{in the cylindrical bed.}$$

Equation (3-39) can be rewritten in dimensionless form as

$$P^*(x^*,z^*) = (1-z^*) + \frac{Q^*-a^*}{1-a^*}\frac{2}{a^*H^*}\sum_{n=1}^{\infty}\frac{\sin\alpha_n^* a^*}{\alpha_n^{*2}\cosh\alpha_n^* H^*}\cos\alpha_n^* x^* \sinh\alpha_n^* H^*(1-z^*)$$

where here $\alpha_n^* = \alpha_n R = n.\pi$.

Equations (3-57) and (3-59) can be rewritten as

$$P^*(x^*,z^*) = 2\{\frac{K_1}{K_o}\frac{Q_o^*}{a^*} - \frac{1-Q_o^*}{1-a^*}\}\sum_{n=0}^{\infty}\frac{\cos\alpha_n^* z^*}{\alpha_n^{*2}\{1+\frac{K_1}{K_o}\frac{H^*}{a^*}\frac{B_n}{\alpha_n^*}\}}\frac{\cosh\alpha_n^*\frac{R^*-x^*}{H^*}}{\cosh\alpha_n^*\frac{R^*-a^*}{H^*}} +$$

$$+ \frac{1-Q_o^*}{1-a^*}(1-z^*)$$

$$P^*(x^*,z^*) = P^*(a^*,z^*) \qquad \text{for } |x^*| < a^*$$

assuming that $\alpha_n^* = \alpha_n.H = (n+\frac{1}{2})\pi$.

From equation (3-33) it follows that:

$$P^*(r^*,z^*) = (1-z^*) + \frac{Q_o^*-a^{*2}}{1-a^{*2}}\frac{2}{a^*H^*}\sum_{n=1}^{\infty}\frac{J_1(\alpha_n^* a^*)}{J_o^2(\alpha_n^*)}\frac{J_o(\alpha_n^* r^*)\sinh\alpha_n^* H^*(1-z^*)}{\alpha_n^{*2}\cosh\alpha_n^* H}$$

Assume now that $\alpha_n^* = \alpha_n.R$, i.e. the n^{th} root of $J_1(\alpha_n^*) = 0$.

Equations (3-45) and (3-56) can be rewritten to obtain

$$P^*(r^*,z^*) = 2\{\frac{K_1}{K_o}\frac{Q_o^*}{a^{*2}} - \frac{1-Q_o}{1-a^{*2}}\} \sum_{n=0}^{\infty} \frac{\cos \alpha_n^* z^*}{\alpha_n^{*2}\,(1 + \frac{K_1}{K_o}\frac{2H^*}{a^*}\frac{B_n}{\alpha_n^*})}$$

$$\cdot \frac{I_o(\alpha_n^* \frac{r^*}{H^*}) I_1(\frac{\alpha_n^*}{H^*}) + I_o(\alpha_n^* \frac{r^*}{H^*})\, K_1(\frac{\alpha_n^*}{H^*})}{K_o(\alpha_n^* \frac{r^*}{H^*}) I_1(\frac{\alpha_n^*}{H^*}) + I_o(\alpha_n^* \frac{a^*}{H^*})\, K_1(\frac{\alpha_n^*}{H^*})} + \frac{1-Q_o^*}{1-a^{*2}}\,(1-z^*)$$

$P^*(x^*,z^*) = P^*(a^*,z^*)$ for $r^* < a^*$

assuming that $\alpha_n^* = \alpha_n . H = (n+\frac{1}{2})\pi$.

APPENDIX 3.IV

The spout channel friction factor and permeability

The spout channel flow can be regarded as a turbulent flow in a tube with a porous wall through which spout gas percolates into the annular region.
The relation between the pressure drop and the flow velocity in a long cylindrical tube can be expressed by

$$-\frac{dP}{dz} = \frac{\lambda}{2a} \cdot \frac{1}{2} \rho V_{sp}^2$$

where the friction factor λ is dependent on the Reynolds number of the tube and on the relative wall roughness.
Figure 3.IV.1 shows friction factors λ as a function of the Reynolds number for several values of the relative wall roughness.
The Reynolds number of the flow in the tube is defined by

$$Re = \frac{\rho_g V_{sp}\, 2a}{\eta}$$

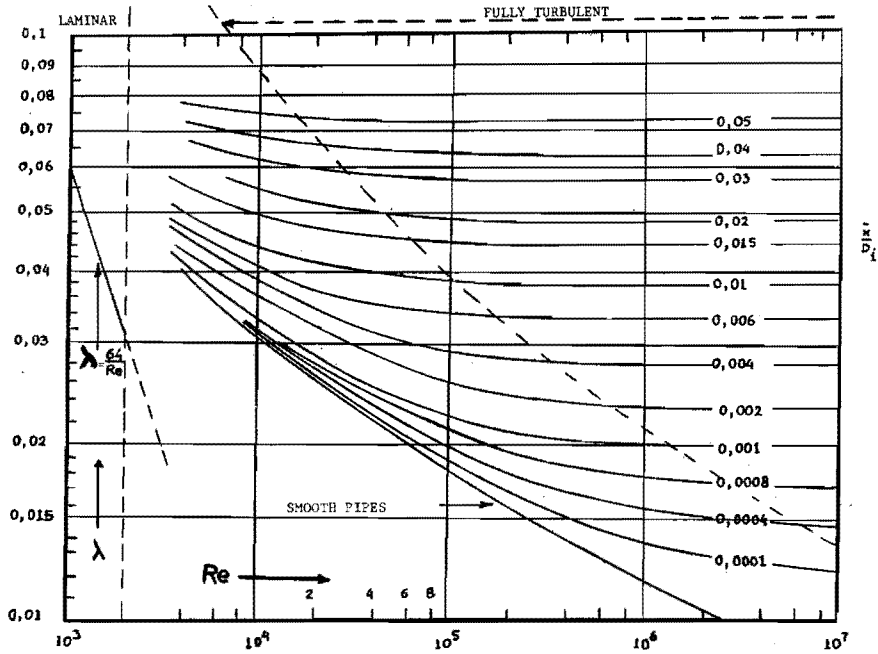

Figure 3.IV-1. Friction factors smooth and rough pipes against Reynolds number and relative roughness $\bar{x}/D_i$.
λ = friction factor of the pipe.
Re = Reynolds number of the flow in the pipe.
$\bar{x}$ = mean height of the pipe wall roughness.
D_i = diameter of the pipe.
Figure is from H.Schlichting, "Grenzschichttheorie", Karlsruhe, 5th printing 1965.

The wall roughness of the spout channel is defined as the mean height of the wall roughness divided by the diameter of the channel. The mean height of the roughness is set equal to the mean radius $\frac{1}{2}\bar{d}_p$ of the bed particles.
The relative roughness is thus set equal to $\frac{1}{2}\bar{d}_p/2a$.
At high values of the Reynolds number the friction factor is independent of the Reynolds number. Figure 3.IV.2 shows a plot of the relation between the relative wall roughness and the friction factor at high values of Re that can be read from figure 3.IV.1.

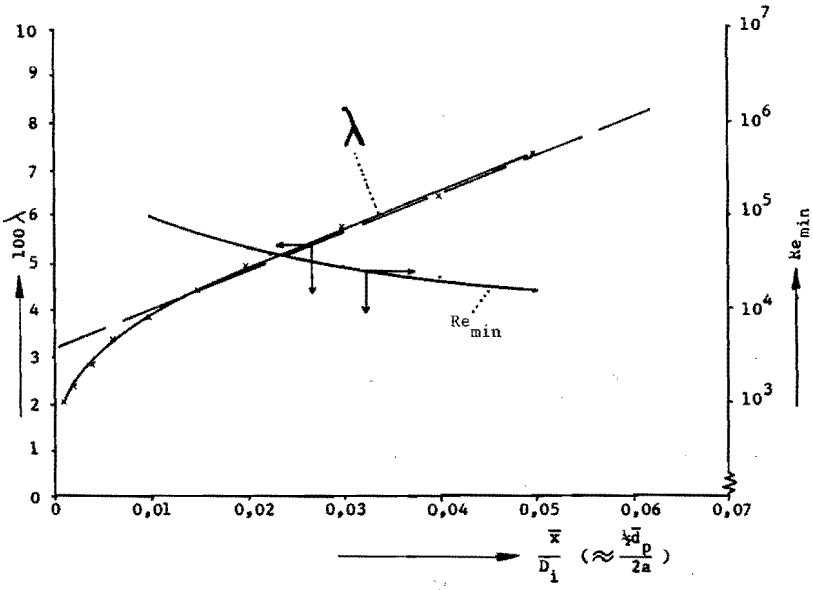

Figure 3.IV-2. Friction factors at high values of Re as a function of the wall roughness, obtained from figure 3.IV-1. The minimum value of Re above which λ is independent of Re as a function of the wall roughness.

It is found that the friction factor λ can be approximated by

$$\lambda = 3.2.10^{-2} + 0.815\ \bar{d}_p/4a$$

Figure 3.IV.2 also shows the Reynolds number Re_{min} above which the friction factor λ is independent of the Reynolds number as a function of the wall roughness.

Appendix 3.V Gas and particle flow in the spout channel

The momentum equation that can be applied to the gas flow in the spout channel reads:

$$\text{div } \varepsilon\rho_g \vec{\vec{V}}\vec{\vec{V}} = -\varepsilon\vec{\nabla}.\bar{\bar{\tau}}_c - \vec{\nabla}.\bar{\bar{R}}_c - \varepsilon\vec{\nabla}p + \varepsilon\rho_g\vec{g} + \vec{F}_s \qquad (3.V\text{-}1)$$

The left hand side of eq.(3.V-1) can be rewritten to obtain:

$$\text{div } \varepsilon\rho_g \vec{\vec{V}}\vec{\vec{V}} = \vec{V} \text{ div } \varepsilon\rho_g \vec{V} + \varepsilon\rho_g \vec{V}.\text{grad } \vec{V} \qquad (3.V\text{-}2)$$

In the case where div $\varepsilon\rho_g \vec{V} = 0$ and when the gravitational forces are neglected eq. (3.V-1) simplifies to:

$$\varepsilon\rho_g \vec{V} \text{ . grad } \vec{V} = -\varepsilon \vec{\nabla}.\bar{\bar{\tau}}_c - \vec{\nabla}.\bar{\bar{R}}_c - \varepsilon\vec{\nabla}p + \vec{F}_s \qquad (3.V\text{-}3)$$

which is identital with equation (3-14).

When the Reynolds stresses are neglected the z-component of equation (3.V-3) can be written as:

$$\varepsilon\rho_g V_z \frac{\partial V_z}{\partial z} = -\varepsilon \frac{1}{r} \frac{\partial r\tau_{rz}}{\partial r} - \varepsilon \frac{dP_{sp}}{dz} + F_s \qquad (3.V\text{-}4)$$

which is equivalent to .

$$\frac{1}{2} \varepsilon\rho_g \frac{\partial}{\partial z} V_z^2 = -\varepsilon \frac{1}{r} \frac{\partial r\tau_{rz}}{\partial r} - \varepsilon \frac{dP_{sp}}{dz} + F_s \qquad (3.V\text{-}5)$$

Equation (3.V-5) will now be integrated over the cross section of the spout channel.
Assume that

$$V_{sp}^2 = \frac{2}{a^2} \int_0^a V_z^2 \, r \, dr \qquad (3.V\text{-}6)$$

where a is the spout channel radius.

It can be verified that

$$\frac{2}{a^2}\int_0^a \frac{1}{r}\frac{\partial r\tau_{rz}}{\partial r}\,r\,dr = \frac{2\tau_w}{a} \qquad (3.V\text{-}7)$$

where τ_w is the shear stress at the spout channel wall.

It then follows from equations (3.V-5), (3.V-6) and (3.V-7) that

$$\frac{1}{2}\varepsilon\rho_g\frac{d}{dz}V_{sp}^2 = -\varepsilon\frac{2\tau_w}{a} - \varepsilon\frac{dP_{sp}}{dz} + F_s \qquad (3.V\text{-}8)$$

The first term of the right hand side of equation (3.V-8) is related to the gas velocity V_{sp} by

$$\frac{2\tau_w}{a} = \frac{\lambda}{2a}\frac{1}{2}\rho_g V_{sp}^2 \qquad (3.V\text{-}9)$$

The third term of the right hand side of equation (3.V-8) is related to the spout gas velocity relative to that of the bed particles in the spout channel by

$$F_s = \beta(V_{sp} - V_d)^2 \qquad (3.V\text{-}10)$$

where β is a multiplication factor that has been proposed by Barnea and Mizrahi [15].

The momentum equation that can be applied to the particle flow in the spout channel reads:

$$\text{div}\,(1-\varepsilon)\rho_d\vec{V}_d\vec{V}_d = -(1-\varepsilon)\vec{\nabla}.\bar{\bar{\tau}}_c - \vec{\nabla}.(1-\varepsilon)\bar{\bar{T}}_d - (1-\varepsilon)\vec{\nabla}p$$

$$-(1-\varepsilon)\rho_d\vec{g} - \vec{F}_s \qquad (3.V\text{-}11)$$

When the shear stresses and the interparticle forces are neglected the z-component of equation (3.V-11) can be written as ($V_r = V_\phi = 0$):

$$\rho_d\frac{d}{dz}(1-\varepsilon)V_{dz}^2 = -(1-\varepsilon)\frac{dP_{sp}}{dz} + (1-\varepsilon)\rho_d g - F_s \qquad (3.V\text{-}12)$$

It is noted that it is assumed that the particle velocity $\vec{V}_d$ has no radial component over the whole cross section of the spout channel. This assumption implies that $\text{div}(1-\varepsilon)\vec{V}_d$ must have a defined non-zero value over that whole cross section of the spout channel:

$$\text{div}(1-\varepsilon)\vec{V}_d = \frac{d}{dz}(1-\varepsilon)V_{dz} = \text{source term}$$

$$= 2\pi a\, V_{da} \qquad (3.V\text{-}13)$$

where V_{da} is the entrainment velocity of the bed particles at the spout channel wall.

Equation (3.V-12) will now be integrated over the cross section of the spout channel.
Assume that

$$(1-\varepsilon)V_d^2 = \frac{2}{a^2}\int_0^a (1-\varepsilon)V_{dz}^2\, r\, dr \qquad (3.V\text{-}14)$$

or when the hold-up is constant over the cross section:

$$V_d^2 = \frac{2}{a^2}\int_0^a V_{dz}^2\, r\, dr \qquad (3.V\text{-}15)$$

It then follows from equations (3.V-12) and (3.V-15) that

$$\rho_d \frac{d}{dz}(1-\varepsilon)V_d^2 = -(1-\varepsilon)\frac{dP_{sp}}{dz} + (1-\varepsilon)\rho_d\, g - F_s \qquad (3.V\text{-}16)$$

When the relationship that Barnea and Mizrahi [15] have proposed for the interaction force F_s is substituted into equation (3.V-16), equation (3-71) is obtained.

List of symbols

A_n	coefficient defined by eq. (3-27) (n=0,1,2,..)	[N/m^2]
a	orifice radius (packed bed regime)	
	spout channel radius (stable spouted bed regime)	[m]
a^*	dimensionless orifice or spout channel radius (a/R)	[-]
B_n	coefficient defined by eq.(3-48) or (3-59)	[-]
B	multiplication factor (Lefroy and Davidson [8])	[-]
C	constant defined by eq. (3-62)	[kg/m^4]
C_D	drag coefficient of one particle	[-]
D	bed depth (thickness)	[m]
D	constant defined by eq.(3-62)	[kg/m^4]
D_C	column diameter	[m]
d_p	particle diameter	[m]
$\vec{F}_s$	interaction force per unit volume dense phase between gas and solid phase	[N/m^3]
H	bed height	[m]
H^*	dimensionless bed height (H/R)	[-]
H_m	maximum spoutable bed height	[m]
$I_0()$	zero order modified Bessel function of the first kind	
$I_1()$	first order modified Bessel function of the first kind	
$J_0()$	zero order Bessel function of the first kind	
$J_1()$	first order Bessel function of the first kind	
$K_0()$	zero order modified Bessel function of the second kind	
$K_1()$	first order modified Bessel function of the second kind	
K	permeability (general)	[m^2]
K_0	permeability of the spout channel	[m^2]
K_1	permeability of the dense phase	[m^2]
k	summation variable	[-]
ℓ	summation variable	[-]
m	$\pi/2H$ (Lefroy and Davidson [8])	[-]
n	summation variable	[-]
P	pressure in the bed	[N/m^2]
P_H	pressure above the bed (Lefroy and Davidson [8])	[N/m^2]

P_x	x-dependent solution of diff.eq.(3-35)	
P_r	r-dependent solution of diff.eq.(3-21)	
P_z	z-dependent solution of diff.eq.(3-21) or (3-35)	
P^*	dimensionless pressure defined by eq.(3-40A or B)	[-]
P_{sp}	pressure in the spout channel	[N/m^2]
P_{fl}	pressure beneath the sieve plate	[N/m^2]
ΔP_s	pressure drop over a spouted bed	[N/m^2]
ΔP_{fl}	pressure drop over a fluidised bed	[N/m^2]
Q_o	spout gas flow rate	[m^3/s]
Q_1	fluidisation gas flow rate	[m^3/s]
Q_o^*	dimensionless spout gas flow rate ($Q_o/(Q_o+Q_1)$)	[-]
R	bed radius	[m]
$\bar{\bar{R}}_c$	space averaged Reynolds stresses in the gas phase	[N/m^2]
r	radial distance	[m]
r^*	dimensionless radial distance (r/R)	[-]
s	distance to the orifice (section 3.3.3)	[m]
$\bar{\bar{T}}_d$	stress tensor in the dense phase	[N/m^2]
t	time	[s]
t_m	mean circulation time	[s]
$\vec{V}$	linear gas velocity	[m/s]
V_{fl}	vertical gas velocity at the sieve plate	[m/s]
V_{sp}	vertical gas velocity at the orifice	[m/s]
V_{ra}	radial component of gas velocity at the spout channel wall	[m/s]
$\vec{V}_d$	dispersed phase velocity	[m/s]
$V_{z,H}$	linear gas velocity at the top of a bed with height H	[m/s]
V_{z,H_m}	linear gas velocity at the top of a bed with maximum spoutable bed height	[m/s]
V_{mf}	minimum fluidisation velocity	[m/s]
V_x	component of the gas velocity in the x-direction	[m/s]
V_z	component of gas velocity in the z-direction	[m/s]
V_{spo}	gas velocity in the spout channel at z=0	[m/s]
V_{spH}	gas velocity in the spout channel at z=H	[m/s]
V_{da}	particle entrainment velocity	[m/s]
W	circulation rate of the bed material	[m^3/s]

x	horizontal coordinate in the plane of the flat bed	[m]
x^*	dimensionless horizontal coordinate (x/R)	[-]
$Y_o()$	zero order Bessel function of the second kind	
y	horizontal coordinate perpendicular to the plane of the flat bed	[m]
z	vertical coordinate	[m]
$z*$	dimensionless vertical coordinate	[-]
α	constant in eq.(3-22) and (3-23) or eq.(3-36) and (3-37)	[-]
α_n	coefficient in pressure distribution model	[m^{-1}]
α_n^*	dimensionless coefficient in pressure distribution model	[-]
β	factor defined by eq.(3-17)	
ε	porosity (in the annulus or in the spout channel)	[-]
ε_s	spout channel porosity at z=H	[-]
η	dynamic viscosity of the gas phase	[Ns/m^2]
λ	friction factor of the spout channel	[-]
ρ_g	density of the gas phase	[kg/m^3]
ρ_d	density of the dispersed phase	[kg/m^3]
$\bar{\bar{\tau}}_c$	shear stresses in the gas phase	[N/m^2]
ϕ	function (Nagarkatti and Chatterjee [9])	[-]

4. EXPERIMENTAL PRESSURE DISTRIBUTIONS IN SPOUT-FLUID BEDS

4.1 The 15.2 cm diameter spout-fluid bed

4.1.1 The equipment

The 15.2 cm diameter spout-fluid bed was fitted with a pressure probe that could be placed in any position in the bed. The probe was mounted on the top cover of the bed and could be rotated and moved in vertical direction (figure 4.1).

The pressure drop was measured between the probe tip and the top of the bed when the bed was operated in a given flow regime at constant flow rates of fluidisation and spouting gas.

The probe was designed in such a way that it would affect the bed structure as little as possible (figure 4.2). The pressures that were

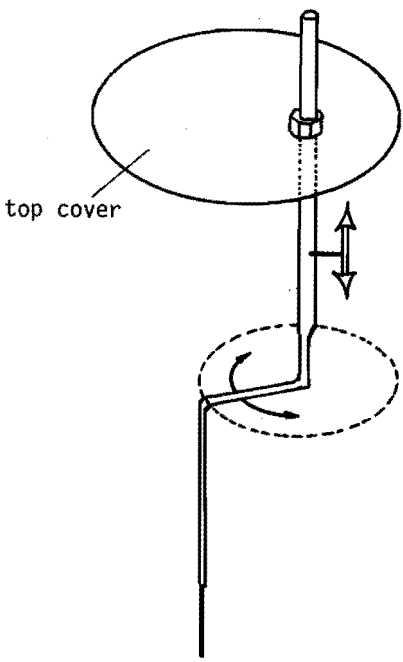

Figure 4.1. The pressure probe mounted at the top cover of the bed.

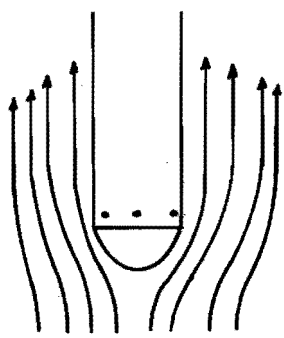

Figure 4.2. The round tip of the pressure probe (diameter probe = 3 mm, diameter holes = 0.3 mm).

measured by means of the probe proved to be most reliable when the probe was fitted with a round tip (diameter 3 mm).
The probe was mounted excentrically on the top cover to make it possible to place the probe tip in any point of the annulus by turning the probe (figure 4.3).
The radial positions of the probe could be read from a graduated scale. The vertical positions of the probe was read from measuring marks made on the stem of the probe. The probe tip was fitted with some holes of 0.3 mm diameter to permit the pressure measurement to be made.
Pressures were measured by means of an inductive difference pressure transducer (type Hottinger-Baldwin PD1/0.1). The inductive transducer was connected with a Hottinger-Baldwin KWS 6A-5 measuring bridge and amplifier. The output signal was recorded. It was calibrated with a water manometer.

4.1.2 Measuring method and results

As pressure distributions tend to be flat when fluidisation gas is also introduced the pressure data were obtained at zero fluidisation gas velocity.
The results of the pressure measurements are greatly influenced by the

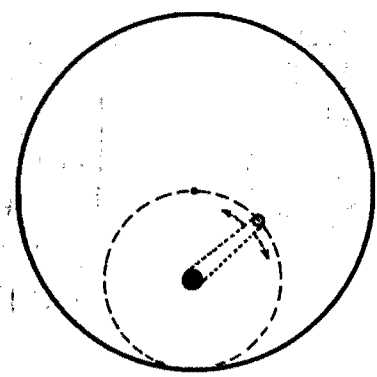

Figure 4.3. The excentrical mounting of the pressure at the top cover (top view).

difficulty of obtaining a reproducible bed structure. It was not possible to obtain sufficiently reproducible measurements with the bed in the packed bed flow regime in the 15.2 cm diameter spout-fluid bed. The probe did disturb the static bed structure in the packed bed regime when the probe was inserted from above. The reason probably is that vertical channels of high permeability are formed near the stem of the probe (figure 4.4).
Pressure measurements were reasonably reproducible when the bed was in the spouted bed flow regime except at locations close to the spout channel. In the stable spouted bed regime the probe hardly disturbed the bed structure. The reason is that the dynamic behaviour of the bed in the stable spouted bed regime prevents channeling.

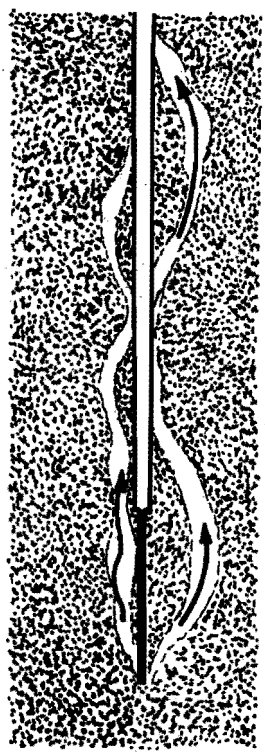

Figure 4.4. Assumed formation of vertical flow channels near the stem of the pressure probe.

Measurements were carried out at spout gas rates that varied from 4.53 ℓ/s to 7.25 ℓ/s.
Measurements were carried out at a fixed position of the probe while the spout gas flow was varied. This was done to reduce the errors that result from the poor reproducibility of the bed structure. Fluctuations in the measurements were smoothed out by plotting the measured pressure data against spout gas rate for each position in the bed and fitting a smooth curve to these data points.
Pressures read from such curves are shown in figure 4.5 for 25 positions in the bed at spout gas rates of 5, 6 and 7 ℓ/s.

4.2 The 45 cm diameter spout-fluid bed

4.2.1 The equipment

The 45 cm diameter bed was fitted at the bed wall with four sets of 27 holes placed in a vertical line at regular distances. Pressure probes can be introduced into the bed through these holes. At every level 4 holes were positioned in a horizontal plane at 90 degrees intervals (figure 4.6). A pressure probe that was inserted into the bed through a hole could be moved in radial direction only.
Pressure differences were measured between the probe tip at a given position in the bed and the free space above the bed.
As in the case of the 15.2 cm bed the probe tip had a diameter of 3 mm and was fitted with pressure taps of 0.3 mm diameter. The probe was found to have little effect on the bed structure.
Pressures were measured by means of the Hottinger-Baldwin inductive difference pressure transducer and the measuring bridge that were mentioned above.

4.2.2 Measuring method and results

Sufficiently reproducible measurements with the bed in the stable spouted bed regime could not be obtained in this spout-fluid bed. Pressure measurements with the bed in the packed bed flow regime were reasonably reproducible. The probe tip did not affect the bed to any marked degree. This is probably due to the fact that in this regime horizontally inserted probes do not lead to the formation of long vertical channels in the bed that show high permeability (figure 4.7).

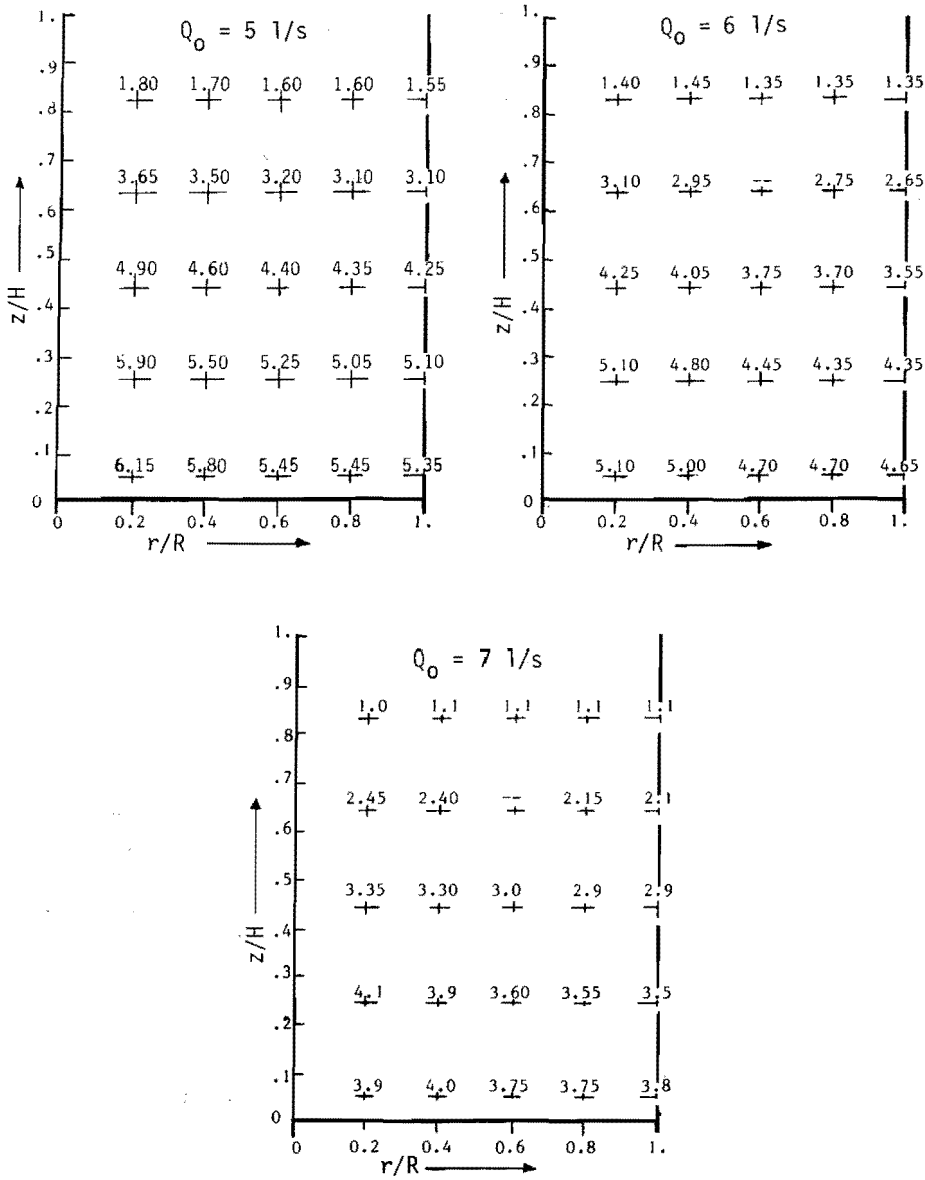

Figure 4.5. Measured pressures with respect to the pressure above the bed for 25 positions in the bed (10^{-3} bar).

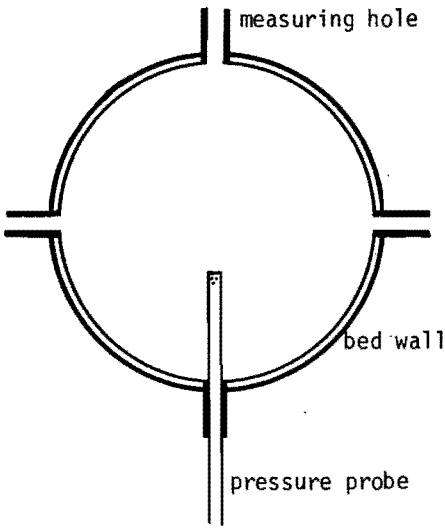

Figure 4.6. Cross section of 4 measurement holes in the bed wall. View of the pressure probe that is inserted into the bed.

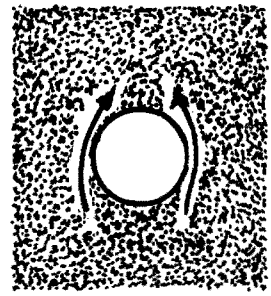

Figure 4.7. Assumed vertical flow channels near a horizontal probe (cross section).

Measurements were carried out at spout gas rates that varied from 3.96 ℓ/s to 17.84 ℓ/s, corresponding to superficial gas velocities ranging from 2.5 m/s to 11.2 m/s, while no fluidisation gas was introduced. In order to reduce errors that might result from poor reproducibility the measurements were carried out by keeping the probe point in a given fixed position while the spout gas rate was varied in the range that was specified above.

Figure 4.8 presents graphs of the measured dimensionless pressures that were measured at several radial positions and at a height of 5.5 cm and 15.5 cm above the sieve plate as a function of the superficial spout gas velocity with zero fluidisation gas velocity. The dimensionless pressures were obtained by dividing the experimental results by the pressure drop over the bed that would exist if the bed were fluidised at a gas rate equal to the spout gas flow rate that was used in the actual experiment.

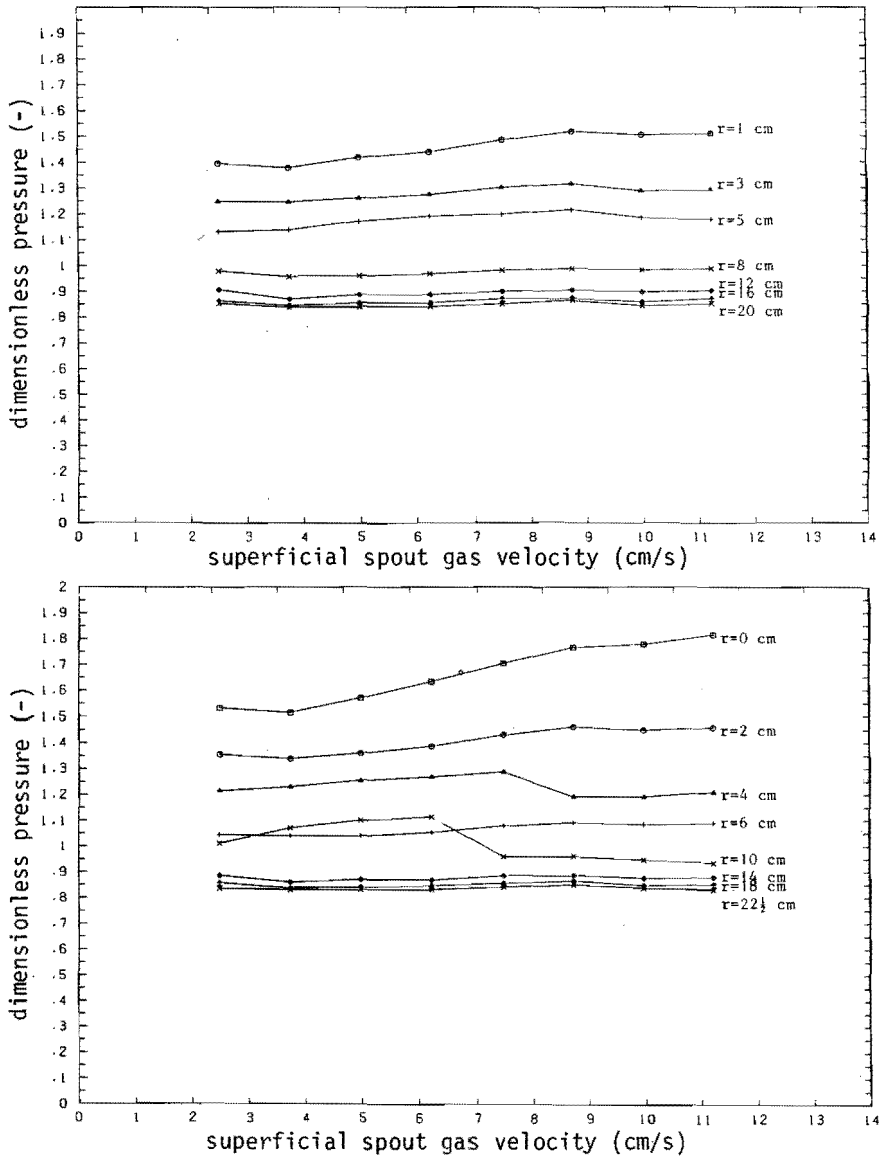

Figure 4.8A. Measured dimensionless pressures P for several radial positions (z=5.5 cm). The bed is in the packed bed flow regime. Introduction of spout gas only.*

$P^* = P/(\frac{\eta}{K_1} \cdot V_{spsup} \cdot H)$.

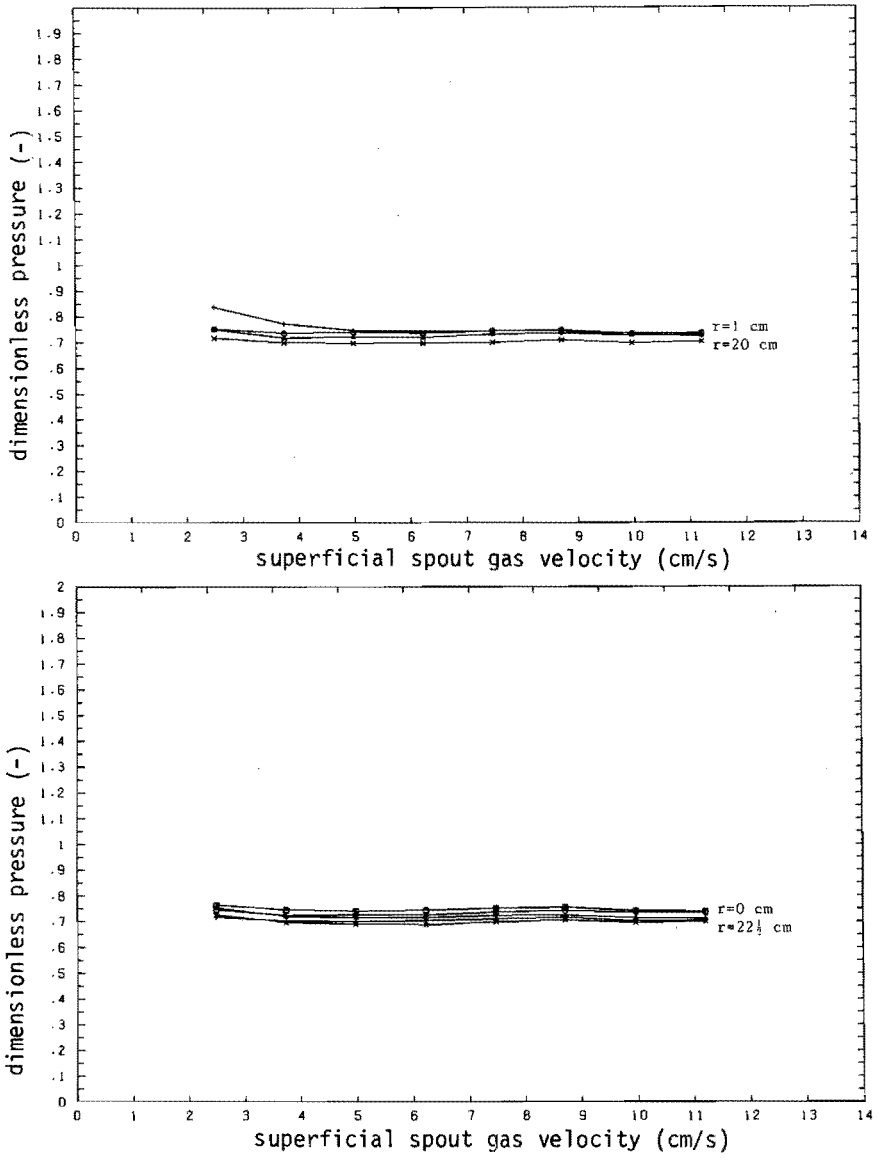

Figure 4.8B. Measured dimensionless pressures P for several radial positions (z=15.5 cm). The bed is in the packed bed flow regime. Introduction of spout gas only.*
$P^* = P/(\frac{\eta}{K_1} \cdot V_{spsup} \cdot H)$.

It can be seen that at all positions the dimensionless pressure varies with the gas rate at all radial positions where measurements were carried out. This does not agree with the prediction from the flow model.

4.3 Comparison of the experiments with the flow models

The results of the pressure measurements carried out in the 45 cm diameter bed and in the 15.2 cm diameter bed were compared to calculated pressures, using the model for the packed bed and for the stable spouted bed regime.
The properties of the bed material (fluidisation pressure drop curve and particle size distribution) are given in figures 2.1 and 2.2 of chapter 2.

4.3.1 The 45 cm diameter bed

The pressure measurements in the packed bed regime are compared to the results of the theoretical model. The bed used for this comparison had the following properties:

H = 60 cm, R = 22.5 cm, a = 1.5 cm

No fluidisation gas was introduced, so that $Q_1=0$.
Figure 4.9 presents a comparison of dimensionless pressures that were measured at various positions in the bed which was operated in the packed bed regime to the corresponding dimensionless pressures that were calculated from the model described in chapter 3.

It is seen that the agreement between the model and most of the measured pressures is reasonable. The measurements that were carried out near the orifice were subject to very considerable errors. There was a considerable increase of the dimensionless pressure near the orifice when the spout gas rate increases (figure 4.8A).

This may be due to the following reasons:

1. The formation of a strong and densely packed region above the orifice that is formed under the influence of a high pressure gradient at that position, the diameter of which increases with the gas rate.
2. The influence of the quadratic part of the Ergun relation for the

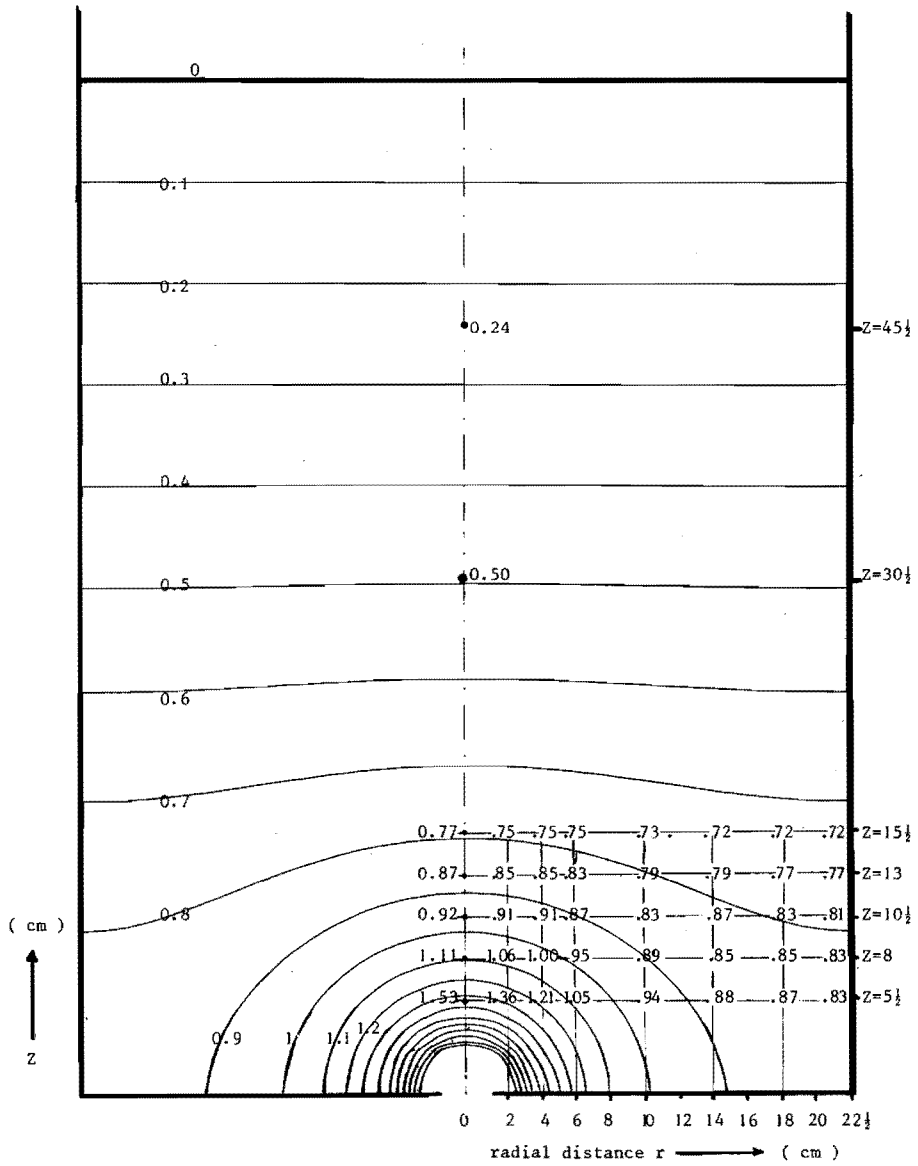

Figure 4.9. Measured dimensionless pressures at several places in the bed (H = 60 cm, R = 22.5 cm, a = 1.5 cm) and the calculated distribution of the dimensionless pressure when the bed is in the packed bed flow regime (H/R = 1.33, a/R = 0.0667). No fluidisation gas is introduced.

bed material probably cannot be neglected near the orifice.

3. The permeability of the gas distributor plate influences the pressure distribution near the plate and the orifice.

The first and second point would lead to a measured pressure drop that is higher than the one that is calculated from the model.
The third point should cause the measured pressure profile near the distributor plate to be flatter than the one that is calculated from the model.

4.3.2 The 15.2 cm diameter bed

The pressure measurements in the stable spouted bed regime cannot be compared directly to the results from the models because several parameters such as the spout channel diameter and the hold-up of entrained particles in the spout channel are not known.
As was already pointed out earlier the calculated pressure distribution in the spouted bed depends to a large extent on the assumptions that have been made concerning the flow of gas in the spout channel.
Calculations have been carried out using the models for stable spouted bed flow. The following parameter values were applied:

$R = 7.62$ cm, $H = 20.5$ cm.

The bed porosity was assumed to be 0.42, the mean particle diameter was set at 0.56 mm. The spout gas flow rates were taken to be 5, 6 and 7 ℓ/s in accordance with the conditions used during the actual measurements. The mean particle diameter is employed as a measure of the roughness of the spout channel wall which is required to compute the friction factor of the spout channel (see Appendix 3-IV). It is also used to compute the gas to particle interaction forces in the spout channel (see section 3.2.3).

4.3.2.1 The simple pressure distribution model

The simple model that only takes pressure and wall friction forces into account is considered first. The simple model is based on the assumption that a linear relationship exists between the wall friction in the spout channel and the local gas velocity in the spout channel. The value of the unknown spout channel radius is obtained by a curve fitting procedure of the calculated values of the bed wall pressures to

the experimentally measured bed wall pressures.
Bed wall pressures were computed for this purpose for several values of the spout channel radius and compared to the measured data. The comparison is shown in figure 4.10. It is seen from this figure that the measured and computed values of the pressure at the bed wall show the closest agreement for a spout channel radius of a = 0.59 cm when Q_0 = 5 ℓ/s. For Q_0 = 6 ℓ/s the best agreement is obtained when the spout channel radius is a = 0.65 cm. At Q_0 = 7 ℓ/s a spout radius a = 0.73 cm gives the best fit.

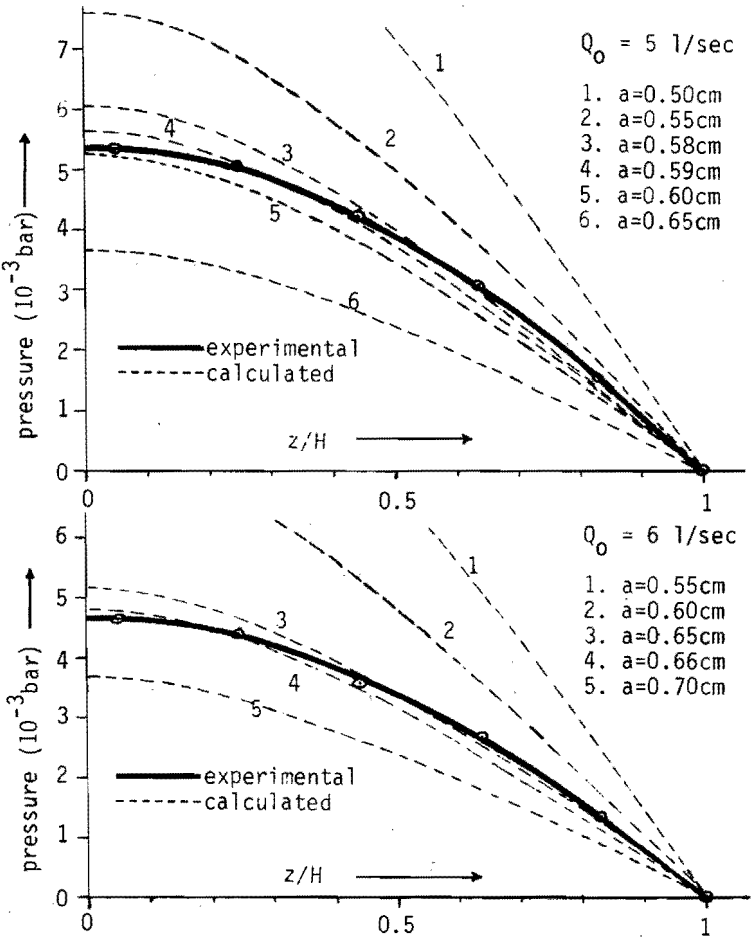

Figure 4.10. Comparison between measured and computed bed wall pressures using the simple pressure distribution model.
(R = 7.6 cm, H = 20.5 cm, assumed spout channel radius a as indicated).

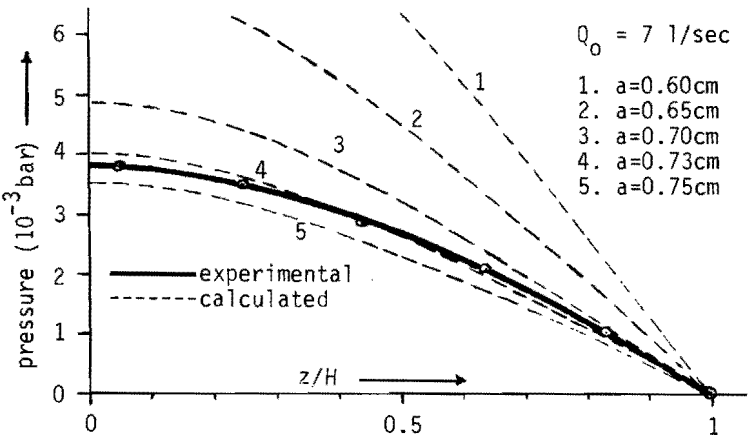

Figure 4.10. Comparison between measured and computed bed wall pressures using the simple pressure distribution model. (R = 7.6 cm, H = 20.5 cm, assumed spout channel radius a as indicated).

Figure 4.11 presents the experimentally determined values of the pressure together with the pressures that were calculated from the model, using the above best fit values of the channel radius.
It follows from the comparisons in figures 4.10 and 4.11 that the calculated values of the pressure are too high in the bottom and too low in the top section of the bed. This discrepancy between experimental and calculated values was to be expected, because of the linear relationship that was assumed to exist between wall friction and local spout gas velocity and because the inertial forces and interaction forces in the gas flow were neglected.
The simple model can be used for a first approximation. However, this model is too much of an oversimplification to give reliable pressure data.

4.3.2.2 The extended model

The more extensive model that also takes inertial and interaction forces into account is now compared to the pressure distributions that were measured in the stable spouted bed regime.
The same curve fitting procedure that was described above was again applied to obtain the best values of the spout channel radius at

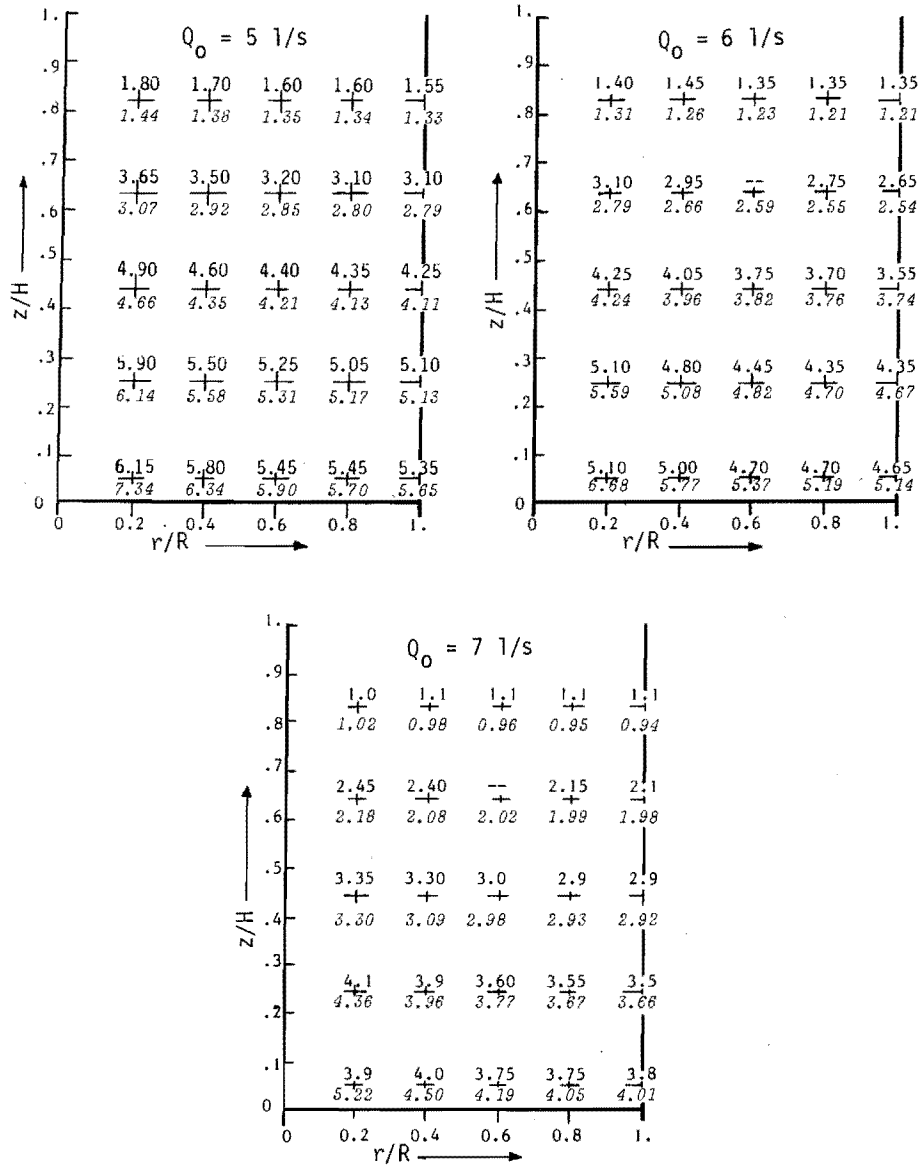

Figure 4.11. Comparison between measured and calculated pressures for 25 positions in the bed (in 10^{-3} bar). Calculated pressures in italics are based on spout channel radii obtained from the best fit in figure 4.10. Pressures are given with respect to the pressure above the bed.

assumed maximum hold-ups of bed particles in the spout channel of 0.001, 0.002, 0.003 and 0.004.
Table 4-1 summarizes the results of the curve fitting procedure.

$1-\varepsilon_s$	Q_0 = 5 ℓ/s	Q_0 = 6 ℓ/s	Q_0 = 7 ℓ/s
0	a = 0.51 cm	a = 0.59 cm	a = 0.68 cm
0.001	a = 0.54 cm	a = 0.62 cm	a = 0.72 cm
0.002	a = 0.57 cm	a = 0.65 cm	a = 0.76 cm
0.003	a = 0.59 cm	a = 0.68 cm	a = 0.79 cm
0.004	a = 0.62 cm	a = 0.72 cm	a = 0.82 cm

Table 4-1. Results of the curve fitting procedure to the pressure distribution at the bed wall r=R
$1-\varepsilon_s$ = assumed hold-up of bed particles at the top of the spout channel
Q_0 = spout gas flow rate
a = assumed spout channel radius

Figures 4.12A, B and C show some comparisons of the measured pressures at the bed wall r=R and at the position r = 0.2 R to computed values. The hold-up $1-\varepsilon_s$ is seen to have only a negligible influence on the bed wall pressures (curve 2 in figures 4.12A, B and C that represent the pressures for the values of the spout channel hold-up that were considered).
The curves which were obtained by calculation at a value of $1-\varepsilon_s = 0.004$ (curve 5) fit the experimental data at r = 0.2 R better than the curve that was obtained by calculation at $1-\varepsilon_s = 0$ (curve 4).
It can thus be concluded that the pressure distribution in the annulus of the spout-fluid bed is reasonably well described by the extended flow model when some degree of particle to gas interaction is assumed to exist in the spout channel, while the particle hold-up in the spout channel is held to depend linearly on the height in the bed.
It is found that the agreement between measured and calculated pres-

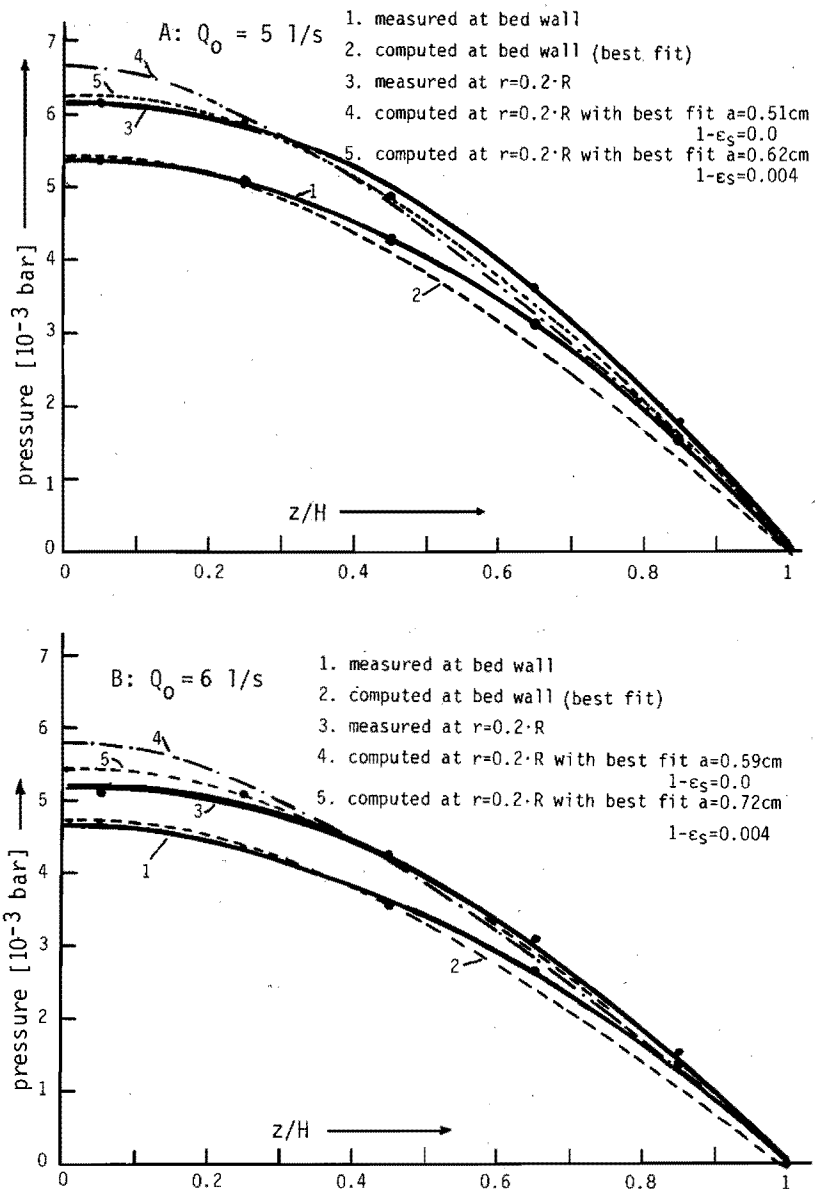

Figure 4.12A-B. Comparison of measured pressures at r=R and r=0.2R to pressures calculated from the extended flow model for spouted beds.

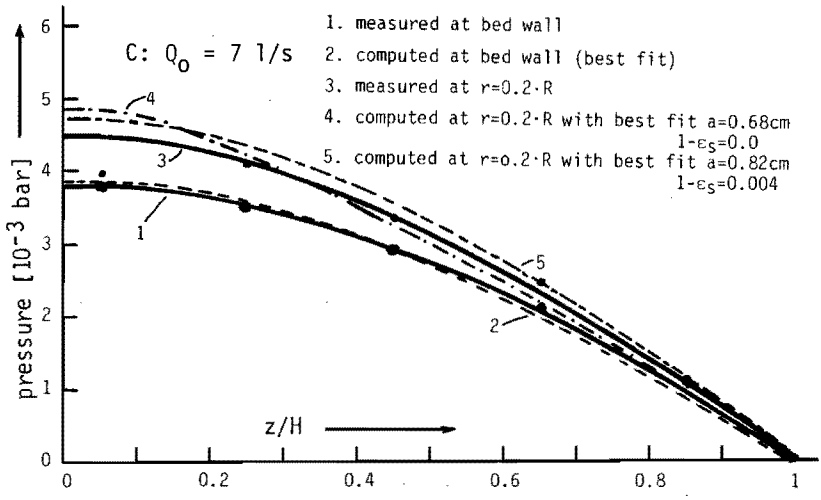

Figure 4.12C. Comparison of measured pressures at r=R and r=0.2R to pressures calculated from the extended flow model for spouted beds.

sure values is reasonably good when a maximum hold-up $1-\varepsilon_s = 0.004$ is assumed to exist in the spout channel together with a value of the spout channel radius which is obtained form the curve fitting procedure.

The figures 4.13A and 4.13B show pressures measured at r = 0.2R and r = R respectively as functions of height z for a spout gas flow rate Q_o = 5 l/s. These profiles are compared to the longitudinal pressure profiles at the same radial distances that were calculated by means of the simple model and of the extended model assuming $1-\varepsilon_s = 0.004$. It is clear from the comparisons that the extended model fits the measured pressure profile better than the simple model. The differences between the results of the two models diminish with increasing radial distance from the bed axis (compare figure 4.13A (r =0.2R) and 4.13B (r=R)).

In judging the value of the resemblances between the measured and calculated pressure profiles it should of course be recalled that the spout channel radius has been selected such that the calculated pressure profile fits the measured pressure profile best. The spout channel radii that produced the closest pressure profile fit were different for the two models (compare figure 4.10, figure 4.12 and table 4-I).

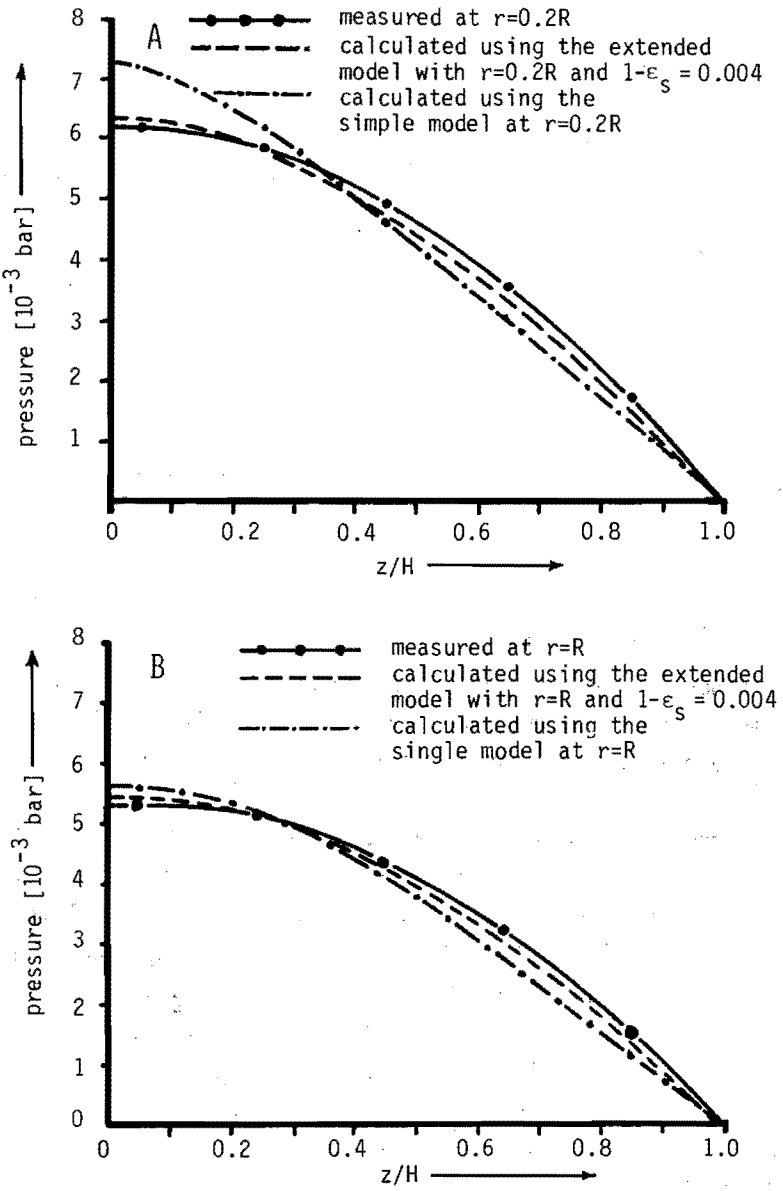

Figure 4.13. Comparison between measured pressures and calculated longitudinal pressure profiles using the simple model and the extended model assuming $1-\varepsilon_s = 0.004$ *(*Q_o *= 5 ℓ/s, r = 0.2R and r = R).*

4.4 Conclusions

4.4.1 The packed bed flow regime

The pressures that were measured in the packed bed regime by means of a probe that was horizontally inserted into the bed were reasonably reproducible. The relationship between the pressures obtained in this manner and the spout gas rate was not linear. This does not agree with what the pressure distribution model for the packed bed flow regime predicts.

This non-linearity is probably caused by the occurence of a region near the spout orifice that has a more densely packed structure than the remaining part of the bed. This region of relatively low porosity expands slightly at increasing spout gas flow rate due to the reaction of the bed solids to the pressure gradients that exists in the bed structure. The model, however, assumes a bed porosity that is constant over the bed and independent of the gas rate.

The influence of this non-uniformity in the packing of the solids diminishes at low spout gas rates. The measured pressure distribution is then well described by the model for the packed bed flow regime (see the comparison in figure 4.9).

4.4.2 The stable spouted bed regime

-The pressures which were measured in a bed that shows a stable spout channel by means of a probe that was inserted vertically into the bed were reasonably reproducible. These pressures were found to depend on the spout gas rate.

Pressure measurements that were carried out near the spout channel showed irregularities and fluctuations which are due to the fact that the pressure probe interferes with the flow of the bed solids near the wall of the spout channel and disturbs the spout channel wall itself.

-An equilibrium exists at each point on the spout channel wall between the local gas pressure in the spout channel and the hydrostatic pressure which is caused by the weight of the bed solids in the annulus above that point.

The diameter of the spout channel is determined by the spout gas flow rate. When the spout gas rate is increased the spout channel is widened until a new equilibrium has been established at the spout channel

wall. This can even result in a decrease of the gas pressure in the spout channel at increasing spout gas flow rate (figure 4.10).

-In the limiting case where no fluidisation gas is introduced into the bed the longitudinal pressure profile can be approximated by a quarter cosine curve. Lefroy and Davidson have found that this cosine relation applies under minimum spouting condition and at maximum spoutable bed height. The pressure distribution model presented here is, however, generally valid. Its applicability is not limited to specific spouting conditions or to beds of special heights. In addition the present model not only holds for spouted beds but also for spout-fluid beds.

-In the limiting case where a relatively large amount of fluidisation gas is introduced into the spout-fluid bed the longitudinal pressure profile can be approximated by a straight line. This can be understood as follows:

1. When the fluidisation gas rate is increased the hydrostatic pressure due to the weight of the bed solids in the annulus approximates a straight line. This fact is explained by the influence that the gas flow in the interstitial space has on the stresses between the annulus solids. These stresses diminish as the interstitial gas velocities increase. The fraction of the weight of the bed that the vertical bed wall can carry therefore decreases. The hydrostatic pressure profile thus becomes more nearly linear.
2. It may be assumed that the pressure profile in the spout channel also approximates a straight line more closely as the fluidisation gas rate is increased.
   This is explained by the decrease of the dissipation of the kinetic energy of the gas flow in the spout channel at the bottom of the bed. As the fluidisation gas rate increases the cross flow of gas from the spout channel into the annulus must decrease. Therefore the diameter of the spout channel must decrease so that it becomes more nearly equal to the diameter of the spout orifice. The dissipation that is required for channel wall maintenance must thus diminish.

List of symbols

a	orifice radius (packed bed regime)	
	spout channel radius (stable spouted bed regime)	[m]
a^*	dimensionless orifice or spout channel radius (a/R)	[-]
H	bed height	[m]
H^*	dimensionless bed height (H/R)	[-]
K_1	permeability of the dense phase	[m^2]
P	pressure in the bed relative to that above the bed	[N/m^2]
P^*	dimensionless pressure	[-]
Q_o	spout gas flow rate	[m^3/s]
Q_1	fluidisation gas flow rate	[m^3/s]
Q_o^*	dimensionless spout gas flow rate ($Q_o/(Q_o+Q_1)$)	[-]
R	bed radius	[m]
r	radial distance from bed axis	[m]
$V_{sp\ sup}$	superficial spout gas velocity	[m/s]
z	vertical coordinate	[m]
ε_s	porosity of the spout channel at z=H	[-]
η	dynamic viscosity of the gas phase	[Ns/m^2]

5. SOLIDS CIRCULATION IN A SPOUT-FLUID BED

5.1 Introduction

It was stated in chapter 1 that the spout-fluid bed is suitable for handling dispersions that contain both fine and coarse solid particles. It can also be used for handling mixed dispersions which contain material that cannot be fluidised as such in addition to material that can be fluidised. Good mixing is established in the same way as in a spouted bed, i.e. by a well developed overall circulation of the bed material, comprising the total volume of the bed, a large variation in the circulation times of the bed particles, and a sufficient degree of particle exchange between the circulation paths.
The overall circulation is induced by an upwards flow of bed material in the spout channel. The exchange of particles between the circulation paths mainly occurs in the fountain region.

Several publications are available that deal with properties of circulating systems or continuous flow systems with recycle in general and the mixing and circulation behaviour of solids in spouted beds in particular.
Chatterjee [1] studied the internal solid circulation rate in a spouted bed. He obtained data on unsteady state mixing by letting spouting air flow for limited periods of time through beds that contain two sorts of particles that had different colours.
The circulation rates of the solid particles were correlated with fluid flow rate, particle diameter and particle density. The circulation rate appeared to depend much more on the spout gas flow rate than on the other factors. This author also found that the circulation rate of the solid particles increases with increasing gas flow rate and with increasing particle diameter while it decreases with increasing particle density.
Mann and Crosby [2] determined the circulation time distribution of a magnetic particle by means of a coil that was located around the spout channel just inside the fountain region above the bed. They concluded that both their own technique and the one that was used by van Velsen et al. [7] who used a radioactive particle are suitable for measuring circulation time distributions in spouted beds. The method that employs

a radioactive particle provides detailed information on the particle trajectories and axial velocities not only in the fountain but also in the bed. It can be applied to any spouted bed the particles of which can contain a traceable amount of radioactive material. However, elaborate monitoring equipment is required. The technique in which a magnetic tracer particle is used is, in the opinion of Mann and Crosby, relatively simple and does not require very expensive monitoring apparatus. Its application is, however, limited to spouted beds with relatively large and heavy particles.

Takeda and Yamanoto [3] analysed the mixing of particles in a spouted bed. They proposed a mixing model in which the spout is assumed to be a perfect mixer while piston flow with decreasing downward velocity is assumed to occur in the annulus. The bed material is entrained from the spout channel wall into the spout channel below a certain height. Tracer particles were injected into a bed that was being operated under constant flow conditions. The concentration of tracer particles in the spout was then measured. The above model proposed by Takeda and Yamanoto was found to describe the mixing in the bed satisfactory when the particle concentration in the spout is corrected to take a certain amount of mixing in the annulus into account. Increasing the flow rate of the spout gas shortened the cycle time but did not significantly affect the mixing rate.

Vadja [4] calculated the residence time distributions of solids in a spouted bed. He developed a model in which a spouted bed is represented as a continuous flow system with a recirculation flow. Solids flow into the spouted bed at the top of the annulus and out of the bed at the bottom. The author calculated the response to a step signal assuming the existence of two extreme mixing patterns.

In the first pattern plug flow occurs in all regions of the spouted bed apparatus. In the second pattern mixing is ideal in the spout channel and fountain region while plug flow occurs in the annulus region.

It was found that the model did not yield significantly different results for these two extremes.

Robinson and Waldie [5] describe an experimental study on the circulation behaviour of solids in a spouted bed of particles that show a particle size distribution. The circulation of the solids were determined by means of optical techniques in which coloured tracer particles were

used that were observed at the flat face of a half-cylindrical column. They found that in the same bed large particles more often follow short cycle paths in short cycle times whereas small particles more often follow long cycle paths that they complete in longer cycle times. They explained this observation on the basis of two mechanisms: In the first place the radial component of the gas velocity in the annulus prevents smaller particles from reaching the spout channel. In the second place smaller particles may percolate through layers of larger ones under the influence of strains that occur in the annulus and of vibrations that are due to minor pulsations. Another feature of the trajectories that they observed was the tendency that medium and small size particles showed to travel nearly vertically downwards in the annulus just before they reached the spout channel.
Suciu and Patrascu [6] investigated particle circulation in a half-cylindrical column by means of a high speed camera. They found from characteristic pictures that show the particle trajectories in the spout channel and in the annulus that the particle velocity in the annulus depends on the radial position of the particle in the annulus.
Van Velzen et al. [7] determined the movements of the solid particles in a spouted bed by means of a radioactive tracer particle. These authors found that the circulation rate of the solid particles was proportional to the gas flow rate. The circulation rate also was a function of the bed geometry, the gas density and the particle diameter.
Mann and Crosby [8] studied the circulation time distribution of solid particles in closed, steady state circulating systems and related them to the residence time distributions in the regions which make up these systems. The theory that these authors propose applies only to systems that consist of regions that have closed boundaries through which no diffusion can take place. The analysis that these authors have published is discussed in section 5.2.

5.2 Model of circulation flow

5.2.1 Introduction

A model is developed which describes circulating systems. The model is analogous to many models that describe continuous flow systems.
A circulating system is defined as a closed system in which all fluid

elements pass periodically through at least one specified cross section. In circulating systems no tracer material leaves the system. In general such a system can be represented schematically by figure 5.1 where the system is symbolized by the rectangle and by the circulation path. The circulation path denotes the passage of the material in the system through that specified cross section where all fluid passes periodically. Each cycle of an element of material is assumed to be independent of each previous cycle of that element of material.
In general the material may be composed of different kinds of elements that have different properties, for example particles which have different sizes or densities. Since the flow characteristics may vary between the elements of the material the flow of each element should be considered separately.

The cycle time or circulation time is defined as the time that elapses between two consecutive passages of a certain element of the material past the cross section through which all material passes.
Because elements of the flowing material follow different paths or because fluctuations in the flow occur the cycle time is a random variable with the probability density function $h(t)$. Therefore $h(t).\Delta t$ is the probability that the random variable representing the

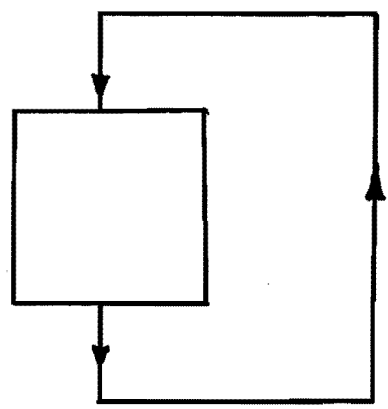

Figure 5.1. Schematic presentation of a circulating system.

cycle time of an element of material lies within the interval between t and t+Δt.
The mean circulation time θ of the material element and its variance σ^2 can be found from the probability density function h(t) of the cycle time (appendix 5.I). The circulation time distribution of an element of the flowing material depends on the geometry of the system and on the flow condition of the material in the system.
Some relationships that have to do with circulation flow are introduced in section 5.2.2.
Section 5.2.3 deals with a circulation flow model that is applied to spout-fluid beds. The model proposes that the mixing of the bed solids in the annulus occurs because particles in different radial positions follow different trajectories and because the bed particles while flowing over an individual trajectory undergo mixing by fluctuations in the flow.
Results obtained from the model are shown at the end of this chapter.

5.2.2 Modelling circulation time distribution

5.2.2.1 Systems with purely convective recirculation

General relationships which hold for circulating systems can be developed in analogy with continuous flow systems. The circulation time distribution depends on the flow pattern of the material in the system. When the circulating system consists of several separate flow regions the circulation time distribution depends on the residence time distributions of the individual regions.
When the circulating system consists of several flow regions that are connected in series the random cycle time is the sum of the times a particle has spent in those regions. The resulting circulation time distribution is then a convolution of the distribution functions of the residence times of the separate flow regions. For example when the residence times of 2 regions in series (denoted as "1" and "2" in figure 5.2) are assumed to be independent random variables with distribution function $f_1(t)$ and $f_2(t)$ respectively then the distribution function h(t) of the cycle time is expressed by

$$h(t) = \int_0^t f_1(t')\, f_2(t-t')\, dt' \qquad (5\text{-}1)$$

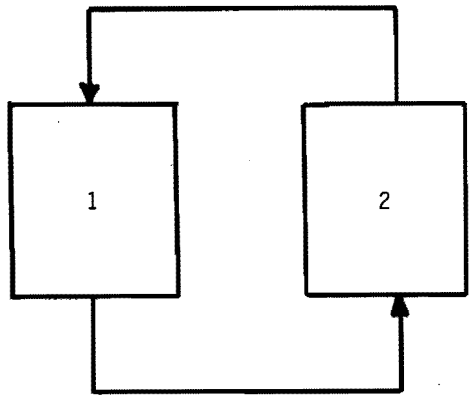

Figure 5.2. Circulating system with two regions in series.

Equation (5-1) can be understood as follows: The probability that a particle resides in region 1 for a time between t_1 and t_1+dt_1 is equal to $f_1(t_1)dt_1$ while the probability that a particle resides in region 2 for a time between t_2 and t_2+dt is equal to $f_2(t)dt_2$. The probability that a particle completes a cycle in a time between t and t+dt is equal to the conditional probability that having spent a time $t'<t$ in region 1 it will spend a time t-t' in region 2.

When the circulating system consists of several flow regions that are connected in parallel the circulation time distribution h(t) can be expressed in terms of the distribution functions $f_i(t)$ of the flow regions by:

$$h(t) = \sum_{i=1}^{n} q_i \, f_i(t) \qquad (5\text{-}2)$$

where q_i is the fraction of the material that passes the i^{th} region ($\sum_{i=1}^{n} q_i = 1$).

For example when the residence times of 2 regions "1" and "2" in parallel are independent random variables with distribution functions $f_1(t)$ and $f_2(t)$ respectively (figure 5.3), then the distribution function h(t) can be expressed by

$$h(t) = q_1 f_1(t) + q_2 f_2(t) \qquad (5\text{-}3)$$

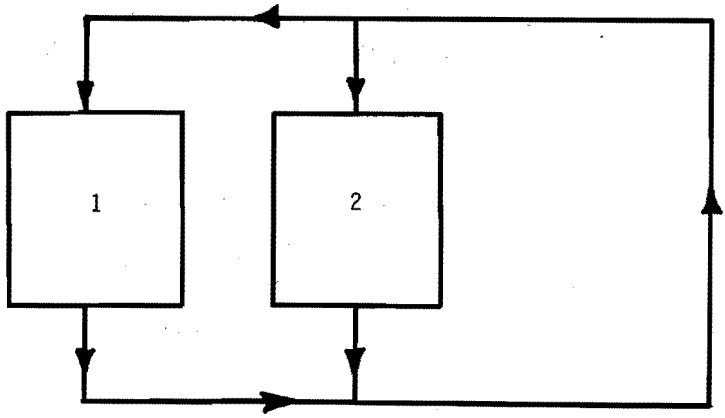

Figure 5.3. Circulating system with two regions in parallel.

It follows that whenever the residence time distribution of each of the flow regions is known the circulation time distribution of the material in the system can be evaluated.

The experimental investigation into the circulation time distribution can be achieved either by use of a single tagged particle or by injection of a certain amount of tracer material to which a concentration can be assigned. Use of a single tagged particle allows direct measurement of the time elapsed between two consecutive passages of the particle past the detection point. Measurements are continued until enough data have been collected for the determination of a reliable circulation time distribution. It should be noted, however, that the measured circulation time distribution generally depends on the properties of the tagged particle. When the circulation properties of a fluid are to be determined the tagged particle should have a negligible slip velocity with respect to the surrounding material. The tagged particle then must have the same density and size as the elements of the material in the system. When, in general, the circulation behaviour of the different elements of a non-homogeneous material are to be determined the experiments have to be repeated with a series of tagged particles. This method is simple and yields the circulation time distribution directly. It is, however, time consuming.
A second experimental method is the injection of an amount of tracer material, that is injected into the system at the point where all the

material in the system passes. The tracer concentration is measured at that point as a function of time. However, the response differs from that which is obtained in a continuous flow system since the tracer material remains in the system.

A relationship between the measured concentration of the tracer C(t), the injection rate T(t) of the tracer material and the probability density function h(t) of the circulation time can easily be derived for systems where convective recirculation flow only occurs along the recirculation path (figure 5.4).
When a tracer is injected into the recirculation path the tracer concentration downstream the injection point, C'(t), can be expressed by:

$$C'(t) = C(t) + \frac{1}{Q} T(t) \qquad (5\text{-}4)$$

where Q is defined as the circulation rate of the material in the system and C(t) is the tracer concentration in the recirculation path upstream the injection point. The amount of injected tracer material is assumed to be negligible with respect to the total amount of

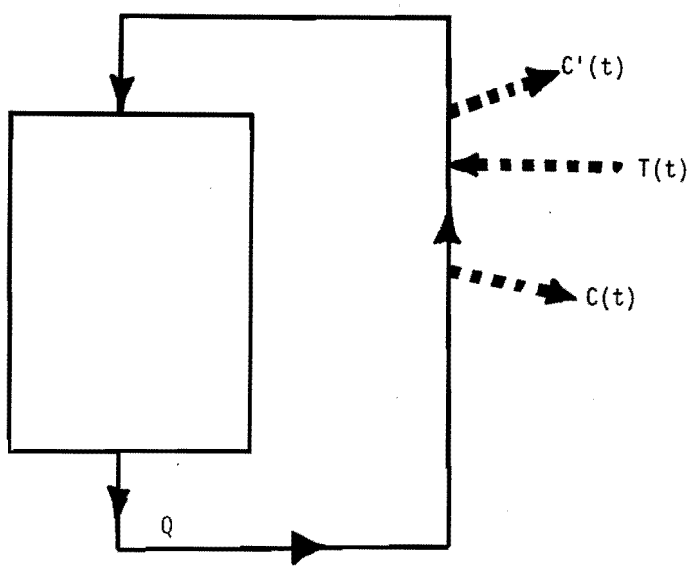

Figure 5.4. The points of tracer injection and detection at the circulating system.

material in the system.
After passage through the system the concentration is as follows:

$$C(t) = \int_0^t C'(t-y)\, h(y)\, dy \qquad (5\text{-}5)$$

where h(t) is the circulation time distribution of the circulating system under consideration and is indicated in figure 5.4.
Combination of equation (5-4) and equation (5-5) gives

$$C(t) = \int_0^t C(t-y)\, h(y)\, dy + \frac{1}{Q} \int_0^t T(t-y)\, h(y)\, dy \qquad (5\text{-}6)$$

which shows a recurrence relationship in the expression for C(t).
When the tracer injection is an ideal pulse, i.e.

$$T(t) = A.\delta(t) \qquad (5\text{-}7)$$

equation(5-6) then reduces to

$$C(t) = \int_0^t C(t-y)\, h(y)\, dy + \frac{A}{Q} h(t) \qquad (5\text{-}8)$$

where A is the total amount of tracer that was injected into the system.
system.
Equation (5-8) yields a stationary concentration C_{stat} in the limit $t \to \infty$. C_{stat} depends on the amount of tracer, A, and on the volume, V, of the system:

$$C_{stat} = \frac{A}{V} = \frac{A}{Q\tau} \qquad (5\text{-}9)$$

where τ is the characteristic circulation time of the material in the system.
The stationary concentration $C(t)=C_{stat}$ for $t \to \infty$ can be understood on the basis of the equation (5-8) as follows:

1. $h(t) \to 0$ when $t \to \infty$
2. $C(t) \to C_{stat}$ when $t \to \infty$
   $C(t-y) \to C_{stat}$ when $t \to \infty$ and when $y<t$

For the case $t \to \infty$ equation (5-8) can then be written as

$$C_{stat} = C_{stat} \int_0^\infty h(y)\, dy \qquad (5\text{-}10)$$

Equation (5-10) is in accordance with the definition of the probability density function h(t) that states

$$\int_0^\infty h(t)\, dt = 1 \qquad (5\text{-}11)$$

Equation (5-8) shows that a stationary concentration C_{stat} is reached at the limit $t \to \infty$ but the value of C_{stat} cannot be deduced directly from that equation.

It can be found from equation (5-8) that when the recirculated system is an ideal mixer the stationary value of C(t) is reached immediately after the tracer injection has taken place at t=0:
When the residence time distribution of an ideal mixer

$$h(t) = \frac{1}{\tau} e^{-t/\tau} \qquad (5\text{-}12)$$

is substituted into equation (5-8), it then follows from equation (5-8) that:

$$C(t) = \int_0^t C(t-y) \frac{1}{\tau} e^{-y/\tau} dy + \frac{A}{Q} \frac{1}{\tau} e^{-t/\tau} \qquad (5\text{-}13)$$

the only solution for C(t) that obeys equation (5-13) reads

$$C(t) = C(t-y) = \frac{A}{Q\tau} = \frac{A}{V} \text{ for } t \to 0 \qquad (5\text{-}14)$$

This can be shown by substituting (5-14) into equation (5-13):

$$C(t) = \int_0^t \frac{A}{Q\tau} \frac{1}{\tau} e^{-y/\tau}\, dy + \frac{A}{Q} \frac{1}{\tau} e^{-t/\tau} = \frac{A}{Q\tau} (1 - e^{-t/\tau}) + \frac{A}{Q\tau} e^{-t/\tau} \qquad (5\text{-}15)$$

from which the equivalence with equation (5-14) is immediately apparent.

The theory of Laplace transforms can be applied to calculate the mean and the variance of the probability distribution of the circulation times. Assume that the Laplace transform of h(t) is denoted as G(s):

$$G(s) = \int_0^\infty h(t)\, e^{-st}\, dt \tag{5-16}$$

and that

$$h(t) = \frac{1}{2\pi i} \int_{-\infty}^{\infty} G(s)\, e^{st}\, ds \tag{5-17}$$

where G(s) is a complex function of a complex variable s.

It can be found from equation (5-16) and from the definitions of the mean circulation time θ and its variance σ^2 (appendix 5.I):

$$\theta = \lim_{s \to 0} \left(-\frac{dG}{ds}\right) \tag{5-18}$$

$$\sigma^2 = \lim_{s \to 0} \left(\frac{d^2G}{ds^2} - \left(\frac{dG}{ds}\right)^2\right) \tag{5-19}$$

Assume I(s) and C(s) to be the Laplace transforms of I(t) and C(t) respectively:

$$I(s) = \int_0^\infty T(t)\, e^{-st}\, dt \tag{5-20}$$

$$C(s) = \int_0^\infty C(t)\, e^{-st}\, dt \tag{5-21}$$

Equation (5-6) and (5-8) then become respectively:

$$C(s) = C(s) \cdot G(s) + \frac{1}{Q} I(s) \cdot G(s) \tag{5-22}$$

$$C(s) = C(s) \cdot G(s) + \frac{A}{Q} G(s) \tag{5-23}$$

It follows from equation (5-22) that

$$C(s) = \frac{1}{Q} I(s) \cdot \frac{G(s)}{1-G(s)} \tag{5-24}$$

which provides an explicit expression in the Laplace transform of C(t) when the injection rate T(t) is an arbitrary function. The relationship between the Laplace transform G(s) of the circulation time distribution h(t) and the Laplace transforms of the response concentration C(t) and the injection rate T(t) is given by

$$G(s) = \frac{C(s)}{C(s) + I(s)/Q} \tag{5-25}$$

Equation (5-23) leads to

$$C(s) = \frac{A}{Q} \frac{G(s)}{1-G(s)} \tag{5-26}$$

and

$$G(s) = \frac{C(s)}{C(s) + A/Q} \tag{5-27}$$

The equations (5-26) and (5-27) provide relations between the Laplace transforms of C(t) and h(t), when C(t) is the response of a tracer injection that is a δ-pulse at t=0 (T(t) according to equation (5-7)).

Equation (5-26) can be approximated by means of a Taylor series development of G(s) around s=0:

$$G(s) = G(s=0) + \left(\frac{dG}{ds}\right)_{s=0} .s + \frac{1}{2} \left(\frac{d^2G}{ds^2}\right)_{s=0} \cdot s^2 + ... \tag{5-28}$$

Using equation (5-16) for $s \to 0$ together with equation (5-11) and equations (5-18) and (5-19), equation (5-28) can be rewritten to yield

$$G(s) = 1 - \theta \cdot s + \frac{1}{2}(\sigma^2 + \theta^2).s^2 - \frac{1}{6} M_3 s^3 + ... \tag{5-29}$$

where M_3 is the third moment of the probability function of the circulation time distribution.
With equation (5-29) equation (5-26) becomes

$$C(s) = \frac{A}{Q} \frac{1-\theta.s}{\theta.s} + \varepsilon(s) = \frac{A}{Q\theta} \frac{1-\theta.s}{s} + \varepsilon(s) \tag{5-30}$$

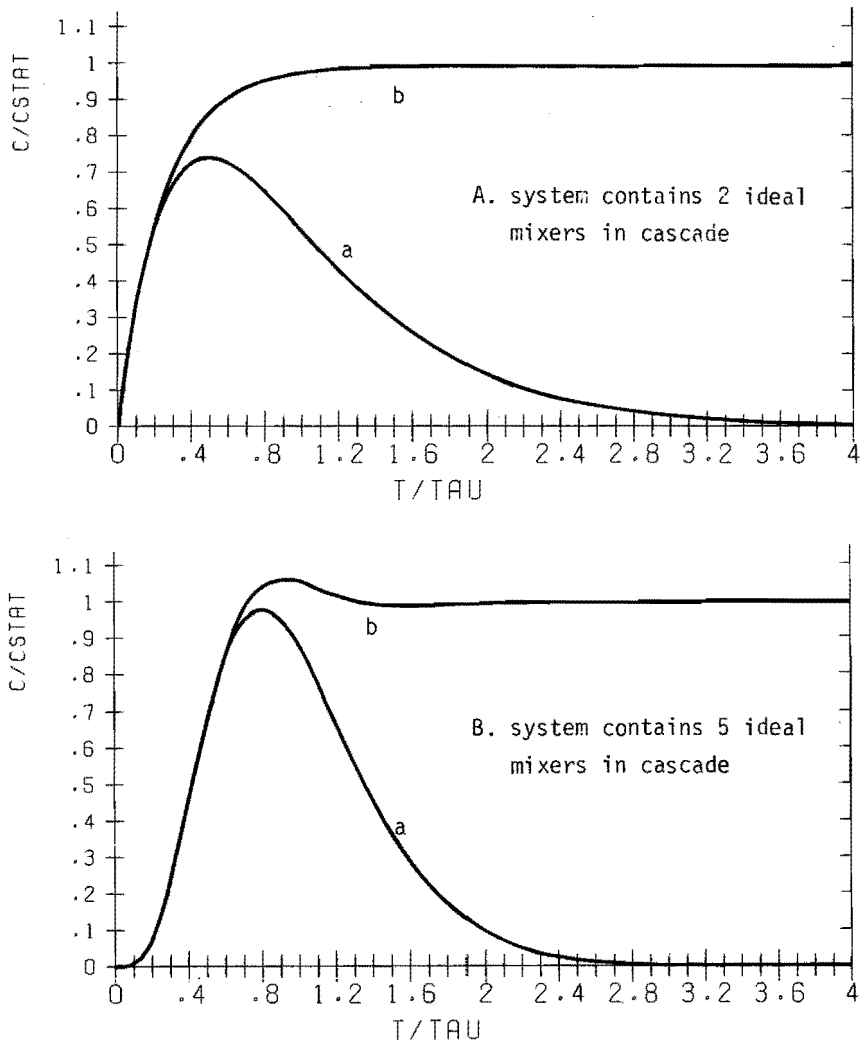

Figure 5.5 A-B Response of a purely convective flow system to a pulse injection at t=0.
a. continuous flow system with no recirculation
b. circulating system
The flow system was modelled by a cascade of ideal mixers of equal volume.

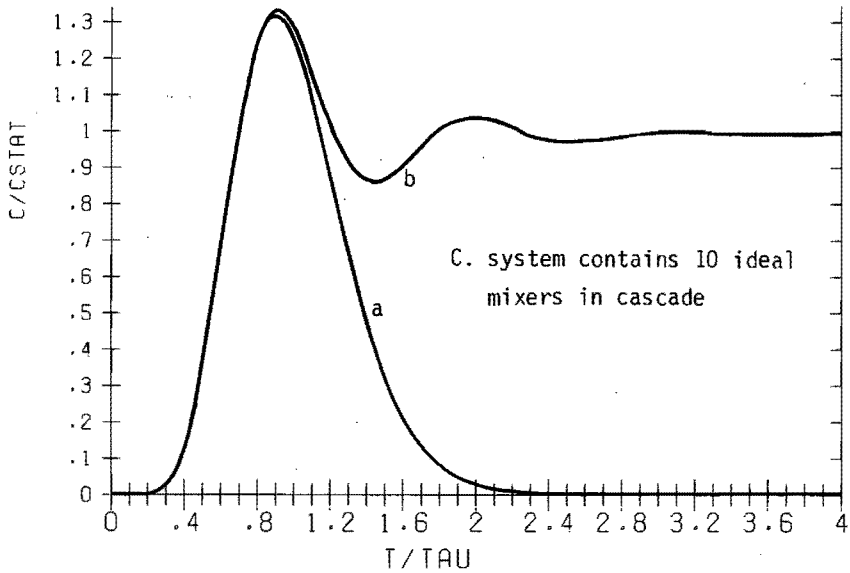

Figure 5.5 C Response of a purely convective flow system to a pulse injection at t=0.
a. continuous flow system with no recirculation
b. circulating system
The flow system was modelled by a cascade of ideal mixers of equal volume.

where $\varepsilon(s)$ is a rest function ($\varepsilon(s) \to 0$ when $s \to 0$).

It should be noted again that the relationship that is given by equation (5-4) is valid only when the recirculation flow is purely convective. The mean circulation time θ is then equal to the characteristic circulation time of the material in the system, i.e. $\theta = \tau$. In that case the application of Laplace transform theory to equation (5-30) shows that

$$\lim_{t\to\infty} C(t) = \lim_{t\to\infty} C(s) = \frac{A}{Q\theta} = \frac{A}{Q\tau} = C_{stat} \qquad (5\text{-}31)$$

which is again in accordance with equation (5-9).
Figure 5.5 shows a typical response of a circulating system to a pulse injection. It also shows the response of the circulating system to that pulse injection when the tracer material resides only one

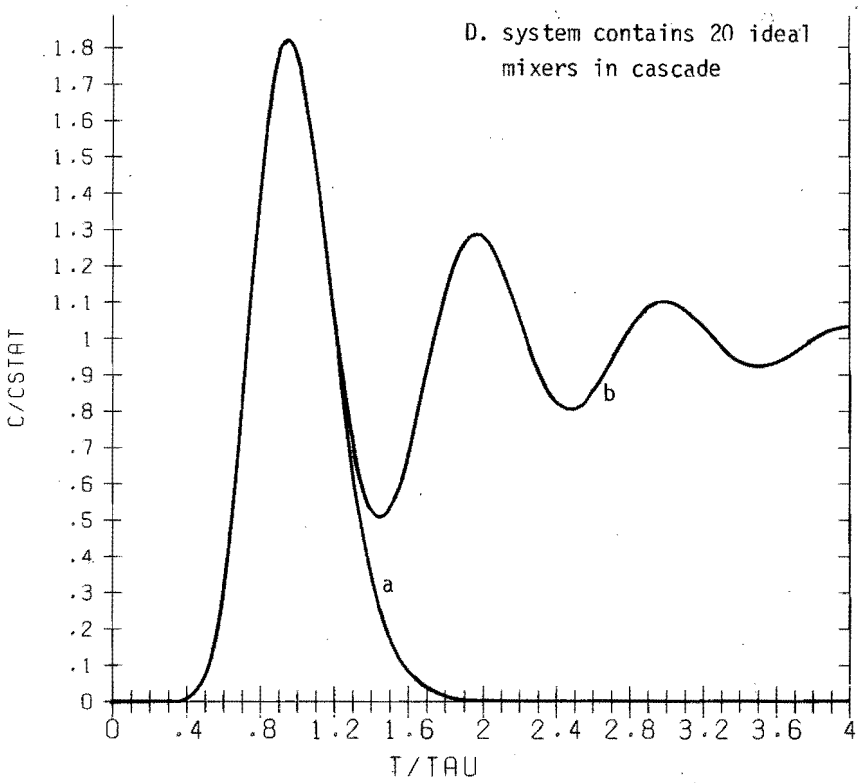

Figure 5.5 D Response of a purely convective flow system to a pulse injection at t=0.
a. continuous flow system with no recirculation
b. circulating system
The flow system was modelled by a cascade of ideal mixers of equal volume.

time in that system.
Note the damped fluctuating curve in the figures 5.5C and 5.5D. The tops of these fluctuating curve are due to the occurence of a region of high concentration of tracer material which passes the detection point each cycle at the moment that a maximum of C(t) is measured. This region is spread out over the whole volume of the circulating system when a certain period of time has elapsed after the moment of the pulse injection.

5.2.2.2 Systems with both diffusive and convective recirculation

A circulation flow channel where both convective and diffusive flow can occur will now be considered. Tracer particles can at any time show motions relative to that of the average flow. This is not possible in the case where purely convective recirculation flow only is assumed to occur. In comparison to what occurs in purely convective recirculation an additional response is observed at t=0 at the detection point, that is located just upstream the point of injection (figure 5.6). This additional response is the result of backmixing, i.e. movement of particles in the direction opposite to that of the average flow due to diffusion. No discontinuity in the tracer concentration can occur in the recirculation path at the injection point. Such a discontinuity must necessarily occur in the case of purely convective recirculation (compare equation (5-4)).
Material is circulating in the flow channel, while the mixing coefficient is constant over the length of the channel. The injection point is located at x=0 (= x=L) The differential equation that governs the transport of tracer material in the channel is well known and reads

$$\frac{\partial C}{\partial t} + v \frac{\partial C}{\partial x} - E \frac{\partial^2 C}{\partial x^2} = 0 \qquad (5\text{-}32)$$

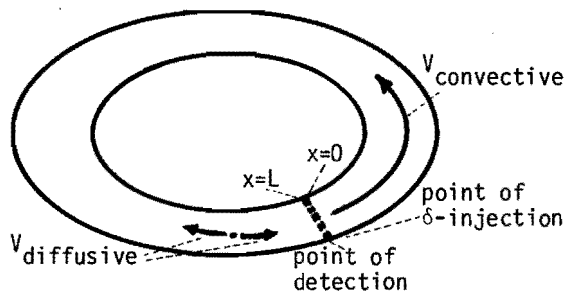

Figure 5.6. Schematic view of a circulation flow channel. linear coordinate x; flow velocity v; channel length L; system volume V; dispersion coefficient E; amount of injected tracer A.

in which E stands for a dispersion or mixing coefficient of the tracer material in the circulating system. Boundary conditions at x=0 and x=L are

$$C(x=0,t) = C(x=L,t)$$
$$\left(\frac{\partial C}{\partial x}\right)_{x=0} = \left(\frac{\partial C}{\partial x}\right)_{x=L} \qquad (5\text{-}33)$$

The initial condition (at t=0 and $0 \leq x < L$) reads

$$C(x,0) = A.\delta(x)/\left(\frac{V}{L}\right) \qquad (5\text{-}34)$$

where A is the total amount of injected tracer while V/L denotes the area of the cross section of the flow channel that is assumed to be constant for reason of simplicity of the calculations.
It can be shown that the solution of the differential equation which meets the boundary conditions (5-33) and the initial condition (5-34) reads (appendix 5.II):

$$\frac{C(x,t)}{C_{stat}} = 1 + 2 \sum_{n=1}^{\infty} \exp\left(-\frac{4\pi^2 n^2}{Pe}\frac{t}{\tau}\right).\cos\left(2\pi n\left(\frac{x}{L} - \frac{t}{\tau}\right)\right) \qquad (5\text{-}35)$$

where $C_{stat} = A/V$
$Pe = vL/E$
$\tau = L/v.$

The tracer concentration C(x,t) in the flow channel which results from the δ-injection approaches a stationary value $C_{stat} = A/V$ for large values of t. The rate of attenuation of the fluctuations around $C(x,t) = C_{stat}$ depends on the Péclet number that exists in the channel. The rate of attenuation increases when the Péclet number decreases. Figure 5.7 shows some typical responses of the circulation flow channel. The tracer concentration is measured just upstream from the point where the tracer injection has been carried out (C = C(0,t)).

The pulse responses of figure 5.5, where circulation occurs through a cascade of 5, 10 and 20 ideal mixers correspond to the pulse responses of figure 5.7, where circulation takes place through a flow channel at Péclet numbers of 10, 20 and 40 respectively (figure 5.8). This agrees

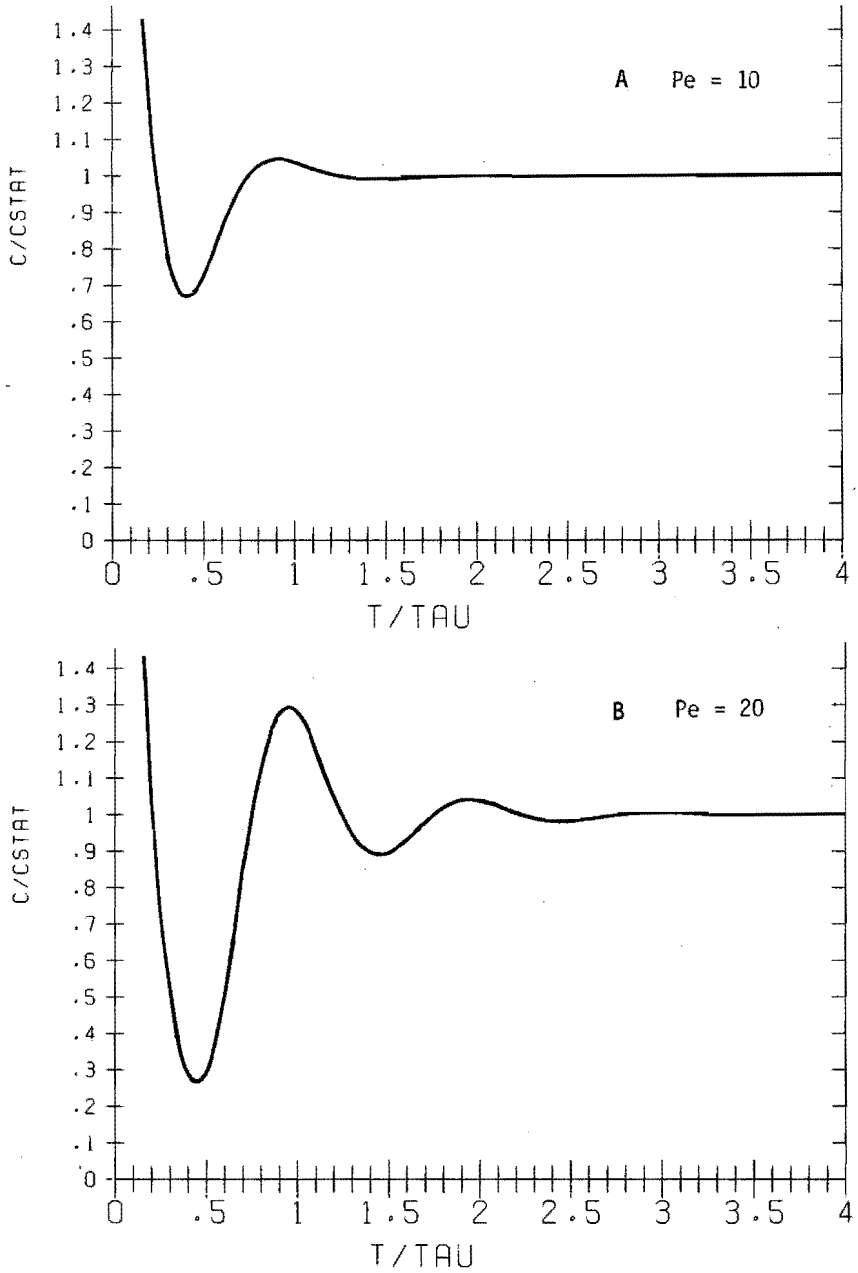

Figure 5.7 A-B Response of a circulation flow channel to a pulse injection (Pe = vL/E). The tracer concentration is measured just upstream from the point where the tracer injection has been carried out (C = C(x=0,t).

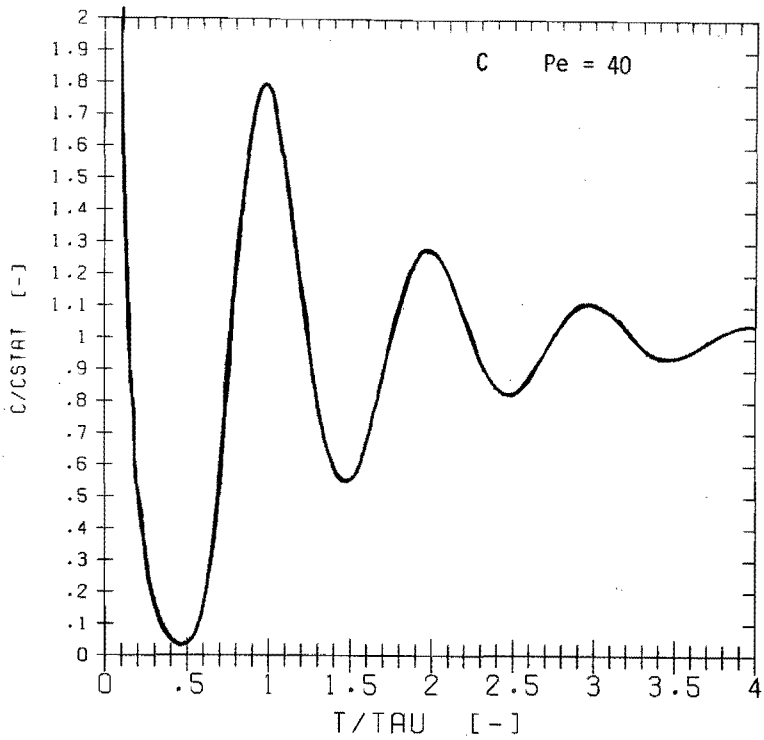

Figure 5.7 C Response of a circulation flow channel to a pulse injection (Pe = vL/E). The tracer concentration is measured just upstream from the point where the tracer injection has been carried out (C = C(x=0,t).

with the fact that the response of a system that consists of a cascade of N ideal mixers is similar to the response of a flow channel with a Péclet number that is equal to 2 x N, if the residence time of the fluid in the channel is equal to that in the cascade and if N is high enough.

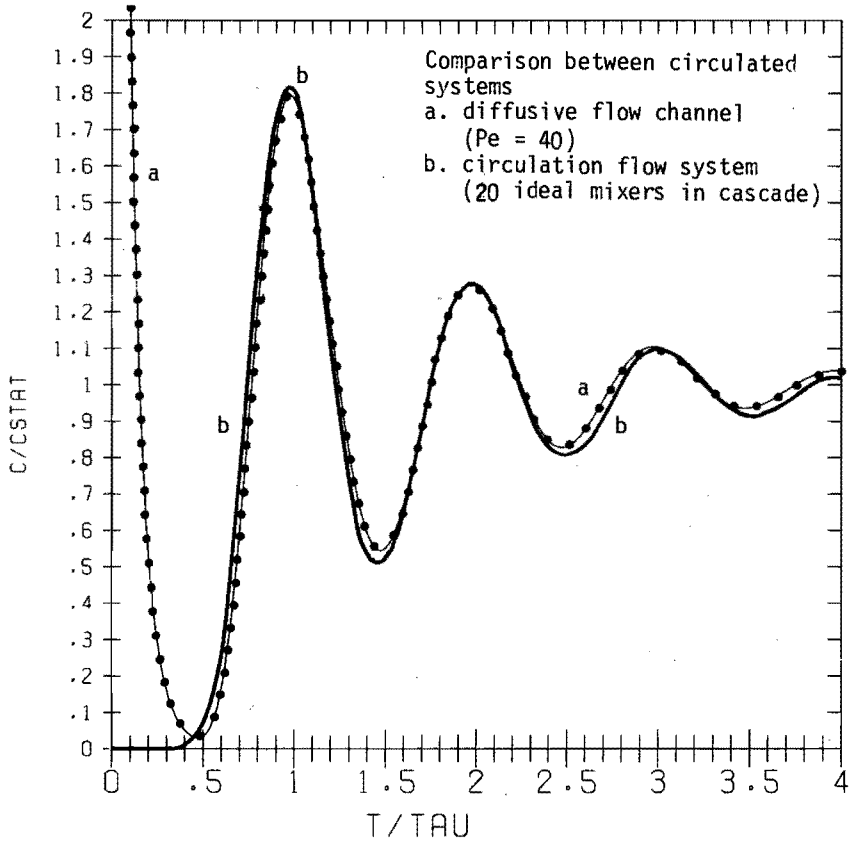

Figure 5.8. Comparison between the response to a pulse injection in a circulated diffusive flow channel with Pe = vL/E = 40 (curve a) and that in a circulation flow system that can be modelled by a cascade of 20 ideal mixers (curve b, figure 5.5D).

5.2.3. Solids circulation in fluctuating spout-fluid beds

A model is proposed in this section that deals with the flow behaviour of particles in the annulus of a bed which is operated in the fluctuating spouted bed regime (fluctuating spout-fluid bed). The model features solids flow along different paths in the annulus and the dispersion in the solids flow over each path (figure 5.9).

It is assumed that the flow of the solids in a fluctuating spouted bed proceeds as follows: Gas bubbles that form a bubble train rise from

the spout orifice to the top of the bed. At the bottom of each bubble the bubble wall collapses inward so that solid material bridges are formed that separate the bubbles from each other. As a bubbles rises it transports part of the solid material bridge above it upwards. Another part of this bridge above the rising gas bubble that is being considered is moved outwards out of the path of the bubble train. The bridge on top of the rising bubble remains intact, however, as bed material also collapses into the lower part of the gas bubble above the one we have considered.

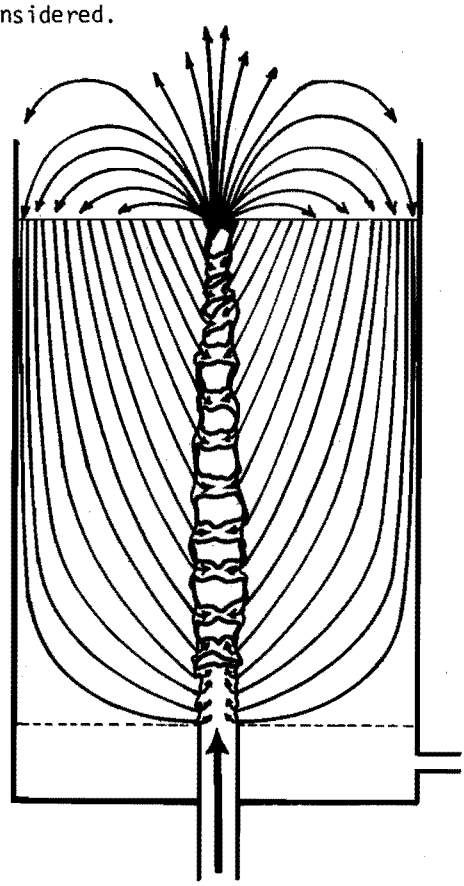

Figure 5.9. Assumed particle trajectories in a bed that is being operated in the fluctuating spouted bed regime.

The bubble train is thus regarded as an unstable spout channel, interrupted by solid material bridges. These bridges rise together with the gas in the unstable spout channel as solids continually flow into the bubbles onto the tops of the bridges. At the same time solids are continually removed from the bottoms of the bridges and moved outward out of the spout channel.
It is pointed out here that in this model solids can move both into the spout channel and out of it. This will prove to be of some importance in a later part of this thesis.
Figure 5.9 shows circulation paths in a spout-fluid bed that is being operated in the fluctuating spouted bed regime. This figure is to be compared to figure 3.17 which shows paths the bed material follows when the bed is in the stable spouted bed regime. It should be noted that the solids flow in the two flow regimes differ in nature.
The solids flow in a stable spouted bed is determined by the entrainment of the bed solids at the wall of the spout channel.
The upward flow of the solids in a fluctuating spout channel, on the other hand, is defined by the velocity at which a bubble train that contains both bubbles of spout gas and bridges that contain bed solids transports the solids to the top of the bed. This velocity is lower than the velocity with which spout gas transports entrained bed solids when the bed is being operated in the stable spouted bed regime.
It will be shown, however, that the mass of bed solids that is being transported upwards per unit time in a fluctuating spouted bed is much larger than that which is being entrained and transported per unit time in a comparable stable spouted bed that is being operated at the same rates of spout and fluidisation gas.

It is assumed that the annulus consists of a number of solid flow channels that are arranged in parallel with respect to each other. The lengths of the channels vary approximately linearly between 0 near the wall of the spout channel to almost the bed height H at the bed wall. A loose structure of the solids in the annulus and a uniform downwards flow of the bed solids are established when fluidisation gas is introduced into the bed at a sufficient rate. It is assumed that the same loose structure exists at each place in the annulus. This causes the fluctuations that may occur in the flow of the solids to have inten-

sities that are nearly independent of the position in the annulus. The dispersion coefficient, which will be used to express the longitudinal dispersion in the solids flow, has thus the same value at any position in the annulus. Transversal dispersion in the annulus (exchange of solids between the separate paths) is neglected. Transversal dispersion only occurs in the fountain region where the solids are spread out at random over the top surface of the bed. Each solid particle then enters a new path at a position that is entirely independent of previous cycles. The residence times of the solid particles in the spout and fountain region is neglected in comparison to the residence time in the annulus region.
The model for circulation flow is thus reduced to a description of the residence time distribution of the bed material in the annulus (figure 5.10).

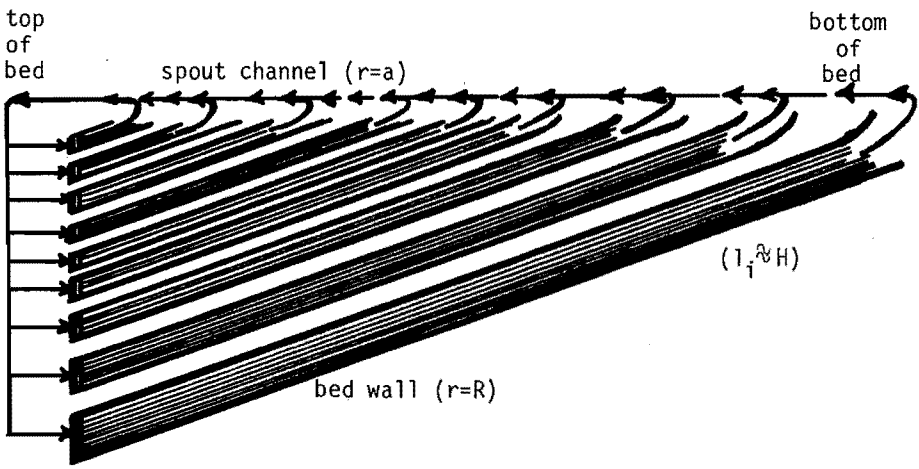

Figure 5.10. Schematic view of the parallel sets of particle trajectories in the annulus.

The transport of bed solids from the annulus into the spout channel region includes contributions of both a convective transport and a transport by dispersion due to fluctuations in the movement of the bed material. These fluctuating movements are associated with the transport of solids into and out of the spout channel which was described above. Bed solids are dropped onto the top surface of the annulus. There is no

possibility of backmixing at this fountain-annulus interface. A closed boundary with convective transport only is therefore assumed to exist at the entrance of each trajectory at the top of the annulus.
The fraction of the total circulating bed material that passes the set of trajectories that begin between r and r+Δr at the bed surface is equal to $2\pi r\Delta r/\pi(R^2-a^2)$ (figure 5.11). It follows that the contribution of that set of trajectories to the residence time distribution of solid particles in the annulus is equal to the residence time distribution in that set trajectories multiplied by the factor $2r\Delta r/(R^2-a^2)$.

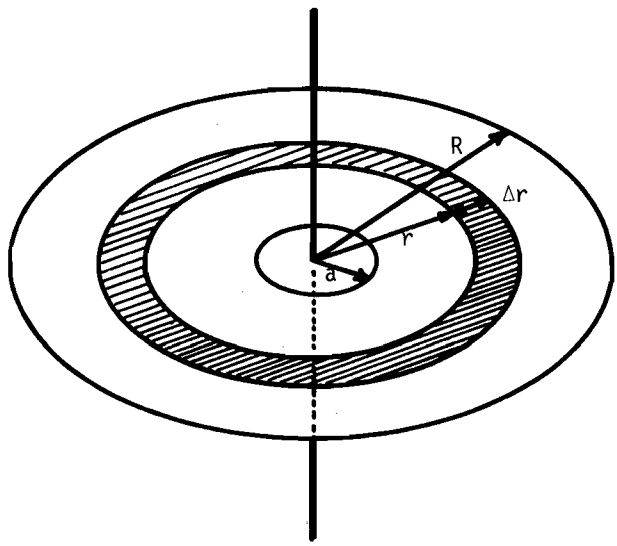

Figure 5.11. View of the top of the annulus.

A single set of trajectories is now considered. The dispersion that occurs in this set of trajectories must obey the conditions that a closed boundary must exist at the entry at the top of the annulus while an open boundary must exist at the exit to the spout channel.
Van der Laan [9] derived an expression for the Laplace transform of the residence time distribution of tracer material that is injected at x=0 and measured at $x = l_i$, where l_i is the length of the set of trajectories that is denoted by "i". The mean residence time θ_i of the solids in the i^{th} set of trajectories and the variance σ_i^2 of the residence time of the solids can be derived from this Laplace transform of the residence

time distribution.
In analogy with equations (5-18) and (5-19) that apply to circulation time distributions it can be found that

$$\theta_i = \lim_{s\to 0}\left[-\frac{dF_i}{ds}\right] = \frac{1 + Pe_i}{Pe_i}\ \tau_i \qquad (5\text{-}36)$$

and

$$\sigma_i^2 = \lim_{s\to 0}\left[\frac{d^2F_i}{ds^2}\right] - \theta_i^2 = \frac{2Pe_i + 3}{Pe_i^2}\ \tau_i^2 \qquad (5\text{-}37)$$

where F_i = the Laplace transform of the residence time distribution in the i^{th} set of trajectories $f_i(t)$

$= \tau_i . e^{-(p_i-\frac{1}{2}).Pe_i/(p_i+\frac{1}{2})}$

$p_i = \sqrt{s/Pe_i + \frac{1}{4}}$

Pe_i = the Péclet number of the flow in the i^{th} set of trajectories

$= vl_i/E$

τ_i = the residence time of the solids in the i^{th} set of trajectories

$= l_i/v$

No analytical solution of the residence time distribution $f_i(t)$ is available. Computed values of the distribution are presented in figure 5.12 for some values of the Peclet number.

The residence time distribution in the entire annulus is approximated by the summation of the contributions of each of the sets of trajectories in the annulus:

$$f(t) = \int_a^R f_i(t)\ \frac{2r}{R^2-a^2}\ dr \qquad (5\text{-}38)$$

where $f(t)$ = residence time distribution of the entire annulus

$f_i(t)$ = residence time distribution of a single set of trajectories in the annulus with the entry at radial distance r at the top surface of the bed

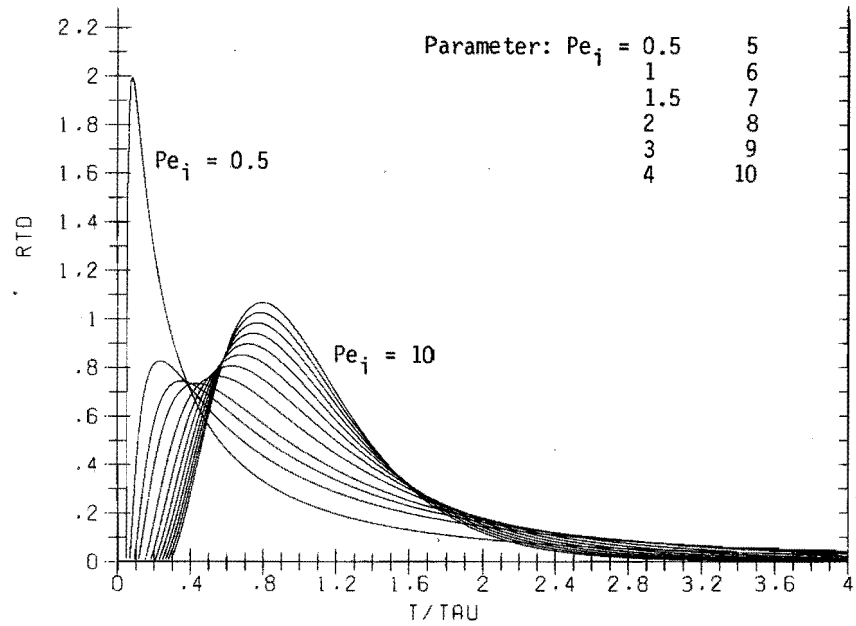

Figure 5.12. Residence time distributions (R.T.D.) of solids in individual sets of trajectories with a closed and an open boundary for some values of the Péclet number Pé$_i$ = vl$_i$/E as a function of the reduced time t/τ_i = vt/l$_i$.

The mean residence time in the entire annulus θ is obtained from the mean residence times θ_i of the individual sets of trajectories by means of a weighted integration of equation (5-36):

$$\theta = \int_a^R \theta_i \frac{2r}{R^2-a^2}\, dr \qquad (5\text{-}39)$$

which is analogous to equation (5-38).
Assume that $\tau_i = \frac{r}{R}\tau_R$ with $\tau_R = H/v$ and that $Pe_i = \frac{r}{R} Pe_H$ with $Pe_H = vH/E$. τ_R is the residence time for the set of trajectories that are closest to the bed wall, while Pe_H is the Péclet number that belongs to the set of trajectories that begin at r=R. It can then be found from equation (5-39) using equation (5-36) that

$$\theta = \int_a^R \tau_R \frac{r}{R}\left(1 + \frac{R}{Pe_H \cdot r}\right) \frac{2r}{R^2-a^2}\, dr = \tau_R \left(\frac{2}{3}\frac{R^3-a^3}{R^2-a^2} + \frac{R}{Pe_H}\right)\frac{1}{R} \qquad (5\text{-}40)$$

When a<<R equation (5-40) reduces to

$$\theta = \tau_R \left(\frac{2}{3} + \frac{1}{Pe_H}\right) \tag{5-41}$$

The second moment M_2 of the residence time distribution in the annulus which is equal to $\sigma^2+\theta^2$ is derived from the second moments M_{2i} of the individual sets of trajectories by

$$M_2 = \int_a^R M_{2i} \frac{2r}{R^2-a^2}\, dr \tag{5-42}$$

which is also analogous to equation (5-38) while $M_{2i} = \sigma_i^2 + \theta_i^2$. It is found from equation (5-42) using equations (5-36) and (5-37) that

$$M_2 = \int_a^R \tau_i^2 \frac{2Pe_i + 3 + (1+Pe_i)^2}{Pe_i^2} \cdot \frac{2r}{R^2-a^2}\, dr \tag{5-43}$$

which yields

$$\sigma^2 = \tau_R^2 \left(\frac{4}{3}\frac{R}{Pe_H}\frac{R^3-a^3}{R^2-a^2} + 3\frac{R^2}{Pe_H^2} + \frac{1}{2}(R^2+a^2) - \frac{4}{9}\left(\frac{R^3-a^3}{R^2-a^2}\right)^2\right)\frac{1}{R^2} \tag{5-44}$$

When a<<R equation (5-44) reduces to

$$\sigma^2 = \tau_R^2\left(\frac{3}{Pe_H^2} + \frac{4/3}{Pe_H} + \frac{1}{18}\right) \tag{5-45}$$

Combination of equation (5-41) and equation(5-45) gives

$$\frac{\sigma^2}{\theta^2} = \frac{\frac{1}{18}Pe_H^2 + \frac{4}{3}Pe_H + 3}{\left(1 + \frac{2}{3}Pe_H\right)^2} \tag{5-46}$$

The equations (5-41), (5-45) and (5-46) characterise the flow of the bed material in the annulus of the bed in terms of the Péclet number Pe_H and the residence time τ_R that are related to the set of trajectories that are closest to the bed wall (r=R, $l_i \approx H$).

The residence time distribution for the entire annulus is computed by summing the contributions of each of the individual sets of trajectories in the annulus according tot equation (5-38). The trajectories in the annulus have a different length l_i and thus a different residence time τ_i and Péclet number Pe_i. The summation according to equation (5-38) should thus be carried out using residence time distribution functions $f_i(t)$ that are to be found from the reduced residence time distribution by the relationship

$$f_i(t) = \frac{1}{\tau_i} f_i^*(t/\tau_i, Pe_i) \qquad (5\text{-}47)$$

where $f_i^*(t^*,Pe)$ is the reduced residence time distribution that is a function of the reduced time $\tau^* = t/\tau$ and of the Péclet number $Pe = vL/E$.

The values of τ_i and Pe_i can be found from the Péclet number Pe_H and from the residence time τ_R for the set of trajectories that are closest to the bed wall, as was indicated above.

5.2.4. Calculated results of the dispersion model

Figure 5.13A and 5.13B show plots of calculated residence time distributions for the entire annulus for some values of Pe_H and for given mean residence times θ of 5 and 10 seconds respectively.
Note the limiting residence time distribution for $Pe_H = \infty$ for the case that piston flow occurs in the particle trajectories in the annulus:

$$f(t) = 0 \qquad \text{for } t > \tau_R$$
$$f(t) = (2/\tau_R^2)t \qquad \text{for } t < \tau_R \qquad (5\text{-}48)$$

The circulation time distributions in cases where roughly $Pe_H < 4$ show a high maximum at low circulation times and a long tail section at higher values of the circulation time. The maximum becomes lower and shifts to longer circulation times when the Péclet number Pe_H increases, while the tailing effect diminishes. The maximum of the circulation time distribution passes a minimum with respect to Pe_H when $Pe_H \approx 6$ while the maximum at high Pe_H is limited by the case where $Pe_H = \infty$ which corresponds to piston flow in the annulus, as described above (equation 5-48).

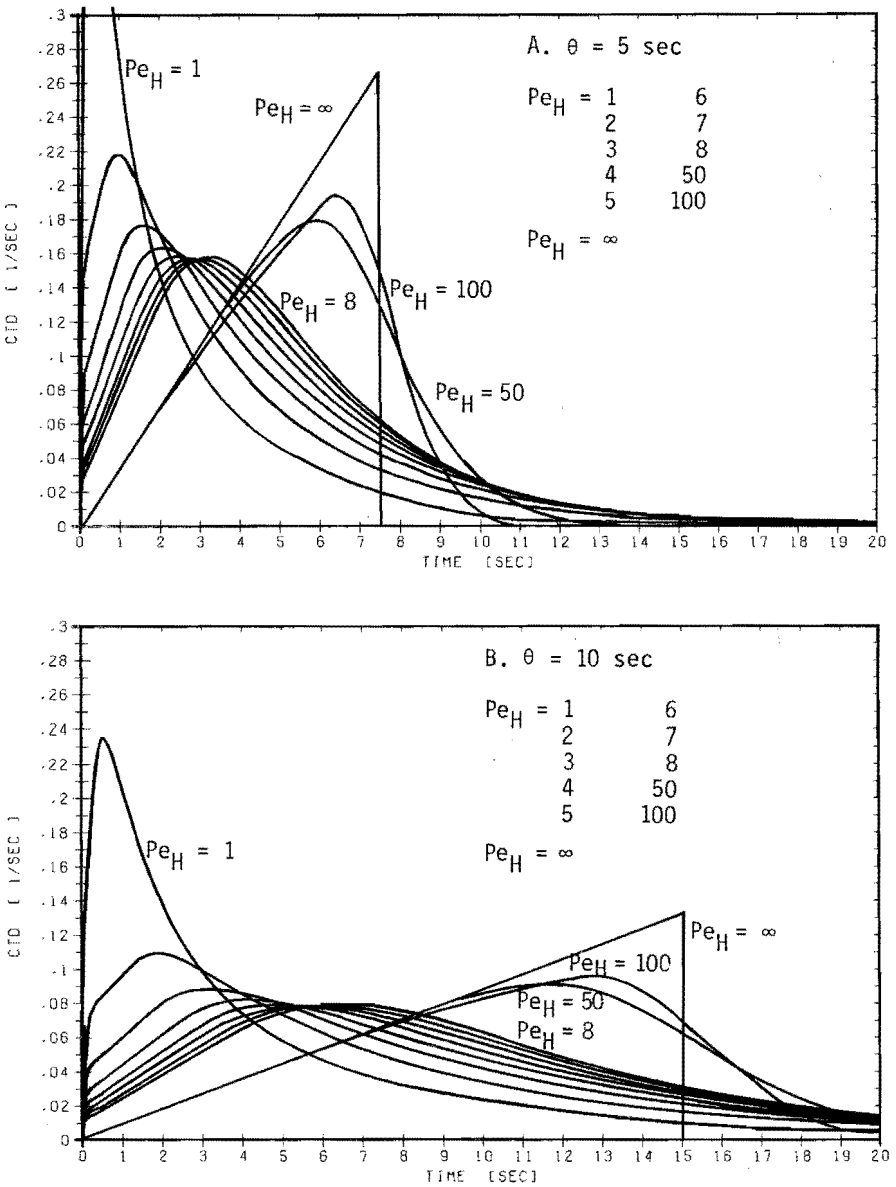

Figure 5.13. Calculated residence time distributions for the entire annulus, that is equal to the circulation time distribution (C.T.D.) in the spout-fluid bed, for some values of $Pé_H$ *and* θ.

Literature

[1] Chatterjee, A.
Ind.Eng.Chem.Proc.Des.Dev. 9, 531-536 (1970)

[2] Mann, U. and Crosby, E.J.
Can.J.Chem.Eng. 53, 579-581 (1975)

[3] Takeda, H. and Yamanoto, Y.
J.Nuclear Sc. and Techn. 13, 372-381 (1976)

[4] Vadja, T.
Int.Chem.Eng. 16, 543-551 (1976)

[5] Robinson, T. and Waldie, B.
Can. J. Chem.Eng. 56, 632-635 (1978)

[6] Suciu, G.C. and Patrascu, M.
Powder Technology 19, 109-114 (1978)

[7] van Velsen, D., Flamm, H.J., Langenkamp, H. and Casile, A.
Can.J.Chem.Eng. 52, 156 (1974)

[8] Mann, U. and Crosby, E.J.
Chem.Eng.Science 28, 623-627 (1973)

[9] van der Laan, E.Th.
Chem.Eng.Science 7, 187 (1958)

Appendix 5.I

Circulation time distributions

The circulation time is a random variable having a probability density function $h(t)$. $h(t).\Delta t$ is the probability that the random variable T, representing the circulation time lies within the interval between t and $t+\Delta t$:

$$h(t).\Delta t = Pr\{t < T < t+\Delta t\} \qquad (5.I\text{-}1)$$

Because $h(t)$ is a density function of the probability it follows that

$$\int_0^\infty h(t)dt = 1 \qquad (5.I\text{-}2)$$

The mean or first moment of the circulation time distribution is

$$\theta = \int_0^\infty t\, h(t)\, dt \qquad (5.I\text{-}2)$$

and its variance

$$\sigma^2 = \int_0^\infty (t-\theta)^2\, h(t)\, dt \qquad (5.I\text{-}4)$$

which also can be written as

$$\sigma^2 = \int_0^\infty t^2\, h(t)\, dt - \theta^2 \qquad (5.I\text{-}5)$$

The first term of the right hand side of eq. (5.I-5) is the second moment of the circulation time distribution.

Appendix 5.II

Response to a pulse injection in a circulation flow channel

The differential equation that governs the diffusive and convective transport of tracer material in the flow channel (equation (5-32)) can be written in dimensionless form as:

$$\frac{\partial C^*}{\partial t^*} + \frac{\partial C^*}{\partial x^*} - \frac{1}{Pe}\frac{\partial^2 C^*}{\partial x^{*2}} = 0 \qquad (5.II\text{-}1)$$

where $t^* = t/\tau = t \cdot v/L$

$x^* = x/L$

$Pe = vL/E$

$C^* = C/C_{stat} = C \cdot V/A$

The conditions (5-33) and (5-34) then read:

$$C^*(0,t^*) = C(1,t^*)$$

$$\left(\frac{\partial C^*}{\partial x^*}\right)_{x^*=0} = \left(\frac{\partial C^*}{\partial x^*}\right)_{x^*=1}$$

$$C^*(x^*,0) = \delta(x^*)$$

Because of the periodicity in x^*, C^* can be written as:

$$C^*(x^*,t^*) = \sum_k C_{kt}\, e^{ikx^*} = \sum_{n=0}^{\infty} C_{kt}\, e^{2\pi i n x^*} \qquad (5.II\text{-}2)$$

$$k = 2\pi n,\ n=0,1,2,3,.....$$

Combination of (5.II-2) in (5.II-1) gives:

$$\frac{\partial C_{kt}}{\partial t^*} + ik\, C_{kt} + k^2/Pe\, C_{kt} = 0 \qquad (5.II\text{-}3)$$

the solution of which is $C_{kt} = C_k\, e^{-(k^2/Pe + i)t^*}$ (5.II-4)

thus

$$C^*(x^*,t^*) = \sum_k C_k \, e^{-(k^2/Pe)\,t^*} e^{ik(x^*-t^*)} \qquad (5.II\text{-}5)$$

its <u>real part</u> being:

$$C^*(x^*,t^*) = \sum_{n=0}^{\infty} C_n \, e^{-\frac{4\pi^2 n^2 t^*}{Pe}} \cos(2\pi n(x^*-t^*)) \qquad (5.II\text{-}6)$$

At $t^*=0$ the initial condition reads:

$$C^*(x^*,0) = \sum_{n=0}^{\infty} C_n \cos(2\pi n x^*) = \delta(x^*) \qquad (5.II\text{-}7)$$

It then follows for C_n $(n=0,1,2,\ldots)$:

$$C_n = \frac{1}{1/2} \int_{-1/2}^{1/2} \delta(x^*) \cos(2\pi n x^*) dx^* = 2 \qquad n\neq 0$$

$$C_0 = \int_{-1/2}^{1/2} \delta(x^*)\, dx^* = 1 \qquad (5.II\text{-}8)$$

Equation (5.II-6) then becomes

$$C^*(x^*,t^*) = 1 + 2 \sum_{n=1}^{\infty} e^{-\frac{4\pi^2 n^2}{Pe}\, t^*} \cos(2\pi n(x^*-t^*)) \qquad (5.II\text{-}9)$$

which results in solution (5-35) in section 5.2.2.

List of symbols

A	total amount of injected tracer	[kmol]
a	spout channel radius	[m]
C(s)	Laplace transform of tracer concentration C(t)	[kmol.s/m^3]
C(t)	tracer concentration (upstream the injection point)	[kmol/m^3]
C'(t)	tracer concentration (downstream the injection point)	[kmol/m^3]
C_{stat}	stationary tracer concentration	[kmol/m^3]
E	diffusion (dispersion) coefficient	[m^2/s]
F(s)	Laplace transform of residence time distribution (R.T.D.)	[-]
$F_i(s)$	Laplace transform of R.T.D. of the i^{th} trajectory	[-]
f(t)	residence time distribution (R.T.D.) of entire annulus	[1/s]
$f_i(t)$	R.T.D. of the i^{th} trajectory	[1/s]
f*(t*,Pe)	reduced residence time distribution	[-]
G(s)	Laplace transform of circulation time distribution	[-]
H	bed height	[m]
h(t)	circulation time distribution	[1/s]
I(s)	Laplace transform of tracer injection rate	[kmol]
L	length of circulation flow channel	[m]
l_i	length of the i^{th} trajectory	[m]
M_2	second moment of R.T.D.	[s^2]
M_3	third moment of R.T.D.	[s^3]
p_i	variable defined in eq. (5-37)	[-]
Pé	Péclet number	[-]
$Pé_i$	Péclet number of i^{th} trajectory	[-]
$Pé_H$	Péclet number of the trajectory near r=R	[-]
Q	circulation rate of material in system	[m^3/s]
q_i	fraction of material passing through the i^{th} region	[-]
R	bed radius	[m]
r	radial distance in the bed	[m]
s	Laplace transform variable	[1/s]
T(t)	tracer injection rate	[kmol/s]
t	time	[s]

t'	integration variable in equation (5-1)	[s]
t^*	reduced time	[-]
V	capacity of the circulating system	[m^3]
v	fluid velocity in the flow channel and trajectories	[m/s]
x	linear coordinate	[m]
y	integration variable in equations (5-6), (5-8), (5-10), (5-13), (5-14)	
$\delta(t)$	delta-function in time domain	[1/s]
$\delta(x)$	delta function in x domain	[1/m]
$\varepsilon(s)$	rest function in equation (5-30)	
θ	mean residence (circulation) time of tracer	[s]
σ	standard deviation of the residence (circulation) time	[s]
τ	fluid residence (circulation) time	[s]
τ_i	fluid residence time in channel "i"	[s]
τ_R	fluid residence time in channel at r=R	[s]

6. THE CIRCULATION BEHAVIOUR OF TRACER PARTICLES IN A SPOUT-FLUID BED

6.1 Introduction

The mixing of particles in a spout-fluid bed can be described either by considering the time-average concentration distribution of the particles or by considering the period of time the bed smooths out concentration gradients that occur in the bed when a large amount of tracer particles has been injected into the bed. The time-average concentration distribution of the particles results from an equilibrium between a segregation mechanism and a mechanism that tends to disperse the particles throughout the annulus. If it acted alone, the segregation mechanism would result in an inhomogeneous distribution of the particles in the annulus when they do not have the same size, shape and density as the surrounding bed material.
Large and heavy particles tend to be concentrated in the lower part of the bed, while the smaller and lighter particles predominate more in the upper part.

Mixing results from the variance in the circulation times of the bed particles. This variance in the circulation times is established by the exchange of the bed particles between the separate trajectories in the annulus. The exchange between the trajectories takes place in the spout channel and fountain region only.

It was mentioned in section 5.1 that the circulation behaviour of particles in the bed is best studied by measuring the circulation times of these particles. The distribution of the circulation times can be obtained either by a pulse injection of an amount of tracer material or by measuring the time that elapses between consecutive passages of one tracer particle. The last method is rather time consuming when one wishes to obtain a reliable histogram of the measured circulation times. The first method is fast but does not result in the determination of a direct circulation time distribution for the system when the responses of tracer particles that have completed different numbers of cycles overlap (figure 5.5). This method is therefore less suitable.

This chapter presents a method for determining the circulation behaviour

of a tracer particle that has been put into the bed. This way of studying the mixing behaviour has been selected because it provides the possibility to carry out measurements continuously while the bed is in stationary operation. This method is also suitable for automatic registration of the tracer particle circulation.
The circulation time distribution of a tracer particle is determined by measuring the consecutive passages of the tracer particle through the horizontal plane at the top of the annulus through which all circulating bed material must pass. Sufficient data must be collected to construct a reliable histogram.
Figure 6.1 shows an example of a comparison between the result of circulation time measurements with one tracer particle, the response to a pulse injection of a unit mass of tracer material and the actual circulation time distribution of the system.

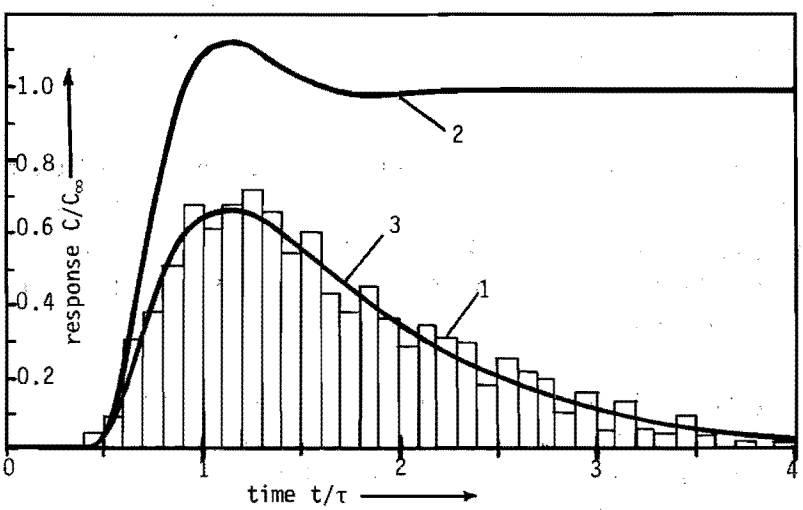

Figure 6.1 Example of a comparison between a result of cycle time measurements (histogram 1), a response to a puls injection of a unit mass of tracer material (curve 2) and the actual cycle time distribution of a circulating system (curve 3).

Pulse response measurements require accurate and reliable measuring equipment. The mean concentration of tracer material should be determined at any time in the cross section of that part of the bed through which all bed material passes. Examples of types of equipment that allow

such measurements over an entire cross section are chromatographs and conductivity cell devices.
The registration of one tracer particle, however, only requires an apparatus that is equiped with a simple threshold mechanism which controls a counter or timer.
Because of the reasons indicated above the second measurement method was chosen.

When one wishes to measure circulation properties of the bed material one requires tracer particles that have zero slip velocity with respect to the bed material. The tracer particles thus must show the same sizes, shapes and densities as the bed particles. When tracer particles are to be used that are large with respect to the bed particles then a density is required that is equal to the bulk density of the bed material.

6.2 The experimental apparatus

A flat ferroxcube core with two poles was mounted around a 15.2 cm spout-fluid bed wound with two inductive coils in series to measure the passage of a tracer particle with a high magnetic permeability. The measured cycle times were used to compute the histogram of the density function of the circulation time distribution of that tracer particle. Figure 6.2 shows a sketch of the inductive coil. The measuring coil was placed around the glass column at the top of the annulus. A reference coil was placed outside the equipment and is a reference in comparison to which changes in the induction of the measuring coil were determined. The measuring coil and the reference coil form one half of a Wheatstone inductive bridge. The other half of the bridge is part of a Hottinger-Baldwin KWS-6A-5 device.
The presence of a tracer particle in the magnetic field between the poles of the core causes the self-induction of the measuring coil to increase. The passage of the tracer particle past the coil is thus denoted by a pulse in the output signal of the bridge.
The bed material has a magnetic permeability that is negligible in comparison to the permeability of the tracer particle. It can be shown that the extra induction generated in the coil is roughly proportional to the volume of that tracer particle. It can also be shown that when

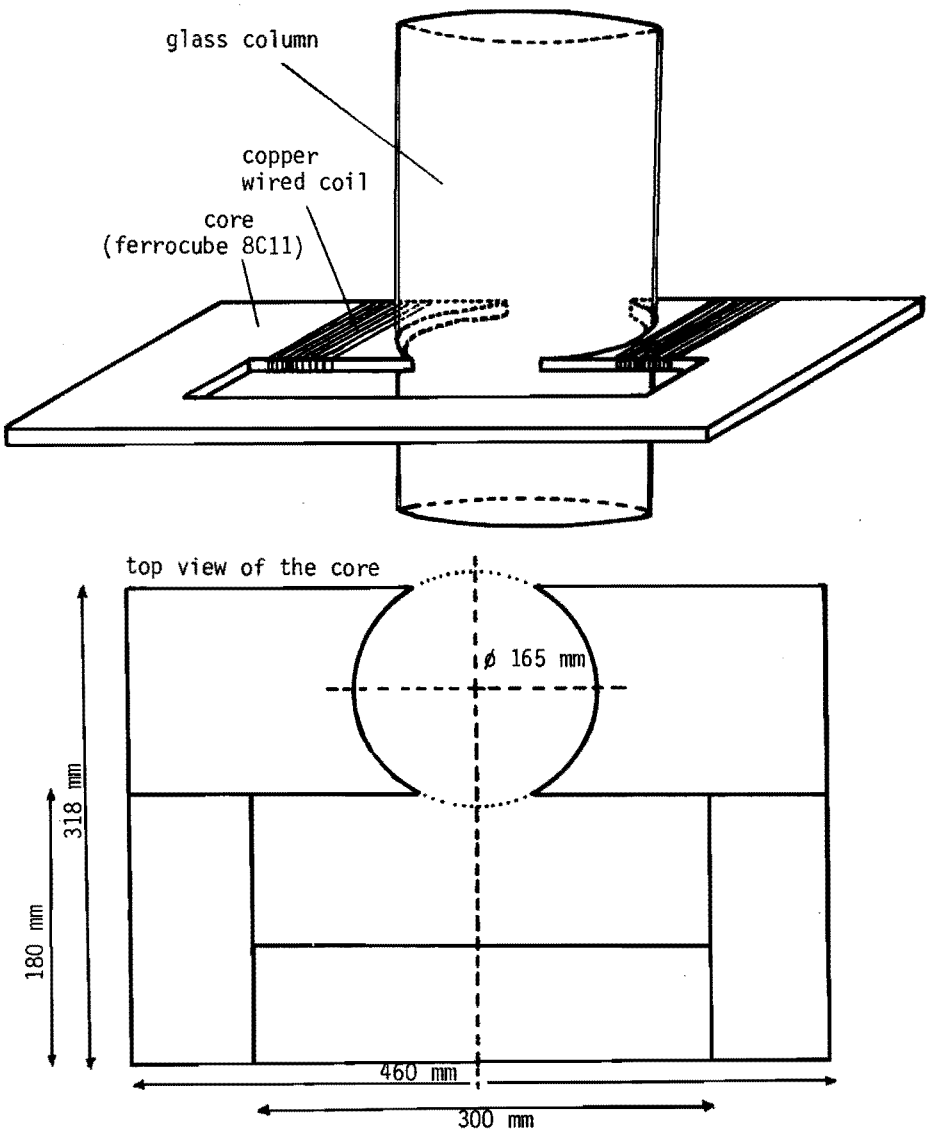

Figure 6.2 Sketch of the measuring core at the spout-fluid bed.

a 4 mm diameter tracer particle is used the increment of the self-induction of the coil relative to its original self-induction amounts to approximately 4.10^{-5}.

The time that elapsed between two consecutive passages of the particle through the plane of the coil was measured by means of a Hewlett Packard 5233 L counter.

Figure 6.3 shows a scheme of the experimental equipment. It indicates the way in which the measuring and reference coil are connected to the peripheral devices. Effects of noise and bed vibrations are reduced by filtering the frequency components higher than roughly 50 Hz of the output signal of the inductive measuring bridge.
The threshold value of the counter mechanism must be adjusted in order to register a reliable signal that results from the passage of the tracer particle.

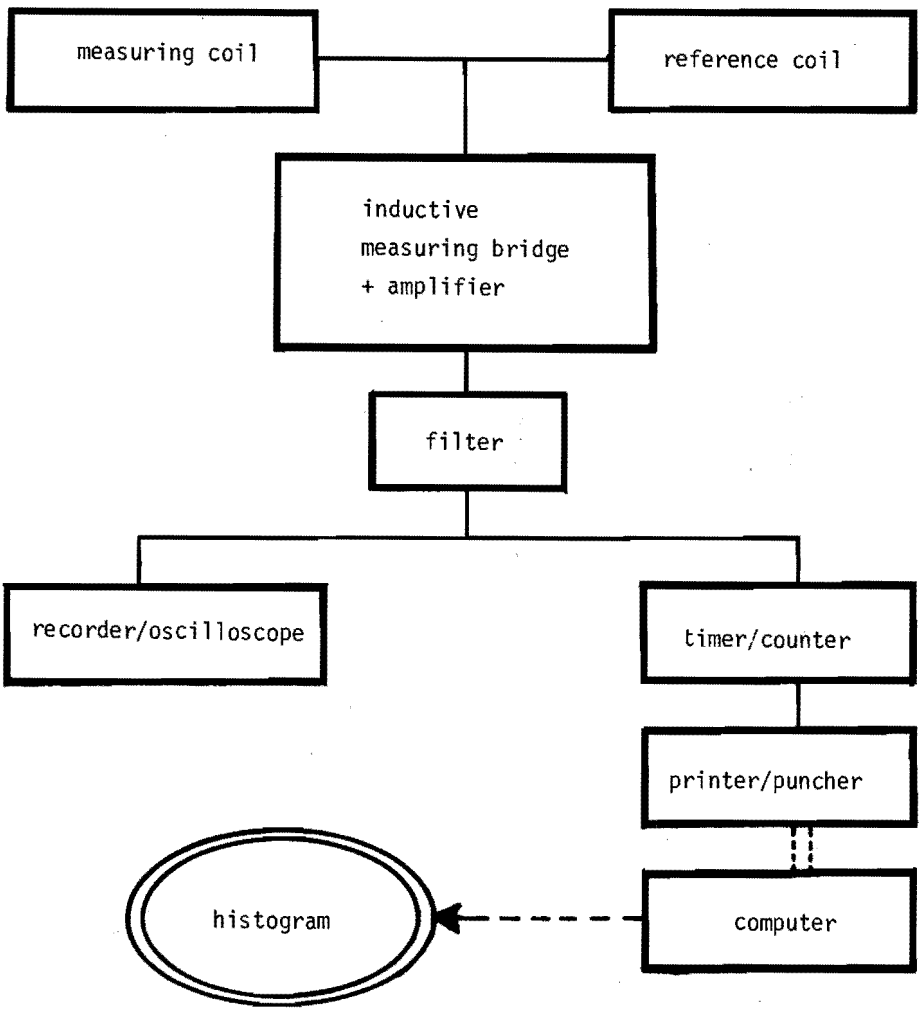

Figure 6.3 Scheme of the connection of the measuring coil to the peripheral devices.

Figure 6.4 shows the experimentally determined relation between the amount of registered pulses per minute at the output of the bridge and the adjusted threshold value of the counter. This experimental relation was obtained at constant spout and fluidisation gas flow rates while the bed was being operated in the fluctuating spouted bed regime. A large number of pulses were registered per unit time at a low value of the threshold. This is due to noise and bed vibrations. The number of pulses measured per unit time decreases as the threshold value is increased. At a sufficient high threshold value the number of pulses that are measured per unit time becomes nearly independent of the threshold value. Circulation time measurements are best carried out when the value of the threshold is adjusted in such a way that the frequency with which the counter detects pulses does not depend too strongly on the threshold value.

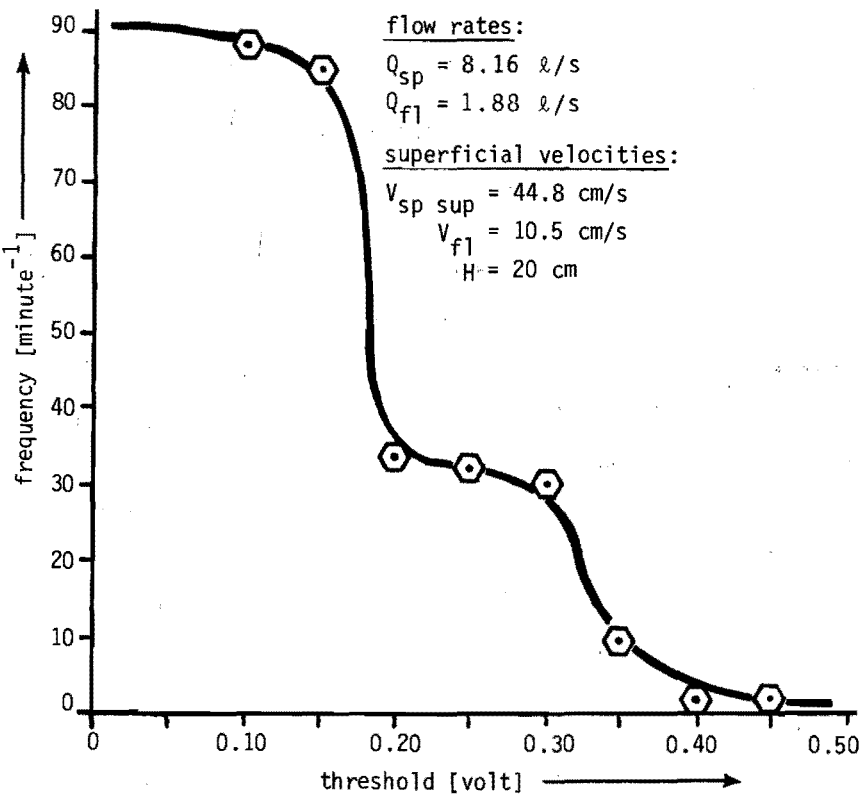

Figure 6.4 Example of a measured relation between the frequency of registered pulses and the threshold value of the counter.

Four different tracer particles have been used in the circulation time measurements in order to investigate the effect of the size and density of the tracer particles that were applied. The sizes and densities of these tracer particles, that were identified by "A", "B", "C" and "D", are summarized in table 6-I.

Table 6-I Summary of the sizes and densities of the used tracer particles

	A	B	C	D
size	3.5 mm	6.2 mm	5.5 mm	7.0 mm
density	4.74 g/cm^3	1.98 g/cm^3	3.85 g/cm^3	4.74 g/cm^3

Figures 6.5 through 6.8 show experimentally determined circulation time distributions of the 4 tracer particles. The cycle time distribution of the small particle with high density (particle A) and that of the large particle with very low density (particle B) are similar (compare figures 6.5 and 6.6). It is seen, however, that the large particles with high densities (the particles C and D) in their cycles tend to follow circulation paths of greater length than do the smaller and lighter particles (figures 6.7 and 6.8).
This can be explained by assuming, as seems reasonable, that large particles tend to move more frequently through the bottom section of the bed than the small particles. The large particles do not follow the same trajectories as the bed material because they have a higher density than the bed material (figure 6.9).
It was already mentioned that the circulation properties of the bed material are best studied by using tracer particles that have densities near to that of the bed material. Particle B, of which the cycle time distribution is given in figure 6.6, approximates this condition most closely. On the basis of the similarity between the figures 6.5 and 6.6 it is assumed that the circulation time distributions of the particles A (size 3.5 mm, density 4.7 g/cm^3) and B (size 6.2 mm, density 1.98 g/cm^3) both roughly describe the circulation behaviour of the bed material.

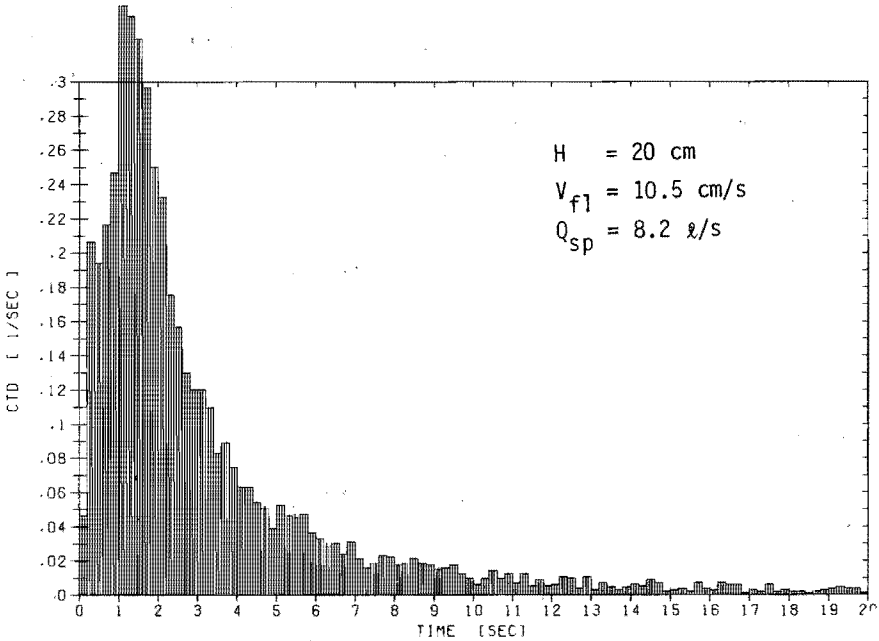

Figure 6.5 Measured cycle time distribution of tracer particle A (size = 3.5 mm, density = 4.74 g/cm^3).

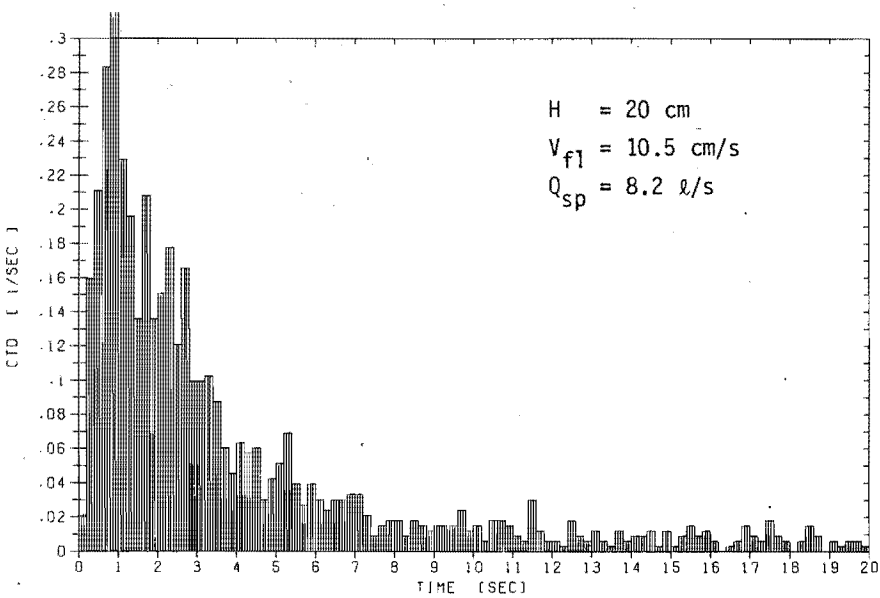

Figure 6.6 Measured cycle time distribution of tracer particle B (size = 6.2 mm, density = 1.98 g/cm^3).

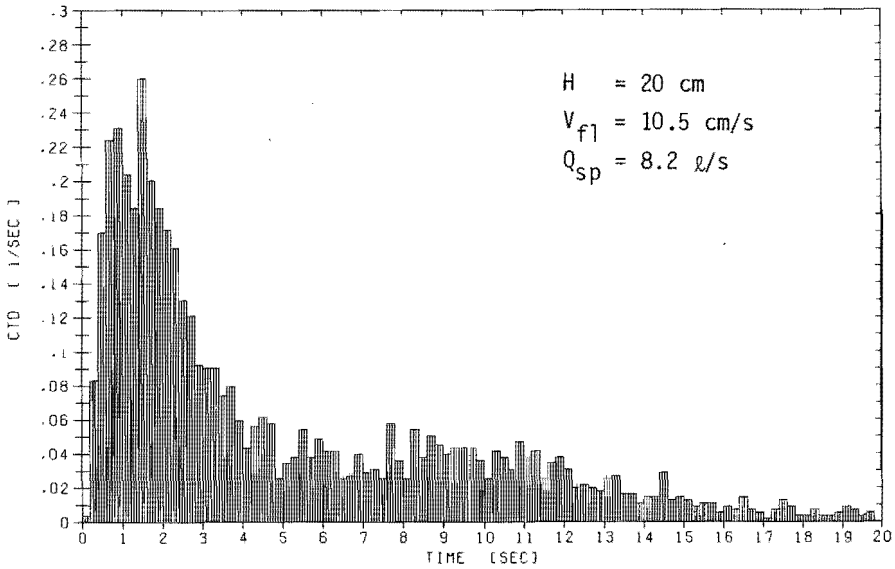

Figure 6.7 Measured cycle time distribution of tracer particle C (size = 5.5 mm, density = 3.85 g/cm^3).

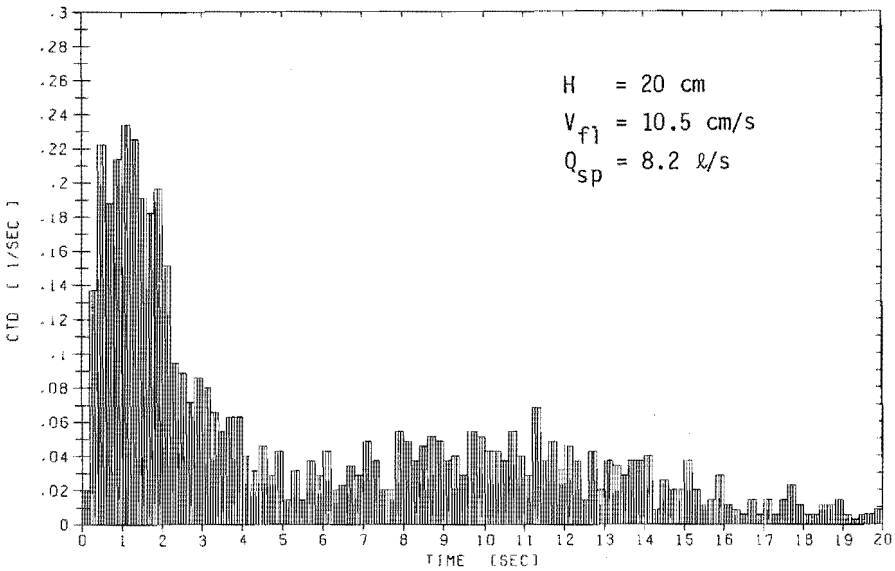

Figure 6.8 Measured cycle time distribution of tracer particle D (size = 7 mm, density = 4.74 g/cm^3).

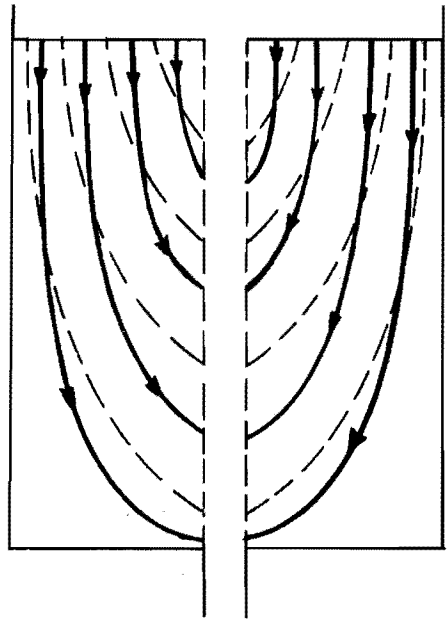

Figure 6.9. Scheme of the imagined trajectories of the bed material (----) and of the relatively heavy and large tracer particles (———) in a spout-fluid bed.

The circulation time measurements described in this thesis were carried out with tracer particle A.

6.3 Experimental results

Circulation time measurements were carried out in the bed at different values of the spout and fluidisation gas flow rates. The bed heights employed in these measurements were 20 and 35 cm respectively, while the 3.5 mm diameter tracer particle that had a density of 4.7 g/cm^3 (particle A) was used in the experiments.
The circulation paths that the bed particles follow should include a plane through which all bed material passes at each cycle to obtain a reliable cycle time distribution.
Circulation times in a bed that is being operated in the stable spouted bed regime tend to be relatively long. The tracer particles show a tendency to stay a relatively long time in the bottom section of the

bed in that regime. Bed material is entrained from the spout channel wall at a much lower rate than in a bed that is being operated in the fluctuating spouted bed regime as was stated earlier.
An example is shown in figure 6.10 of a comparison between the circulation time distributions that are measured in beds in the fluctuating and stable spouted bed flow regimes respectively and at the same rates of spout and fluidisation gas.
The results shown in figure 6.10 indicate that the spout-fluid bed is being operated in the fluctuating spouted bed regime at increasing spout gas rate, while the bed is being operated in the stable spouted bed regime at decreasing spout gas rate. The mean circulation times in the fluctuating spouted bed regime were in the range between 2 and 7 seconds. The mean circulation times in the bed at stable spouted bed condition, however, appear to be at least one order of magnitude longer.
Because of the interest in the high rate of mixing in spout-fluid beds measurements have only been carried out when the bed was being operated in the fluctuating spouted bed regime.
Figure 6.11 shows measured circulation time distributions for different values of the fluidisation and spout gas rate. The histograms show a number of maxima and minima. These maxima and minima are caused by the stochastic variation due to the finite number of cycle time measurements that have been used for computing the histograms. It is well known that a large number of measurements results in a histogram that has a low relative error in the value of each class of the histogram. Assume for example that the number of measurements in a certain class is n. The absolute and relative error in the number of measurements in that class are represented by its standard deviation $\sigma = \sqrt{n}$ and its relative deviation $\sigma/n = 1/\sqrt{n}$ respectively.
Most histograms have been computed from a total of over 1000 measurements. The maximum relative errors in the values for each class of the middle section of the histograms were less than 20%. The relative error for each class of the tail section, however, amounts to almost 50%.

The dispersion model that was discussed in chapter 5 has been applied to the measured cycle time distributions. The dispersion coefficient

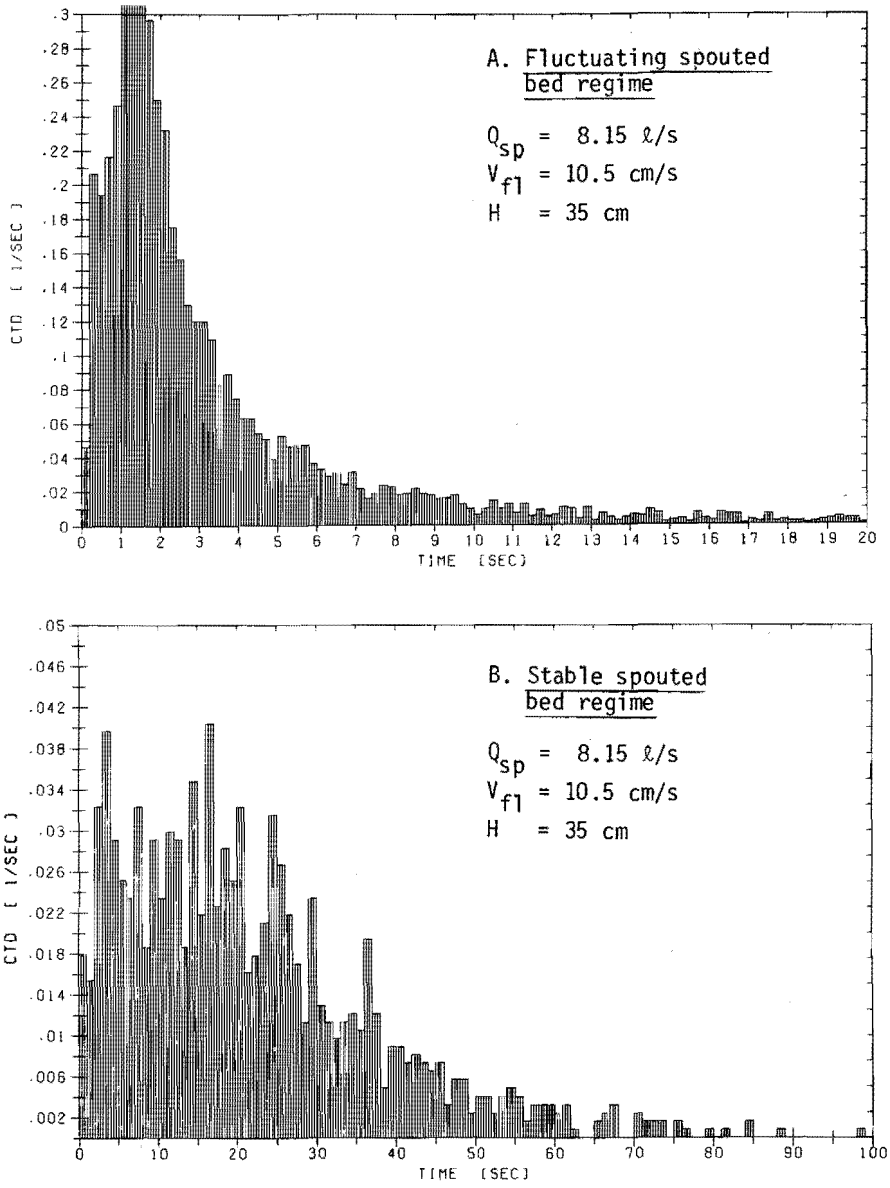

Figure 6.10. Circulation time distributions (C.T.D.) in a spout-fluid bed that is being operated in two regimes at the same spout and fluidisation gas rates. The bed is being operated in the hysteresis zone between the fluctuating spouted and stable spouted bed regime.

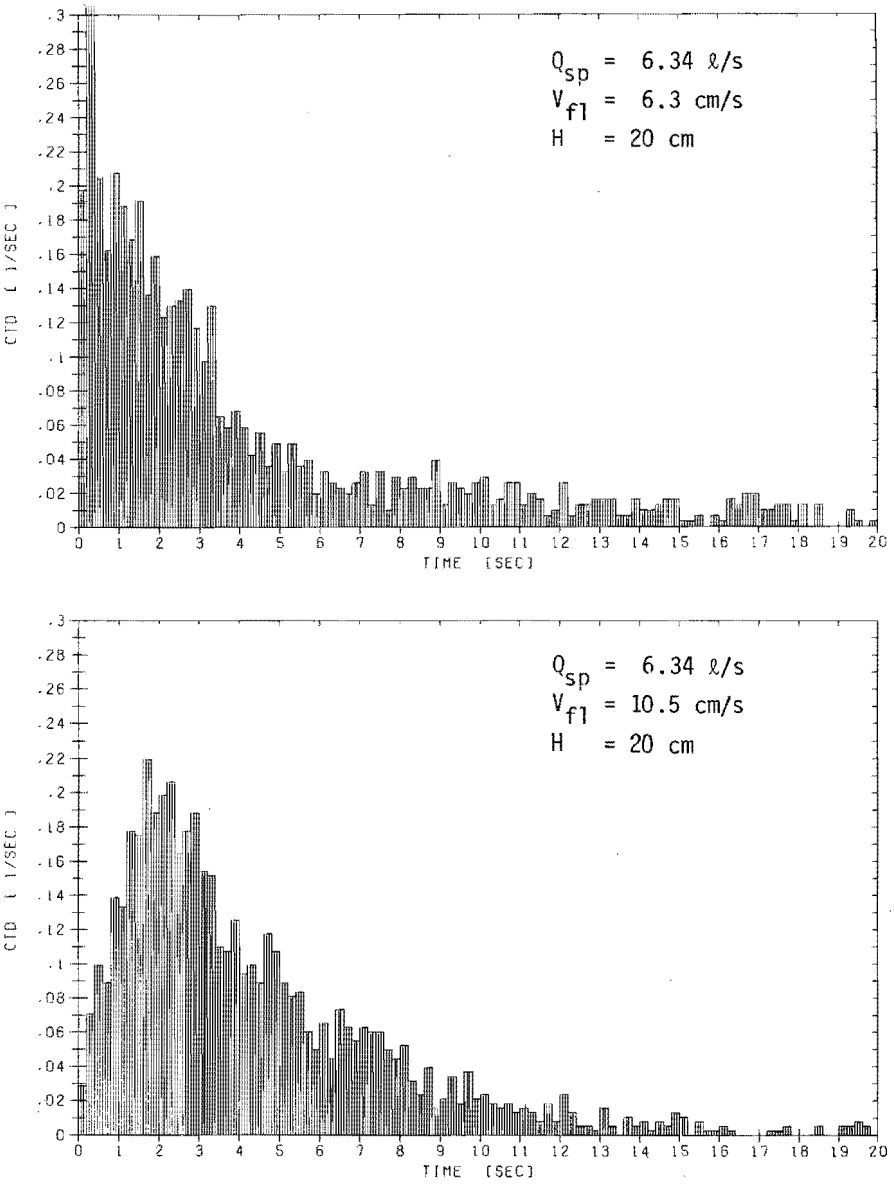

Figure 6.11. Examples of measured circulation time distributions (C.T.D.) in a spout-fluid bed that is being operated in the fluctuating spouted bed regime (H = 20 cm).

and the rate of solids circulation in the spout-fluid bed were computed from this model.
The solids circulation rate is described by the residence time τ_R of the bed material that is flowing along the bed wall:

$$\tau_R = H/v \qquad (6\text{-}1)$$

where H is the bed height
and v is the downward flow velocity of the bed material.
The dispersion coefficient is described by the Peclet number Pe_H that applies to the flow of the bed material along the bed wall:

$$Pe_H = v.H/E \qquad (6\text{-}2)$$

The dispersion coefficient E represents the effect that fluctuations in the movement of the bed particles have on the downward flow of the bed material.

The parameters τ_R and Pe_H were obtained by successive application of equation (5-46) and of either equation (5-41) or equation (5-45) to the measured circulation time distribution. The dispersion model was checked by calculating the circulation time distribution according to that model using the values of τ_R and Pe_H which had been found from the histograms that were measured.
Figure 6.12 and 6.13 show some experimentally determined histograms of the cycle times together with cycle time distributions that were calculated from the dispersion model. Figure 6.12 shows cycle time distributions in the spout-fluid bed with a bed height 35 cm and with spout gas rates of 8.15 ℓ/s and 4.53 ℓ/s (varying fluidisation gas velocity). Figure 6.13 shows distributions in the bed with a bed height of 20 cm and with a spout gas rate of 8.15 ℓ/s while the fluidisation gas velocity was also varied.
It is seen that the correspondence between the experimental distribution and the dispersion model is reasonable.
The circulation time distribution of the bed material in the spout-fluid bed can thus be described reasonably well by the dispersion model in most cases.

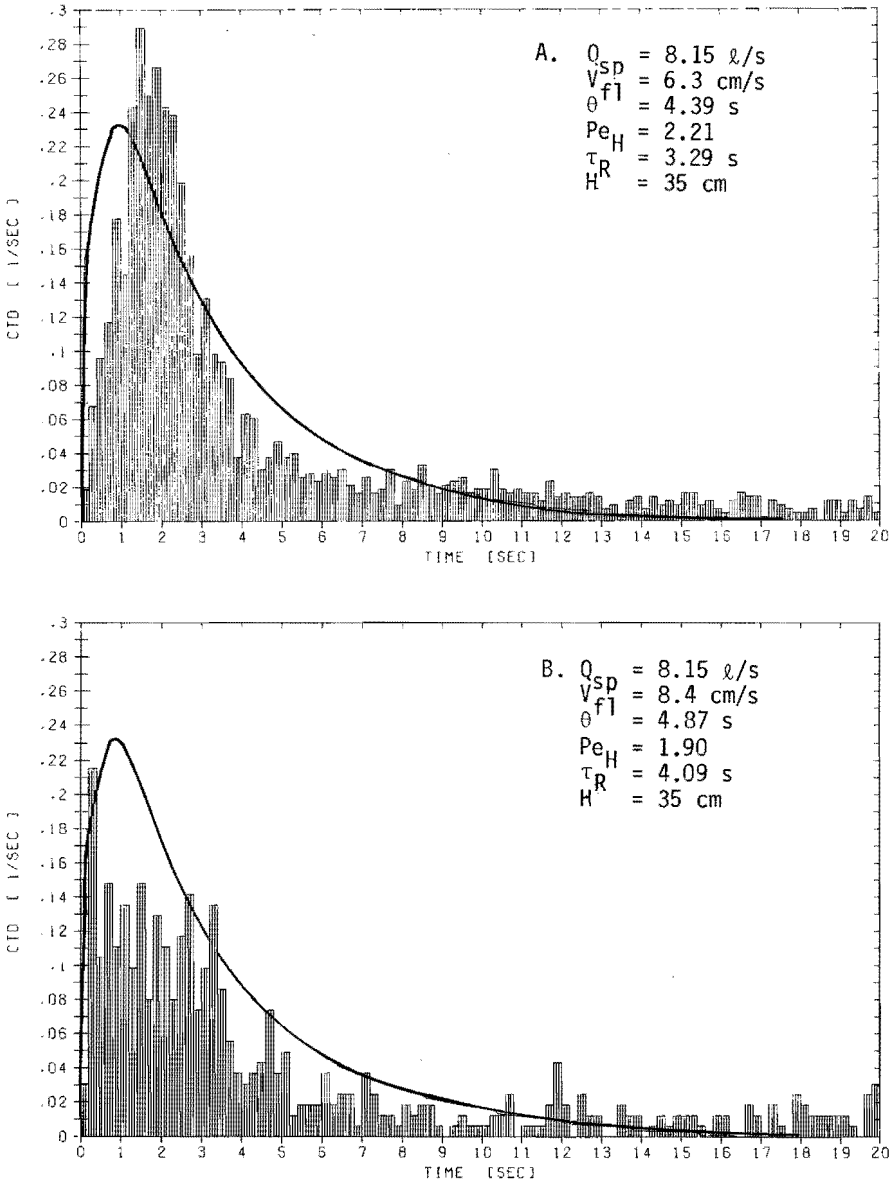

Figure 6.12A-B. Measured histograms and calculated curves from the dispersion model with the same values of τ_R and Pe_H (H = 35 cm).

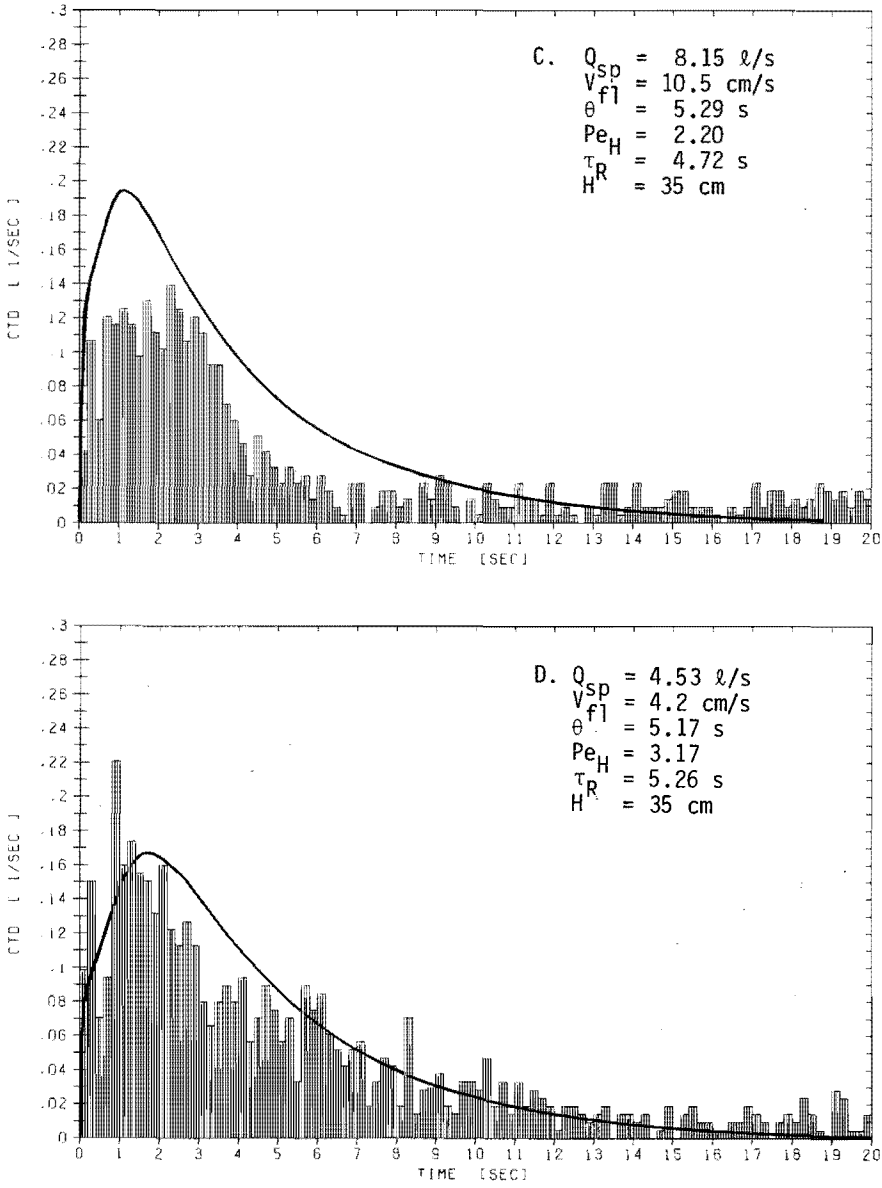

Figure 6.12C-D. Measured histograms and calculated curves from the dispersion model with the same values of τ_R and Pe_H (H = 35 cm).

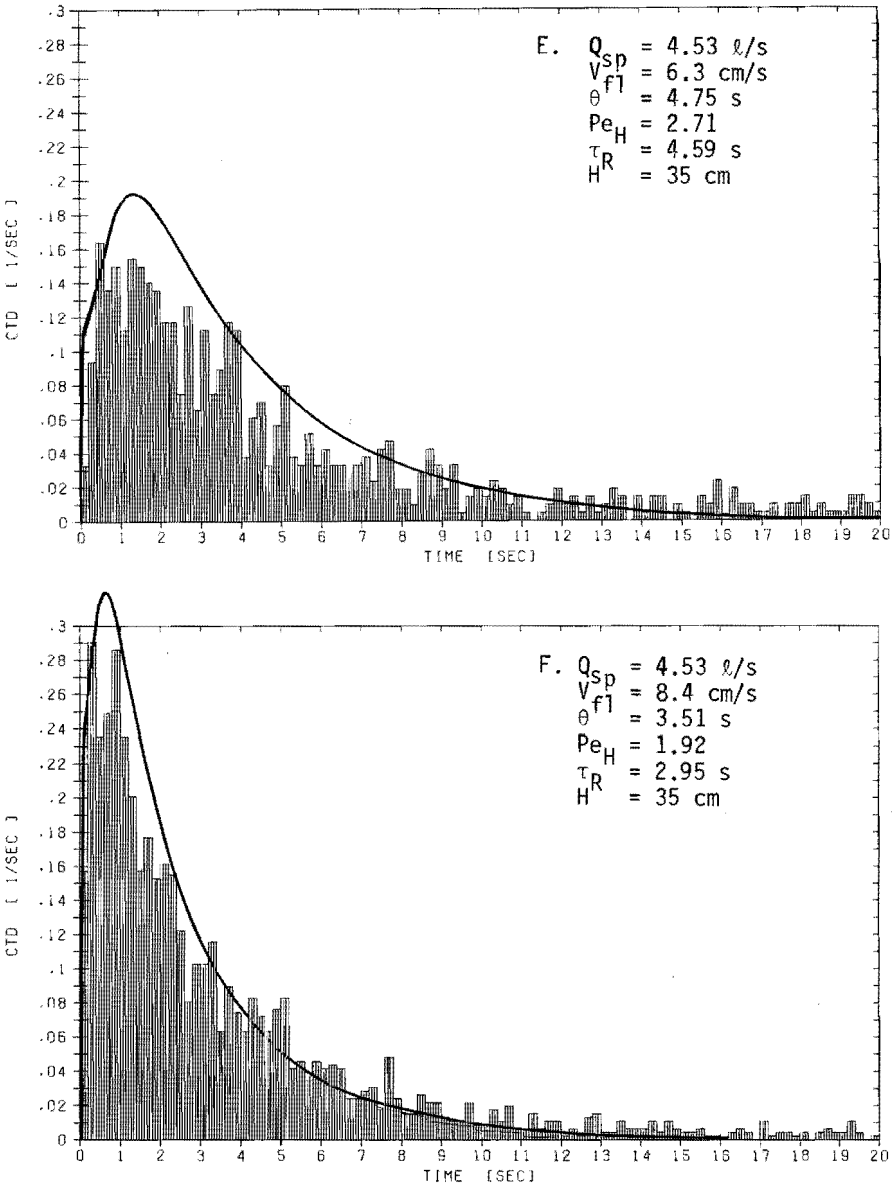

Figure 6.12E-F. Measured histograms and calculated curves from the dispersion model with the same values of τ_R and Pe_H (H = 35 cm).

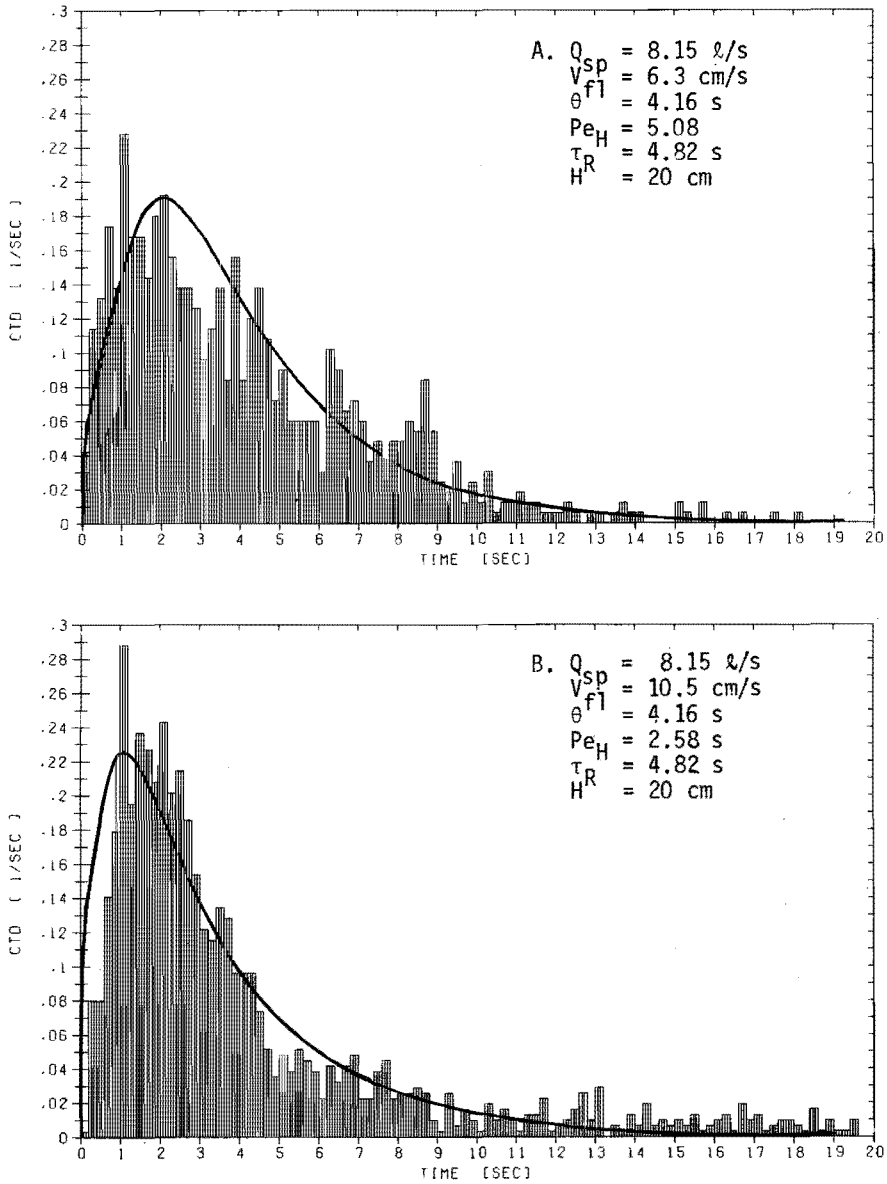

Figure 6.13A-B. Measured histograms and calculated curves from the dispersion model with the same values of τ_R and Pe_H (H = 20 cm).

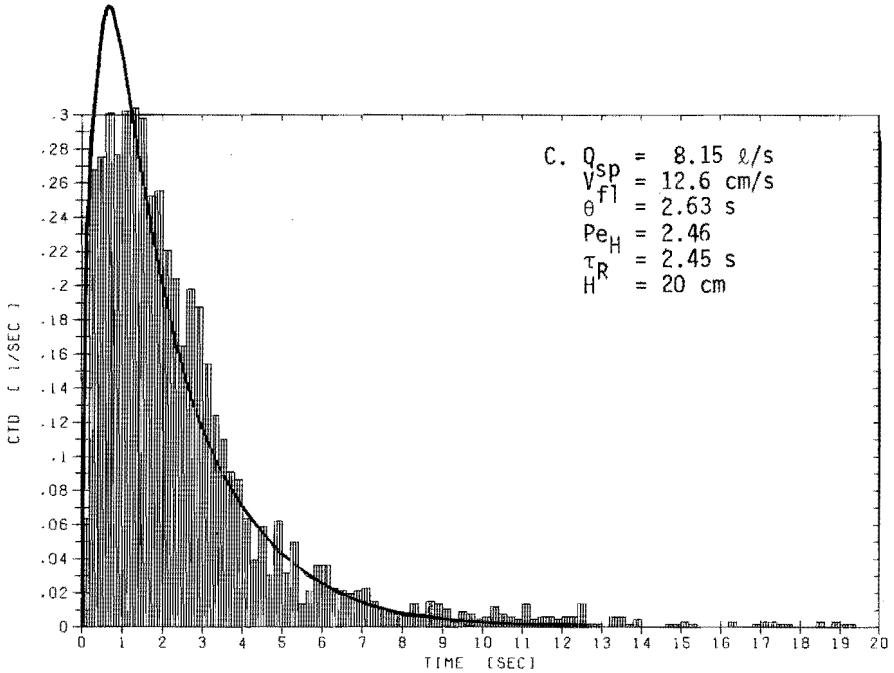

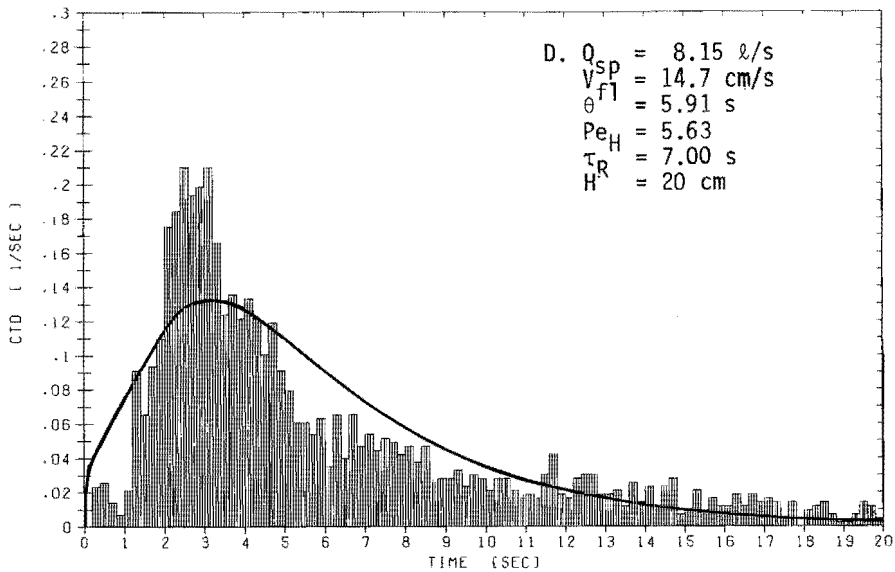

Figure 6.13C-D. Measureed histograms and calculated curves from the dispersion model with the same values of τ_R and Pe_H (H = 20 cm).

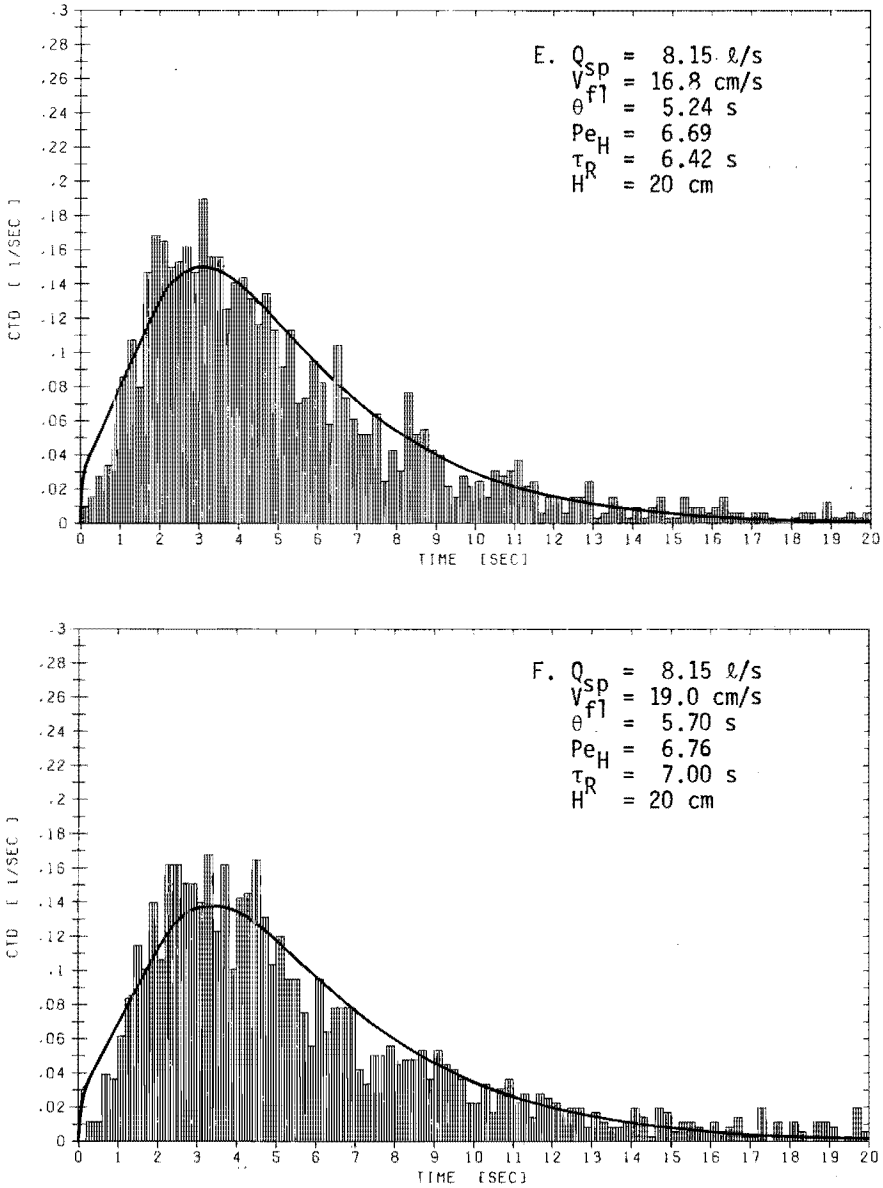

Figure 6.13E-F. Measured histograms and calculated curves from the dispersion model with the same values of τ_R and Pe_H (H = 20 cm).

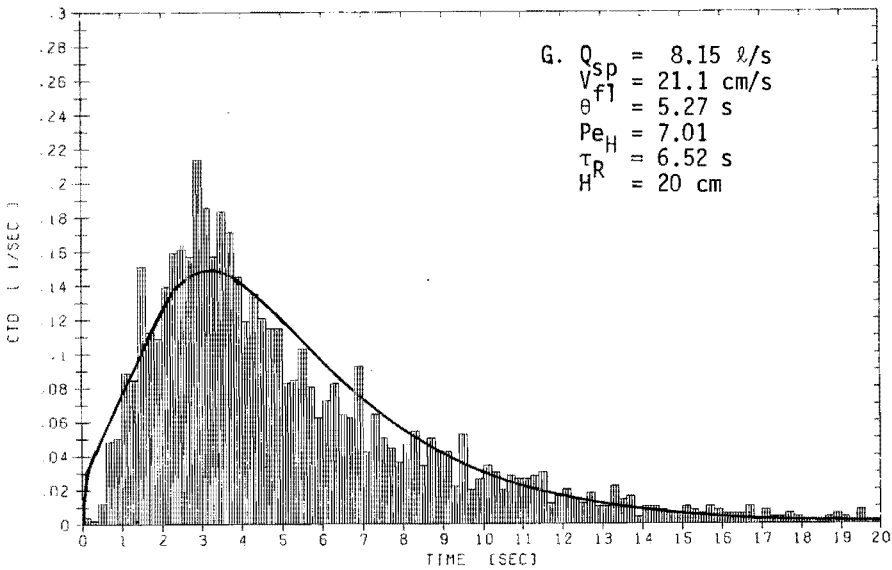

Figure 6.13G. Measured histograms and calculated curves from the dispersion model with the same values of τ_R and Pe_H (H = 20 cm).

Results of circulation time measurements in the spout-fluid beds with bed heights of 35 cm and 20 cm are summarized in table 6-II and table 6-III respectively. The computed mean cycle time θ, its standard deviation σ, the residence time τ_R and the Peclet number Pe_H are given as functions of spout and fluidisation gas flow rates. The bed and orifice diameter were 15.2 and 1 cm respectively.

The dispersion coefficient E and the downward velocity v of the bed material are derived from τ_R and Pe_H by the simple relations

$$v = H/\tau_R \qquad (6\text{-}3)$$

and

$$E = H^2/(Pe_H \cdot \tau_R) \qquad (6\text{-}4)$$

Numerical values of the downward solids flow velocity and the dispersion coefficient are given in the tables 6.IV and 6.V for the gas

V_{fl}		4.2 cm/s	6.3 cm/s	8.4 cm/s	10.5 cm/s	12.6 cm/s
Q_{sp} = 9.06 ℓ/s	θ	2.60 s		5.61 s	4.80 s	
	σ	3.67 s		5.76 s	5.23 s	
	τ_R	1.05 s		4.90 s	3.83 s	
	Pe_H	0.55		2.09	1.71	
Q_{sp} = 8.15 ℓ/s	θ		4.39 s	4.87 s	5.29 s	
	σ		4.43 s	5.15 s	5.35 s	
	τ_R		3.92 s	4.09 s	4.72 s	
	Pe_H		2.21	1.90	2.20	
Q_{sp} = 7.25 ℓ/s	θ	4.36 s	3.46 s	3.61 s	2.99 s	2.62 s
	σ	4.99 s	3.98 s	4.02 s	3.63 s	3.18 s
	τ_R	3.21 s	2.53 s	2.78 s	1.96 s	1.72 s
	Pe_H	1.45	1.43	1.59	1.17	1.17
Q_{sp} = 6.34 ℓ/s	θ	4.10 s	2.33 s	3.23 s	2.19 s	2.07 s
	σ	4.32 s	3.06 s	3.66 s	2.46 s	2.88 s
	τ_R	3.46 s	1.24 s	2.42 s	1.67 s	0.91 s
	Pe_H	1.92	0.83	1.50	1.54	0.62
Q_{sp} = 5.44 ℓ/s	θ	4.46 s		4.80 s	4.60 s	
	σ	4.44 s		4.11 s	3.58 s	
	τ_R	4.06 s		3.65 s	5.26 s	
	Pe_H	2.31		2.22	4.81	
Q_{sp} = 4.53 ℓ/s	θ	5.17 s	4.75 s	3.51 s		
	σ	4.64 s	4.99 s	3.70 s		
	τ_R	5.26 s	4.59 s	2.95 s		
	Pe_H	3.17	2.71	1.92		

Table 6-II Results of measured circulation time distributions in a spout-fluid bed (D = 15.2 cm, a = 0,5 cm, H = 35 cm). Tracer particle: d_p = 3½ mm.

V_{fl}		4.2 cm/s	6.3 cm/s	8.4 cm/s	10.5 cm/s	12.6 cm/s
Q_{sp} = 8.15 ℓ/s	θ		4.16 s		4.16 s	2.63 s
	σ		3.18 s		4.00 s	2.57 s
	τ_R		4.82 s		3.94 s	2.45 s
	Pe_H		5.08		2.58	2.46
Q_{sp} = 6.34 ℓ/s	θ	4.86 s	4.08 s	3.56 s	4.33 s	4.90 s
	σ	5.04 s	4.43 s	2.94 s	3.36 s	3.59 s
	τ_R	4.19 s	3.30 s	3.90 s	4.95 s	5.83 s
	Pe_H	2.02	1.75	4.04	4.83	5.74
Q_{sp} = 4.53 ℓ/s	θ	6.68 s	5.41 s		3.64 s	3.75 s
	σ	5.62 s	5.05 s		2.77 s	3.14 s
	τ_R	7.20 s	5.29 s		4.23 s	4.07 s
	Pe_H	3.83	2.81		5.14	3.92

V_{fl}		14.7 cm/s	16.8 cm/s	19.0 cm/s	21.1 cm/s
Q_{sp} = 8.15 ℓ/s	θ	5.91 s	5.24 s	5.70 s	5.27 s
	σ	4.36 s	3.65 s	3.95 s	3.62 s
	τ_R	7.00 s	6.42 s	7.00 s	6.52 s
	Pe_H	5.63	6.69	6.76	7.01
Q_{sp} = 6.34 ℓ/s	θ	6.30 s	6.12 s	6.37 s	6.80 s
	σ	4.50 s	4.11 s	4.37 s	4.40 s
	τ_R	7.60 s	7.64 s	7.86 s	8.65 s
	Pe_H	6.17	7.47	6.98	8.34
Q_{sp} = 4.53 ℓ/s	θ	4.87 s	4.99 s		6.23 s
	σ	3.87 s	4.01 s		4.64 s
	τ_R	5.48 s	5.59 s		7.33 s
	Pe_H	4.51	4.40		5.46

Table 6-III Results of measured circulation time distributions in a spout-fluid bed (D = 15.2 cm, a = 0.5 cm, H = 20 cm). Tracer particle: d_p = 3½ mm.

V_{fl}		4.2 cm/s	6.3 cm/s	8.4 cm/s	10.5 cm/s	12.6 cm/s
Q_{sp} = 9.06 ℓ/s	v	33 cm/s		7.1 cm/s	9.1 cm/s	
	E	0.21 m^2/s		0.014 m^2/s	0.019 m^2/s	
Q_{sp} = 8.15 ℓ/s	v		8.9 cm/s	8.6 cm/s	7.4 cm/s	
	E		0.014 m^2/s	0.016 m^2/s	0.012 m^2/s	
Q_{sp} = 7.25 ℓ/s	v	10.9 cm/s	13.8 cm/s	12.6 cm/s	17.9 cm/s	20.3 cm/s
	E	0.026 m^2/s	0.034 m^2/s	0.028 m^2/s	0.053 m^2/s	0.061 m^2/s
Q_{sp} = 6.34 ℓ/s	v	10.1 cm/s	28.2 cm/s	14.5 cm/s	21.0 cm/s	38 cm/s
	E	0.018 m^2/s	0.119 m^2/s	0.034 m^2/s	0.048 m^2/s	0.217 m^2/s
Q_{sp} = 5.44 ℓ/s	v	8.6 cm/s		9.6 cm/s	6.7 cm/s	
	E	0.013 m^2/s		0.015 m^2/s	0.005 m^2/s	
Q_{sp} = 4.53 ℓ/s	v	6.7 cm/s	7.6 cm/s	11.9 cm/s		
	E	0.007 m^2/s	0.010 m^2/s	0.022 m^2/s		

Table 6-IV Measured downward particle velocity and dispersion in the annulus (D = 15.2 cm, a = 0.5 cm, H = 35 cm). Results are obtained from table 6-I.

V_{fl}		4.2 cm/s	6.3 cm/s	8.4 cm/s	10.5 cm/s	12.6 cm/s
Q_{sp} = 8.15 ℓ/s	v		4.1 cm/s		5.1 cm/s	8.2 cm/s
	E		0.0016 m^2/s		0.0039 m^2/s	0.0066 m^2/s
Q_{sp} = 6.34 ℓ/s	v	4.8 cm/s	6.1 cm/s	5.1 cm/s	4.0 cm/s	3.4 cm/s
	E	0.0047 m^2/s	0.0069 m^2/s	0.0025 m^2/s	0.0017 m^2/s	0.0012 m^2/s
Q_{sp} = 4.53 ℓ/s	v	2.8 cm/s	3.8 cm/s		5.5 cm/s	4.9 cm/s
	E	0.0015 m^2/s	0.0027 m^2/s		0.0018 m^2/s	0.0025 m^2/s

V_{fl}		14.7 cm/s	16.8 cm/s	19.0 cm/s	21.1 cm/s
Q_{sp} = 8.15 ℓ/s	v	2.9 cm/s	3.1 cm/s	2.9 cm/s	6.1 cm/s
	E	0.0010 m^2/s	0.0009 m^2/s	0.0008 m^2/s	0.0009 m^2/s
Q_{sp} = 6.34 ℓ/s	v	2.6 cm/s	2.6 cm/s	2.5 cm/s	2.3 cm/s
	E	0.0009 m^2/s	0.0007 m^2/s	0.0007 m^2/s	0.0006 m^2/s
Q_{sp} = 4.53 ℓ/s	v	3.6 cm/s	3.6 cm/s		2.7 cm/s
	E	0.0016 m^2/s	0.0016 m^2/s		0.0010 m^2/s

Table 6-V Measured downward particle velocity and dispersion in the annulus (D = 15.2 cm, a = 0.5 cm, H = 20 cm). Results are obtained from table 6-II.

rates and bed heights that were used in this investigation. Figure 6.14 shows a diagram where the solids flow velocity v is plotted against the spout gas flow rate Q_{sp} for the spout-fluid bed with bed height 35 cm. Figure 6.15 shows a plot of the solids flow velocity v versus the superficial fluidisation gas velocity V_{fl} that was measured in the bed with bed height 20 cm.

Figure 6.14 shows that the circulation rate increases at increasing spout gas rate when the rates of both spout and fluidisation gas are low. This might perhaps be explained as follows: Increasing the spout gas rate results in a higher gas velocity in the spout channel region and therefore in a higher circulation rate of the bed solids. Increasing the local gas velocity in the spout channel thus means increasing the circulation rate of the bed solids as long as the gas

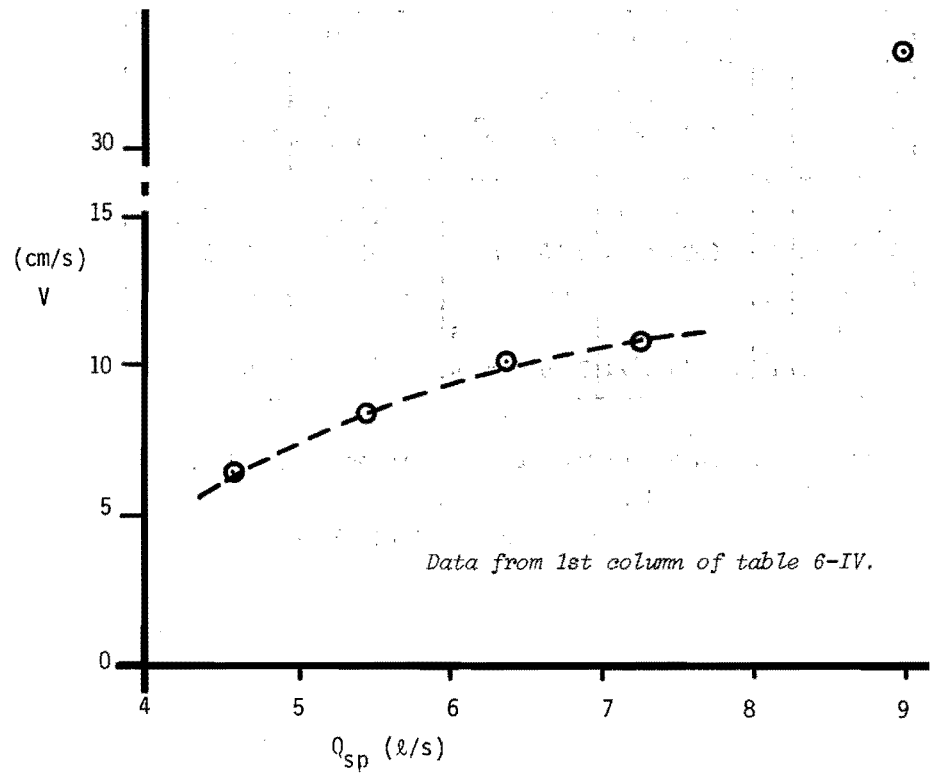

Figure 6.14A. Solids flow velocity obtained from measured histograms as a function of the spout gas flow rate.
Bed height = 35 cm, V_{fl} = 4.2 cm/s.

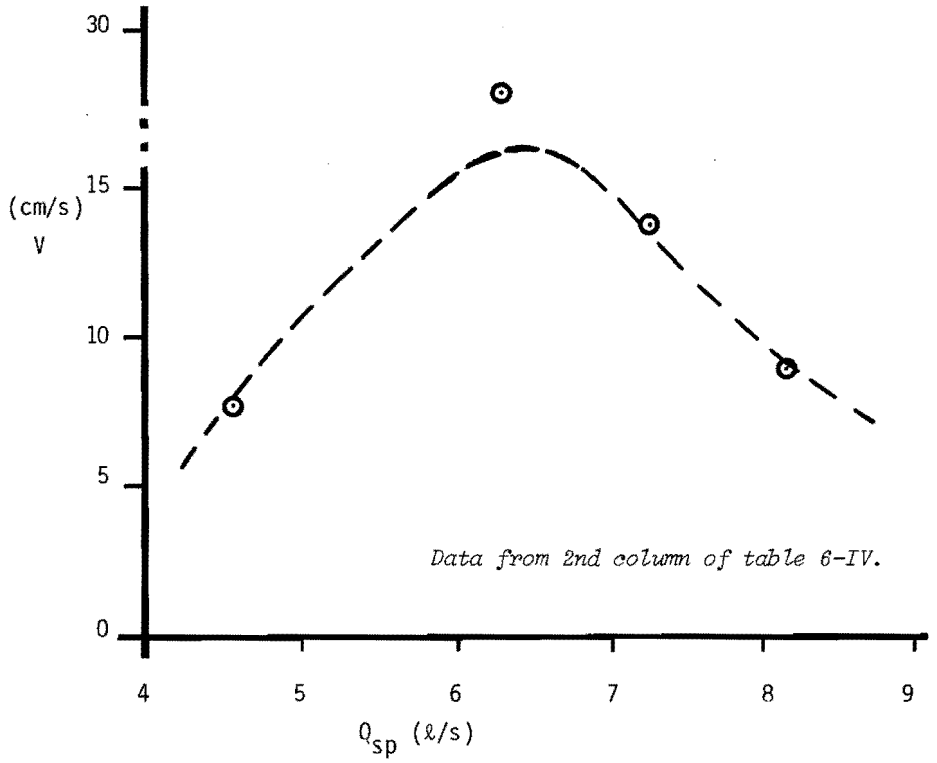

Figure 6.14B. Bed height = 35 cm, V_{fl} = 6.3 cm/s.

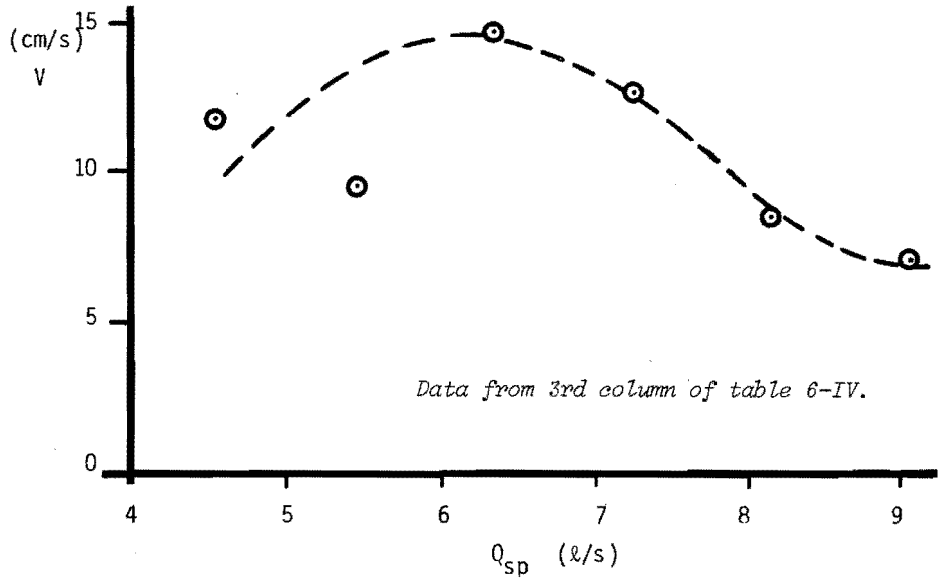

Figure 6.14C. Bed height = 35 cm, V_{fl} = 8.4 cm/s.

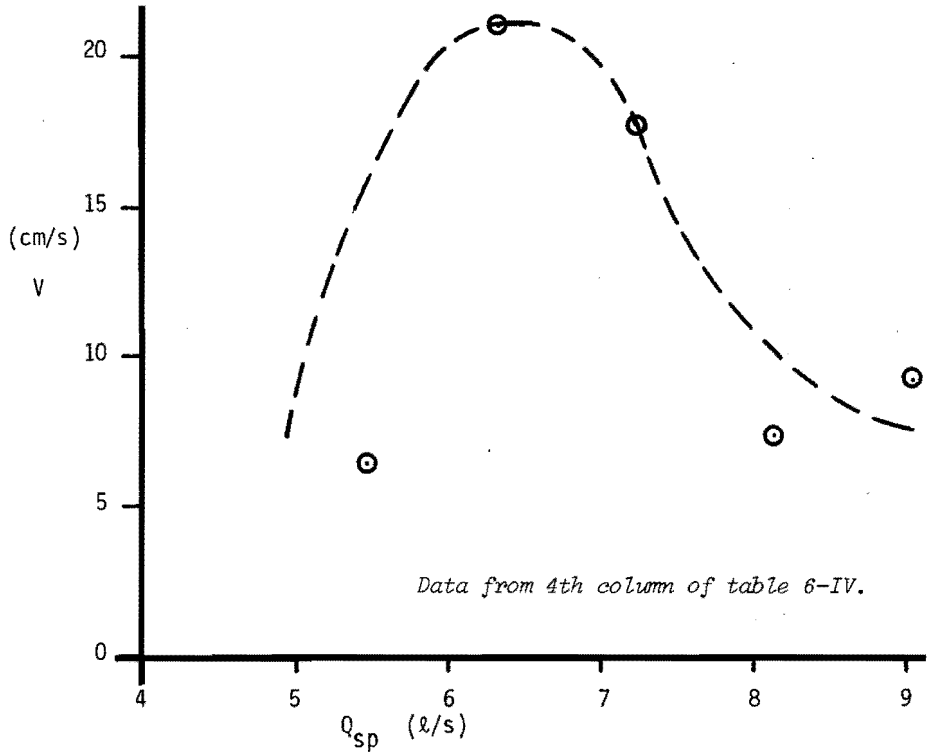

Figure 6.14D. Solids flow velocity obtained from measured histograms as a function of the spout gas flow rate. Bed height = 35 cm, V_{fl} = 10.5 cm/s.

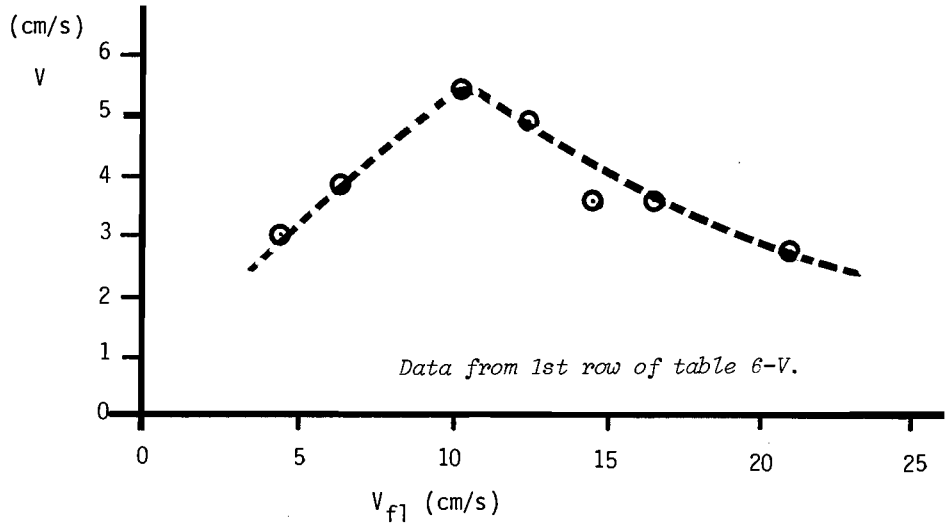

Figure 6.15A. Solids flow velocity obtained from measured histograms as a function of the superficial fluidisation gas velocity.
Bed height = 20 cm, Q_{sp} = 4.53 ℓ/s.

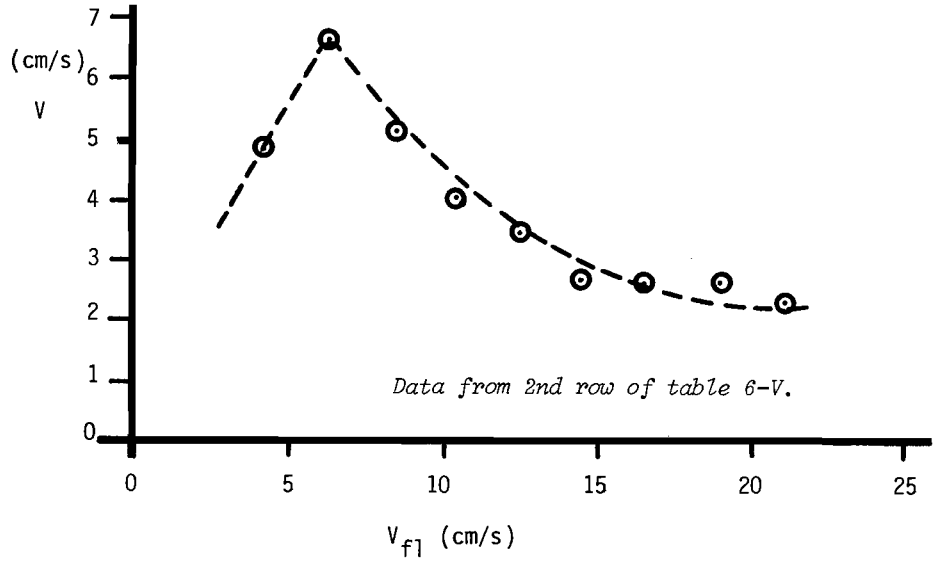

Figure 6.15B. Bed height = 20 cm, Q_{sp} = 6.34 ℓ/s.

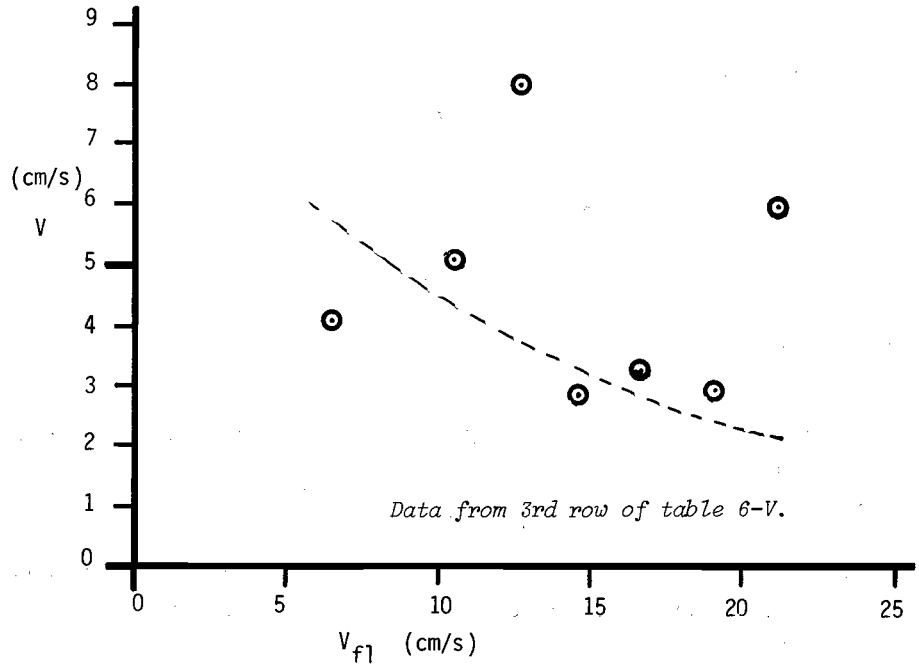

Figure 6.15C. Solids flow velocity obtained from measured histograms as a function of the superficial fluidisation gas velocity.
Bed height = 20 cm, Q_{sp} = 8.15 ℓ/s.

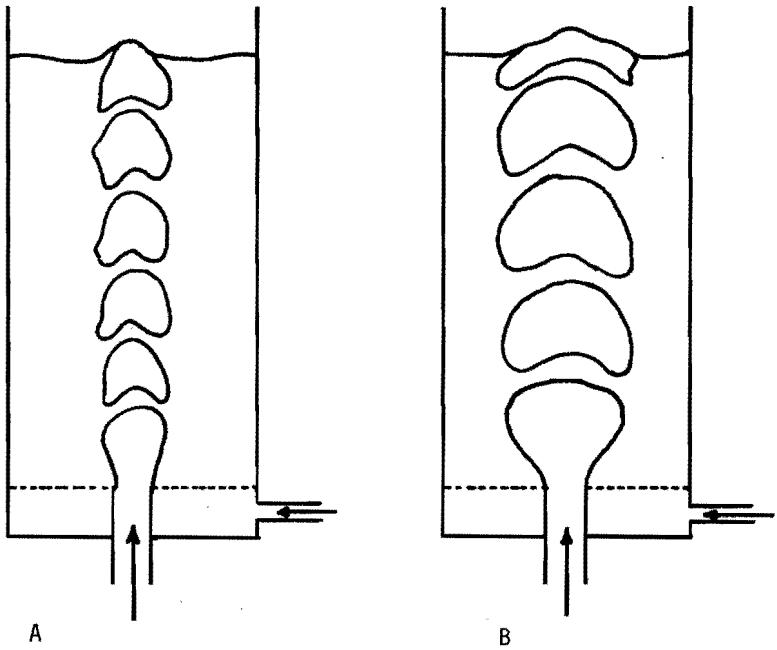

Figure 6.16. Scheme of a spout-fluid bed with a fluctuating spout channel (A) and a region with large bubbles (B) in the center of the bed.
Case A for relatively low values of Q_{sp} and V_{fl}.
Case B for relatively high values of Q_{sp} and V_{fl}.

velocity in the spout channel region is low.
The gas velocity in the spout channel increases when either the spout gas rate or the fluidisation gas rate is increased.
When the spout and fluidisation gas flow rates are increased beyond the values that correspond to the maxima of the downward solids flow velocity that are shown in figure 6.14, the circulation rate seems to decrease. This might be caused by relatively large bubbles that ascend from the spout orifice to the top of the bed under these conditions. Large bubbles have only few bridges from which bed material flows into the upward gas flow in the central region of the bed (figure 6.16). The occurrence of large bubbles also diminish the volume of the annulus region. Large bubbles therefore interfere with the downward solids flow in the annulus and slow it down. The formation of large bubbles

therefore might result in a lower solids circulation rate.
It is to be noted that at high values of the gas rates the introduction of both spout gas and fluidisation gas results in the formation of large bubbles. In the top section of the bed it is then no longer possible to distinguish between the gas that originated from the spout orifice and gas that originated from the sieve plate.

A relationship was found to exist between the rate of dispersion and the downward flow of the solids in the spout-fluid bed. This relation-

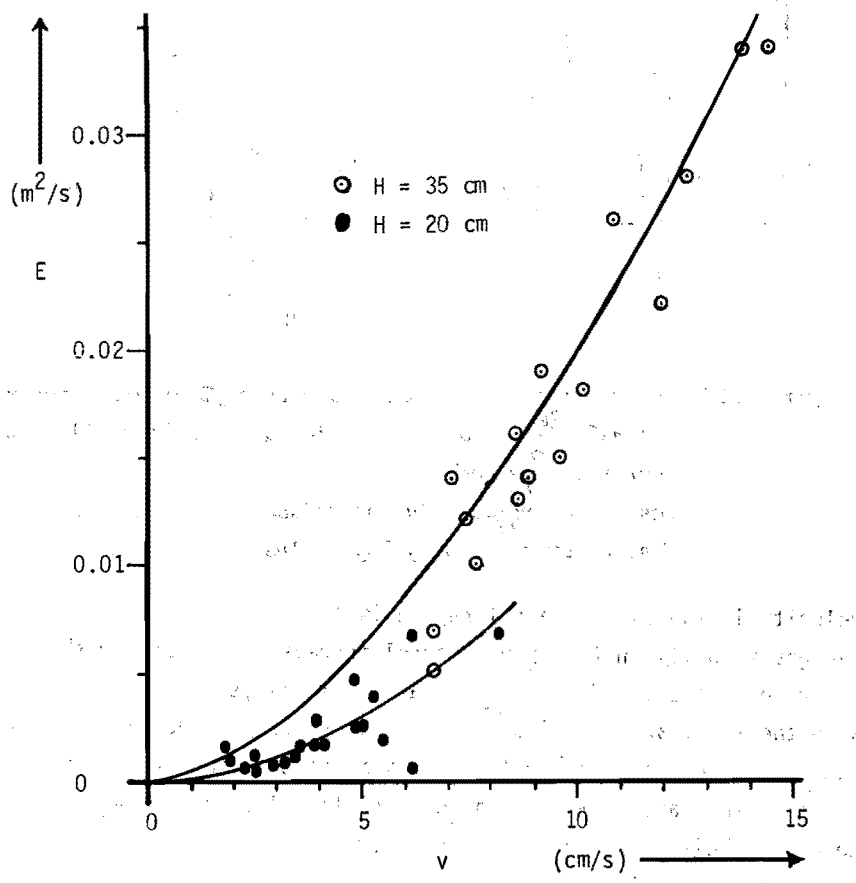

Figure 6.17A. Dispersion coefficient as a function of the solids flow velocity (H = 20 cm and 35 cm).

ship is shown in figure 6.17 which is a plot of the dispersion coefficient E versus the solids flow velocity v.
The dispersion is related to the solids flow velocity by a power function. The power of the function is found to be equal to 1.65 for a bed height H = 35 cm while a power equal to 1.9 resulted from the best fit for H = 20 cm.

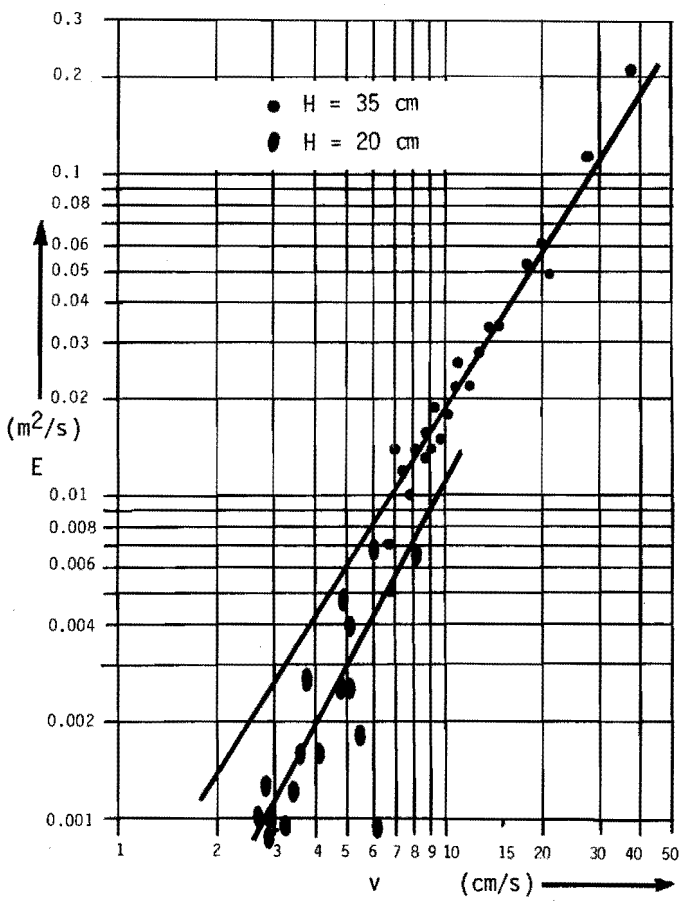

Figure 6.17B. Dispersion coefficient as a function of the solids flow velocity (H = 35 cm and 20 cm).

6.4. Conclusions

-Because of the short circulation times in spout-fluid beds in the fluctuating spouted bed regime the mixing behaviour in these beds can best be investigated by measuring the circulation time distribution of a single tracer particle, rather than by measuring the response of a pulse injection of an amount of tracer material.

-The technique of measuring the circulation behaviour of the bed material by means of a tracer particle with a high magnetic permeability requires relatively inexpensive and relatively simple equipment for the detection of the particle.
This technique has the disadvantage that it is very difficult to produce a particle with high magnetic permeability that has a density that is comparable to that of the bed particles or to the bulk density of the bed.

-Bed solids that are present in a bed in the fluctuating spouted bed regime undergo a much higher rate of mixing than the solids that are present in a bed that is being operated in the stable spouted bed regime and at the same rates of spout and fluidisation gas.

-It was found that the dispersion model of a spout-fluid bed which assumes the existence of a series of particle trajectories of different length is able to provide a rough description of the circulation flow rate distribution of the bed solids in a fluctuating spouted bed.

-The rate of solids circulation in the fluctuating spout-fluid beds increases with increasing bed height. This rate also increases at increasing spout and fluidisation gas flow rates when these gas rates are low.

-Relatively high values of the spout and fluidisation gas rates do not result in a high circulation rate because of limitations which are due to the formation of large bubbles in the bed.

List of symbols

E	dispersion coefficient	$[m^2/s]$
H	bed height	[m]
Q_{fl}	fluidisation gas flow rate	$[m^3/s]$
Q_{sp}	spout gas flow rate	$[m^3/s]$
Pe_H	Peclet number that applies to the trajectory along the bed wall	[-]
R	bed radius	[m]
v	downward solids flow velocity	[m/s]
V_{fl}	superficial fluidisation gas velocity	[m/s]
θ	mean circulation time	[s]
σ	standard deviation of the circulation time	[s]
τ_R	residence time of the bed material in the trajectory along the bed wall	[s]

S T E L L I N G E N

behorende bij

het proefschrift

S O M E P R O P E R T I E S

O F

S P O U T - F L U I D B E D S

van

C. Heil

Eindhoven, 18 mei 1984

STELLINGEN

1. De maximale hoogte van een nog te spouten bed is een grootheid, die onvoldoende eenduidig bepaald kan worden. Deze grootheid kan daarom beter niet betrokken worden bij een analyse van het gedrag van een spouted bed.

   Mamuro, T., Hattori, H., J.Chem.Eng.Japan 1, 1 (1968)
   Epstein, N. et al., Can.J.Chem.Eng. 56, 436 (1978)
   Grbavcić, Z.B. et al., Can.J.Chem.Eng. 54, 33 (1976)

2. De drukverdeling in een spout-fluid bed met een stabiel spoutkanaal hangt grotendeels af van de condities, die geschapen worden op de grens tussen het spoutkanaal en de annulus alsmede in de onmiddellijke nabijheid van die grens.

   Dit proefschrift, hoofdstuk 4
   Mamuro, T., Hattori, H., J.Chem.Eng.Japan 1, 1 (1968)
   Yokogawa, A. et al., Trans.Jap.Soc.Mech.Eng. 38, 148 (1972)

3. Het gebruik van een tracerdeeltje met een hoge magnetische permeabiliteit voor circulatietijdmetingen is te verkiezen boven het gebruik van een magnetisch tracerdeeltje.

   Mann, U., Crosby, E.J., Can.J.Chem.Eng. 53, 579 (1975)
   Dit proefschrift, hoofdstuk 6

4. De vorming van één of meer bellen in het zoggebied van een grotere opstijgende bel onder omstandigheden waarbij een bellentrein in het centrum van het bed overgaat in een fluctuerend spoutkanaal, verklaart, dat verschillende auteurs onder ruwweg dezelfde bedomstandigheden verschillende belfrequenties meten.

   Rowe, P.N. et al., Trans.Inst.Chem.Eng. 57, 194 (1979)
   Harrison, D., Lueng, L.S., Trans.Inst.Chem.Eng. 39, 407 (1961)
   Payne, G.J., Prince, R., Trans.Inst.Chem.Eng. 53, 209 (1975)
   Dit proefschrift, hoofdstuk 2

5. De door Tsubaki en Jimbo gevonden relatie tussen de adhesie tussen poederdeeltjes en de grootte van de voordruk in een poederstapeling berust niet op experimenten, maar op het veronderstelde zuiver theoretische verband tussen de adhesiekrachten in, en de porositeit en cohesie van een poederstapeling.

   Tsubaki, J., Jimbo, G., Intern.Symp. EFChE., Eindhoven, August 29-31, 1983, EFChE Publication Series no. 28.

6. Het weergeven van resultaten van warmteoverdrachtsexperimenten in gefluidiseerde bedden in de vorm van correlaties is niet zinvol zolang het stromingsgedrag van het poeder aan het warmteoverdragend oppervlak niet afdoende beschreven kan worden.

   Gupta, S.N. et al., Chem.Eng.Sci. 29, 839 (1974)
   Gutfinger, C., Abuaf, N., Heat transfer in fluidised beds, in: Advances in Heat Transfer, Vol.10, 1974, Ac.Press, New York, p.167-214.

7. Het verdient aanbeveling bij de analyse van de energie-degradatie bij voorgestelde thermodynamische processen gebruik te maken van het exergiebegrip, daar dit begrip het mogelijk maakt op aanschouwelijke wijze met de tweede hoofdwet van de thermodynamica te werken. Discussies over voorgestelde processen zullen daardoor meer inhoud krijgen.

   van Lier, J.J.C., Brennst.-Wärme-Kraft 30, 475 (1978)

8. De huidige methode ter berekening van de kWh-prijs mag niet zonder meer toegepast worden op de grootschalige electriciteitsopwekking zoals die met behulp van windturbines in de toekomst plaats zou kunnen vinden.

   Halberg, N., Electrotechniek 61, 250 (1983)

9. Het afremmen van de ontwikkeling van commerciële kolenvergassingssystemen wanneer de brandstofprijzen relatief lager worden getuigt van een grote kortzichtigheid. Het gevolg hiervan zal zijn, dat bij het

weer stijgen van de brandstofprijzen of bij het steeds verder toenemen van de milieuhinder door kolenstokers, de benodigde tijd zal ontbreken om de research uit te voeren die nodig is om de dan noodzakelijk geworden beslissingen te nemen omtrent de optimalisatie van de Nederlandse energievoorziening.

10. De door de Minister van Onderwijs en Wetenschappen voorgenomen wijziging van de naam "Technische Hogeschool" in "Universiteit" miskent zowel het wezen van de universiteit als dat van de Technische Hogeschool.